UNIVERSIDAD AUTÓNOMA DE MADRID

Facultad de Ciencias

Sección de Ingeniería Química

Removal of naphthenic acids from water by persulfate and Fenton-like oxidation

Eliminacion de ácidos nafténicos en agua por oxidación con persulfato y mediante el sistema Fenton

环烷酸溶液的过硫酸盐及类芬顿氧化处理

Tesis Doctoral

XU XIYAN

Madrid, 2017

UNIVERSIDAD AUTÓNOMA DE MADRID
Facultad de Ciencias
Sección de Ingeniería Química

Eliminacion de ácidos nafténicos en agua por oxidación con persulfato y mediante el sistema Fenton

MEMORIA
Para optar al grado de
Doctor
Mención Internacional
presenta
XU XIYAN

Directores: Dr. Juan José Rodríguez Jiménez
Dra. Gema Pliego Rodríguez

Madrid, 2017

D. Juan José Rodríguez Jiménez, Catedrático de Universidad, y Dña. **Gema Pliego Rodríguez**, Profesora ayudante de Universidad, ambos profesores de la Sección de Ingeniería Química perteneciente al Departamento de Química-Física Aplicada de la Universidad Autónoma de Madrid.

HACEN CONSTAR: que el presente trabajo, titulado "*Eliminacion de ácidos nafténicos en agua por oxidación con persulfato y mediante el sistema Fenton",* presentado por D. Xiyan Xu, ha sido realizado bajo su dirección, en los laboratorios de la Sección de Ingeniería Química, en la Universidad Autónoma de Madrid, y que a su juicio reúne los requisitos de originalidad y rigor científico necesarios para ser presentado como Tesis Doctoral.

Y para que conste a efectos oportunos, firmamos el presente informe en Madrid, a 23 de mayo de 2017.

Juan José Rodríguez Jiménez

Gema Pliego Rodríguez

Contents/Índice/目录

OBJECTIVES AND SUMMARY

OBJETIVOS Y RESUMEN

序

Objectives and summary

The growing energy demand of traditional fossil fuels along with the expansion of human population promotes the exploration of other energy resources, including non-conventional hydrocarbon deposits. This trend has been eventually enhanced by the intermittent raise of oil prices. Among the non-conventional hydrocarbons, shale oil and tar sands represent the most available resources with the current extraction processing technologies. However, their exploitation is associated to very important environmental problems. In particular, high amounts of wastewaters have been generated in the last decades from those activities. Huge volumes of aqueous wastes are simply spilled in tailing ponds, implying a highly concerning risk for human health and the environment. As representative example, in the tar sands area of Alberta (Canada), around 1,500 hm^3 of those wastewaters are currently stored.

The main harmful components of the oil shales and oil sands process-affected waters (OSPWs) are naphthenic acids (NAs). They are highly resistant to biodegradation due to their saturated ring-structures and toxicity. Different physical, chemical and biological techniques have been studied so far for the abatement of NAs. Activated carbon adsorption can remove those pollutants from the aqueous phase, but further disposal is still needed since the harmful components are not destroyed but simply transferred to the solid adsorbent. Biodegradation approaches do not allow effective removal of NAs due to the abovementioned bio-recalcitrant character of those compounds. Advanced oxidation processes (AOPs) have been investigated for NAs treatment. They include ozonation, UV/H_2O_2 and persulfate (PS) oxidation under thermal, UV, zero valent iron (ZVI) activation. However, none of these techniques have been demonstrated as cost-effective solutions at full-scale and further research efforts

need to be accomplished to evaluate potential application.

The current Ph.D. Thesis is aimed to investigate the abatement of NAs by advanced oxidation with thermally-activated persulfate and its combination with conventional and heterogeneous Fenton treatment, this last being also named Catalytic Wet Peroxide Oxidation (CWPO). In the case of PS oxidation, fairly substoichiometric amount of this reagent were found sufficient for complete mineralization of the NAs tested. The source of that extra oxidation capacity was investigated in depth. Comparing the results obtained under dissolved oxygen and inert conditions, it was found that oxygen plays an important role in the oxidation process, so that the stoichiometry of the overall reactions needed to be reformulated. The analysis of the effluents from the oxidation experiments allowed identifying intermediate and end-products to stablish the corresponding reaction pathways. The kinetics of the process was studied as well to describe the time-course of TOC (mineralization) and individual species. Although PS oxidation showed to be highly effective towards NAs degradation, the cost of reagent is fairly high compared with that of H_2O_2 and moreover it introduces the corresponding amount of sulfate, which can be a concerning issue looking at the stoichiometry of the reaction. Based on these considerations, alternative approaches, combining PS and Fenton-like oxidation have been studied. Regarding to the Fenton step, both conventional (homogeneous) and heterogeneous (CWPO) have been tested. For this second, activated carbon or γ-alumina-supported iron catalysts were used. These combined systems allowed reducing the cost associated to reagents consumption while providing high mineralization (> 80%), being the remaining TOC due to low molecular-weight carboxylic acids of low significance in terms of toxicity. The resulting effluents were readily biodegradable as determined from respirometric tests.

The Thesis is structured in the following chapters:

I. Introduction: It presents a review of the properties, identification techniques and treatment approaches for NAs. Because of the structural complexity of NAs, the identification of these species becomes a task to which important efforts have been devoted in the last decade. Regarding the treatment methods, particular attention is paid to advanced oxidation processes (AOPs).

II. Materials and methods: This chapter collects the information on the starting NAs and the reagents used, the analytical techniques and the setups and operating conditions for the oxidation experiments.

III. Results and discussion: The first section investigates the mineralization of model naphthenic acids (NAs) by catalyst-free thermally-activated PS oxidation in aqueous solution. The NAs tested include saturated-ring (cyclohexanecarboxylic (CHA) and cyclohexanebutyric acids (CHBA)) and aromatic (2-naphthoic (2-NA) and 1,2,3,4-tetrahydro-2-naphthoic acids (1234-T-2-NA)) structures. The effects of PS dose and working temperature are checked. Complete mineralization of NAs was achieved with frankly substoichiometric amounts of PS which is explained by the important contribution of dissolved oxygen. The structural features of the NAs was found to play also a significant role. The effect of chloride and bicarbonate as potential scavengers has been also tested. The kinetics of NAs mineralization has been studied and values of the normalized rate constants and the corresponding apparent activation energy are given.

The second section of this chapter analyzes the reaction pathways and kinetics of PS oxidation of individual NAs (CHA, CHBA, 2-NA and 1234-T-2-NA) in presence and absence of dissolved oxygen. The identification of the reaction intermediates was conducted by GC-MS. That allowed establishing the corresponding degradation pathways. The structure-based differences between

the saturated and aromatic ring-bearing NAs are discussed and the mineralization kinetics of each NA is provided with the role of oxygen quantitatively discussed.

In the third section of Chapter III, a combined treatment consisting of PS oxidation at circumneutral initial pH followed by Fenton oxidation is studied. The effect of the amount of reactants and the temperature are investigated with CHA as model NA. The biodegradability before and after reaction was assessed from the specific oxygen uptake rates (SOUR). The treatment efficiency for various individual and mixed NAs was also tested. A kinetic model considering both the PS and Fenton stages is proposed and the corresponding apparent activation energy values are also provided. The system was successfully tested with other NAs including saturated ring as well as aromatic structures, namely CHBA, 2-NA and 1234-T-2-NA. The results allow considering this approach as a promising cost-effective solution for the treatment of NAs-bearing aqueous wastes.

In the fourth section, heterogeneous Fenton systems catalyzed by home-made activated carbon and γ-alumina supported iron (Fe/AC and Fe/γ-Al_2O_3) are tested after PS pretreatment for the abatement of NAs at circumneutral initial pH. The performance of the two catalysts is compared under different working conditions. Iron leaching is checked as well as the reusability of the catalysts. Their textural characteristics and surface composition before and after reaction were evaluated by 77 K N_2 adsorption-desorption, TXRF and XPS. The effect of oxalic acid formed upon reaction, the enhanced acidity after the PS pretreatment and the metal-support interaction on iron leaching are discussed.

IV. Conclusions and outlook: This chapter summarizes the main conclusions of the work and suggests some ideas to address further research.

Objetivos y resumen

El incremento en la demanda de combustibles fósiles, vinculado al crecimiento paulatino de la población y a un mayor grado de desarrollo, ha impulsado la búsqueda de fuentes alternativas de hidrocarburos. Esta tendencia, favorecida por las subidas intermitentes de los precios del petróleo, ha puesto en valor las reservas de gas de esquisto y arenas bituminosas, principales fuentes de hidrocarburos no convencionales. No obstante, el aprovechamiento de estas reservas acarrea graves problemas medioambientales, en especial la generación de grandes volúmenes de aguas residuales que se han ido almacenando en balsas de decantación, con el consiguiente riesgo para la salud humana y para el medio ambiente. A modo de ejemplo, en la región de Alberta (Canadá), una de las principales zonas de explotación de este tipo de hidrocarburos, el volumen de agua embalsada asciende a 1.500 hm^3.

Entre los compuestos orgánicos presentes en el sobrenadante de las balsas de decantación, los ácidos nafténicos son los que concentran mayor atención, debido a su escasa biodegradabilidad, producto de su estructura y toxicidad.

Hasta la fecha, las alternativas estudiadas para su eliminación abarcan procesos físicos, químicos y biológicos. La adsorción sobre carbón activo permite retirar estos contaminantes de la fase acuosa, pero con la necesidad de regenerar o gestionar adecuadamente el adsorbente utilizado. Por su parte, los procesos biológicos no consiguen eliminar de manera efectiva los ácidos nafténicos, debido a su carácter biorecalcitrante. Entre los procesos avanzados de oxidación avanzada (POAs; AOPs en sus siglas en inglés) investigados cabe citar la ozonación, UV/H_2O_2 y oxidación con persulfato, ya sea activado térmicamente o mediante UV o hierro zerovalente. Sin embargo, ninguna de estas opciones ha demostrado su viabilidad a escala industrial, por lo que se requiere un esfuerzo investigador sostenido para

desarrollar soluciones efectivas.

La presente Tesis Doctoral tiene como objetivo estudiar la eliminación de ácidos nafténicos en agua mediante procesos avanzados de oxidación, empleando persulfato activado térmicamente, solo y en combinación con el sistema Fenton homogéneo y heterogéneo, este último también llamado oxidación catalítica con peróxido de hidrógeno (CWPO, en sus siglas en inglés).

En la oxidación con persulfato, se ha conseguido la mineralización total de los ácidos nafténicos seleccionados con dosis de este reactivo significativamente inferiores a las que, en principio, se deducen de la estequiometría de las correspondientes reacciones. Esta aparente anormalidad se explica por el papel desempeñado por el oxígeno disuelto, experimentalmente demostrado en el trabajo, lo que ha permitido reformular dichas reacciones incluyendo su contribución.

A partir del análisis de los efluentes, se identificaron una serie de intermedios y productos finales de degradación, con lo que se han planteado los correspondientes esquemas de reacción. Con dicha información se han elaborado los modelos cinéticos que describen la evolución de las especies individuales y del carbono orgánico total (COT).

Si bien la oxidación con persulfato representa una opción muy eficaz en términos de mineralización de los ácidos nafténicos, el coste relativamente alto en concepto de reactivo y la incorporación de sulfato derivada de su empleo constituyen dos de los principales problemas de esta tecnología.

En base a estas consideraciones, se ha investigado la combinación de este tratamiento con una etapa posterior vía Fenton, tanto homogéneo como heterogéneo. Para el proceso Fenton heterogéneo se han ensayado catalizadores

de hierro soportado sobre carbón activo o γ-alúmina.

Estas alternativas permiten reducir los costes asociados al consumo de reactivos, manteniendo niveles de mineralización superiores al 80%. La materia orgánica residual está constituida por ácidos carboxílicos ligeros, de escasa toxicidad y fácil biodegradabilidad, constatada en ensayos respirométricos.

La Tesis Doctoral se estructura en los siguientes capítulos.

I. Introducción: Presenta una revisión de las propiedades y técnicas de identificación de los ácidos nafténicos, así como de los procesos investigados en la bibliografía para su tratamiento. Debido a su complejidad estructural, el análisis de estas especies constituye uno de los aspectos clave en relación con este grupo de contaminantes. En lo que respecta a los métodos de tratamiento, la mayor parte de las investigaciones se orientan hacia la aplicación de procesos de avanzados oxidación.

II. Materiales y métodos: Este capítulo recoge la información sobre los ácidos nafténicos de partida y los reactivos utilizados, las técnicas y equipos de análisis empleados y los sistemas y condiciones de operación para los experimentos realizados.

III. Resultados y discusión: La primera sección investiga la mineralización de los ácidos nafténicos empleados, en disolución acuosa, mediante persulfato activado térmicamente. Entre los compuestos estudiados se incluyen estructuras cíclicas saturadas (ácido ciclohexanocarboxílico (CHA) y ácido ciclohexanobutírico (CHBA) y estructuras aromáticas (ácido 2 naftoico (2-NA) y ácido 1,2,3,4-tetrahidro-2-naftoico (1234-T-2-NA)). Se ha analizado el efecto de la dosis de persulfato y de la temperatura de operación. Los resultados obtenidos ponen de manifiesto que es posible mineralizar dichos compuestos con dosis de

persulfato muy por debajo de la estequiométrica, lo que se explica por la contribución del oxígeno disuelto. La estructura de los ácidos nafténicos también se ha demostrado que constituye un factor importante para su degradación.

Otro de los aspectos analizados ha sido la capacidad inhibitoria de cloruros y bicarbonatos. Por último, dentro de esta primera sección se ha llevado a cabo un estudio cinético de la mineralización de los ácidos nafténicos, obteniéndose los valores de las constantes de velocidad y la correspondiente energía de activación aparente.

La segunda parte de este capítulo analiza la ruta de degradación y las cinéticas de oxidación individuales de cada uno de los ácidos nafténicos estudiados, en presencia y en ausencia de oxígeno disuelto. La identificación de los intermedios de reacción se realizó mediante GC-MS. En base a esta información se proponen los correspondientes esquemas de reacción.

La tercera parte recoge los resultados obtenidos mediante el tratamiento de oxidación en dos etapas, consistente en una primera oxidación con persulfato a dosis francamente subestequiométricas, seguida de Fenton. Se ha estudiado el efecto de la dosis de reactivos y de la temperatura, empleando CHA como compuesto modelo. La biodegradabilidad, antes y después de la reacción se evalúa a partir de la velocidad específica de consumo de oxígeno (SOUR). El estudio se amplió a los restantes ácidos nafténicos ensayados y a mezclas de los mismos. Los resultados obtenidos demuestran la mejora que supone este sistema combinado en cuanto al coste en concepto de reactivos. Se ha desarrollado un modelo cinético capaz de describir la evolución del COT en ambas etapas, obteniéndose las correspondientes energías de activación aparentes.

Por último, dentro de este capítulo se han ensayado catalizadores preparados a base de hierro soportado sobre carbón activo y alúmina (Fe/AC and Fe/γ-Al_2O_3)

para el tratamiento vía Fenton heterogéneo de los efluentes de la oxidación con persulfato de los ácidos nafténicos. Las características texturales y la composición de los catalizadores se analizaron, antes y después de la reacción, mediante adsorción-desorción de N_2 a 77 K, TXRF y XPS. Se compara la eficacia de ambos catalizadores bajo diferentes condiciones de operación, analizando la cantidad de hierro lixiviada y relacionándola con el pH del medio, la concentración de ácido oxálico y la interacción hierro-soporte, factores que afectan la estabilidad del catalizador.

IV. Conclusiones y perspectivas: En este capítulo se recogen las conclusiones originales de la investigación y se sugieren algunas ideas para futuras investigaciones.

序

世界人口的日益增长和传统矿石燃料需求的不断增加，促使着人们对包括非传统烃类矿藏在内的替代能源进行探索和发掘。同时，国际油价的阶段性变化也间接导致了这种趋势的加深。页岩油和焦油砂是非传统能源中的代表，人们可应用现有提纯处理技术从中得到烃类燃料。然而，对于这些非传统能源的开发可能会导致严重的环境问题。尤其是过去的几十年中对这些能源的开采产生了大量的含油废水，而这些废水被简单地排放到尾矿池中，威胁到附近居民的身体健康。例如，在加拿大阿尔伯塔省的焦油砂开采区，就储放着约 1500 公顷的此类有害废水。

环烷酸(naphthenic acids, NAs)是油页岩和油砂处理过程所产生的废水(oil sands process-affected waters, OSPWs)中所含的主要有害物质。此类物质具有坚固的饱和烃环结构和高毒性，因此极难被生物降解。为此，已有多种基于物理，化学和生物的处理技术被开发出来。活性炭吸附法可以有效将其从水溶液中去除，但由于有害物质仅是被吸附到吸附剂而未被完全分解，因此需要对该固体废物进行进一步处理。生物降解法成本低廉，但是由于 NAs 的难生化降解性而无法有效去除部分有害物质。高级氧化法(Advanced oxidation processes, AOPs)也被用于 NAs 的处理，包括经加热，紫外辐射(UV)或零价铁(zero valent iron, ZVI)催化的臭氧法，UV/H_2O_2 和过硫酸盐氧化法(persulfate, PS)。然而，虽然这些方法可以有效矿化 NAs 的有害组分，但它们的成本普遍较高，因此需要进一步研究以提高其实用性。

此博士论文以高级氧化法去除 NAs 为目的，使用热催化过硫酸盐氧化法并使其与传统芬顿(Fenton treatment)和非均相芬顿体系(heterogeneous Fenton, 亦即湿式过氧化氢催化氧化(Catalytic Wet Peroxide Oxidation, CWPO))相结合，对 NAs 进行降解。在 PS 氧化降解 NAs 过程中，实验结果发现，使用低于理论化学计量的 PS 即可导致模型 NAs 的全部矿化。因此，进一步深入研究了此额外氧化能力的来源。有氧和无氧条件下 PS 氧化降解 NAs 效果的对比，揭示了溶解氧在该氧化过程中起到了重要作用。考虑到氧气的作用，化学计量方程式被重列。同时，本研究通过对反应后溶液进行分析，鉴定了可能的反应中间物和最终产物，并据此推断了反应机理。另外，进一步研究了此过程的反应动力学以描述 NAs 的矿化和部分反应产物的演化过程。然而，尽管 PS 氧化对 NAs 的降解有极高的效率，但其成本仍较高于过氧化氢，并且此法会向目标溶液中引入相应量的硫元素。基于上述考虑，本研究进一步开发了一些替代方法，如将 PS 和类芬顿体系相结合，形成 PS-Fenton 两步降解体系，而在芬顿反应阶段分别使用了传统(均相，homogeneous)和非均相(湿式催化过氧化氢氧化法 CWPO)芬顿法。这些两步结合体系能够通过减少 PS 的消耗有效降低处理成本，并得到较高的矿化效率(80%)。通过微生物呼吸实验研究了反应前后的可生物降解性。结果发现，NAs 经上述两步氧化法处理后所产生的有机残留物物被测定为可生物降解的小分子有机酸。

此博士论文由以下章节组成：

I. 引言：此章综述了 NAs 的性质，检测技术和处理方法。由于 NAs 结构的复杂性，NAs 有效检测技术的发展成为近十年的一项工作焦点。同时，该章重点

总结了已应用于 NAs 处理的高级氧化技术。

II. 材料与方法：此章包括所使用模型 NAs 和其他药剂的信息，所使用的分析技术和实验设备及所涉及的实验反应条件等内容。

III. 结果与讨论：本章第一节研究了热催化 PS 氧化矿化降解模型 NAs。所使用的模型 NAs 包括具有饱和烃环的 NAs(cyclohexanecarboxylic (CHA) and cyclohexanebutyric acids (CHBA)) 和具有芳香环的 NAs(2-naphthoic (2-NA) and 1,2,3,4-tetrahydro-2-naphthoic acids (1234-T-2-NA))。研究了 PS 剂量和反应温度对 NAs 矿化效率的影响。实验结果表明，低于理论化学计量的 PS 可以导致全部 NAs 的矿化，而体系中的溶解氧在此过程中有着重要作用。同时，研究发现不同种类 NAs 的分子结构对其矿化也有显著影响。考察了潜在的自由基猝灭剂如氯离子和碳酸氢根的影响。此外，研究了 NAs 矿化的反应动力学，并得到了标准化的反应速率常数和相应的反应活化能。

第二节研究了有氧及无氧条件下 PS 氧化降解模型 NAs(CHA, CHBA, 2-NA and 1234-T-2-NA) 的反应机理和动力学。反应产物由 GC-MS 鉴定得到，并据此推测了相应的反应路径。讨论了含有饱和碳环和芳香环的 NAs 氧化过程的差异，并基于对体系中氧气和反应产物的考虑，进一步研究了各模型 NA 的反应动力学。

第三节开发了一种结合 PS 氧化和芬顿法的两步式氧化体系，在碱性初始条件下对 NA 进行处理。以 CHA 为模型污染物，考虑了反应物剂量和反应温度的

影响。以特定氧化率(specific oxygen uptake rates, SOUR)为指标，评估了 CHA 反应前后的可生物降解性，同时考察了此反应体系对其他 NAs 的降解效率。提出一个兼顾 PS 氧化和芬顿两步的反应动力学模型，并得到了相应的反应活化能。实验结果表明该体系为含 NAs 废水的处理提供了一种有效并低成本的解决方案。

第四节研究了经热催化 PS 氧化预处理后，由活性炭和 γ-氧化铝负载铁催化的非均相芬顿体系对 NAs 的处理(初始 pH=8)。研究对比了这两种催化剂在不同反应条件下的处理效率，并考察了反应过程中的铁流失效应和催化剂的复用性。使用 77 K 氮气吸附-脱附法，TXRF 和 XPS 技术检测了催化剂反应前后的表面特征和组分。最后，综合分析了反应过程中所生成草酸的浓度，PS 预处理后较低的 pH 值和金属-载体之间的相互作用等因素对催化剂铁流失效应的影响。

IV. 结论与展望：此章总结了此博士论文所得到的主要结论并为未来的相关工作提供了一些建议。

CHAPTER I/ CAPÍTULO I /首卷

INTRODUCTION

INTRODUCCIÓN

引言

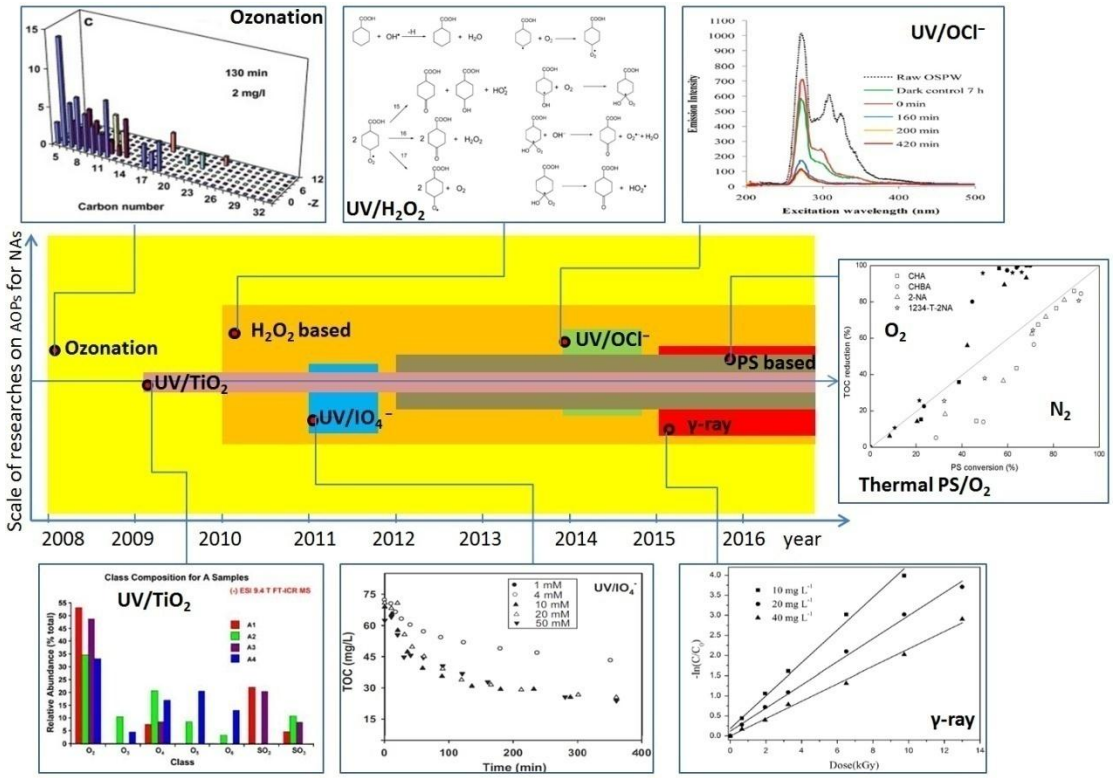

The application of advanced oxidation processes for the removal of naphthenic acids from water

La aplicación de procesos avanzados de oxidación para la eliminación de ácidos nafténicos en agua

环烷酸溶液的高级氧化处理

In the last two decades, there has been an increasing interest on the exploitation of non-conventional oil resources in the context of the growing energy demand (Gautier et al., 2009; Hughes, 2013). Oil sands (tar sands) or, more technically, bituminous sands and shales, are available non-conventional oil deposits, from which important amounts are refined nowadays (Kannel and Gan, 2012; Wang et al., 2015b). Taking the Alberta's oil sands in Canada for instance, over 1 million barrels of oil were produced daily in 2006 and it has been estimated to reach up to 3 million per day by 2020 (Schindler, 2010). In spite of the intermittent variation of oil prices due to different mixed reasons, continuous exploration of new sources is a growing activity (Baffes et al., 2015; Tokic, 2015). The fast development of non-conventional oil refining industry brings not only more available energy supply and the corresponding potential economic benefits, but also concerning environmental impacts.

Amid 2–5 volumes of water are needed per unit volume of oil in the exploitation of oil or tar sands (Schindler, 2010). Those so-called oil sand process-affected waters (OSPWs) ultimately converge into tailing ponds. The area occupied by these ponds in Alberta was around 130 km^2 in 2009 (Kean, 2009) which denotes the magnitude of the problem. OSPWs have been demonstrated to be toxic and able to cause malformation of aquatic organisms and even affect people downstream the oil sand fields (Schindler, 2010).

Naphthenic acids (NAs) have been found as series of the emblematic toxic and recalcitrant organic compounds in OSPWs. Increasing research is being addressed toward their identification (Headley et al., 2016), toxicity assessment (Clemente and Fedorak, 2005) and treatment methods (Brown and Ulrich, 2015; Headley and McMartin, 2004) for the sake of providing useful knowledge to control the environmental impact of those species. The current review presents a summary of the properties of NAs, the available techniques for their analysis and the potential

solutions for their abatement, with special emphasis on the application of advanced oxidation processes (AOPs).

1.1 Naphthenic acids

1.1.1 Chemical structure

The term naphthenic acids refers to a group of organic acids consisting in saturated alkyl-substituted acyclic and cycloaliphatic carboxylic structures, represented by a common formula of $C_nH_{2n+m}O_2$, where "n" stands for the number of carbon atoms and "m" is zero or a negative integer specifying the homologous series through hydrogen atoms deficiency with respect to saturated structures (Brown and Ulrich, 2015; Clemente and Fedorak, 2005). The diverse combination manners of the hydrocarbon rings and branches of the side chains determine the complexity of the NAs (Grewer et al., 2010b; Johnson et al., 2011; Rowland et al., 2012). However, the above expression serves only to describe the "classic" NAs but does not afford the intricacy of all the transformed or derived NAs found in the OSPWs tailing ponds. For this reason, more complicated formulas have been suggested, like $C_nH_{2n+m}O_aN_bS_c$, including more oxygen as well as the possible formation of nitrogen- and sulfate-bearing groups during the long-term retention in the tailing ponds (Pereira et al., 2013a; Quinlan and Tam, 2015). Instead of the oxygen number "a" being 2 in the "classic" NAs, oxy-NAs with more oxygen (a=3, 4 or 5) in the structure are found as the intermediates frequently identified in the matured tailings or after the aerobic microbial biodegradation of OSPW (Bataineh et al., 2006; Han et al., 2009; Han et al., 2008; Hindle et al., 2013; Islam et al., 2014; Wang et al., 2013a).

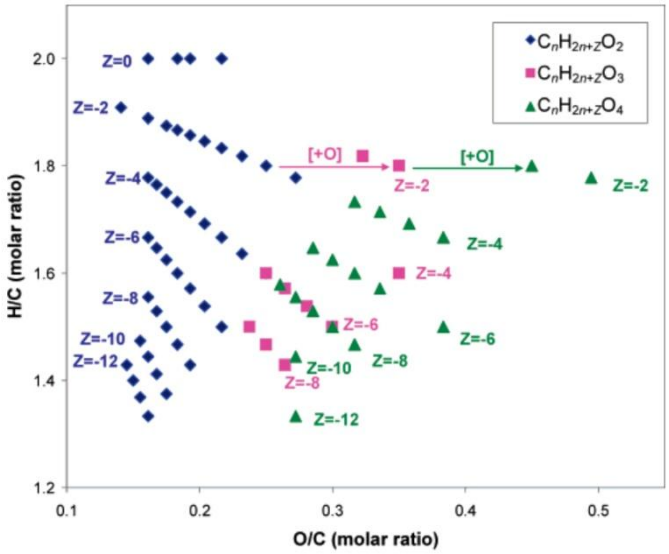

Fig. 1.1 HPLC/QTOF-MS derived Van Krevelen diagram showing parent NA species and their oxidation byproducts in Syncrude tailing wastewaters. (adopted from Bataineh et al., 2006)

Oxy-NAs were firstly reported by Bataineh et al. (2006) from the OSPWs of Syncrude Canada Ltd. postulated as possible byproducts of biodegradation (Fig. 1.1). Wang et al. (2013a) determined the NAs components from the oilfield wastewater in Hebei province and the oil sands extraction plants in Xinjiang province of China. A great diversity of NAs within a wide range of carbon atoms (from 5 to 41) were identified, including fairly considerable proportions of oxy-NAs (in terms of O_a-NAs or (OH)-NAs) with "m" ranging from -14 to 0.

The differences found in the oxy-NAs proportions among various kinds of industrial OSPWs were attributed to the particular pretreatment or storage conditions. These compounds have been claimed as biodegradation intermediates (Islam et al., 2014) during the long-term storage in the tailing ponds (Grewer et al., 2010b; Han et al., 2009). The evolution of oxy- and aromatic NAs was followed in a wastewater treatment plant in North China which included physicochemical and biological processes (Wang et al., 2015a). The changes in the relative proportion of those species provided information on the biodegradation of NAs and on the observed seasonal differences in terms of removal efficiency.

The structural characteristics of aromatic ring-bearing NAs have also been considered in relation with their similarity with some estrogens and the corresponding potential disturbance toward living organisms (Rowland et al., 2011b; Johnson et al., 2012; Jones et al., 2012; Johnson et al., 2013; Reinardy et al., 2013). Scarlett et al. (2013) tested the impact of aromatic ring-bearing NAs toward larval zebrafish and LC50 values of 5 – 8 mg L^{-1} were determined for acute toxicity. Johnson et al. (2013) investigated the ability of *Pseudomonas putida KT2440* to degrade different alkyl-branched aromatic NAs with (4'-n-butylphenyl)-4-butanoic acid (n-BPBA). Those compounds were readily degraded within several days via beta-oxidation of the alkanoic acid side chain. However, this degradation was significantly inhibited by increasing the concentration of n-BPBA. Anaerobic biodegradation of polycyclic aromatic NAs was recently studied and 40% conversion upon 260 days was reported, being identified 2-naphthoic acid as one of the main byproducts (Folwell et al., 2016).

A group of special tricyclic diamondoid NAs structures have also been detected as biodegradation byproducts in OSPWs (Wang et al., 2006; Rowland et al., 2011a; Rowland et al., 2012) (Fig. 1.2). These adamantine structures have been proved to be persistent and their adverse environmental effect has been analyzed in the literature (Jones et al., 2011; Dissanayake et al., 2016). For instance, in-vivo exposure for mussels were carried out in the presence of two diamondoid acids with varying degrees of genotoxicity displayed to hemocytes at a concentration of 30 μmol L^{-1} (Dissanayake et al., 2016).

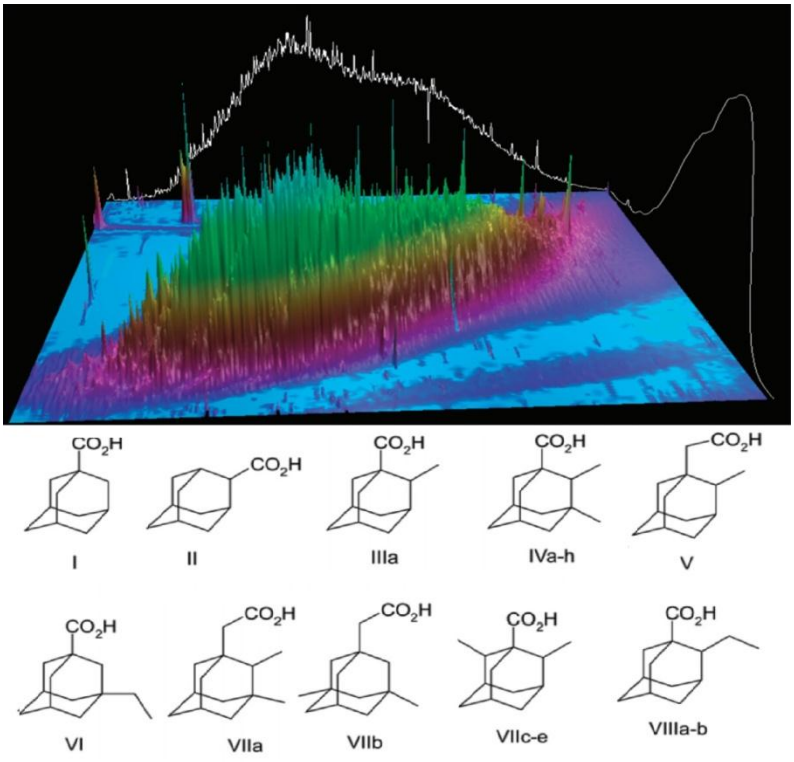

Fig. 1.2 Total ion current chromatogram of OSPW NAs (methyl esters) examined by GCxGC-ToF-MS illustrating high chromatographic resolution by GCxGC compared with GCMS. (adopted from Rowland et al., 2011a)

1.1.2 Physical properties

Oil sand containing NAs is a mixture of clay, sand, water and bitumen (Barrow et al., 2010). The appearance of NAs in aquatic solution is viscous and the color varies from light yellow to dark amber according to the components, showing high volatility with a musty hydrocarbon-like smell (Brient et al., 1995). The tailing pond of OSPWs possess weak alkaline pH, in the vicinity of 8 (Schramm et al., 2000). As kind of weak acids, NAs with dissociation constants (pKa) around 5–6 can be well dissolved in mild alkaline solutions, like OSPWs, but show poor solubility in acidic or neutral conditions (Drzewicz et al., 2012). High solubility of NAs in organic solvents has also been reported (Armstrong, 2008). The boiling point of individual NAs ranges from 250 to 300 ^{o}C, which must be considered for

analysis since some of the available identification approaches include evaporation, like in gas chromatography. In alkaline aqueous solutions, NAs always exist in the ionized form and can be associated to metal ions as the corresponding metal salts (Brient et al., 1995).

1.1.3 Toxicity

NAs have been frequently reported among the most toxic components of OSPWs (Schramm et al., 2000; Madill et al., 2001; Biryukova et al., 2007; Frank et al., 2008; Toor et al., 2013; Mahdavi et al., 2015). There are numerous studies focusing on the toxicity of NAs toward various organisms covering almost the entire biological taxonomy both aquatic and terrestrial, including microorganisms (Dokholyan and Magomedov, 1984; Leung et al., 2001; Leung et al., 2003; Hayes, 2007; West et al., 2011), plants (Wort and Patel, 1970; Kamaluddin and Zwiazek, 2002) and animals (Myhre and Fonnum, 2001; Melvin and Trudeau, 2012; Tollefsen et al., 2012).

So far, no conclusive structure-toxicity relationship has been established for NAs. However, it has been determined that, in general, NAs with more carbon atoms and cyclic structures are more harmful, while branched chains imply less toxicity (Kannel and Gan, 2012). Previous reviews summarized the toxic properties of NAs in various aspects (Clemente and Fedorak, 2005; Kannel and Gan, 2012). Recently, Marentette et al. (2015) comprehensively examined the toxicity of extracted NAs fraction components (NAFCs) from fresh and aged OSPW as well as commercial ones toward the fathead minnow embryonic survival, growth and deformities. Both NAFC and commercial NA mixtures reduced hatch success, with NAFCs from OSPW showing less toxicity (EC_{50} = 5–12 mg L^{-1}) than the commercial NAs (≈2 mg L^{-1}) tested.

1.2 Analysis of NAs

The structural features of NAs demand the development of high resolution (semi-)quantitative analytical methods beyond the classical well-stablished techniques. Clemente and Fedorak (2005) reported an standard method for the determination of NAs, based on Fourier transform infrared spectroscopy (FTIR) after acidification, dichloromethane extraction and concentration of the sample. Other analytical procedures of higher resolution have been developed more recently, but a universally accepted analytical approach is not available so far (Brown and Ulrich, 2015). Different mass spectrometry (MS)-based techniques have been used, like time-of-flight MS (ToF-MS) (Hao et al., 2005; Bataineh et al., 2006; Rowland et al., 2011a; Rowland et al., 2012; Hindle et al., 2013; Wang et al., 2013a; Brunswick et al., 2016), Linear trap quadropole MS (LTQ-Orbitrap-MS) (Pereira et al., 2013a; Pereira et al., 2013b) or Fourier transform ion cyclotron resonance MS (FT-ICR-MS) (Purcell et al., 2006; Da Campo et al., 2009; Headley et al., 2013; Dias et al., 2014; Ortiz et al., 2014; Rowland et al., 2014; Barrow et al., 2015). Other techniques, like FTIR (Luna et al., 2008; Scott et al., 2008a; Grewer et al., 2010a), synchronous fluorescence spectroscopy (SFS) (Kister et al., 1996; Kavanagh et al., 2009; Martin et al., 2014; Bauer et al., 2015; Klamerth et al., 2015) or Flame ionization (FID) detection (Pollard et al., 1992; Jones et al., 2001; Vaiopoulou et al., 2015) have been also successfully applied for NAs when specific structural analysis is not required. FTIR serves to determine not only NAs but also a total signal of various detectable characteristic bonds that may not correspond to NAs (Grewer et al., 2010b). SFS has been used to analyze the OSPW from Syncrude Canada Ltd. operations in Alberta (Kavanagh et al., 2009). In general, it is necessary to consider the structural particularity of NAs when using these approaches.

FID and MS detections are always associated to gas or high-performance

liquid chromatography (GC or HPLC). A GC-FID method with a low-polarity capillary column was reported by Ré-Poppi et al. (2009) with lots of NAs being detected from Brazilian gasoline samples, yielding values of relative standard deviation lower than those of standard methods. FT-ICR-MS was used to analyze crude oil samples, providing some practical information on the size and composition of NAs, but with uncertainty about the presence of NAs with higher hydrogen deficiency. To avoid this drawback, other approaches like ToF-MS have been used (Barrow et al., 2003). A two-dimensional gas chromatography/ToF-MS (GC×GC/ToF-MS) technique was reported for the characterization of commercial mixtures and tailing extractions which provided detailed structural information on individual NAs (Hao et al., 2005). This approach has also been tested to effectively analyze diamondoid and aromatic NAs in OSPWs (Rowland et al., 2011a; Jones et al., 2012). Hindle et al. (2013) combined HPLC with ToF-MS for quantitative analysis of NAs from OSPW with particular sensitivity toward oxy-NAs. HPLC-LTQ-Orbitrap-MS was successfully used to detect about 3000 species in each OSPW sample including classical as well as S- and N-containing related compounds (Pereira et al., 2013a). Clemente and Fedorak (2005) and Brown and Ulrich (2015) summarized analytical methods for NAs determination. Table 1.1 collects the available identification approaches for non-conventional NAs including aromatic, oxy- and diamondoid ones from petroleum-sources worldwide.

Table 1.1 Identification approaches for non-conventional NAs

Categories of NAs	Source of NAs	Sample preparation	Identification Techniques	Reference
Saturated and aromatic	Distilled Brazilian petroleum supplied by PETROBRAS	Not mentioned	FTIR Spectrometer	Luna et al. (2008)
Aromatic	Syncrude Canada Ltd.'s West In-pit settling basin	Acidified by HCl and dissolved in NaOH	GC-MS; Synchronous fluorescence spectroscopy (SFS)	Kavanagh et al. (2009)
Aromatic	Individual butylphenylbutanoic acid (BPBA) isomers	Acidified by HCl; Use N,O-bis(trimethylsilyl)trifluoroacetamide to form trimethylsilyl derivatives; Extracted with ethyl acetate	GC-MS	Johnson et al. (2011)
Aromatic	OSPW	Demethylated by BF_3-MeOH; argentation solid phase extraction (SPE) by elution with hexane	Multidimensional comprehensive gas chromatography–mass spectrometry (GC × GC–MS)	Jones et al. (2012)
Aromatic	Hydrocarbon-contaminated sediments from Avonmouth, UK	Acidified by HCl; Use N,O-bis(trimethylsilyl)trifluoroacetamide to form trimethylsilyl derivatives; Extracted with ethyl acetate	GC-MS	Johnson et al. (2012)
Aromatic	Synthesized by n-BPBA and t- BPBA	Acidified by HCl; Use N,O-bis(trimethylsilyl)trifluoroacetamide to form trimethylsilyl derivatives; Extracted with ethyl acetate	GC-MS	Johnson et al. (2013)
Aromatic	Concentrated OSPW from Syncrude Canada Ltd. West In-pit settling basin in Fort McMurray, Alberta, Canada	Demethylated by BF_3-MeOH; acidified with HCl; extracted with ethyl acetate	GC × GC–MS	Reinardy et al. (2013); Rowland et al. (2011b); Scarlett et al. (2013)
Polycyclic aromatic hydrocarbons and NAs	Individual NAs; Tailings pond water in Alberta, Canada	Acidified by HCl; Use N,O-bis(trimethylsilyl)trifluoroacetamide to form trimethylsilyl derivatives; Extracted with ethyl	GC–MS	Folwell et al. (2016)

		acetate		
Oxy-NAs	Individual oxy-NAs; Syncrude Canada Ltd. from the clarified zone of the West In-pit	Liquid-liquid extraction and solid-phase extraction (SPE); dissolved in ethyl acetate	HPLC/QTOF-MS	Bataineh et al. (2006)
Classic and Oxy-NAs	Individual NAs; Mildred Lake Settling Basin OSPWs, Canada	Liquid-liquid extraction and solid-phase extraction (SPE). dissolved in ethyl acetate	FTIR; HPLC/HRMS	Han et al. (2009)
Classic and Oxy-NAs	Individual 14 NAs and 3 oxy-NAs; oil production platform in Hebei; oil sands extraction plants in Xinjiang, China; OSPWs in North China	Derivatized with dansyl chloride; a solid-phase extraction (SPE) and resolved in acetonitrile	An ACQUITY UPLC system coupled to a Xevo QTOF-MS equipped with an electrospray ionization (ESI) source. (UPLC-ESI+-QTOF-MS)	Wang et al. (2013a) Wang et al. (2015a)
Classic and Oxy-NAs	35 model NAs and 4 oxy-NAS; Acros and Merichem mixed NAs	Dissolved in isopropyl alcohol (IPA)	HPLC high resolution accurate mass time-of-flight mass spectrometry (HPLC-HRQTOF-MS)	Hindle et al. (2013)
Diamondoids	Oils and petroleum products (including gasoline, kerosene, diesel fuels, residual, bunker B, and bunker C lubricating oils) from various oil companies worldwide	Eluted in order with n-hexane (12 mL) and followed by n-hexane DCM	GC-MS and GC-FID	Wang et al. (2006)
Diamondoids	Individual and Syncrude Canada Ltd. West Endpit settling basin in Fort McMurray, Alberta, Canada	Refluxing with BF_3-methanol	Two-dimensional comprehensive gas chromatography-timeof-flight-mass spectrometry (GCxGC-ToF-MS) analyses	Rowland et al. (2011a)
Isomeric diamondoid-structure like acids	A: a currently used tailings pond in Alberta, Canada; B: storage in-pit settling basin	Demethylated by BF_3-MeOH; extracted into hexane	GCxGC/ToF-MS	Rowland et al. (2012)

1.3 Treatment of NAs-containing wastewaters

Research on the abatement of NAs from aqueous effluents has been carried out in the past half century, including biological, physical and chemical techniques. The substrates used in these studies mainly fall into three categories: surrogate NAs, commercial NAs and NAs in real industrial wastewaters (Vaiopoulou et al., 2015; Klamerth et al., 2015; Xu et al., 2016).

Scott et al. (2008a) claimed that biodegradation is the most cost-effective solution for mitigating the hazard of NAs-containing wastewaters. The study of Herman et al. (1994) concluded that NAs collected from OSPWs were more recalcitrant than the commercial ones. Hwang et al. (2013) demonstrated the important role of aerobic bacteria in the degradation of NAs. Specific bacterial groups were found able to partially degrade those methyl-substituted NAs (Smith et al., 2008). In a more recent study, Mahdavi et al. (2015) reported an algae–bacteria consortium allowing NAs degradation with significant toxicity reduction.

The biodegradation of aliphatic or alicyclic acids may occur via β-oxidation (Biryukova et al., 2007), α- and β- co-oxidation (Rontani and Bonin, 1992) and aromatization (Han et al., 2008) depending on the structural characteristics. NAs with lower molecular weight and fewer rings are more susceptible to biodegradation (Clemente and Fedorak, 2005) whereas those with higher branching were found much more recalcitrant (Han et al., 2008). Besides, the number of carbon atoms also affects to the resistance of NAs to biodegradation. It has been reported that those with even numbers commonly give rise to cyclohexyl acetic acid formation, which possibly hinders the β- oxidation reactions in the biodegradation pathway (Kannel and Gan, 2012).

The high bio-recalcitrance of the NAs from real OSPWs is due to their higher molecular weight and cyclicity. Marsh (2006) reported that the indigenous microorganisms found in the OSPWs of the tailing ponds were not able to degrade a significant percentage of NAs even upon long time periods. Long-term evolution of OSPWs in the tailing ponds suggests that considerable amounts of NAs can remain for over 10 years (Kannel and Gan, 2012). Therefore, effective solutions are needed, based on chemical or physic-chemical approaches.

Adsorption has been reported for the removal of NAs. Several adsorbents, like organic-rich soil (Janfada et al., 2006), petroleum coke (El-Din et al., 2011; Alam et al., 2016) cyclodextrin-based polymers (Mohamed et al., 2011) and activated carbon (Iranmanesh et al., 2014) have been tested for that purpose. Mohamed et al. (2011) demonstrated that granular activated carbon yield better performance for NAs removal than organic polymeric adsorbents. Petroleum coke showed to efficiently remove NAs allowing significant detoxification (El-Din et al., 2011). However, health and operational maintenance concerns are associated to petroleum-coke, since vanadium and/or other heavy metals can be leached (Jia et al., 2002). Anyway, the main drawback of adsorption derives from its non-destructive character, which determines the need of further treatment and/or disposal of the exhausted adsorbent.

1.3.1 Application of AOPs for NAs abatement

Advanced oxidation processes (AOPs) have been widely studied in the literature for the removal of water pollutants mainly focused on recalcitrant harmful species. The traditional AOP concept refers to a series of techniques based on the oxidizing capacity of $HO^{\bullet}$ radicals under ambient-like conditions. However, this concept is currently accepted in a broader sense since it is well known the contribution of other radical species and temperature and pressure beyond the

ambient have been used in many cases. There is a diversity of recognized AOPs, depending on the reagents or activation approaches used. Among the former, ozone, hydrogen peroxide and persulfate (PS) are the most common (Andreozzi et al., 1999; Yang et al., 2014).

The oxidation of NAs proceeds through a complex network of multiple series-parallel reactions involving radical species derived from the oxidizing reagents as well as from the organic substrate and the intermediates in the reaction pathway. Under appropriate operating conditions, the end products consist of CO_2 and H_2O (mineralization) but also low molecular-weight carboxylic acids can remain in different extent depending on the specific character and strength of the oxidation process. The kinetics of such complex systems has been commonly described by useful approaches like simple pseudo-first or second order models rather than rigorous ones involving the time-course of radical species whose validation is hindered by analytical limitations (Beltran, 2003).

Fig. 1.3 depicts the time-course and the relative presence in the literature of different AOPs for NAs. In the following, those contributions are reviewed. Table 1.2 contains a list of the most recent works on AOPs application to NAs abatement.

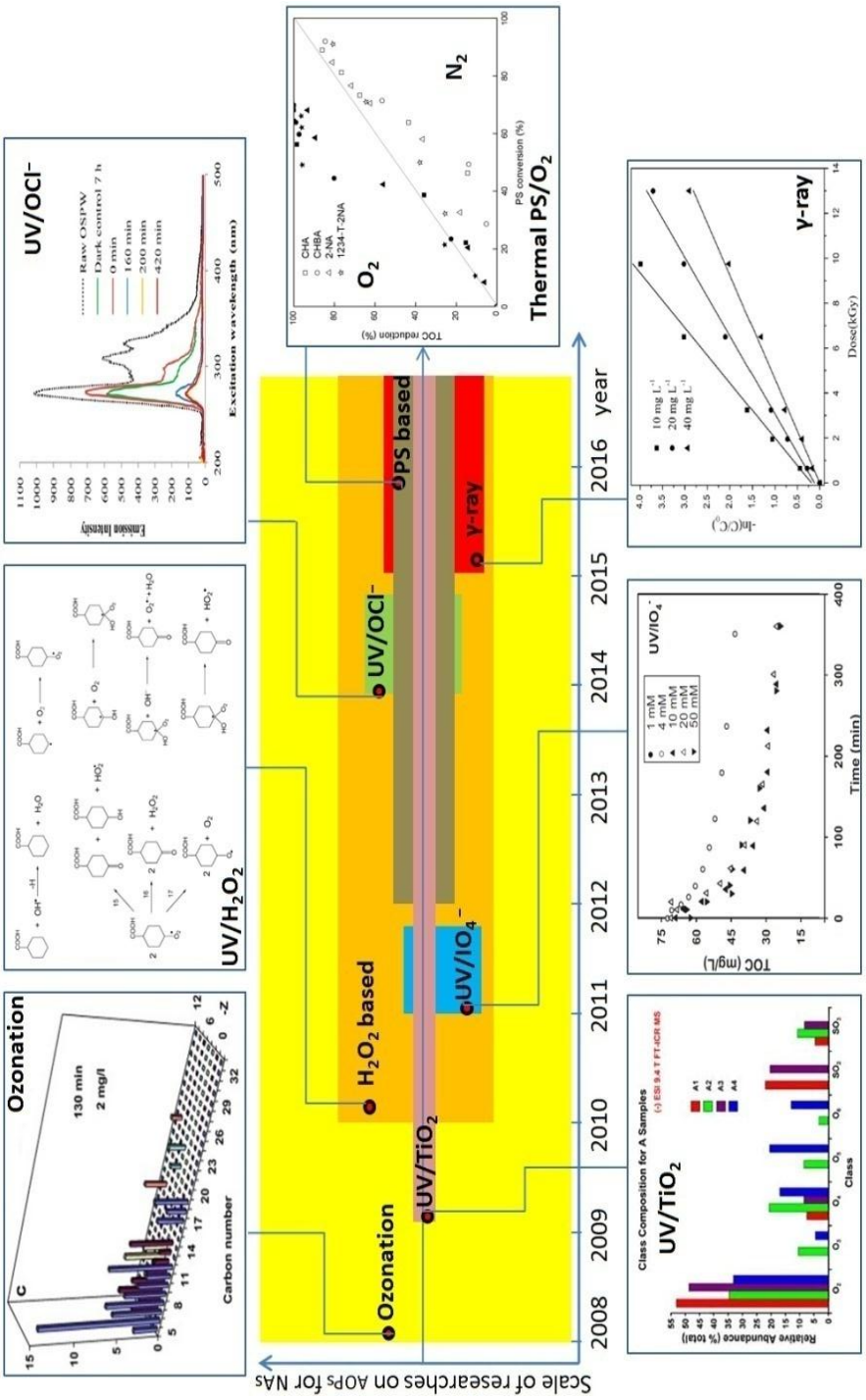

Fig. 1.3 The brief time-course of the development of AOPs for NAs treatment categorized by oxidizing sources. The area of each block stands for the period and the relative number of publications ascribed to each AOP group with the figures of iconic works. (adopted from Drzewicz et al. (2010), Headley et al. (2010), Jia et al. (2015), Liang et al. (2011), Scott et al. (2008b), Shu et al. (2014) and Xu et al. (2016), respectively.)

Table 1.2 Summary of AOPs for NAs treatment

AOPs	NAs source	Reaction conditions	Main results	Other conclusions	references
Ozone-based AOPs (from 2015)					
Ozonation; O_3/H_2O_2	Cyclohexa-noic acid (CHA) and OSPW from Syncrude Canada Ltd.	pH = 9, in the presence and absence of scavengers	NA removal = 97.7% by O_3 and 99% by O_3/H_2O_2	$HO^{\bullet}$ radicals are responsible and direct ozonaton is quite significant	Afzal et al. (2015)
Ozonation; ozonation-biodegradation combination	Commercial mixture and individual NAs	[NA] = 25−35 mg L^{-1}; $[O_3]$ = 9.3 mg L^{-1}; T = 23 ^oC	NA removal = 89% by ozonation-biodegradation combined system	Ozone reacted preferentially with NAs of higher cyclicity and molecular weight, toxicity decreased by 6.7-fold	Vaiopoulou et al. (2015)
Ozonation	four fractions of OSPW	[NA] = 50 mg L^{-1}; $[O_3]$ = 37−41 mg L^{-1}; pH = 8	NA removal = 55% to 98% with different NA categories	Organic extracts at different pH differentiate NAs; Residual toxicity attributed to degradation products	Klamerth et al. (2015)
Ozonation	model NAs	T = 5, 15 and 25 ^oC	k = 0.67, 2.71 and 8.85 M^{-1} s^{-1} at 5, 15 and 25 ^oC, respectively	E_a = 88.85 kJ mol^{-1}	Al-jibouri et al. (2015)
Ozonation combined with integrated fixed-film activated sludge (IFAS)	OSPW	$[O_3]$ = 30mg L^{-1}; 11 months of retention time	Acid extractable fraction (AEF) removal = 42%	NA biodegradation decreased as the NA cyclization number increased	Huang (2016)
Ozonation	OSPW	$[O_3]$ = 2.0 mM	Complete removal	Efficient reduction of the acute toxicity towards *Vibrio fischeri* was observed by ozonation	Wang et al. (2016)
Ozonation followed by modified Luzack-Ettinger membrane bioreactor (MLE-MBR)	OSPW	$[O_3]$ = 30 mg L^{-1}; Retention time = 426 days	Classical NAs removal = 70%	No severe membrane fouling was observed as the transmembrane pressure controlled below 12 kPa	Zhang et al. (2016d)

Ozone pretreated noxic-aerobic membrane bioreactor	OSPW	$[O_3]$ = 30mg L^{-1}; Retention time = 742 days	Ozonation pretreatment enhanced the OSPW NA degradation and the system's fouling control	Ozonation reshaped the microbial community structure of the MBR by changing relative abundances of the dominating species	Xue et al. (2016)
Fenton-based AOPs					
NTA-modified Fenton	CHA	[CHA] = 0.39 mM; $[H_2O_2]$ = 0.29−5.88 Mm; $[Fe^{III}NTA]$ = 0.27−0.89 mM; [NTA:Fe] = 1:1; pH = 8	CHA removal reached 90%	$HO^{\bullet}$ radicals played the main role with minor role of $O_2^{\bullet-}$ found for CHA degradation	Zhang et al. (2016b)
EDDS-modified Fenton	CHA	[CHA] = 0.39 mM; $[H_2O_2]$ = 0.74 mM; $[Fe^{II}]$ = 0.11 mM; [EDDS:Fe] = 2:1; pH=7−9	84% CHA removal	$E_{1/2}$ = 186 mV, −39 mV, and −89 mV at pH = 7, 8 and 9; The EDDS and $HO^{\bullet}$ reaction rate constant k = 2.48 ± 0.43 × 109 M^{-1} s^{-1} at pH 8	Zhang et al. (2016c)
Chelate-UV/Fenton	OSPW	UV lamp (200 nm to 530 nm); $[H_2O_2]$ = 5.88 Mm; [Fe] = 0.8 − 3 mg L^{-1}; [NTA] = [EDDS] = 0.72 mM	At optimal conditions: NA removal = 66.8% for UV-NTA-Fenton and 50.0% for UV-EDDS-Fenton)	No significant toxicity change of the NTA containing systems; EDDS increased the acute toxicity of the solution	Zhang et al. (2016a)
PS-based AOPs					
UV/PS	CHA	[CHA] = 100 mg L^{-1}; [PS] = 1−20 mM; pH=8−10	Half-life: 18.3 to over 360 min	Not mentioned	Liang et al. (2011)
Thermally-activated PS; ZVI/PS	CHA and OSPW	[CHA] = 50 mg L^{-1}; [NAs] = 30 mg L^{-1}; [PS] = 0−2000 mg L^{-1}; [ZVI] = 20g L^{-1}; T = 40, 60, 80 °C; pH = 9	100% CHA removal with 2000mg L^{-1} PS at 80 °C; over 90% OSPW NA removal with 100 mg L^{-1} PS and ZVI	Chloride show little effect on NA removal, but chloro-CHA was formed	Drzewicz et al. (2012)
Thermally-activated PS with O_2	Model NAs: CHA, Cyclohexa-nebutyric acid (CHBA), 1234-T-	[NAs] = 50 mg L^{-1}; [PS] = 10−100% stoichiometric; T = 40−97 °C, pH = 8	100% CHA removal achieved with 40% stoichiometric PS at 80 °C	Oxygen were demonstrated to take a role in NA mineralization	Xu et al. (2016)

	2NA, 2-NA				
Other AOPs					
Vacuum UV/H_2O_2; UV/H_2O_2	CHA	[CHA] = 20 mg L^{-1}; Vacuum UV lamp (172 nm); UV lamp (254 nm)	4-oxo-CHA, and hydroxy-CHA are the main intermediates; oxyl radical may be formed during the process	Scission of the cyclohexane ring was also observed from the acyclic byproducts including heptadioic acid and other short-chain carboxylic acids	Drzewicz et al. (2010)
UV/H_2O_2	CHA	[CHA] = 100 mg L^{-1}; [H_2O_2] = 1−50 mM pH = 8−12	Half-life: 17.2 to over 360 min; TOC drop from 64 to 3.4 mg L^{-1}	-	Liang et al. (2011)
UV/H_2O_2	CHA	[CHA] = 10−50 mg L^{-1} ; UV lamp (254 nm); irradiance = 0.11 mW cm^2	Highest reaction rate k = 2.5 × 10^{-2} min^{-1} at [H_2O_2] = 80 mg L^{-1}	pH had no significant effect on the CHA degradation; Chloride and carbonate ions decreased the treatment efficiency	Afzal et al. (2012a)
UV/H_2O_2	Model NAs and OSPW NAs	[NA] = 10−50 mg L^{-1}; UV lamp (254 nm); irradiance = 0.11 mW cm^2	Large, branched and cyclic NAs may be better oxidized in the UV/H_2O_2 process than small, linear and acyclic ones	No structure–reactivity was observed in the case of OSPW NAs	Afzal et al. (2012b)
UV/H_2O_2	OSPW	H_2O_2 = 2.0 mM; UV dose = 950 mJ cm^{-2} UV	Classical NAs removal = 42.4%	^{1}H NMR analyses confirmed the removal of aromatics NAs	Wang et al. (2016)
fluorescent and natural solar with TiO_2	oil sands NA mixtures; NAs mixture (FlukaNAs); model-NAs (4MACH)	[NA] = 40−100 mg L^{-1}; [TiO_2] = 0.3 g L^{-1}	75% removal of compounds in the oil sands NA mixture; 100% removal of 4MACH	The efficacy of the photo-catalysis was structure of NA related that ones with –z < 6 were more readily degraded	Headley et al. (2009)
UV/TiO_2; Microwave+UV /TiO_2	OSPW NA; Fluka NAs	[NA] = 40−100 mg L^{-1}; [TiO_2] = 0.3 g L^{-1}; UV lamp: 245nm; Microwave: 1200 W, 2.45 GHz	Samples treated with UV and microwave radiation have a lower relative abundance of other heteroatomic classes	Species containing SO_2 were found only in non-UV-treated samples which may serve as possible indicators of process-amended OSPW	Headley et al. (2010)

UV/TiO_2	OSPW NA; Fluka NAs	[NA] = 40−100 mg L^{-1}; $[TiO_2]$ = 0.3 g L^{-1}; UV lamp: 245 nm	Commercial NAs and OSPW NA degraded rapidly, with half-life values ranging between 1.55 and 17.37 h	Complete toxicity of NAs as confirmed using Microtox tests	Sabyasachi et al. (2010)
$Solar/TiO_2$	OSPW NAs	[NA] = 54 mg L^{-1}; $[TiO_2]$ = 0.5 g L^{-1}; Solar light: 25 MJ m^2 over 14 h daylight	Acid extractable organics (AEO): 39.8→0.6 mg L^{-1}; total organic carbon: (TOC): 45.1→3.5 mg L^{-1}; chemical oxygen demand (COD): 135→54 mg L^{-1}; biological oxygen demand (BOD): 0.2→4.4 mg L^{-1}; Microtox 15 min IC20 (% v/v): 77.2→>90	Complete mineralization was achieved within 7 days; A mechanism of superoxide bond cleavage was suggested	Leshuk et al. (2016)
Solar/film-fixed TiO_2	Fluka NAs	[NA] = 63 mg L^{-1}; Thickness of silicone film < 0.2 cm, 28 × 43 cm; solution deep < 1 cm	NA removal > 90%; removal rate: 15.5 mg L^{-1} h^{-1}; half-life: 2 h	Complete toxicity was achieved	McQueen et al. (2016)
UV alone, UV/TiO_2, UV/TiO_2-Graphene	Commercial NAs mixture	[NA] = 100 mg L^{-1}; GO:P25 = 0.5, 1, 5 and 10 wt%; [catalyst] = 100 mg L^{-1}; UV lamp: 254 nm	NA removal > 90% in UV/TiO_2-Graphene; 80% with UV/TiO_2	Lower pH is better for NA treatment; macromolecular NAs were easier to be degraded than the micromolecular ones	Liu et al. (2016b)
UV/chlorine	OSPW NAs and fluorophore organic compounds	[NA] = 21.6 mg L^{-1}; $[OCl^-]$ = 200-300 mg L^{-1}; pH = 8−10; UV (303 nm) irradiance = 0.50 mW cm^{-2}	NA removal = 75 − 84%	Structure-dependent effect is observed that the NAs with higher molecular weight are easier to degrade	Shu et al. (2014)
Gamma radiation	CHBA	[CHBA] = 10−40 mg L^{-1}; absorbed doses: 0–13 kGy	CHBA removal = 99%; COD removal = 92%	The removal rate of CHBA increased with the absorbed dose and the decrease of its initial concentration	Jia et al. (2015)

Gamma radiation	OSPW and fluid fine tailings (FFT)	90% by volume was gamma irradiated mixed with 10% untreated inoculum from the pond source; Retention time: 2-52 weeks	NAs removal = 97%; FFT removal = 85%	Acute toxicity to *Vibrio fischeri* was reduced by gamma radiation of OSPW	Boudens et al. (2016)
UV/IO_4^-	CHA	[CHA] = 100 mg L^{-1}; [IO_4^-] = 4−50 mg L^{-1}; pH = 8−12	Half-life = 100 → > 300min	Not mentioned	Liang et al. (2011)

1.3.1.1 Ozonation

Ozonation is a clean and efficient approach for the breakdown of organic pollutants with ozone playing the role of the oxidant and precursor of other oxidizing radicals.

Earlier work on NAs abatement by ozonation was conducted by Scott et al. (2008b). Ozonation of NAs-containing OSPW significantly improved the biodegradability, according to El-Din et al. (2011). Highly recalcitrant alkyl-branched NAs can be readily converted into more biodegradable species (Hwang et al., 2013). It was postulated that the reactive species from O_3, including $O_3^{\bullet-}$ and $HO^{\bullet}$ radicals, attack selectively the hydrogen atoms of the tertiary carbons which exist mainly in the more complex NAs, like alkyl-branched and ring-bearing structures. Scott et al. (2008b) found that the proportion of higher molecular weight NAs in the effluent from OSPW ozonation decreased by over 95 %. In the meantime, an increase of lower ones also occurred, which has been confirmed by Pérez-Estrada et al. (2011) and Wang et al. (2013b). A recent study reports the synergistic effect of ozone coupled with H_2O_2 allowing almost complete degradation of NAs from OSPW (Afzal et al., 2015).

Based on the improved biodegradability, biological treatment following previous ozonation has been studied for OSPW treatment with fairly good results (Martin et al., 2010; Wang and Kasperski, 2010). Ozonation hardly allows complete mineralization, especially for the lower molecular weight components, thus uncertainty about the remaining toxicity is a major issue and it is necessary to assess the health risk for practical application (Langlais et al., 1993; He et al., 2012).

Islam et al. (2014) fitted the time-course of surrogate NAs, including the acid-extractable fraction (AEF), COD, NAs, oxy-NAs, and (classical + oxy)-NAs upon ozone oxidation to a first-order kinetic model, which provided fairly good prediction. That simple approach was used by Al-jibouri et al. (2015) for the ozonation of model NAs at various temperatures. The values of the rate constants ranged within 0.67 and 8.85 M^{-1} s^{-1} and ≈ 89 kJ mol^{-1} was reported for the activation energy (Al-jibouri et al., 2015). Most recently, Wu and Upreti (2017) proposed models based on mass balance to describe the evolution of commercial NAs, dissolved ozone and gaseous ozone during NAs ozonation. Although the developed models successfully predicted the concentrations of commercial NAs and gaseous ozone, the actual ozone consumption was higher than the predicted within the earlier process due to the inapplicability of the gas-liquid equilibrium condition in the initial high-rate stage of reaction.

The most recent works on NAs ozonation are included in Table 1.2. Those before 2015 can be seen in the review of Brown and Ulrich (2015).

1.3.1.2 Fenton-based technologies

The Fenton process is a well-known oxidation system using H_2O_2 as starting reagent and Fe^{2+} as catalyst, which promotes the generation of strongly oxidizing

hydroxyl radicals through the main reaction:

$$H_2O_2 + Fe^{2+} + H^+ \rightarrow Fe^{3+} + HO^{\bullet} + H_2O \quad (1)$$

Regeneration of Fe^{2+} takes place, among other, by:

$$H_2O_2 + Fe^{3+} \rightarrow Fe^{2+} + HOO^{\bullet} + H^+ \quad (2)$$

which produces hydroperoxide radicals, also powerful oxidizing species. There are other numerous reactions participating in this complex chemical system which represents so far the most stablished advanced oxidation technology, together with ozonation.

Based on this concept, a number of related approaches have been developed, which can be considered as emerging technologies. The application (real or potential) of Fenton and Fenton-like oxidation to the abatement of recalcitrant water pollutants has been widely reported in the literature (Neyens and Baeyens, 2003; Bautista et al., 2008; Munoz et al., 2015; Pliego et al., 2015).

The pH of NAs-containing OSPWs (≈ 8) hinders the application of conventional Fenton oxidation to these effluents, since this process requires a pH around 3. To overcome this drawback, iron chelates have been used for the activation of H_2O_2 to prevent iron precipitation. Cyclohexanoic acid (CHA) has been effectively removed by Zhang et al. (2016a, b and c) using Fe-nitrilotriacetic acid (NTA) and Fe-Ethylenediamine-N, N'-disuccinic acid (EDDS) chelates. They also studied the reaction mechanism and kinetics involved. A competition-kinetic model was used with p-chlorobenzoic acid (pCBA) as reference compound to study the evolution of CHA by chelate-Fenton oxidation at pH = 8 under initial H_2O_2 concentration in excess respect to the chelates, CHA, and pCBA.

A further study thoroughly investigated the effects of EDDS and NTA as

chelate agents in the treatment of OSPW by UV/Fenton. EDDS was found not only to reduce the reaction rate by scavenging the HO• radicals but also showed worse toxicity effects (Zhang et al., 2016a). Therefore, the scavenging effect of chelating agents can reduce the efficiency of H_2O_2 consumption, which is a critical issue on the economy of Fenton-based technologies. Besides, the addition of chelate agents bring about the concern on the effect on the toxicity of the resulting effluents.

Those studies followed the disappearance of the model NAs tested but results on mineralization, namely TOC reduction, were not provided. Further research on the oxidation intermediates and byproducts is still needed to gain insight into the potential application of Fenton-based treatments to the abatement of NAs.

1.3.1.3 Persulfate (PS)-based oxidation

The PS ion ($S_2O_8^{2-}$) is a well-known oxidant, whose action is based on the formation of highly oxidizing sulfate radicals ($SO_4^{\bullet-}$) (E_0 = 2.5 – 3.1) (Neta et al., 1988; Fang et al., 2012) upon energy- or metal-activated decomposition. The application of PS-based oxidation to the abatement of a diversity of priority and emerging pollutants is widely represented in the literature, with a growing presence in the last fifteen years (Anipsitakis and Dionysiou, 2003 and 2004; Furman et al., 2010; Xu et al., 2012; Yang et al., 2014; Liu et al., 2016; Peng et al., 2017). Differing from Fenton-based processes, PS oxidation can efficiently work within a wide pH range from acidic to basic with the sulfate radicals as the dominant reactive species, but with other also participating. In fact, numerous studies provide evidences that PS can react with OH^- ions or even water to produce HO• radicals:

$$SO_4^{\bullet-} + HO^- \rightarrow SO_4^{2-} + HO^{\bullet} \quad (3)$$

$$SO_4^{\bullet-} + H_2O \rightarrow SO_4^{2-} + HO^{\bullet} + H^+ \quad (4)$$

Moreover, dissolved oxygen has been demonstrated to increase the oxidizing efficiency of PS with the positive effect of $O_2^{\bullet-}$ radicals (Fang et al., 2013; Liu et al., 2016a; Xu et al., 2016).

Thermally-activated PS has been used for the abatement of model and OSPW NAs. Complete conversion of CHA was observed upon 2 h of reaction with 1.2 times the stoichiometric amount of persulfate (Drzewicz et al., 2012). Similarly, high efficiency was reported by Liang et al. (2011) with model NAs in a comparative study. Recently, Xu et al. (2016) reported the important role of dissolved oxygen in thermally-activated PS oxidation of model NAs at 80 ^{o}C. Oxygen molecules were found not only to increase the reaction rate but also allow complete mineralization of NAs under PS doses well below the corresponding stoichiometric amount, due to the contribution of superoxide and hydroperoxide radicals resulting from:

$$SO_4^{\bullet-} + R{-}H \rightarrow HSO_4^- + {}^{\bullet}R \quad (5)$$

$$^{\bullet}R + O_2 \rightarrow R^+ + O_2^{\bullet-} \quad (6)$$

$$O_2^{\bullet-} + H^+ \leftrightarrow HO_2^{\bullet} \quad (7)$$

Based on the experimental findings, the overall oxidation reactions for the model NAs tested in that work were reformulated to include the contribution of oxygen. The kinetics of mineralization was described by a pseudo-first-order rate equation and normalized values of the rate constants were provided (Fig. 1.4).

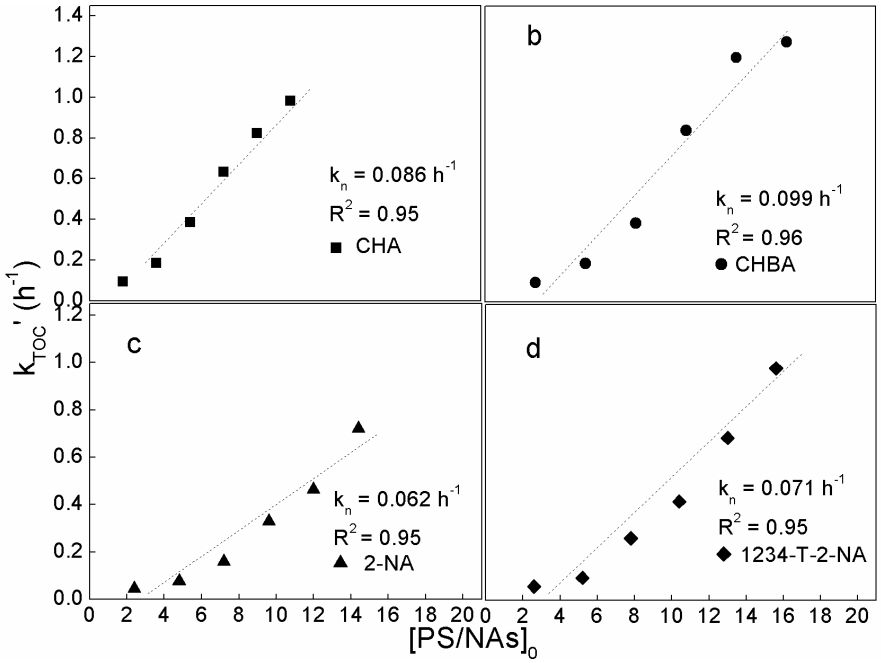

Fig 1.4. Values of the pseudo-first order rate constant of NAs mineralization at different initial PS/NAs molar ratios (adopted from Xu et al., 2016).

Compared to the HO• radical-driven processes, PS readily causes the decarboxylation of NAs giving rise to the corresponding aliphatic radicals which undergo further decomposition. Therefore, the sulfate radical becomes a more effective oxidant than HO• for aliphatic acids oxidation (Madhavan et al., 1978; Drzewicz et al., 2012). Nevertheless, the PS-based systems have some drawbacks, such as the high relative cost of the reagent and the increased conductivity of the resulting effluent due to sulfates.

1.3.1.4 NAs abatement by other AOPs

Degradation of model NAs with UV-activated H_2O_2 has been studied by Drzewicz et al. (2010) and Afzal et al. (2012 a and b). The former identified 4-oxo-CHA as the main intermediate, resulting from the attack of HO• to the para-position on the saturated ring. Ring-opening starts by β-scission of the cyclohexane ring according to the acyclic byproducts, which included heptadioic acid and various

short-chain carboxylic acids. Liang et al. (2011) compared UV-activated H_2O_2, TiO_2, IO_4^-, and $S_2O_8^{2-}$ treatments applied to CHA. The efficiency of $HO^\bullet$ for the breakdown of saturated hydrocarbon chains is lower than for unsaturated ones (Drzewicz et al., 2012). However, classical NAs do not contain olefin structures so that $HO^\bullet$ radicals provoke mainly hydrogen abstraction. This reaction is less effective than the decarboxylation caused by sulfate radicals which can yield aliphatic radicals from saturated rings allowing more in-depth degradation (Madhavan et al., 1978; Drzewicz et al., 2012). Most recently, Wang et al. (2016) compared the efficiency of UV/H_2O_2, potassium ferrate(VI), and ozone in the oxidation of the organic fraction of OSPW. The important role of molecular ozone and $HO^\bullet$ radicals was confirmed by scavenging tests and ^{1}H NMR analyses further suggested the removal of aromatic NAs. Those three oxidation systems reduced the acute toxicity towards *Vibrio fischeri* and goldfish primary kidney macrophages (PKMs), being ozonation the most efficient.

UV/TiO_2 and solar/TiO_2 treatments have been applied to degrade NAs (Headley et al., 2009; Leshuk et al., 2016). The light radiation can cause electron-hole pairs on TiO_2 which promote the formation of $O_2^{\bullet-}$ and $HO^\bullet$ radicals from water and dissolved oxygen. Headley et al. (2009) reported complete conversion of 4-methyl-cyclohexaneaceticic acid (4-MCHAA) with close to 75% TOC reduction upon 8 h under solar radiation over a TiO_2 suspension. In a further work, Sabyasachi et al. (2010) reported half-life values of OSPW NAs by UV/TiO_2 degradation ranging between 1.55 and 4.80 h. Significant toxicity reduction was achieved. Headley et al. (2010) used an UV/microwave system to activate TiO_2 for the abatement of OSPW NAs. More recently, Leshuk et al. (2016) reported on the effective solar-driven TiO_2 degradation of NAs in OSPW. Acid extractable organics in OSPW disappeared after one day of natural solar irradiation (25 MJ m^{-2} for 14 h daylight) in the presence of TiO_2. Complete mineralization was achieved within 7 days where toxicity reduction also occurred.

UV/chlorine oxidation has also been tested for the degradation of OSPW NAs (Shu et al., 2014). This process effectively removed NAs (75–84% conversion) from OSPW. Structure-dependent effects were also observed, being NAs with higher number of rings and carbon atoms more readily degradable. $HO^{\bullet}$, $O^{\bullet-}$ and $Cl^{\bullet}$ were claimed as the main oxidizing species from photo-excitation of water and chloride.

The breakdown of model NAs with gamma-ray irradiation was checked by Jia et al. (2015). Reactive species like $HO^{\bullet}$ radicals, hydrated electrons (e_{aq}^{-}) and atomic hydrogen can be formed by γ-excitation (Wang and Wang, 2007). Liang et al. (2011) attempted UV/IO_4^- oxidation of CHA. This system showed to be less efficient than H_2O_2- and PS-based approaches. The time-course of NAs upon UV/TiO_2 (Leshuk et al., 2016) and gamma-ray (Jia et al., 2015) treatments was fitted to pseudo-first-order rate equation.

The scavenging effect of certain components of real NAs-containing wastewaters, like chloride and bicarbonate, must be considered and addressed. Adverse environmental effects can even result from the formation of related toxic species, like chlorate and organo-chlorinated byproducts. This aspect has been not considered so far in the literature on Fenton-based oxidation of NAs (Zhang et al., 2016c), while several interesting works have been conducted for PS-based oxidation of NAs. Drzewicz et al. (2012) investigated the role of chloride in CHA degradation by PS upon thermal and zero-valent iron activation. Although no significant hampering effect was observed in terms of CHA removal, they reported the formation of chloro-CHA during PS oxidation in the presence of chloride anions. Xu et al. (2016) studied the effect of chloride and bicarbonate on thermally-activated PS oxidation of model NAs. The former showed negative effect whereas it was negligible or even positive in the case of bicarbonate. Apart from those inorganic components, the scavenging potential of some organic species in the

OSPW tailing ponds, such as unrecovered bitumen (oil and grease), polyaromatic hydrocarbons (PAH), BTEX (benzene, toluene, ethyl benzene, and xylenes), as well as fulvic and humic acids, should also be addressed in the future regarding the application of AOP systems (Zhang et al., 2016c).

1.4 Conclusion and outlook

The exploitation of unconventional hydrocarbon sources causes serious environmental problems, derived from the generation of large volumes of wastewater containing a series of recalcitrant species (mainly NAs) of high toxicity. Different advanced oxidation treatments have been reported in the literature as promising solutions for the abatement of those pollutants. Among them, O_3-, H_2O_2- and PS-based techniques appear as the most likely for potential application in the next future. PS-based systems with thermal-activation have proved a high efficiency in terms of mineralization. The contribution of dissolved oxygen has shown to reduce the amount of reagent needed. Compared with O_3 and H_2O_2, however, PS introduces sulfur-containing ionic species into the final effluent. Future development of cost-effective solutions based on AOPs is a main challenge, given the growing environmental concern associated to OSPW and other related NAs-containing effluents. In that sense, advanced oxidation technologies can be used alone or combined. The tandem based on PS followed by further Fenton oxidation has proved to be highly efficient for NAs mineralization, reducing the cost derived from reagents consumption. Also, AOP-based treatments can be used as previous step addressed to improve the biodegradability, thus allowing an effective application of further biological treatment.

An important issue refers to the implementation of more sensitive analytical techniques for NAs and their related oxidation species. That would allow a more in-depth understanding of the reaction mechanisms involved, which is a crucial

issue regarding the selection and design of potential solutions for the effective treatment of aqueous waste streams containing this kind of pollutants.

References

Afzal, A., Chelme-Ayala, P., Drzewicz, P., Martin, J.W. and Gamal El-Din, M. (2015) Effects of ozone and ozone/hydrogen peroxide on the degradation of model and real oil-sands-process-affected-water naphthenic acids. Ozone: Science & Engineering 37(1), 45-54.

Afzal, A., Drzewicz, P., Martin, J.W. and Gamal El-Din, M. (2012a) Decomposition of cyclohexanoic acid by the UV/H_2O_2 process under various conditions. Sci. Total. Environ. 426, 387-392.

Afzal, A., Drzewicz, P., Pérez-Estrada, L.n.A., Chen, Y., Martin, J.W. and Gamal El-Din, M. (2012b) Effect of molecular structure on the relative reactivity of naphthenic acids in the UV/H_2O_2 advanced oxidation process. Environ. Sci. Technol. 46(19), 10727-10734.

Al-jibouri, A.K.H., Wu, J. and Upreti, S.R. (2015) Ozonation of Naphthenic Acids in Water: Kinetic Study. Water, Air, & Soil Pollution 226(10), 1-11.

Alam MS, Cossio M, Robinson L, Wang X, Kenney JP, Konhauser KO, et al. Removal of organic acids from water using biochar and petroleum coke. Environ. Technol. Innov. 2016; 6: 141-151.

Andreozzi, R., Caprio, V., Insola, A. and Marotta, R. (1999) Advanced oxidation processes (AOP) for water purification and recovery. Catal. Today 53(1), 51-59.

Anipsitakis, G.P. and Dionysiou, D.D. (2003) Degradation of organic contaminants in water with sulfate radicals generated by the conjunction of peroxymonosulfate with cobalt. Environ. Sci. Technol. 37(20), 4790-4797.

Anipsitakis, G.P. and Dionysiou, D.D. (2004) Radical generation by the interaction of transition metals with common oxidants. Environ. Sci. Technol. 38(13), 3705-3712.

Armstrong, S.A. (2008) Dissipation and phytotoxicity of oil sands naphthenic acids in wetland plants. (Doctoral dissertation)

Baffes, J., Kose, M.A., Ohnsorge, F. and Stocker, M. (2015) The great plunge in oil prices: Causes, consequences, and policy responses. Consequences, and Policy Responses (June 2015).

Barrow, M.P., McDonnell, L.A., Feng, X., Walker, J. and Derrick, P.J. (2003) Determination of the nature of naphthenic acids present in crude oils using nanospray Fourier transform ion cyclotron resonance mass spectrometry: The continued battle against corrosion. Anal. Chem. 75(4), 860-866.

Barrow, M.P., Peru, K.M., Fahlman, B., Hewitt, L.M., Frank, R.A. and Headley, J.V. (2015) Beyond naphthenic acids: Environmental screening of water from natural sources and the Athabasca oil sands industry using atmospheric pressure photoionization Fourier transform ion cyclotron resonance mass spectrometry. J. Am. Soc. Mass Spectr. 26(9), 1508-1521.

Barrow, M.P., Witt, M., Headley, J.V. and Peru, K.M. (2010) Athabasca oil sands process water: Characterization by atmospheric pressure photoionization and electrospray ionization Fourier transform ion cyclotron resonance mass spectrometry. Anal. Chem. 82(9), 3727-3735.

Bataineh, M., Scott, A., Fedorak, P. and Martin, J. (2006) Capillary HPLC/QTOF-MS for characterizing complex naphthenic acid mixtures and their microbial transformation. Anal. Chem. 78(24), 8354-8361.

Bauer, A.E., Frank, R.A., Headley, J.V., Peru, K.M., Hewitt, L.M. and Dixon, D.G. (2015) Enhanced characterization of oil sands acid-extractable organics fractions using electrospray ionization–high-resolution mass spectrometry and synchronous fluorescence spectroscopy. Environ. Toxicol. Chem. 34(5), 1001-1008.

Bautista, P., Mohedano, A., Casas, J., Zazo, J. and Rodriguez, J. (2008) An overview of the application of Fenton oxidation to industrial wastewaters treatment. J. Chem. Technol. Biot. 83(10), 1323-1338.

Beltran, F.J. (2003) Ozone reaction kinetics for water and wastewater systems, CRC Press.

Biryukova, O.V., Fedorak, P.M. and Quideau, S.A. (2007) Biodegradation of naphthenic acids by rhizosphere microorganisms. Chemosphere 67(10), 2058-2064.

Boudens, R., Reid, T., VanMensel, D., MR, S.P., Ciborowski, J.J. and Weisener, C.G. (2016) Bio-physicochemical effects of gamma irradiation treatment for naphthenic acids in oil sands fluid fine tailings. Sci. Total. Environ. 539, 114-124.

Brient, J.A., Wessner, P.J. and Doyle, M.N. (1995) Naphthenic acids. Kirk-Othmer encyclopedia of chemical technology.

Brown, L.D. and Ulrich, A.C. (2015) Oil sands naphthenic acids: A review of properties, measurement, and treatment. Chemosphere 127, 276-290.

Brunswick, P., Hewitt, L.M., Frank, R.A., van Aggelen, G., Kim, M. and Shang, D. (2016) Specificity of high resolution analysis of naphthenic acids in aqueous environmental matrices. Anal. Methods, 8(37), 6764-6773.

Clemente, J.S. and Fedorak, P.M. (2005) A review of the occurrence, analyses, toxicity, and biodegradation of naphthenic acids. Chemosphere 60(5), 585-600.

Da Campo, R., Barrow, M.P., Shepherd, A.G., Salisbury, M. and Derrick, P.J. (2009) Characterization of naphthenic acid singly charged noncovalent dimers and their dependence on the accumulation time within a hexapole in Fourier transform ion cyclotron resonance mass spectrometry. Energ. Fuel 23(11), 5544-5549.

Dias, H.P., Pereira, T.M., Vanini, G., Dixini, P.V., Celante, V.G., Castro, E.V., Vaz, B.G., Fleming, F.P., Gomes, A.O. and Aquije, G.M. (2014) Monitoring the degradation and the corrosion of naphthenic acids by electrospray ionization Fourier transform ion cyclotron resonance mass spectrometry and atomic force microscopy. Fuel 126, 85-95.

Dissanayake, A., Scarlett, A.G. and Jha, A.N. (2016) Diamondoid naphthenic acids cause in vivo genetic damage in gills and haemocytes of marine mussels. Environ. Sci. Pollut. R., 23(7), 7060-7066.

Dokholyan, B. and Magomedov, A. (1984) The effect of sodium naphthenate on the viability and physiological and biochemical indices of fish. Voprosy Ikhtiologii 23(6), 1013-1019.

Drzewicz, P., Afzal, A., El-Din, M.G. and Martin, J.W. (2010) Degradation of a model naphthenic acid, cyclohexanoic acid, by vacuum UV (172 nm) and UV (254 nm)/H_2O_2. J Phys Chem A 114(45), 12067-12074.

Drzewicz, P., Perez-Estrada, L., Alpatova, A., Martin, J.W. and Gamal El-Din, M. (2012) Impact of peroxydisulfate in the presence of zero valent iron on the oxidation of cyclohexanoic acid and naphthenic acids from oil sands process-affected water. Environ. Sci. Technol. 46(16), 8984-8991.

El-Din, M.G., Fu, H., Wang, N., Chelme-Ayala, P., Pérez-Estrada, L., Drzewicz, P., Martin, J.W., Zubot, W. and Smith, D.W. (2011) Naphthenic acids speciation and removal during petroleum-coke adsorption and ozonation of oil sands process-affected water. Sci. Total. Environ. 409(23), 5119-5125.

Fang, G.-D., Dionysiou, D.D., Al-Abed, S.R. and Zhou, D.-M. (2013) Superoxide radical driving the activation of persulfate by magnetite nanoparticles: Implications for the degradation of PCBs. Appl. Catal. B-Environ. 129, 325-332.

Fang, G.-D., Dionysiou, D.D., Wang, Y., Al-Abed, S.R. and Zhou, D.-M. (2012) Sulfate radical-based degradation of polychlorinated biphenyls: effects of chloride ion and reaction kinetics. J. Hazard. Mater. 227, 394-401.

Folwell, B.D., McGenity, T.J., Price, A., Johnson, R.J. and Whitby, C. (2016) Exploring the capacity for anaerobic biodegradation of polycyclic aromatic hydrocarbons and naphthenic acids by microbes from oil-sands-process-affected waters. Int. Biodeter. Biodegr. 108, 214-221.

Frank, R.A., Fischer, K., Kavanagh, R., Burnison, B.K., Arsenault, G., Headley, J.V., Peru, K.M., Kraak, G.V.D. and Solomon, K.R. (2008) Effect of carboxylic acid content on the acute toxicity of oil sands naphthenic acids. Environ. Sci. Technol. 43(2), 266-271.

Furman, O.S., Teel, A.L. and Watts, R.J. (2010) Mechanism of base activation of persulfate. Environ. Sci. Technol. 44(16), 6423-6428.

Gautier, D.L., Bird, K.J., Charpentier, R.R., Grantz, A., Houseknecht, D.W., Klett, T.R., Moore, T.E., Pitman, J.K., Schenk, C.J. and Schuenemeyer, J.H. (2009) Assessment of undiscovered oil and gas in the Arctic. Science 324(5931), 1175-1179.

Grewer, D.M., Young, R.F., Whittal, R.M. and Fedorak, P.M. (2010a) Naphthenic acids and other acid-extractables in water samples from Alberta: what is being measured? Sci. Total. Environ. 408(23), 5997-6010.

Grewer, D.M., Young, R.F., Whittal, R.M. and Fedorak, P.M. (2010b) Naphthenic acids and other

acid-extractables in water samples from Alberta: what is being measured? Sci. Total. Environ. 408(23), 5997-6010.

Han, X., MacKinnon, M.D. and Martin, J.W. (2009) Estimating the in situ biodegradation of naphthenic acids in oil sands process waters by HPLC/HRMS. Chemosphere 76(1), 63-70.

Han, X., Scott, A.C., Fedorak, P.M., Bataineh, M. and Martin, J.W. (2008) Influence of molecular structure on the biodegradability of naphthenic acids. Environ. Sci. Technol. 42(4), 1290-1295.

Hao, C., Headley, J.V., Peru, K.M., Frank, R., Yang, P. and Solomon, K.R. (2005) Characterization and pattern recognition of oil–sand naphthenic acids using comprehensive two-dimensional gas chromatography/time-of-flight mass spectrometry. J. Chromatogr. A 1067(1), 277-284.

Hayes, T.M.E. (2007) Examining the ecological effects of naphthenic acids and major ions on phytoplankton in the Athabasca oil sands region, Library and Archives Canada= Bibliothèque et Archives Canada.

He, Y., Patterson, S., Wang, N., Hecker, M., Martin, J.W., El-Din, M.G., Giesy, J.P. and Wiseman, S.B. (2012) Toxicity of untreated and ozone-treated oil sands process-affected water (OSPW) to early life stages of the fathead minnow (Pimephales promelas). Water Res. 46(19), 6359-6368.

Headley, J.V., Du, J.-L., Peru, K.M. and McMartin, D.W. (2009) Electrospray ionization mass spectrometry of the photodegradation of naphthenic acids mixtures irradiated with titanium dioxide. J. Environ. Sci. Heal. A 44(6), 591-597.

Headley, J.V. and McMartin, D.W. (2004) A Review of the Occurrence and Fate of Naphthenic Acids in Aquatic Environments. J. Environ. Sci. Heal. A 39(8), 1989-2010.

Headley, J.V., Peru, K.M. and Barrow, M.P. (2016) Advances in mass spectrometric characterization of naphthenic acids fraction compounds in oil sands environmental samples and crude oil—a review. Mass spectrometry reviews 35(2), 311-328.

Headley, J.V., Peru, K.M., Mishra, S., Meda, V., Dalai, A.K., McMartin, D.W., Mapolelo, M.M., Rodgers, R.P. and Marshall, A.G. (2010) Characterization of oil sands naphthenic acids treated with ultraviolet and microwave radiation by negative ion electrospray Fourier transform ion cyclotron resonance mass spectrometry. Rapid Commun. Mass S. 24(21), 3121-3126.

Headley, J.V., Peru, K.M., Mohamed, M.H., Wilson, L., McMartin, D.W., Mapolelo, M.M., Lobodin, V.V., Rodgers, R.P. and Marshall, A.G. (2013) Atmospheric pressure photoionization Fourier transform ion cyclotron resonance mass spectrometry characterization of tunable carbohydrate-based materials for sorption of oil sands naphthenic acids. Energ. Fuel 28(3), 1611-1616.

Herman, D.C., Fedorak, P.M., MacKinnon, M.D. and Costerton, J. (1994) Biodegradation of

naphthenic acids by microbial populations indigenous to oil sands tailings. Can. J. Microbiol. 40(6), 467-477.

Hindle, R., Noestheden, M., Peru, K. and Headley, J. (2013) Quantitative analysis of naphthenic acids in water by liquid chromatography-accurate mass time-of-flight mass spectrometry. J. Chromatogr. A 1286, 166-174.

Huang, C. (2016) Treatment of Oil Sands Process-affected Water (OSPW) Using Integrated Fixed-film Activated Sludge (IFAS) Reactors, University of Alberta.

Hughes, J.D. (2013) Energy: A reality check on the shale revolution. Nature 494(7437), 307-308.

Hwang, G., Dong, T., Islam, M.S., Sheng, Z., Pérez-Estrada, L.A., Liu, Y. and El-Din, M.G. (2013) The impacts of ozonation on oil sands process-affected water biodegradability and biofilm formation characteristics in bioreactors. Bioresource technology 130, 269-277.

Iranmanesh, S., Harding, T., Abedi, J., Seyedeyn-Azad, F. and Layzell, D.B. (2014) Adsorption of naphthenic acids on high surface area activated carbons. J. Environ. Sci. Heal. A 49(8), 913-922.

Islam, M.S., Moreira, J., Chelme-Ayala, P. and Gamal El-Din, M. (2014) Prediction of naphthenic acid species degradation by kinetic and surrogate models during the ozonation of oil sands process-affected water. Sci. Total. Environ. 493, 282-290.

Janfada, A., Headley, J.V., Peru, K.M. and Barbour, S. (2006) A laboratory evaluation of the sorption of oil sands naphthenic acids on organic rich soils. J. Environ. Sci. Heal. A 41(6), 985-997.

Jia, L., Anthony, E. and Charland, J. (2002) Investigation of vanadium compounds in ashes from a CFBC firing 100 petroleum coke. Energ. Fuel 16(2), 397-403.

Jia, W., He, Y., Ling, Y., Hei, D., Shan, Q., Zhang, Y. and Li, J. (2015) Radiation-induced degradation of cyclohexanebutyric acid in aqueous solutions by gamma ray irradiation. Radiat. Phys. Chem. 109, 17-22.

Johnson, R.J., Smith, B.E., Rowland, S.J. and Whitby, C. (2013) Biodegradation of alkyl branched aromatic alkanoic naphthenic acids by Pseudomonas putida KT2440. Int Biodeter Biodegr 81, 3-8.

Johnson, R.J., Smith, B.E., Sutton, P.A., McGenity, T.J., Rowland, S.J. and Whitby, C. (2011) Microbial biodegradation of aromatic alkanoic naphthenic acids is affected by the degree of alkyl side chain branching. ISME J 5(3), 486-496.

Johnson, R.J., West, C.E., Swaih, A.M., Folwell, B.D., Smith, B.E., Rowland, S.J. and Whitby, C. (2012) Aerobic biotransformation of alkyl branched aromatic alkanoic naphthenic acids via two different pathways by a new isolate of Mycobacterium. Environmental microbiology 14(4), 872-882.

Jones, D., Scarlett, A.G., West, C.E. and Rowland, S.J. (2011) Toxicity of individual naphthenic acids to Vibrio fischeri. Environ. Sci. Technol. 45(22), 9776-9782.

Jones, D., Watson, J., Meredith, W., Chen, M. and Bennett, B. (2001) Determination of naphthenic acids in crude oils using nonaqueous ion exchange solid-phase extraction. Anal. Chem. 73(3), 703-707.

Jones, D., West, C.E., Scarlett, A.G., Frank, R.A. and Rowland, S.J. (2012) Isolation and estimation of the 'aromatic' naphthenic acid content of an oil sands process-affected water extract. J. Chromatogr. A 1247, 171-175.

Kamaluddin, M. and Zwiazek, J.J. (2002) Naphthenic acids inhibit root water transport, gas exchange and leaf growth in aspen (Populus tremuloides) seedlings. Tree physiology 22(17), 1265-1270.

Kannel, P.R. and Gan, T.Y. (2012) Naphthenic acids degradation and toxicity mitigation in tailings wastewater systems and aquatic environments: a review. J. Environ. Sci. Health. A 47(1), 1-21.

Kavanagh, R.J., Burnison, B.K., Frank, R.A., Solomon, K.R. and Van Der Kraak, G. (2009) Detecting oil sands process-affected waters in the Alberta oil sands region using synchronous fluorescence spectroscopy. Chemosphere 76(1), 120-126.

Kean, S. (2009) Eco-alchemy in Alberta. Science 326(5956), 1052-1055.

Kister, J., Pieri, N., Alvarez, R., Diez, M. and Pis, J. (1996) Effects of preheating and oxidation on two bituminous coals assessed by synchronous UV fluorescence and FTIR spectroscopy. Energ. Fuel 10(4), 948-957.

Klamerth, N., Moreira, J., Li, C., Singh, A., McPhedran, K.N., Chelme-Ayala, P., Belosevic, M. and El-Din, M.G. (2015) Effect of ozonation on the naphthenic acids' speciation and toxicity of pH-dependent organic extracts of oil sands process-affected water. Sci. Total. Environ. 506, 66-75.

Langlais, B., Legube, B., Beuffe, H. and Dore, M. (1993) Study of the nature of the by-products formed and the risks of toxicity when disinfecting a secondary effluent with ozone. Water. Sci. Technol. 27, 135-135.

Leshuk, T., Wong, T., Linley, S., Peru, K.M., Headley, J.V. and Gu, F. (2016) Solar photocatalytic degradation of naphthenic acids in oil sands process-affected water. Chemosphere 144, 1854-1861.

Leung, S.S., MacKinnon, M.D. and Smith, R.E. (2003) The ecological effects of naphthenic acids and salts on phytoplankton from the Athabasca oil sands region. Aquatic Toxicology 62(1), 11-26.

Leung, S.S.C., MacKinnon, M.D. and Smith, R.E. (2001) Aquatic reclamation in the Athabasca, Canada, oil sands: naphthenate and salt effects on phytoplankton communities. Environ. Toxicol. Chem. 20(7), 1532-1543.

Liang, X., Zhu, X. and Butler, E.C. (2011) Comparison of four advanced oxidation processes for the removal of naphthenic acids from model oil sands process water. J. Hazard. Mater. 190(1-3), 168-176.

Liu, H., Bruton, T.A., Li, W., Buren, J.V., Prasse, C., Doyle, F.M. and Sedlak, D.L. (2016a) Oxidation of benzene by persulfate in the presence of Fe (III)-and Mn (IV)-containing oxides: stoichiometric efficiency and transformation products. Environ. Sci. Technol. 50(2), 890-898.

Liu, J., Wang, L., Tang, J. and Ma, J. (2016b) Photocatalytic degradation of commercially sourced naphthenic acids by TiO_2-graphene composite nanomaterial. Chemosphere 149, 328-335.

Luna, F.M.T., Pontes-Filho, A.A., Trindade, E.D., Silva, I.J., Azevedo, D.C. and Cavalcante, C.L. (2008) Removal of aromatic compounds from mineral naphthenic oil by adsorption. J Ind Eng Chem 47(9), 3207-3212.

Madhavan, V., Levanon, H. and Neta, P. (1978) Decarboxylation by SO_4-radicals. Radiation Research 76(1), 15-22.

Madill, R.E., Orzechowski, M.T., Chen, G., Brownlee, B.G. and Bunce, N.J. (2001) Preliminary risk assessment of the wet landscape option for reclamation of oil sands mine tailings: bioassays with mature fine tailings pore water. Environmental Toxicology 16(3), 197-208.

Mahdavi, H., Prasad, V., Liu, Y. and Ulrich, A.C. (2015) In situ biodegradation of naphthenic acids in oil sands tailings pond water using indigenous algae-bacteria consortium. Bioresour. Technol. 187, 97-105.

Marentette, J.R., Frank, R.A., Bartlett, A.J., Gillis, P.L., Hewitt, L.M., Peru, K.M., Headley, J.V., Brunswick, P., Shang, D. and Parrott, J.L. (2015) Toxicity of naphthenic acid fraction components extracted from fresh and aged oil sands process-affected waters, and commercial naphthenic acid mixtures, to fathead minnow (Pimephales promelas) embryos. Aquatic Toxicology 164, 108-117.

Marsh, W.P. (2006) Sorption of naphthenic acids to soil minerals, Library and Archives Canada= Bibliothèque et Archives Canada.

Martin, J.W., Barri, T., Han, X., Fedorak, P.M., El-Din, M.G., Perez, L., Scott, A.C. and Jiang, J.T. (2010) Ozonation of oil sands process-affected water accelerates microbial bioremediation. Environ. Sci. Technol. 44(21), 8350-8356.

Martin, N., Burkus, Z., McEachern, P. and Yu, T. (2014) Naphthenic acids quantification in organic solvents using fluorescence spectroscopy. J. Environ. Sci. Heal. A 49(3), 294-306.

McQueen, A.D., Kinley, C.M., Kiekhaefer, R.L., Calomeni, A.J., Rodgers Jr, J.H. and Castle, J.W. (2016) Photocatalysis of a Commercial Naphthenic Acid in Water Using Fixed-Film TiO_2. Water, Air, & Soil Pollution 227(5), 1-11.

Melvin, S.D. and Trudeau, V.L. (2012) Toxicity of naphthenic acids to wood frog tadpoles (Lithobates sylvaticus). J. Toxicol. Env. Heal. A 75(3), 170-173.

Mohamed, M.H., Wilson, L.D., Headley, J.V. and Peru, K.M. (2011) Sequestration of naphthenic acids from aqueous solution using β-cyclodextrin-based polyurethanes. Phys Chem Chem Phys 13(3), 1112-1122.

Munoz, M., de Pedro, Z.M., Casas, J.A. and Rodriguez, J.J. (2015) Preparation of magnetite-based catalysts and their application in heterogeneous Fenton oxidation–a review. Appl. Catal. B-Environ. 176, 249-265.

Myhre, O. and Fonnum, F. (2001) The effect of aliphatic, naphthenic, and aromatic hydrocarbons on production of reactive oxygen species and reactive nitrogen species in rat brain synaptosome fraction: the involvement of calcium, nitric oxide synthase, mitochondria, and phospholipase A. Biochem. pharmacol. 62(1), 119-128.

Neta, P., Huie, R.E. and Ross, A.B. (1988) Rate constants for reactions of inorganic radicals in aqueous solution. J. Phys. Chem. ref. Data 17(3), 1027-1284.

Neyens, E. and Baeyens, J. (2003) A review of classic Fenton's peroxidation as an advanced oxidation technique. J. Hazard. Mater. 98(1), 33-50.

Ortiz, X., Jobst, K.J., Reiner, E.J., Backus, S.M., Peru, K.M., McMartin, D.W., O'Sullivan, G., Taguchi, V.Y. and Headley, J.V. (2014) Characterization of naphthenic acids by gas chromatography-Fourier transform ion cyclotron resonance mass spectrometry. Anal. Chem. 86(15), 7666-7673.

Pérez-Estrada, L.A., Han, X., Drzewicz, P., Gamal El-Din, M., Fedorak, P.M. and Martin, J.W. (2011) Structure–reactivity of naphthenic acids in the ozonation process. Environ. Sci. Technol. 45(17), 7431-7437.

Pereira, A.S., Bhattacharjee, S. and Martin, J.W. (2013a) Characterization of oil sands process-affected waters by liquid chromatography orbitrap mass spectrometry. Environ. Sci. Technol. 47(10), 5504-5513.

Pereira, A.S., Islam, M., Gamal El-Din, M. and Martin, J.W. (2013b) Ozonation degrades all detectable organic compound classes in oil sands process-affected water; an application of high-performance liquid chromatography/obitrap mass spectrometry. Rapid Commun. Mass S. 27(21), 2317-2326.

Pliego, G., Zazo, J.A., Garcia-Muñoz, P., Munoz, M., Casas, J.A. and Rodriguez, J.J. (2015) Trends in the intensification of the Fenton process for wastewater treatment: an overview. Crit. Rev. Env. Sci. Tec. 45(24), 2611-2692.

Pollard, S.J., Hrudey, S.E., Fuhr, B.J., Alex, R.F., Holloway, L.R. and Tosto, F. (1992) Hydrocarbon wastes at petroleum-and creosote-contaminated sites: rapid characterization of component classes by thin-layer chromatography with flame ionization detection. Environ. Sci. Technol. 26(12), 2528-2534.

Purcell, J.M., Hendrickson, C.L., Rodgers, R.P. and Marshall, A.G. (2006) Atmospheric pressure photoionization Fourier transform ion cyclotron resonance mass spectrometry for

complex mixture analysis. Anal. Chem. 78(16), 5906-5912.

Quinlan, P.J. and Tam, K.C. (2015) Water treatment technologies for the remediation of naphthenic acids in oil sands process-affected water. Chem. Eng. J. 279, 696-714.

Ré-Poppi, N., Almeida, F., Cardoso, C., Raposo, J., Viana, L., Silva, T., Souza, J. and Ferreira, V. (2009) Screening analysis of type C Brazilian gasoline by gas chromatography–Flame ionization detector. Fuel 88(3), 418-423.

Reinardy, H.C., Scarlett, A.G., Henry, T.B., West, C.E., Hewitt, L.M., Frank, R.A. and Rowland, S.J. (2013) Aromatic naphthenic acids in oil sands process-affected water, resolved by GCxGC-MS, only weakly induce the gene for vitellogenin production in zebrafish (Danio rerio) larvae. Environ. Sci. Technol. 47(12), 6614-6620.

Rontani, J. and Bonin, P. (1992) Utilization of n-alkyl-substituted cyclohexanes by a marine Alcaligenes. Chemosphere 24(10), 1441-1446.

Rowland, S.J., Scarlett, A.G., Jones, D., West, C.E. and Frank, R.A. (2011a) Diamonds in the rough: identification of individual naphthenic acids in oil sands process water. Environ. Sci. Technol. 45(7), 3154-3159.

Rowland, S.J., West, C.E., Jones, D., Scarlett, A.G., Frank, R.A. and Hewitt, L.M. (2011b) Steroidal aromatic 'naphthenic acids' in oil sands process-affected water: structural comparisons with environmental estrogens. Environ. Sci. Technol. 45(22), 9806-9815.

Rowland, S.J., West, C.E., Scarlett, A.G., Ho, C. and Jones, D. (2012) Differentiation of two industrial oil sands process-affected waters by two-dimensional gas chromatography/mass spectrometry of diamondoid acid profiles. Rapid Commun. Mass S. 26(5), 572-576.

Rowland, S.M., Robbins, W.K., Corilo, Y.E., Marshall, A.G. and Rodgers, R.P. (2014) Solid-phase extraction fractionation to extend the characterization of naphthenic acids in crude oil by electrospray ionization Fourier transform ion cyclotron resonance mass spectrometry. Energ. Fuel 28(8), 5043-5048.

Sabyasachi, M., Venkatesh, M., Ajay K, D., Dena W, M., John V, H. and Kerry M, P. (2010) Photocatalysis of naphthenic acids in water. Journal of Water Res.ource and Protection 2010.

Scarlett, A., Reinardy, H., Henry, T., West, C., Frank, R., Hewitt, L. and Rowland, S. (2013) Acute toxicity of aromatic and non-aromatic fractions of naphthenic acids extracted from oil sands process-affected water to larval zebrafish. Chemosphere 93(2), 415-420.

Schindler, D. (2010) Tar sands need solid science. Nature 468(7323), 499-501.

Schramm, L.L., Stasiuk, E.N. and MacKinnon, M. (2000) Surfactants in Athabasca oil sands slurry conditioning, flotation recovery, and tailings processes, Cambridge University Press: Cambridge.

Scott, A.C., Young, R.F. and Fedorak, P.M. (2008a) Comparison of GC-MS and FTIR methods for quantifying naphthenic acids in water samples. Chemosphere 73(8), 1258-1264.

Scott, A.C., Zubot, W., MacKinnon, M.D., Smith, D.W. and Fedorak, P.M. (2008b) Ozonation of oil sands process water removes naphthenic acids and toxicity. Chemosphere 71(1), 156-160.

Shu, Z., Li, C., Belosevic, M., Bolton, J.R. and El-Din, M.G. (2014) Application of a solar UV/chlorine advanced oxidation process to oil sands process-affected water remediation. Environ. Sci. Technol. 48(16), 9692-9701.

Smith, B.E., Lewis, C.A., Belt, S.T., Whitby, C. and Rowland, S.J. (2008) Effects of alkyl chain branching on the biotransformation of naphthenic acids. Environ. Sci. Technol. 42(24), 9323-9328.

Tokic, D. (2015) The 2014 oil bust: Causes and consequences. Energy Policy 85, 162-169.

Tollefsen, K.E., Petersen, K. and Rowland, S.J. (2012) Toxicity of synthetic naphthenic acids and mixtures of these to fish liver cells. Environ. Sci. Technol. 46(9), 5143-5150.

Toor, N.S., Han, X., Franz, E., MacKinnon, M.D., Martin, J.W. and Liber, K. (2013) Selective biodegradation of naphthenic acids and a probable link between mixture profiles and aquatic toxicity. Environ. Toxicol. Chem. 32(10), 2207-2216.

Vaiopoulou, E., Misiti, T.M. and Pavlostathis, S.G. (2015) Removal and toxicity reduction of naphthenic acids by ozonation and combined ozonation-aerobic biodegradation. Bioresour. Technol. 179, 339-347.

Wang, B., Wan, Y., Gao, Y., Yang, M. and Hu, J. (2013a) Determination and characterization of oxy-naphthenic acids in oilfield wastewater. Environ. Sci. Technol. 47(16), 9545-9554.

Wang, B., Wan, Y., Gao, Y., Zheng, G., Yang, M., Wu, S. and Hu, J. (2015a) Occurrences and behaviors of naphthenic acids in a petroleum refinery wastewater treatment plant. Environ. Sci. Technol. 49(9), 5796-5804.

Wang, C., Klamerth, N., Messele, S.A., Singh, A., Belosevic, M. and El-Din, M.G. (2016) Comparison of UV/hydrogen peroxide, potassium ferrate (VI), and ozone in oxidizing the organic fraction of oil sands process-affected water (OSPW). Water Res. 100, 476-485.

Wang, J., Feng, L., Steve, M., Tang, X., Gail, T.E. and Mikael, H. (2015b) China's unconventional oil: A review of its resources and outlook for long-term production. Energy 82, 31-42.

Wang, J. and Wang, J. (2007) Application of radiation technology to sewage sludge processing: a review. J. Hazard. Mater. 143(1), 2-7.

Wang, N., Chelme-Ayala, P., Perez-Estrada, L., Garcia-Garcia, E., Pun, J., Martin, J.W., Belosevic, M. and Gamal El-Din, M. (2013b) Impact of ozonation on naphthenic acids speciation and toxicity of oil sands process-affected water to Vibrio fischeri and mammalian immune system. Environ. Sci. Technol. 47(12), 6518-6526.

Wang, X. and Kasperski, K.L. (2010) Analysis of naphthenic acids in aqueous solution using

HPLC-MS/MS. Anal. Methods 2(11), 1715.

Wang, Z., Yang, C., Hollebone, B. and Fingas, M. (2006) Forensic fingerprinting of diamondoids for correlation and differentiation of spilled oil and petroleum products. Environ. Sci. Technol. 40(18), 5636-5646.

West, C.E., Jones, D., Scarlett, A.G. and Rowland, S.J. (2011) Compositional heterogeneity may limit the usefulness of some commercial naphthenic acids for toxicity assays. Sci. Total. Environ. 409(19), 4125-4131.

Wort, D. and Patel, K. (1970) Response of plants to naphthenic and cycloalkanecarboxylic acids. Agronomy Journal 62(5), 644-646.

Wu, J. and Upreti, S.R. (2017) Application of mass balance models in the process of ozone removal of naphthenic acids from water. Can. J. Chem. Eng. 95(1), 39-45.

Xu, X.-Y., Zeng, G.-M., Peng, Y.-R. and Zeng, Z. (2012) Potassium persulfate promoted catalytic wet oxidation of fulvic acid as a model organic compound in landfill leachate with activated carbon. Chem. Eng. J. 200, 25-31.

Xu, X., Pliego, G., Zazo, J.A., Casas, J.A. and Rodriguez, J.J. (2016) Mineralization of naphtenic acids with thermally-activated persulfate: The important role of oxygen. J. Hazard. Mater. 318, 355-362.

Xue, J., Zhang, Y., Liu, Y. and El-Din, M.G. (2016) Effects of ozone pretreatment and operating conditions on membrane fouling behaviors of an anoxic-aerobic membrane bioreactor for oil sands process-affected water (OSPW) treatment. Water Res. 105, 444-455.

Yang, Y., Pignatello, J.J., Ma, J. and Mitch, W.A. (2014) Comparison of halide impacts on the efficiency of contaminant degradation by sulfate and hydroxyl radical-based advanced oxidation processes (AOPs). Environ. Sci. Technol. 48(4), 2344-2351.

Zhang, Y., Klamerth, N., Chelme-Ayala, P. and Gamal El-Din, M. (2016a) Comparison of nitrilotriacetic acid and [S, S]-ethylenediamine-N, N'-disuccinic acid in UV-Fenton for the treatment of oil sands process-affected water at natural pH. Environ. Sci. Technol., 50(19), 10535-10544.

Zhang, Y., Klamerth, N. and El-Din, M.G. (2016b) Degradation of a model naphthenic acid by nitrilotriacetic acid–modified Fenton process. Chem. Eng. J. 292, 340-347.

Zhang, Y., Klamerth, N., Messele, S.A., Chelme-Ayala, P. and El-Din, M.G. (2016c) Kinetics study on the degradation of a model naphthenic acid by ethylenediamine-N, N'-disuccinic acid-modified Fenton process. J. Hazard. Mater. 318, 371-378.

Zhang, Y., Xue, J., Liu, Y. and El-Din, M.G. (2016d) Treatment of oil sands process-affected water using membrane bioreactor coupled with ozonation: A comparative study. Chem. Eng. J. 302, 485-497.

CHAPTER II/ CAPÍTULO II/卷二

MATERIALS AND METHODS

MATERIALES Y MÉTODOS

材料与方法

2.1 Materials

Model NAs with different structural features have been selected, including cyclohexanoic acid (CHA), cyclohexanebutyric acid (CHBA), 2-naphthoic acid (2-NA) and 1,2,3,4-tetrahydro-2-naphthoic acid (1234-T-2-NA). The former two are saturated ring-bearing structures while the later ones contain aromatic rings (Fig. 2.1). Those compounds were purchased from Sigma-Aldrich with purity ≥ 98%. Oxidants (PS and H_2O_2) and $FeSO_4 \bullet 7H_2O$ (as the iron source for Fenton process) were supplied by Panreac AppliChem company from Spain with purity ≥ 98%. The activated carbon (AC) and γ-alumina (γ-Al_2O_3) used as heterogeneous Fenton catalysts were purchased from Merck company of Germany. Other chemicals used are all from Sigma-Aldrich without further purification.

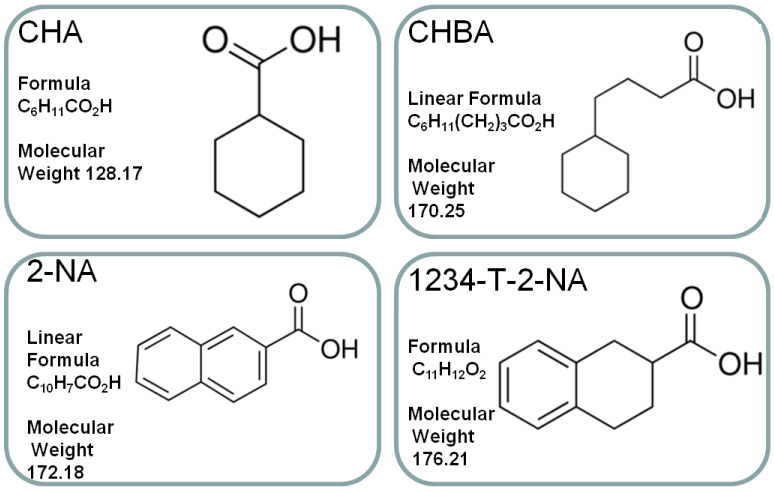

Fig. 2.1 Information on the NAs tested

2.2 Experimental procedures

2.2.1 Preparation of NAs solutions

Because of the acidity and thus the poor water solubility of NAs at neutral pH, pre-alkalinization with NaOH was accomplished. After complete dissolution, the

concentration of NAs was checked and then the pH was adjusted to 8 before the PS-oxidation runs.

2.2.2 PS oxidation experiments

PS oxidation runs were carried out in 100 mL glass batch reactors placed in a constant-temperature water bath with a shacking frequency equivalent to 200 rpm. Given amounts of sodium persulfate ($Na_2S_2O_8$) and/or other reagents (when required) like the scavenging organics (tert-Butyl alcohol, TBA; ethanol, EtOH) and inorganic salts (sodium bicarbonate and chloride) were added into the reactors containing 50 mL of NAs aqueous solution with the desired concentration (50 mg L^{-1}, for instance, which means 0.39, 0.29, 0.29 and 0.28 mM of CHA, CHBA, 2-NA and 1234-T-2-NA respectively). Previous to the addition of PS, the reactors were preheated for 15–30 min to make sure that the reactions were initiated at the testing temperature (40–97 ± 1°C). The degradation of the starting compounds during the preheating stage was always negligible.

The theoretical stoichiometric dose of PS for complete oxidation of CHA, CHBA, 2-NA and 1234-T-2-NA is calculated from the following reactions:

CHA:

$$C_7H_{12}O_2 + 36\ SO_4^{\bullet -} + 12\ H_2O \rightarrow 7\ CO_2 + 36\ SO_4^{2-} + 36\ H^+ \quad (1)$$

CHBA:

CHBA: $C_{10}H_{18}O_2 + 54\ SO_4^{\bullet -} + 18\ H_2O \rightarrow 10\ CO_2 + 54\ SO_4^{2-} + 54\ H^+$ (2)

2-NA:

$$C_{11}H_8O_2 + 48\ SO_4^{\bullet -} + 20\ H_2O \rightarrow 11\ CO_2 + 48\ SO_4^{2-} + 48\ H^+ \quad (3)$$

1234-T-2-NA:

$C_{11}H_{12}O_2 + 52\ SO_4^{\bullet -} + 20\ H_2O \rightarrow 11\ CO_2 + 52\ SO_4^{2-} + 52\ H^+$ (4)

Tests under inert conditions were also carried out, using an inert atmosphere chamber with the NAs samples and PS solutions previously bubbled by N_2 for 30 min. All other operating conditions were as described above.

2.2.3 PS and Fenton oxidation

After PS oxidation during certain reaction time (0.5–2 h), Fenton reagents (10%–80% stoichiometric amount of H_2O_2 and 0.5–20 mg L^{-1} Fe^{2+} as $FeSO_4 \bullet 7H_2O$ or certain amount of catalysts like Fe/AC and Fe/γ-Al_2O_3) were added simultaneously to perform the Fenton process or CWPO step.

The theoretical stoichiometric dose of hydrogen peroxide for the complete oxidation of CHA, CHBA, 2-NA and 1234-T-2-NA is calculated from the reactions:

CHA:

$C_7H_{12}O_2 + 18\ H_2O_2 \rightarrow 7\ CO_2 + 24\ H_2O$ (5)

CHBA:

$C_{10}H_{18}O_2 + 27\ H_2O_2 \rightarrow 10\ CO_2 + 36\ H_2O$ (6)

2-NA

$C_{11}H_8O_2 + 24\ H_2O_2 \rightarrow 11\ CO_2 + 28\ H_2O$ (7)

1234-T-2-NA

$C_{11}H_{12}O_2 + 26\ H_2O_2 \rightarrow 11\ CO_2 + 32\ H_2O$ (8)

2.2.4 Preparation of the catalysts for heterogeneous Fenton

Incipient wetness impregnation was used for the preparation of the home-made Fe/AC(Zazo et al. 2006) and Fe/γ-Al_2O_3(Munoz et al. 2013) catalysts. AC and γ-Al_2O_3 with particle diameter less than 100 μm from Merck (Germany) were impregnated by $Fe(NO_3)_3 \cdot 9H_2O$ solution to adjust the Fe load at nominal 4% (w/w). After left in room ambient for 2 h, the catalysts were dried for 12 h at 60 ^oC and calcined at 300 ^oC for 4 h.

2.2.5 COD and BOD_5 tests

Chemical oxygen demand (COD) was determined by oxidation with potassium dichromate following the Standard Method (ISO 6060) using UV-vis spectrometer (Shimadzu, mod. UV-1603). BOD_5 tests were conducted in a Velps Scientifica apparatus using the standard procedure available from previous work (Sanchis et al. 2013). 400 mL samples of the initial or treated NAs were mixed with activated sludge at 75 mg VSS L^{-1} and pH = 7.2 in the presence of phosphate buffer. $CaCl_2$, KCl and $MgSO_4$ were added as micronutrients and 1.25 mg L^{-1} N-allylthiourea was used as nitrification inhibitor. The biodegradability index was calculated as the BOD_5/COD ratio (Xu et al. 2012). The data of BOD_5 and COD were averages of triplicates with error bars.

2.2.6 Respirometric tests and TOC measurement

A well-developed respirometric test was carried out for the assessment of the biodegradability before and after AOP reactions. A LSS respirometer was used with intermittent aeration during 72 h using (Polo et al. 2011, Sanchis et al. 2014). Two limited values of oxygen concentration were set lower than water-solubility at the given conditions. Each specific oxygen uptake rate (SOUR) data was

recorded once the amount of dissolved oxygen dropped to the bottom limit due to the microbial respiration. The aeration started at the mean time, and then stopped until the oxygen concentration reached the upper limit. A biomass concentration of 350 mg VSS L^{-1} was used according to the preliminary tests. The reactors were placed in a thermostatic water bath at 25 ^{o}C with magnetic stirring at 500 rpm. Total organic carbon (TOC) was also followed throughout the runs, which was measured by a TOC analyzer (Shimadzu, mod. TOC VSCH).

2.2.7 Toxicity analysis

The ecotoxicity of the NAs solutions was determined by the Microtox toxicity test (ISO 11348-3, 1998) (Pliego et al. 2013). The bioluminisence was measured in a M500 Microtox Analyzer (Azur Environmental) to determine the activity of bacteria following previous reported method (Zazo et al. 2007). The light output of the luminescent bacteria was measured and compared with that of a blank negative control sample. The analysis media was 0.34 M NaCl (2% w/v), and the pH of the solution was adjusted to 7±0.5. Phenol (100 mg L^{-1}, EC_{50} = 16 mg L^{-1}) was used as toxicity reference compound. More details are given elsewhere (Zazo et al. 2007).

All the experiments were performed by duplicate if not specifically stated.

2.3 Analytical methods

The samples from the oxidation experiments were cooled in water bath to room temperature and further analyzed immediately.

2.3.1 NAs oxidation byproducts

The concentrations of CHA and CHBA were measured by Gas Chromatography with Flame Ionization Detector (GC-FID) in a GC 3900 Varian provided with a 30 m length × 0.25 mm i.d. capillary column (CP-Wax 52 CB, Varian) using nitrogen as carrier gas. For CHA, the initial oven temperature was set at 70 ^{o}C and then increased up to 240 ^{o}C at a rate of 30 ^{o}C min^{-1}. For CHBA, the only difference was lowering the heating rate to 20 ^{o}C min^{-1}. The concentration of the cyclohexanone as an intermediate of PS oxidation of CHA was also determined by GC-FID according the method for CHA analysis.

2-NA and 1234-T-2-NA were determined by high-performance liquid chromatography (HPLC; Varian Pro-Start 240) with a UV detector and Microsorb C18 5 μm column (250 × 4.6 mm) as stationary phase. Acetonitrile and 4 mM H_2SO_4 (1/1) were used as mobile phase at an injection rate of 1 mL min^{-1} with the oven temperature set at 60 ^{o}C.

A gas chromatography–mass spectrometry (GC-MS) system in electron impact ionization mode was used to analyze the initial NAs and oxidation intermediates. Extraction and 50-folds of concentration of the samples were conducted with n-hexane as the extracting solvent. The analyses were performed by gas chromatography/ion trap mass spectrometry (GC-MS, CP-3800/Saturn 2200, Varian). A 30 m length and 0.25 mm i.d. capillary column (Factor Four VF-5 ms) was used. The samples were injected at 250 °C. The temperature program used in the GC-MS analyses ramped as follows: for CHA, CHBA and 2-NA, the oven was hold at 70 ^{o}C for 1 min and then reached 200 ^{o}C at a rate of 30 ^{o}C min^{-1} and hold for another 1 min, after which the temperature increased up to 300 ^{o}C at rate of 20 ^{o}C min^{-1}; For 1234-T-2-NA, the initial temperature of the oven was set at 50 ^{o}C for 5 min, and then reached 300 ^{o}C at a rate of 15 ^{o}C min^{-1}

Short-chain carboxyl acids were analyzed by ionic chromatography (IC) analysis with chemical suppression (Metrohm 790 IC) using a conductivity detector. A Metrosep A supp 5−250 column (25 cm length, 4 mm i.d.) was used as stationary phase and 0.7 mL of an aqueous solution of 3.2 mM of Na_2CO_3 and 1 mM of $NaHCO_3$ as mobile phase.

2.3.2 PS determination

PS concentration was determined by a spectrophotometric method based on a modification of the iodometric titration analysis. The absorption spectra of a yellow color solution resulted from the reaction of persulfate and iodide in the presence of sodium bicarbonate was analyzed at absorbance at 352 nm, according to the reaction (9) (Liang et al. 2008).

$$S_2O_8^{2-} + 2I^- \rightarrow SO_4^{2-} + I_2 \quad (9)$$

2.3.3 H_2O_2 determination

The concentration of hydrogen peroxide was analyzed by colorimetric titration using the $TiOSO_4$ method (Eisenberg 1943). Yellow color can be produced due to the formation of pertitanic acid following the reaction (10). The absorbance was measured by UV-vis at wavelength of 410 nm.

$$Ti^{4+} + H_2O_2 + 2H_2O \rightarrow H_2TiO_4 + 4H^+ \quad (10)$$

2.3.4 Iron analysis

Iron ions were determined by the o-phenantroline colorimetric method (Sandell 1959). The sample was firstly added with hydroxylamine to reduce Fe^{3+} ions into Fe^{2+} and then titrated with 1,10-phenantroline where a pink color can be

produced. The absorbance at 510 nm was determined on UV-vis.

2.4 Characterization of the catalysts

2.4.1 TXRF analysis

The iron content of the fresh and used catalysts was determined by total reflection X-ray fluorescence (TXRF), using a TXRF spectrometer 8030c.

2.4.2 Porous texture

The BET area, pore volume and micropore size of AC were determined from the N_2 adsorption-desorption isotherms at 77 K using a Micromeritics Tristar 3020 apparatus. The samples were previously degassed overnight at 150 ^{o}C to a residual pressure of 10^{-5} Torr. The isotherms were obtained over a relative pressure (P/P_0) range from 10^{-5} to 1 (Palomar et al. 2009) . The BET surface area (S_{BET}) was calculated using the Brunauer–Emmett–Teller (BET) equation. The t-plot method was used to calculate the micropore area (S_{Micro}) and t-plot micropore volume (V_{Micro}). The total pore volume (V_{Total}) was determined according to single point method at $P/P_0 = 0.99$. The average pore diameter (D_{Ave}) was calculated from 4V/A equation based on BET method.

2.4.3 XPS analysis

X-ray photoelectron spectra (XPS) were recorded with a VGEscalab 200R spectrometer equipped with a Kα Thermo Scientific apparatus with an Al Kα ($h\nu$=1486.68 eV) X-ray source using a voltage of 12 kV under vacuum (2×10^{-7} mbar) condition (Rey et al. 2014). Binding energies were calibrated according to the C 1s peak of carbon samples at 284.6 eV. For the analysis of the peaks a Shirley

type background was used. Peaks were adjusted to a combination of Gaussian and Lorentzian functions using the XPSPeak 4.1 software (Rey et al. 2016).

References

Eisenberg, G. (1943) Colorimetric determination of hydrogen peroxide. Industrial & Engineering Chemistry Analytical Edition 15(5), 327-328.

Liang, C., Huang, C.-F., Mohanty, N. and Kurakalva, R.M. (2008) A rapid spectrophotometric determination of persulfate anion in ISCO. Chemosphere 73(9), 1540-1543.

Munoz, M., de Pedro, Z.M., Menendez, N., Casas, J.A. and Rodriguez, J.J. (2013) A ferromagnetic γ-alumina-supported iron catalyst for CWPO. Application to chlorophenols. Appl. Catal. B-Environ. 136, 218-224.

Palomar, J., Lemus, J., Gilarranz, M. and Rodriguez, J. (2009) Adsorption of ionic liquids from aqueous effluents by activated carbon. Carbon 47(7), 1846-1856.

Pliego, G., Zazo, J.A., Casas, J.A. and Rodriguez, J.J. (2013) Case study of the application of Fenton process to highly polluted wastewater from power plant. J. Hazard. Mater. 252, 180-185.

Polo, A., Tobajas, M., Sanchis, S., Mohedano, A. and Rodriguez, J. (2011) Comparison of experimental methods for determination of toxicity and biodegradability of xenobiotic compounds. Biodegradation 22(4), 751-761.

Rey, A., Garcia-Munoz, P., Hernandez-Alonso, M., Mena, E., Garcia-Rodriguez, S. and Beltran, F. (2014) WO_3–TiO_2 based catalysts for the simulated solar radiation assisted photocatalytic ozonation of emerging contaminants in a municipal wastewater treatment plant effluent. Appl. Catal. B-Environ. 154, 274-284.

Rey, A., Hungria, A., Duran-Valle, C., Faraldos, M., Bahamonde, A., Casas, J. and Rodriguez, J. (2016) On the optimization of activated carbon-supported iron catalysts in catalytic wet peroxide oxidation process. Appl. Catal. B-Environ. 181, 249-259.

Sanchis, S., Polo, A., Tobajas, M., Rodriguez, J. and Mohedano, A. (2014) Coupling Fenton and biological oxidation for the removal of nitrochlorinated herbicides from water. Water Res 49, 197-206.

Sanchis, S., Polo, A.M., Tobajas, M., Rodriguez, J.J. and Mohedano, A.F. (2013) Degradation of chlorophenoxy herbicides by coupled Fenton and biological oxidation. Chemosphere 93(1), 115-122.

Sandell, E.B. (1959) Colorimetric determination of traces of metals. Interscience Pubs. New York.

Xu, X.-Y., Zeng, G.-M., Peng, Y.-R. and Zeng, Z. (2012) Potassium persulfate promoted catalytic wet oxidation of fulvic acid as a model organic compound in landfill leachate with activated carbon. Chem. Eng. J. 200, 25-31.

Zazo, J.A., Casas, J.A., Mohedano, A.F. and Rodríguez, J.J. (2006) Catalytic wet peroxide oxidation of phenol with a Fe/active carbon catalyst. Appl. Catal. B-Environ. 65(3-4), 261-268.

Zazo, J.A., Casas, J.A., Molina, C.B., Quintanilla, A. and Rodriguez, J.J. (2007) Evolution of Ecotoxicity upon Fenton's Oxidation of Phenol in Water. Environ. Sci. Technol. 41(20), 7164-7170.

CHAPTER III/ CAPÍTULO III/卷三

RESULTS AND DISCUSSION

RESULTADOS Y DISCUSIÓN

结果与讨论

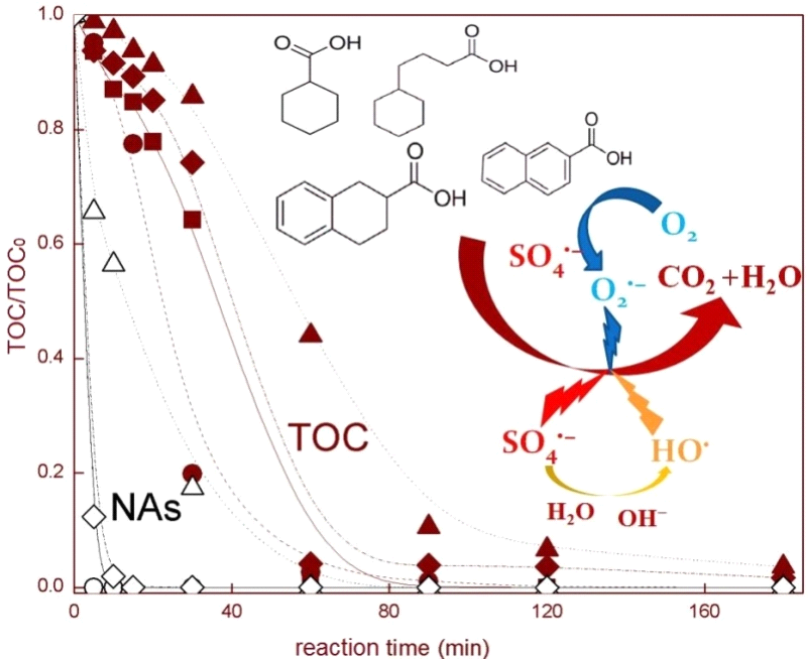

3–1

Mineralization of naphthenic acids with thermally-activated persulfate: The important role of oxygen

La mineralización de los ácidos nafténicos con persulfato activado térmicamente: la importante función de oxígeno

热催化过硫酸盐矿化处理环烷酸：氧气的重要作用

3.1.1 Abstract

This section investigates the mineralization of model naphthenic acids (NAs) in aqueous solution by catalyst-free thermally-activated persulfate (PS) oxidation. The NAs tested include saturated-ring (cyclohexanecarboxylic and cyclohexanebutyric acids) and aromatic (2-naphthoic and 1,2,3,4-tetrahydro-2-naphthoic acids) structures. The starting concentration of the aqueous solution was in all the cases 50 mg L^{-1} and the effect of PS dose within a wide range (10–100% of the theoretical stoichiometric) and working temperature (40–97 ^{o}C) was investigated. At 80 ^{o}C and initial pH=8 complete mineralization of the four NAs was achieved with PS doses frankly bellow the theoretical stoichiometric (40–60% of it). This is explained because of the important contribution of oxygen, which was experimentally verified. That contribution of oxygen was found to be more effective toward the NAs with a single cyclohexane ring than for the bicyclic aromatic-ring-bearing ones. The effect of chloride (10–50 g L^{-1}) and bicarbonate (0.5–10 g L^{-1}) as potential scavengers was also checked. The presence of chloride showed negative effect on the degradation rate of NAs whereas a negligible or even positive effect was found for bicarbonate. The rate of NAs mineralization can be well described by simple pseudo-first order kinetics. The values of the rate constants normalized to the PS dose were within the range of 0.062–0.099 h^{-1}. Fairly similar apparent activation energy values (between 93.7 and 105.3 kJ mol^{-1}) were obtained.

3.1.2 Introduction

As previously mentioned, increasing attention have been paid to the environmental impact of naphthenic acids (NAs) from oil sands process-affected water (OSPW). They have been observed to be of great hazard toward numerous testing organisms due to acute toxicity associated to their complex structure and

their transformation upon long time retention in aquatic systems (Zhang et al. 2011). Various techniques have been developed for the abatement of NAs, but both adsorption and biodegradation have their own limitations for potential application (Quagraine et al. 2005, Janfada et al. 2006, Siddique et al. 2006, Gong et al. 2009, Iranmanesh et al. 2014). Advanced oxidation processes (AOPs) manage to cause mineralization of many recalcitrant compounds (Andreozzi et al. 1999, Pignatello et al. 2006, Pliego et al. 2013). Thermally-activated decomposition of persulfate (PS) is a widely used AOP. Mechanistic studies have shown that hydroxyl radicals, generated from the interaction of PS and hydroxide ions and/or water, could also participate in the breakdown of target pollutants (Criquet and Leitner 2009).

In recent years, several evidences have been reported that oxygen acts positively in PS-based oxidation systems at ambient conditions in the presence of various catalysts by transforming into reactive $O_2^{\bullet-}/HO_2^{\bullet}$ (Ahmed and Chiron 2014, Fang et al. 2013b, Liu et al. 2015). However, the stoichiometric contribution of oxygen as an oxidant in the PS-based systems for the mineralization of the target pollutants has not been documented in the literature.

The mineralization ability of PS-based systems toward different organic contaminants has been investigated. Complete (Criquet and Leitner 2009) as well as partial (Lin et al. 2011, Zhou et al. 2014) TOC removal has been reported. Kinetic studies of PS oxidation activated by different approaches confirm that several reactive species play a role in the mineralization process. As indicated before, those species include sulfate/hydroxyl radicals, but also PS ions and/or other intermediates. Models, such as those based on competitive reactions with steady-state approximation, have been used to describe the kinetics of PS oxidation (Huang et al. 2002, Son et al. 2006, Vicente et al. 2011). In principle, the evolution of target pollutants can be described by a pseudo-first-order rate equation

(Waldemer et al. 2007) and the values of the apparent rate constant and the corresponding normalized rate constants can be used to compare among different systems at a level of generality (Waldemer and Tratnyek 2006) so that they can provide information on the suitability of AOP methods toward given target pollutants. However, the apparent rate constants referred to specific compounds obviously serve only to describe the rate of disappearance of those species whereas TOC-based kinetic studies are needed to learn on the rate of mineralization. So far, there is a lack of information on that respect in the literature.

Because of the well-known stability of PS, remote/localized or even direct heating activation of PS could be used in several in situ thermal remediation (ISTR) technologies. Increasing the temperature will not only promote the decomposition of PS to sulfate radicals, but also would favor the activation of other related radicals (Waldemer et al. 2007). Therefore, the application of ISTR with PS oxidation approach making use of the processing temperature of OSPWs, well above the ambient, is of promising potential for the abatement of NAs from those effluents (Hong et al. 2013).

A few hydroxyl or sulfate radical-based AOPs using different activation approaches have been checked for the degradation of NAs, such as UV/H_2O_2, UV/$S_2O_8^{2-}$ and Zero Valent Iron (ZVI) catalyze(Drzewicz et al. 2010, Drzewicz et al. 2012, Liang et al. 2011). Fenton, that is one of the main hydroxyl radical generating systems, has not been successfully used in NAs abatement, because of the basic pH (around 8) of the OSPW containing those species (Kannel and Gan 2012), whereas Fenton oxidation is strictly pH dependent (pH ≈ 3.5). Opposite to that, PS-based oxidation systems have proved to be effective for the degradation of pollutants within a wide pH range (Criquet and Leitner 2009, Liang et al. 2007). PS oxidation not relying on the action of radicals from PS has also been reported recently. Zhou et al. (2014) investigated the degradation of 2,4-dichlorophenol with PS activated

with CuO.

In the current section, the mineralization of four NAs (with and without aromatic rings) by catalyst-free thermally-activated PS oxidation is investigated and the corresponding constants are given. The NAs used as target pollutants include CHA, CHBA, 2-NA and 1234-T-2-NA. The former two are saturated-ring structures while the last are aromatic ring-bearing bicyclic ones. The role of oxygen is studied, as well as the effect of potential scavenging ions, like chloride and bicarbonate commonly found in OSPWs.

3.1.3 Results and discussion

Fig. 3.1.1 shows the evolution of the four NAs tested upon reaction time using the corresponding stoichiometric amount of PS at 80 ^{o}C and initial pH = 8. Blank experiments were performed under the same conditions in absence of PS where the degradation of the NAs tested was always negligible, thus confirming the thermal stability of those compounds already reported in the literatures (Drzewicz et al. 2012, Liang et al. 2011). The two NAs containing a single cyclohexane ring (CHA and CHBA) were converted in a fairly short time in the presence of PS, most in particular CHBA, whereas the disappearance of the aromatic ring-bearing bicyclic NAs required some more time, especially in the case of the binuclear aromatic 2-NA, although complete conversion was also achieved in less than 1.5 h. The disappearance of the starting NAs consumed fairly low relative amounts of PS as can be seen from its evolution, also depicted in Fig. 3.1.1.

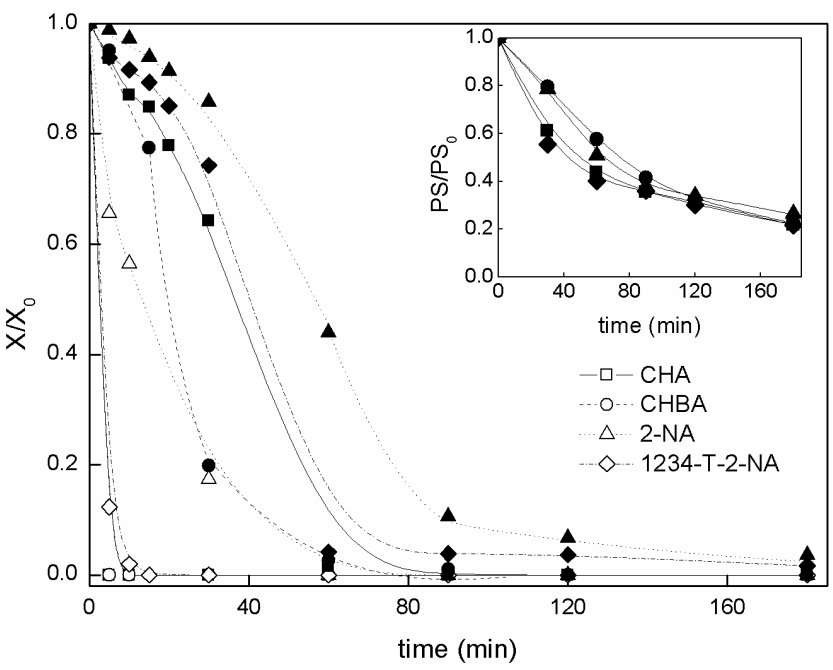

Fig. 3.1.1 Time course of NAs (open symbols) and TOC (solid symbols) upon thermally-activated PS oxidation. [NAs] = 50 mg L-1, T = 80 oC, pH = 8, PS at the corresponding stoichiometric dose.

To learn more on the degradation of the NAs, the evolution of TOC upon reaction time was also followed and is included in Fig. 3.1.1. As expected, the mineralization of NAs was slower than its disappearance since intermediate reaction byproducts are formed along the oxidation process. The reactive radical species attack certain positions of the naphthenic and aromatic rings of NAs giving rise to ring opening which leads to the formation of short-chain carboxylic acids further oxidized to CO_2 and H_2O (Drzewicz et al. 2010, Drzewicz et al. 2012). Complete mineralization was finally achieved in all the cases although upon significantly different reaction times following the same order observed for the disappearance of the starting NAs. TOC reduction takes place from the beginning of the oxidation process suggesting that some extent of direct mineralization of the starting NAs may not be discarded although proceeding at a slower rate as inferred from the lower slope of the initial stage of the TOC curves. The evolution of TOC

has been fitted to a simple pseudo-first order rate equation and the corresponding values of the rate constants are given in Table 3.1.1. In each case, separate values for the initial stage and the rest of the TOC curve have been calculated, showing significant differences among both regions as expected from the shape of the curves. Overall values are also included in Table 3.1.1, together with the corresponding correlation coefficients which confirm the significantly poorer fitting of the data when considering a sole rate equation for the whole TOC curve.

Table 3.1.1 Mineralization rate constants of NAs with the stoichiometric dose of PS: T = 80 °C, pH = 8.

NAs	Stage 1			Stage 2		Overall	
	k_{TOC1}' (h^{-1})	R^2	stage 1 duration (min)	k_{TOC2}' (h^{-1})	R^2	k_{TOC}'(h^{-1})	R^2
CHA	0.72±0.06	0.98	20	6.20±0.65	0.96	4.09±0.81	0.80
CHBA	1.05±0.11	0.97	20	4.07±0.37	0.99	3.64±0.30	0.80
2-NA	0.32±0.02	0.97	30	1.71±0.19	0.96	0.98±0.13	0.87
1234-T-2-NA	0.76±0.06	0.98	20	3.49±0.23	0.96	1.84±0.33	0.86

3.1.3.1 Effect of PS dose

Different relative amounts of PS were tested, varying from 10 to 80% of the corresponding theoretical stoichiometric dose and the results in terms of mineralization are depicted in Fig. 3.1.2. Some differences are observed among the four NAs tested at equivalent PS doses. However, it is interesting that complete mineralization of the four was achieved with PS doses well below the stoichiometric (40% for CHA and CHBA, 50% for 1234-T-2-NA and 60% for 2-NA). The mineralization of non-aromatic NAs consumes less PS than the aromatic ones. These doses are lower than the previously reported in the literatures (Liang et al. 2011, Rodriguez et al. 2014), thus allowing a more favorable view on the potential

application.

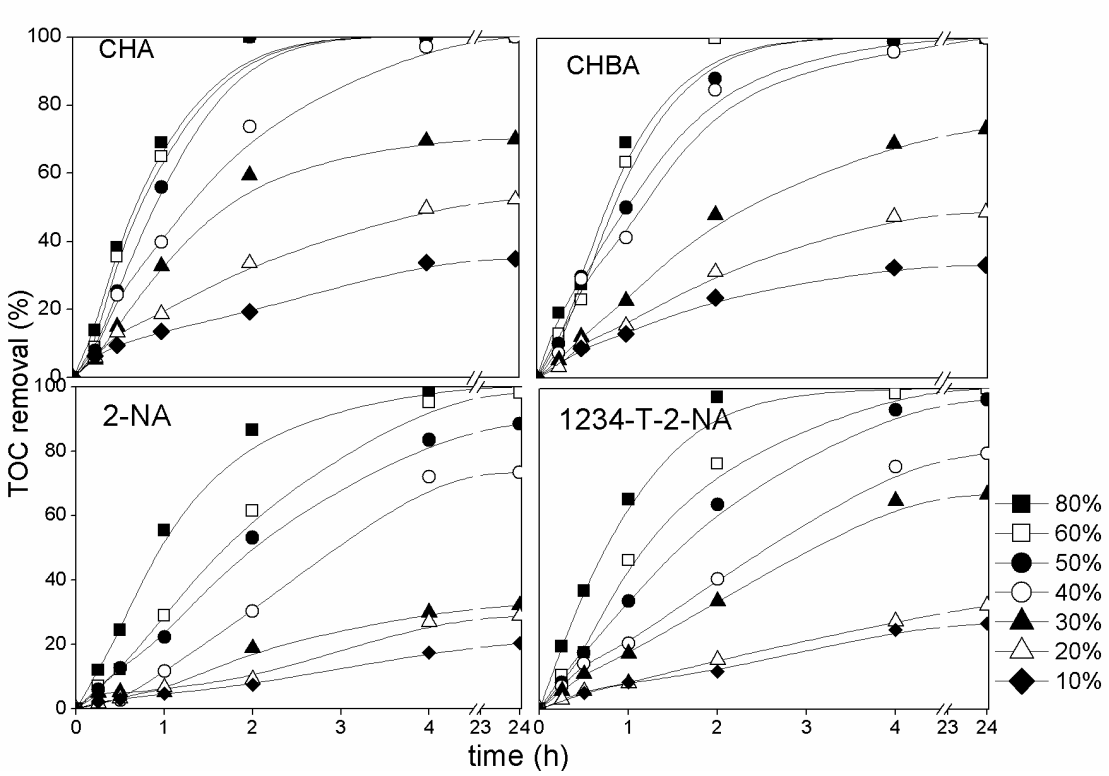

Fig. 3.1.2 TOC evolution upon reaction time at different PS doses (% of the stoichiometric).

Opposite to the observed at 100% and 80% of the stoichiometric PS dose, the kinetics of mineralization under strongly substoichiometric conditions (10%−60%) can be well described in all the cases by a sole rate equation covering the overall TOC vs. time curve with correlation coefficients between 0.95−0.99 (Table 3.1.2).

The values of the pseudo-first order rate constant at different initial PS/NAs molar ratios are plotted in Fig. 3.1.3. Reasonably good linear fits were obtained with the corresponding slopes providing the values of normalized rate constants which serve to compare the reactivity of the NAs tested.

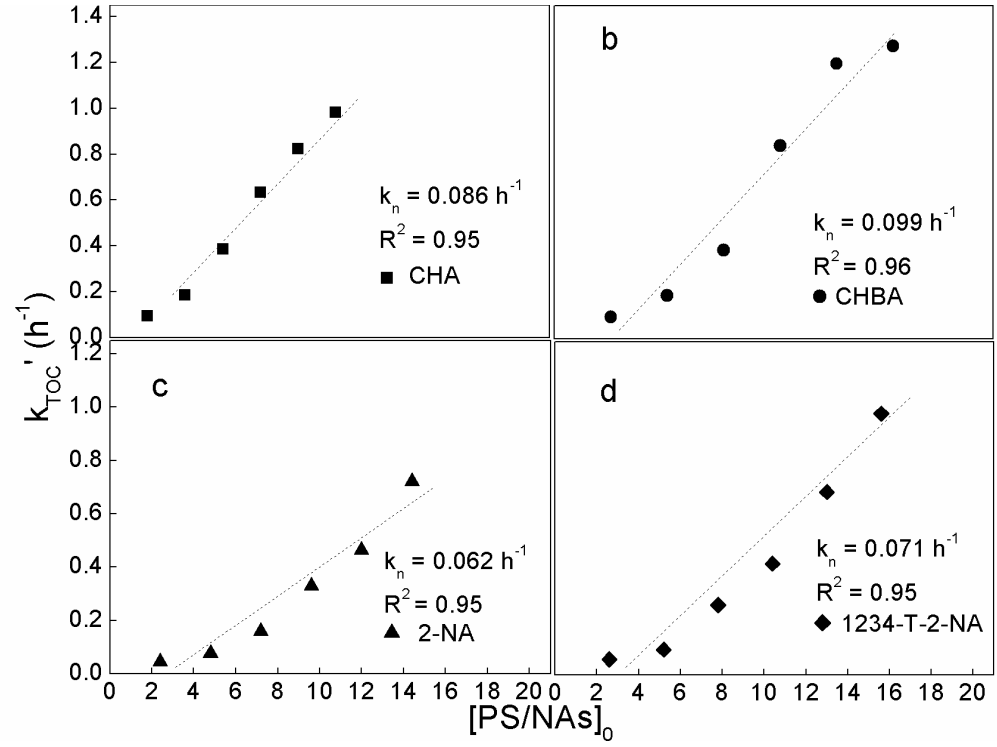

Fig. 3.1.3 Values of the pseudo-first order rate constant of NAs mineralization at different initial PS/NAs molar ratios.

Those values (k_n) are included in Fig. 3.1.3 together with the correlation coefficients. Looking at the k_n values, the reactivity of the four NAs tested are of the same order, differing less than two-fold between the most (CHBA) and the least (2-NA) reactive species. A conclusive structure-to-reactivity relationship cannot be established at this point since the susceptibility to mineralization does not depend exclusively on the starting compound but also on the intermediate oxidation byproducts, being k_n a lumped parameter in that respect, which, anyway, provides useful practical information.

Table 3.1.2 Mineralization rate constants of NAs under different conditions.

Percentage of stoich. dose (%)		CHA		CHBA		2-NA		1234-T-2-NA	
	T (°C)	$k_{TOC}' \times 10$ (h^{-1})	R^2	k_{TOC}' (h^{-1})	R^2	$k_{TOC}' \times 10$ (h^{-1})	R^2	$k_{TOC}' \times 10$ (h^{-1})	R^2
10	80	0.95 ±0.05	0.98	0.10 ±0.01	0.95	0.02 ±0.001	0.95	0.58 ±0.04	0.98
20	80	1.66 ±0.10	0.97	0.19 ±0.02	0.97	0.77 ±0.09	0.95	0.95 ±0.07	0.98
30	80	3.87 ±0.35	0.98	0.39 ±0.02	0.99	1.60 ±0.09	0.99	2.62 ±0.19	0.98
40	40	0.16 ±0.01	0.98	0.07 ±0.007	0.96	0.11 ±0.01	0.95	0.05 ±0.001	0.99
	60	0.77 ±0.08	0.95	0.35 ±0.04	0.97	0.55 ±0.05	0.95	0.20 ±0.01	0.99
	80	6.55 ±0.48	0.95	0.84 ±0.07	0.97	3.29 ±0.44	0.95	4.17 ±0.42	0.95
	97	40.5 ±7.03	0.98	18.9 ±1.75	0.96	16.3 ±1.39	0.98	9.19 ±0.47	0.99
50	80	8.23 ±0.93	0.96	1.20 ±0.08	0.98	4.63 ±0.31	0.98	6.86 ±0.55	0.97
60	80	10.6 ±1.06	0.98	1.38 ±0.08	0.98	7.50 ±0.37	0.98	9.85 ±0.76	0.95

3.1.3.2 Effect of the temperature.

Experiments were carried out at different temperatures (40, 60, 80, and 97 °C) with PS at 40% of the stoichiometric. The results are shown in Fig. 3.1.4, where it can be seen that the oxidation process must work at least around 80 °C to be effective at that low PS dose. At that temperature, more than 90% mineralization of the single-cyclohexane-ring-NAs tested was achieved after 4 h while the bicyclic aromatic ring-bearing ones required substantially higher reaction time. Below 80 °C, TOC reduction was very slow in all cases. Extending the reaction time up to 1 d, complete mineralization of CHA and CHBA was achieved at 60 °C while it still was fairly low in the cases of 2-NA and 1234-T-2-NA (23.6 and 27.7% respectively).

Table 3.1.3 Apparent activation energy of NAs mineralization.

NAs	Ea (kJ mol^{-1})	R^2
CHA	96.2 ±0.7	0.99
CHBA	100.9 ±0.6	0.98
2-NA	93.7 ±0.7	0.99
1234-T-2-NA	105.3 ±1.9	0.97

At 40 °C, less than 10% TOC removal was achieved after one-day reaction time in all the cases since PS conversion remained also below that percentage. The starting colorless solution of the aromatic NAs turned to dark brown, suggesting that although 40 °C is too low for the mineralization, certain transformation seems to be induced. At 97 °C, the TOC abatement was dramatically accelerated (Fig. 3.1.4 and Table 3.1.2). However, complete mineralization was never achieved at this PS dose (40% of the stoichiometric), although PS was completely converted within 1 h. Opposite to that, at 80 °C complete mineralization appears more likely (in particular for the non-aromatic NAs) since the corresponding curves did not reach a saturation level as it was the case at 97 °C. This high-temperature-caused efficiency decline has been previously reported in PS oxidation (Lee et al. 2009, Lee et al. 2010). Increasing the temperature accelerates the release of sulfate radicals leading to a faster breakdown of NAs, but the scavenging effect of those radicals can also be accelerated due to the higher concentration (Criquet and Leitner 2009).

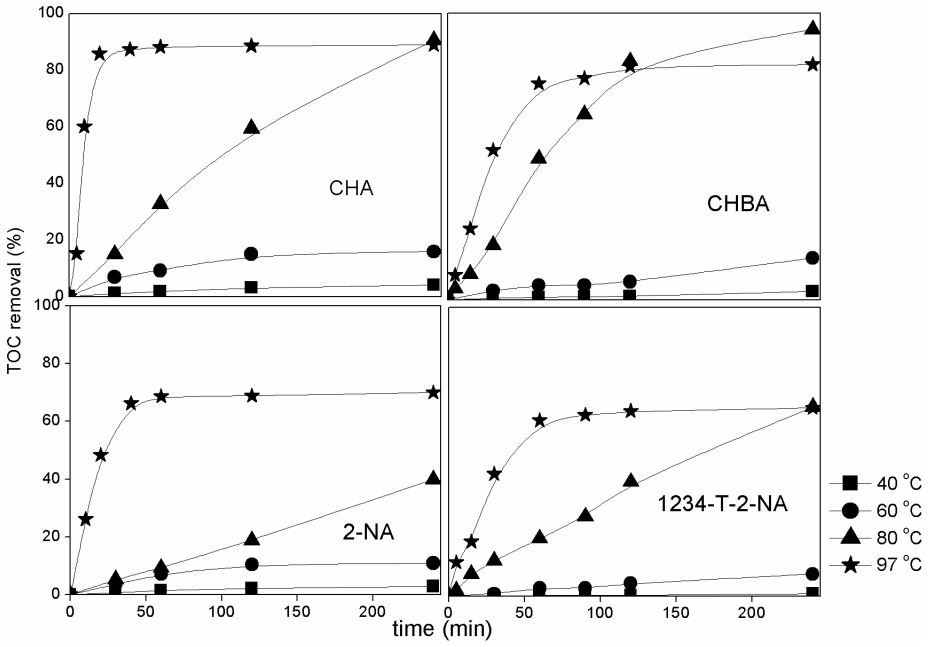

Fig. 3.1.4 Effect of temperature on the mineralization of the NAs tested with PS at 40% of the stoichiometric.

The values of the mineralization first-order rate constants at different temperatures are collected in Table 3.1.2, confirming the important effect of temperature above 60 ^{o}C. Table 3.1.3 summarizes the values of apparent activation energy calculated from the Arrhenius equation. As can be seen, they fall within a fairly narrow range in the vicinity of 100 kJ mol^{-1} for all the NAs tested.

3.1.3.3 The role of oxygen

The results obtained under substoichiometric PS doses suggest that sulfate radicals must not be the only reactive species to degrade NAs but some other must also contribute. In fact it has been reported that PS gives rise to other active species in addition to sulfate radicals in AOP systems (Anipsitakis and Dionysiou 2004, Furman et al. 2010, Lee et al. 2010). PS might react with water or even hydroxide ions in alkaline conditions generating hydroxyl radicals (reactions 2 and 3) (Anipsitakis and Dionysiou 2004). Consistently with those reactions, an important decrease of pH (from 8 to 2 – 4) was observed in all of our experiments in agreement with other authors (Anipsitakis and Dionysiou 2004). However, those hydroxyl radicals result from sulfate ones so that there is no net gain in the stoichiometry towards mineralization and the same occurs with other potentially oxidant species whose occurrence is consequent to PS decomposition or reaction. Therefore, the extra oxidation ability observed with respect to the theoretically expected from PS and PS-derived oxidant species must have other origin. In that respect, oxygen appears the most likely candidate for that extra capacity. Oxygen takes part in catalytic wet air oxidation but that technology operates under fairly different conditions than those of thermally-activated PS oxidation. On the other hand, this last does not use any metallic catalyst capable of activating the oxygen molecule. To investigate the possible role of oxygen, runs under O_2-free conditions were carried out as described before (Materials and methods). The results (depicted in Fig. 3.1.5) differ significantly from the obtained in the previous

regular experiments carried out in presence of oxygen (Fig. 3.1.1). The mineralization proceeds now at lower rate and the extent of mineralization after 4 h of reaction is also lower.

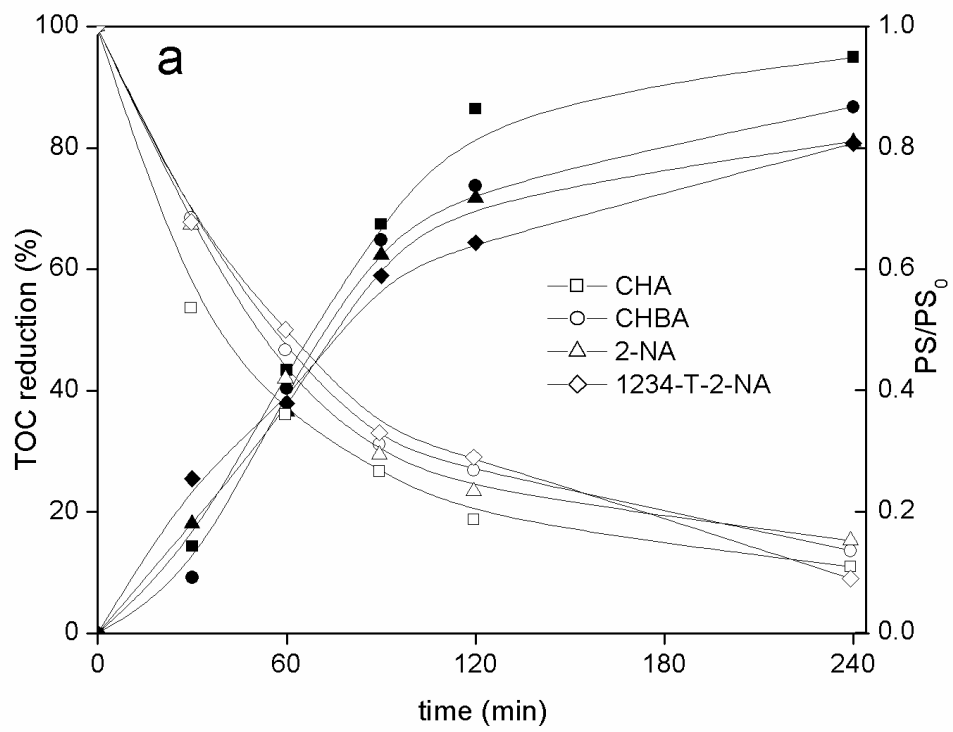

Fig. 3.1.5 Time course of TOC (solid symbols) and PS (open symbols) upon thermally-activated PS oxidation of the NAs tested under oxygen-free conditions. (PS at the stoichiometric dose)

Fig. 3.1.6 shows the TOC removal vs. PS converted in the presence and absence of oxygen. As can be seen, the system is significantly more efficient in the presence of oxygen where the TOC abatement clearly exceeds the maximum expected from the stoichiometry of reactions (4-7). Fang et al. (2013a) found that the $O_2^{\bullet-}$ radicals derived from oxygen could enhance the generation of $SO_4^{\bullet-}$ radicals from PS when investigating the degradation of PCBs with magnetite nanoparticles as catalyst. Very recently, detailed reaction mechanisms of benzene oxidation with PS in the presence of solid catalysts have been established including the contribution of oxygen (Liu et al. 2015). A hydroxylcyclohexadienyl (HCHD) radical formed acted as a key intermediate which tent to react with oxygen to

accelerate the ring-opening process. The current work further verifies quantitatively in terms of mineralization extent that oxygen is not only able to accelerate the PS oxidation process but also acts as an important oxidant enhancing mineralization in thermally-activated catalyst-free systems. The reaction between NAs and sulfate/hydroxyl radicals might give rise to the corresponding organic radicals (Reactions 1 and 2) (Fang et al. 2013a, Liu et al. 2015) that tend to react with oxygen to generate $O_2^{\bullet-}/HO_2^{\bullet}$ (Reaction 3 and 4) (Fang et al. 2013b, Peyton 1993), which have been recognized as reactive species in PS-based oxidation (Ahmed and Chiron 2014).

$$SO_4^{\bullet-} + R{-}H \rightarrow HSO_4^- + {}^{\bullet}R \quad (1)$$

$$HO^{\bullet} + R{-}H \rightarrow H_2O + {}^{\bullet}R \quad (2)$$

$${}^{\bullet}R + O_2 \rightarrow R^+ + O_2^{\bullet-} \quad (3)$$

$$O_2^{\bullet-} + H^+ \leftrightarrow HO_2^{\bullet} \quad (4)$$

The enhanced efficiency of the system under available oxygen is more noticeable as oxidation proceeds which can be explained by the increasing contribution of reaction (4) at lower pH. Also in the earlier stages, at higher PS concentration, self-scavenging reactions are more likely.

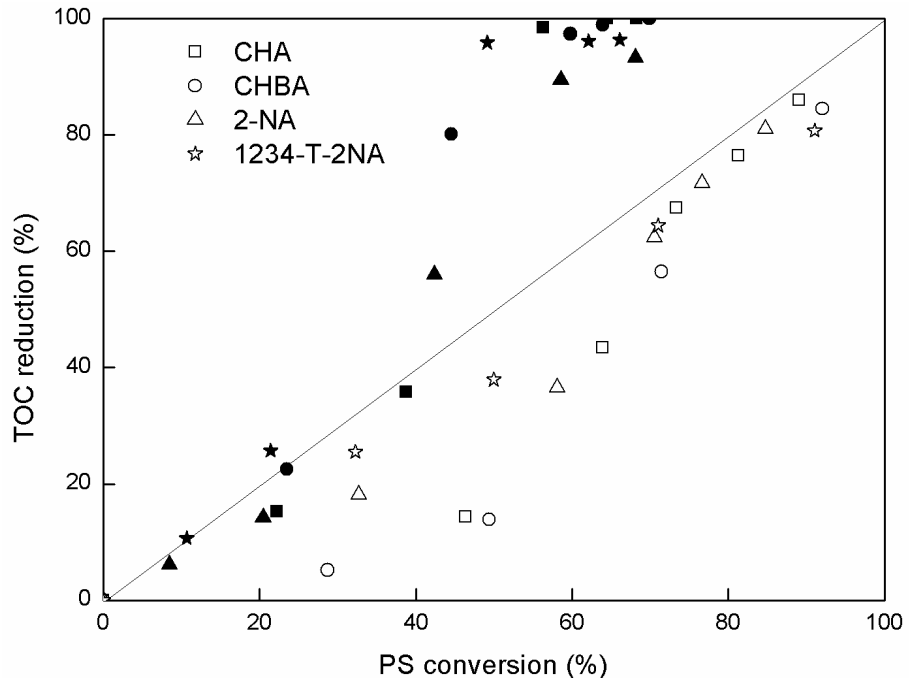

Fig. 3.1.6 TOC removal vs. PS converted in presence (solid symbols) and absence (open symbols) of oxygen. (PS initially at the stoichiometric dose according to reactions 4-7)

According to the results so far, the reaction of PS oxidation can be rewritten to take into account the contribution of oxygen:

CHA:

$$C_7H_{12}O_2 + (36\text{-}4n)\ SO_4^{\bullet -} + n\ O_2 + (12\text{-}2n)\ H_2O \rightarrow$$

$$7\ CO_2 + (36\text{-}4n)\ SO_4^{2-} + (36\text{-}4n)\ H^+,\ (0 \leq n \leq 6) \qquad (5)$$

CHBA:

$$C_{10}H_{18}O_2 + (54\text{-}4n)\ SO_4^{\bullet -} + n\ O_2 + (18\text{-}2n)\ H_2O \rightarrow$$

$$10\ CO_2 + (54\text{-}4n)\ SO_4^{2-} + (54\text{-}4n)\ H^+,\ (0 \leq n \leq 9) \qquad (6)$$

2-NA:

$C_{11}H_8O_2 + (48\text{-}4n)\ SO_4^{\bullet -} + n\ O_2 + (20\text{-}2n)\ H_2O \rightarrow$

$11\ CO_2 + (48\text{-}4n)\ SO_4^{2-} + (48\text{-}4n)\ H^+,\ (0 \leq n \leq 10)$ (7)

1234-T-2-NA:

$C_{11}H_{12}O_2 + (52\text{-}4n)\ SO_4^{\bullet -} + n\ O_2 + (20\text{-}2n)\ H_2O \rightarrow$

$11\ CO_2 + (52\text{-}4n)\ SO_4^{2-} + (52\text{-}4n)\ H^+,\ (0 \leq n \leq 10)$ (8)

According to those reactions and our experimental results, the nature of the target compound is of great importance regarding the contribution of oxygen in thermally-activated PS oxidation. The system is, in that sense, especially more reactive toward saturated rings than to aromatic ones.

To learn more on the radical mechanism involved, some quenching experiments were carried out with 1234-T-2-NA, selected because it contains both naphthenic and aromatic ring. TBA and EtOH were used as quenching agents at 500/1 alcohol/PS molar ratio (Anipsitakis and Dionysiou 2003, 2004, Anipsitakis et al. 2006, Liang et al. 2007, Xu et al. 2012). According to the different reaction rates between alcohols and free radicals, the generation of sulfate and hydroxyl radicals can be readily proved by the comparison of the inhibiting effect of scavengers toward our tested systems (Fig. 3.1.7). Furthermore, TBA was added into the system at different times. The rate of 1234-T-2-NA disappearance increased as the TBA addition was retarded, as can be seen in Fig. 3.1.7, suggesting that the formation of hydroxyl radicals (and thus their contribution) occurs mainly in the early stages.

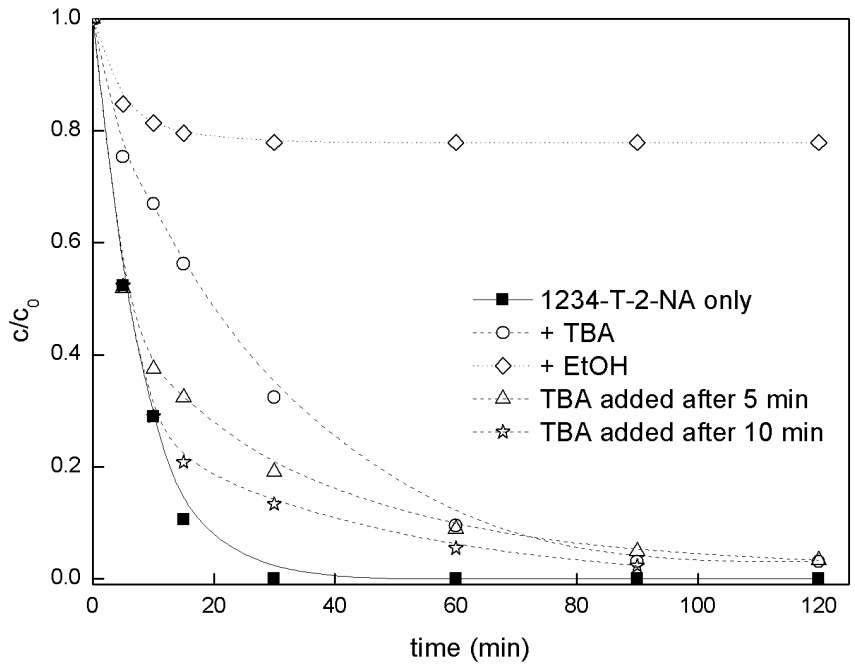

Fig. 3.1.7 Effect of scavengers on the degradation of 1234-T-2-NA. (Scavenger/NA molar ratios = 500/1, PS at 40% of the stoichiometric)

It has been reported in the literature that the role of hydroxyl radicals in PS oxidation systems varies according to the reaction conditions, most in particular the pH of the medium (Criquet and Leitner 2009, Liang et al. 2007). More hydroxyl radicals are believed to be formed by increasing pH. However, a decrease of efficiency has been reported above pH 9 (Criquet and Leitner 2009). The reason is controversial, but one explanation is that reaction between hydroxyl and persulfate radicals might occur giving rise to relatively less reactive radicals. In our case, the initial pH of the NAs solutions was always set at 8 (the common pH of OSPW). At that pH, the contribution of hydroxyl radicals must be appreciable but quite limited compared with that of sulfate ones (Fig. 3.1.7).

Spectroscopic studies by EPR can contribute in the future to better elucidate the radical mechanism involved in persulfate as well as other oxidation processes. In a recent paper, Zhu et al. (Zhu et al. 2016) have used EPR spectroscopy with DMPO as a spin-trapping agent to detect free radicals in the zero-valent iron-

activated persulfate degradation of DDT. They could follow by this the generation of sulfate and hydroxyl radicals upon the reaction. Zhong et al. (Zhong et al. 2015) found a more complex EPR spectrum, including a carbon-centered radical in addition to the sulfate and hydroxyl ones, for a reaction medium from 1,4-dioxane degradation upon persulfate activation by iron filings.

3.1.3.4 Effect of chloride and bicarbonate.

OSPW in general contain fairly high concentrations of chloride as well as bicarbonate, both being potential scavengers (Drzewicz et al. 2012). Some authors have found that the effects of chloride and bicarbonate on PS oxidation systems relies on several factors such as the pH, the activation source and the type of target compounds (Bennedsen et al. 2012, Liang et al. 2006). For example, it has been reported that enhancement rather than inhibition of thermally-activated PS oxidation was observed in the presence of chloride using p-nitrosodimethylaniline as the target molecule, while no significant effect of bicarbonate ions was found (Liang et al. 2006).

To learn on the effect of those ions on the breakdown of 1234-T-2-NAs by PS oxidation, experiments were conducted at 80 ^{o}C with different concentrations of them, using 40% of the stoichiometric PS dose. The results obtained are shown in Fig. 3.1.8, where it can be observed only some small negative effect of chloride. Complex reactions are involved in the interaction between chloride ion and sulfate/hydroxyl radicals. Species like $Cl^{\bullet}$, $Cl_2^{\bullet-}$, $ClHO^{\bullet-}$ can be generated which are believed to be less reactive than sulfate or hydroxyl radicals (Bennedsen et al. 2012, Huang et al. 2002, Liang et al. 2006). Moreover, $Cl^{\bullet}$ can even provoke the formation of chloro-NA according to previous researches (Drzewicz et al. 2012). Therefore, the effect of chloride needs to be considered in practical application of oxidation processes in general. Regarding the impact of bicarbonate ions, it has been

reported that $HCO_3^{\bullet}$ might be generated from the reaction between HCO_3^- and sulfate radicals giving rise to some changes of the redox potential (Liang et al. 2006).

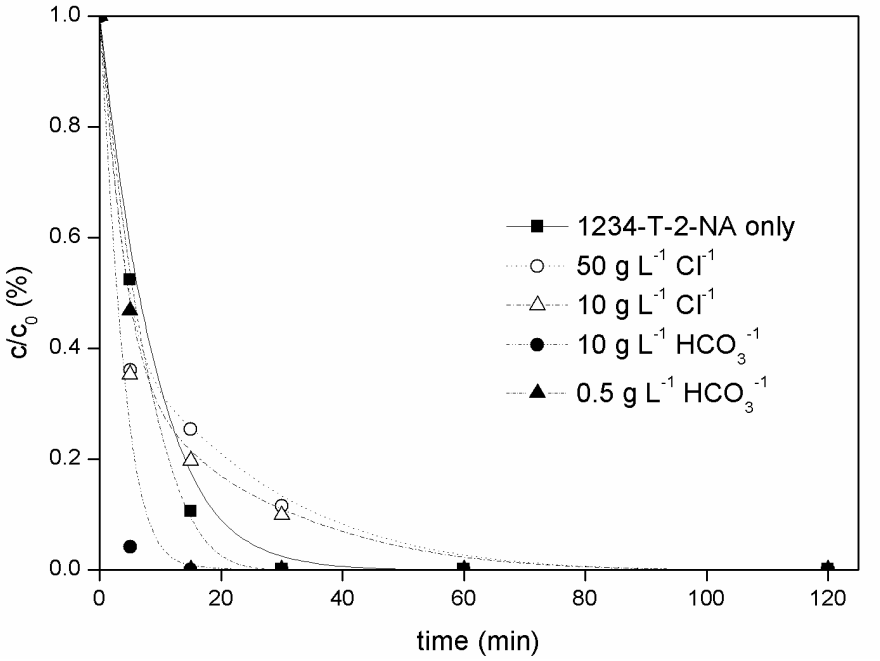

Fig. 3.1.8 Effect of Cl^- and HCO_3^- on the degradation of 1234-T-2-NA upon PS oxidation. (PS at 40% of the stoichiometric, T = 80 ºC)

3.1.4. Conclusions

Oxidation with thermally-activated PS at 80 ºC allowed achieving complete mineralization of the naphthenic acids tested with frankly substoichiometric amount of PS. The rate of TOC removal was well described by a simple pseudo-first order rate equation. The values of the normalized rate constants (k_n) followed the order: CHBA > 1234-T-2-NA > CHA > 2-NA. Fairly similar values of activation energy, in the vicinity of 100 kJ moL^{-1}, were obtained. Oxygen was found to play an important role in the mineralization process and the system showed to be more effective toward the saturated-ring species than for the aromatic ones. Sulfate and

hydroxyl radicals were verified to be the reactive species for NAs breakdown, with the former being by far the dominant ones. The impact of chloride and bicarbonate as potential scavengers was also analyzed. Only certain small negative effect of chloride was observed. The results allow learning on the potential application of this process to the treatment of the OSPWs.

References

Ahmed, M.M. and Chiron, S. (2014) Solar photo-Fenton like using persulphate for carbamazepine removal from domestic wastewater. Water Res 48, 229-236.

Andreozzi, R., Caprio, V., Insola, A. and Marotta, R. (1999) Advanced oxidation processes (AOP) for water purification and recovery. Catal Today 53(1), 51-59.

Anipsitakis, G.P. and Dionysiou, D.D. (2003) Degradation of organic contaminants in water with sulfate radicals generated by the conjunction of peroxymonosulfate with cobalt. Environ Sci Technol 37(20), 4790-4797.

Anipsitakis, G.P. and Dionysiou, D.D. (2004) Radical generation by the interaction of transition metals with common oxidants. Environ Sci Technol 38(13), 3705-3712.

Anipsitakis, G.P., Dionysiou, D.D. and Gonzalez, M.A. (2006) Cobalt-mediated activation of peroxymonosulfate and sulfate radical attack on phenolic compounds. Implications of chloride ions. Environ Sci Technol 40(3), 1000-1007.

Bennedsen, L.R., Muff, J. and Søgaard, E.G. (2012) Influence of chloride and carbonates on the reactivity of activated persulfate. Chemosphere 86(11), 1092-1097.

Criquet, J. and Leitner, N.K.V. (2009) Degradation of acetic acid with sulfate radical generated by persulfate ions photolysis. Chemosphere 77(2), 194-200.

Drzewicz, P., Afzal, A., El-Din, M.G. and Martin, J.W. (2010) Degradation of a model naphthenic acid, cyclohexanoic acid, by vacuum UV (172 nm) and UV (254 nm)/H2O2. The Journal of Physical Chemistry A 114(45), 12067-12074.

Drzewicz, P., Perez-Estrada, L., Alpatova, A., Martin, J.W. and Gamal El-Din, M. (2012) Impact of peroxydisulfate in the presence of zero valent iron on the oxidation of cyclohexanoic acid and naphthenic acids from oil sands process-affected water. Environ Sci Technol 46(16), 8984-8991.

Fang, G.-D., Dionysiou, D.D., Al-Abed, S.R. and Zhou, D.-M. (2013a) Superoxide radical driving the activation of persulfate by magnetite nanoparticles: Implications for the degradation of PCBs. Appl. Catal. B-Environ. 129, 325-332.

Fang, G., Gao, J., Dionysiou, D.D., Liu, C. and Zhou, D. (2013b) Activation of persulfate by quinones: Free radical reactions and implication for the degradation of PCBs. Environ Sci Technol 47(9), 4605-4611.

Furman, O.S., Teel, A.L. and Watts, R.J. (2010) Mechanism of base activation of persulfate. Environ Sci Technol 44(16), 6423-6428.

Gong, J.-L., Wang, B., Zeng, G.-M., Yang, C.-P., Niu, C.-G., Niu, Q.-Y., Zhou, W.-J. and Liang, Y. (2009) Removal of cationic dyes from aqueous solution using magnetic multi-wall carbon nanotube nanocomposite as adsorbent. J Hazard Mater 164(2), 1517-1522.

Hong, P.A., Cha, Z., Zhao, X., Cheng, C.-J. and Duyvesteyn, W. (2013) Extraction of bitumen from oil sands with hot water and pressure cycles. Fuel Processing Technology 106, 460-467.

Huang, K.-C., Couttenye, R.A. and Hoag, G.E. (2002) Kinetics of heat-assisted persulfate oxidation of methyl tert-butyl ether (MTBE). Chemosphere 49(4), 413-420.

Iranmanesh, S., Harding, T., Abedi, J., Seyedeyn-Azad, F. and Layzell, D.B. (2014) Adsorption of naphthenic acids on high surface area activated carbons. Journal of Environmental Science and Health, Part A 49(8), 913-922.

Janfada, A., Headley, J.V., Peru, K.M. and Barbour, S. (2006) A laboratory evaluation of the sorption of oil sands naphthenic acids on organic rich soils. Journal of Environmental Science and Health Part A 41(6), 985-997.

Kannel, P.R. and Gan, T.Y. (2012) Naphthenic acids degradation and toxicity mitigation in tailings wastewater systems and aquatic environments: a review. J Environ Sci Health A Tox Hazard Subst Environ Eng 47(1), 1-21.

Lee, Y.-C., Lo, S.-L., Chiueh, P.-T. and Chang, D.-G. (2009) Efficient decomposition of perfluorocarboxylic acids in aqueous solution using microwave-induced persulfate. Water Res 43(11), 2811-2816.

Lee, Y.-C., Lo, S.-L., Chiueh, P.-T., Liou, Y.-H. and Chen, M.-L. (2010) Microwave-hydrothermal decomposition of perfluorooctanoic acid in water by iron-activated persulfate oxidation. Water Res 44(3), 886-892.

Liang, C., Wang, Z.-S. and Bruell, C.J. (2007) Influence of pH on persulfate oxidation of TCE at ambient temperatures. Chemosphere 66(1), 106-113.

Liang, C., Wang, Z.-S. and Mohanty, N. (2006) Influences of carbonate and chloride ions on persulfate oxidation of trichloroethylene at 20 C. Sci Total Environ 370(2), 271-277.

Liang, X., Zhu, X. and Butler, E.C. (2011) Comparison of four advanced oxidation processes for the removal of naphthenic acids from model oil sands process water. J Hazard Mater 190(1-3), 168-176.

Lin, Y.-T., Liang, C. and Chen, J.-H. (2011) Feasibility study of ultraviolet activated persulfate oxidation of phenol. Chemosphere 82(8), 1168-1172.

Liu, H., Bruton, T.A., Li, W., Van Buren, J., Prasse, C., Doyle, F.M. and Sedlak, D.L. (2015) Oxidation of Benzene by Persulfate in the Presence of Fe (III)-and Mn (IV)-Containing Oxides: Stoichiometric Efficiency and Transformation Products. Environ Sci Technol.

Peyton, G.R. (1993) The free-radical chemistry of persulfate-based total organic carbon analyzers. Marine Chemistry 41(1), 91-103.

Pignatello, J.J., Oliveros, E. and MacKay, A. (2006) Advanced oxidation processes for organic contaminant destruction based on the Fenton reaction and related chemistry. Crit Rev Environ Sci Technol 36(1), 1-84.

Pliego, G., Zazo, J.A., Casas, J.A. and Rodriguez, J.J. (2013) Case study of the application of Fenton process to highly polluted wastewater from power plant. J Hazard Mater 252, 180-185.

Quagraine, E., Peterson, H. and Headley, J. (2005) In situ bioremediation of naphthenic acids contaminated tailing pond waters in the Athabasca oil sands region—demonstrated field studies and plausible options: a review. Journal of Environmental Science and Health 40(3), 685-722.

Rodriguez, S., Vasquez, L., Costa, D., Romero, A. and Santos, A. (2014) Oxidation of Orange G by persulfate activated by Fe (II), Fe (III) and zero valent iron (ZVI). Chemosphere 101, 86-92.

Siddique, T., Fedorak, P.M. and Foght, J.M. (2006) Biodegradation of short-chain n-alkanes in oil sands tailings under methanogenic conditions. Environ Sci Technol 40(17), 5459-5464.

Son, H.-S., Choi, S.-B., Khan, E. and Zoh, K.-D. (2006) Removal of 1, 4-dioxane from water using sonication: Effect of adding oxidants on the degradation kinetics. Water Res 40(4), 692-698.

Vicente, F., Santos, A., Romero, A. and Rodriguez, S. (2011) Kinetic study of diuron oxidation and mineralization by persulphate: effects of temperature, oxidant concentration and iron dosage method. Chem. Eng. J. 170(1), 127-135.

Waldemer, R.H. and Tratnyek, P.G. (2006) Kinetics of contaminant degradation by permanganate. Environ Sci Technol 40(3), 1055-1061.

Waldemer, R.H., Tratnyek, P.G., Johnson, R.L. and Nurmi, J.T. (2007) Oxidation of chlorinated ethenes by heat-activated persulfate: kinetics and products. Environ Sci Technol 41(3), 1010-1015.

Xu, X.-Y., Zeng, G.-M., Peng, Y.-R. and Zeng, Z. (2012) Potassium persulfate promoted catalytic wet oxidation of fulvic acid as a model organic compound in landfill leachate with activated carbon. Chem. Eng. J. 200, 25-31.

Zhang, X., Wiseman, S., Yu, H., Liu, H., Giesy, J.P. and Hecker, M. (2011) Assessing the toxicity of naphthenic acids using a microbial genome wide live cell reporter array system. Environ Sci Technol 45(5), 1984-1991.

Zhong, H., Brusseau, M.L., Wang, Y., Yan, N., Quig, L. and Johnson, G.R. (2015) In-situ activation of persulfate by iron filings and degradation of 1, 4-dioxane. Water Res 83, 104-111.

Zhou, D., Chen, L., Zhang, C., Yu, Y., Zhang, L. and Wu, F. (2014) A novel photochemical system of ferrous sulfite complex: Kinetics and mechanisms of rapid decolorization of Acid Orange 7 in aqueous solutions. Water Res 57, 87-95.

Zhu, C., Fang, G., Dionysiou, D.D., Liu, C., Gao, J., Qin, W. and Zhou, D. (2016) Efficient transformation of DDTs with Persulfate Activation by Zero-valent Iron Nanoparticles: A Mechanistic Study. J Hazard Mater 316, 232-241.

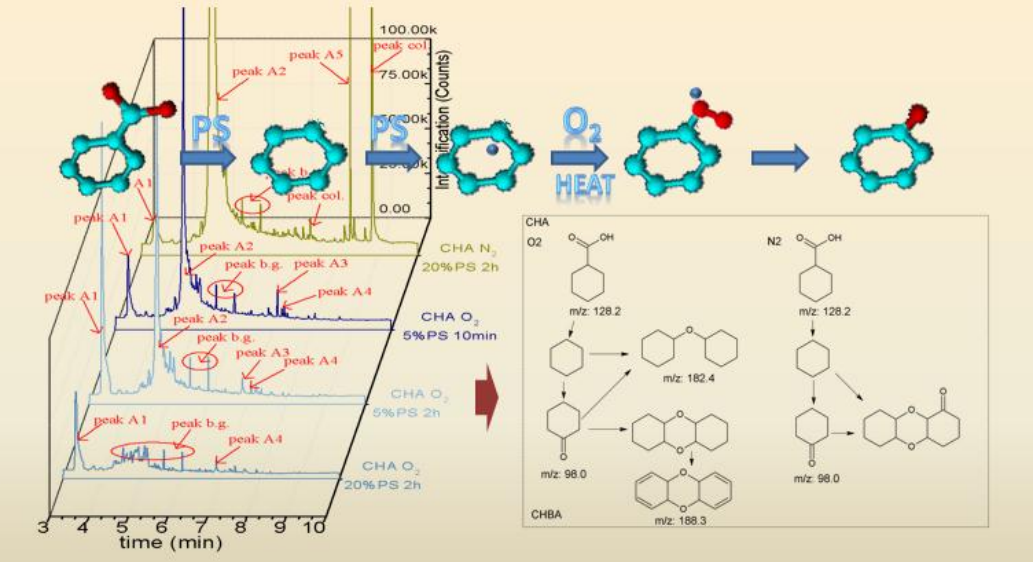

3-2

Mechanism and kinetics of thermally-activated persulfate oxidation of Naphthenic acids in the presence and absence of molecular oxygen

Mecanismo y cinética de la oxidación de ácidos naftenicos mediante persulfato en presencia y ausencia de oxígeno molecular

有氧及无氧条件下过硫酸盐氧化降解环烷酸的反应机理与动力学

3.2.1 Abstract

This research studies the reaction pathways of thermally-activated persulfate (PS) oxidation of model naphthenic acids (NAs) from the analysis of the byproducts upon reaction time. It also provides the kinetics of mineralization. The analyses were performed by gas chromatography with mass spectrometry (GC-MS), flame ionization detector (GC-FID) and ion chromatography (IC). The results suggest that decarboxylation of NAs is the initial step of PS-oxidation under air and inert atmosphere. Cyclohexanone-structured compounds are one of the main intermediates, indicating an oxygen-adding effect upon the reaction. The formation of those compounds relies on the dissolved oxygen since it was significantly hindered in inert atmosphere. This hindering effect was less significant in the case of aromatic rings-bearing NAs than for the saturated ones. The corresponding degradation and ring-opening mechanisms were postulated on the basis of those observations. The mineralization kinetics of each model NA is analyzed. The results demonstrate that the presence of oxygen allows reducing the PS consumption.

3.2.2 Introduction

The previous section showed that thermally-activated (80 °C) PS allows a highly efficient degradation of the NAs tested, where oxygen plays an important role, so that complete mineralization was achieved with PS well below the theoretical stoichiometric amount. This method was more effective toward the NAs with a single cyclohexane ring than for the bicyclic aromatic-ring-bearing ones (Xu et al. 2016). Apart from that, it is of promising applicability also because of the fact that the temperature of 80 °C is about that of the real wastewaters from oil sands processing (Hong et al. 2013, Xu et al. 2016). In fact, the positive effect of oxygen in PS oxidation has been observed by other authors for other organic compounds (Fang et al. 2013, Liu et al. 2016). However, although previous study reported on the decarboxylation of naphthenic rings (Madhavan et al. 1978), further degradation including ring opening mechanism has not been yet elucidated.

The kinetics of PS oxidation of organic contaminants has been described in the literature by pseudo-first-order rate equations (Fang et al. 2013, Waldemer et al. 2007). This approach was also used in the previous section for NAs mineralization, but its validity is restricted since it does not consider the formation of reactive radicals or intermediates (Xu et al. 2016). A model considering distinctive TOC categories has been developed for describing the Fenton mineralization of phenol where the susceptibility of original pollutants and the reaction intermediates towards $HO^{\bullet}$ radicals was considered (Zazo et al. 2009, Pliego et al. 2012). The mineralization kinetics of PS oxidation of NAs, in that respect, can be improved using this model.

The aim of the current section is to investigate the reaction pathway and corresponding mineralization kinetics of PS oxidation of model NAs with

saturated-rings (cyclohexanecarboxylic (CHA) and cyclohexanebutyric acids (CHBA)) and aromatic structures (2-naphthoic (2-NA) and 1,2,3,4-tetrahydro-2-naphthoic acids (1234-T-2-NA)) in the presence and absence of dissolved oxygen. For that purpose, GC-MS and IC has been used to identify the byproducts as a basic information.

3.2.3 Results and discussion

3.2.3.1 Byproducts of thermally-activated PS oxidation of NAs

Oxidation byproducts at various reaction conditions were analyzed. NAs were treated by thermally-activated PS at 80 ^{o}C, with 5 and 20% of the stoichiometric amount for 10 min and 2 h, respectively, under air and inert (N_2) atmosphere. The corresponding total ion chromatographs (TIC) are shown in Fig. 3.2.1 and Table 3.2.1 summarizes the structures assessed to the different peaks.

Four main peaks were detected in the reaction effluents from CHA oxidation but with different intensities depending on the operating conditions. The first peak (A1) with m/z = 98.0 was assessed to cyclohexanone (Cy-one) according to the mass spectra (see Table S1 in the supporting information) and the authentic standard provided by NIST, USA (http://webbook.nist.gov/chemistry). The A2 peak, showing a significant signal, with 128.2 mass ion value corresponded to the remaining CHA. The A3 peak (m/z = 188.3) was tentatively assessed since the authentic standard was unavailable. The molecular weight of this species is higher than that of CHA, so it has been postulated as a condensation compound probably dibenzo-p-dioxin. The species associated to the A4 peak yielded a MS with a high value of m/z (209.3), which can correspond to a condensation product from two decarboxylated CHA with one oxygen atom added (Table 3.2.1).

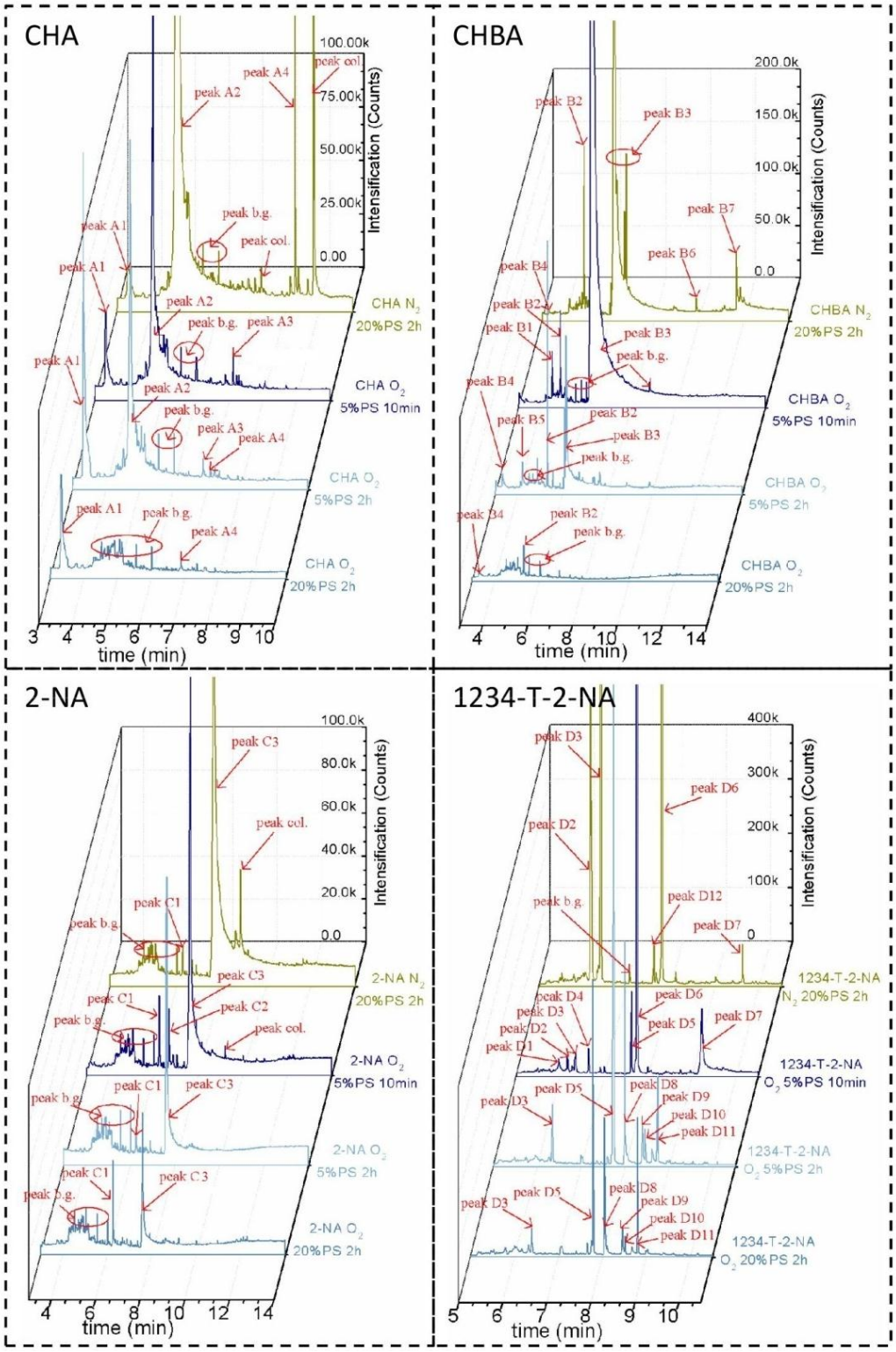

Fig. 3.2.1 TIC of GC-MS analyses of the effluents from PS oxidation of NAs under different conditions.

The oxidation of CHBA with 5% of the stoichiometric amount of PS at short reaction time (10 min) yielded three main peaks. The m/z value of B1 peak was 140.3. The most significant mass ion in its mass spectra is m/z = 97.3 (Table S1), which probably comes from the loss of $–CH_2CH_2CH_3$ (m/z = 43) in the mass spectrometer. That suggests a cyclohexanone-derived structure, as shown in Table 3.2.1. The B2 peak included mass ion of m/z = 122.1 in its structure, which may correspond to decarboxylated CHBA with 4 hydrogen atoms shedding. The B3 peak with m/z = 171.2 was assessed to the remaining CHBA. After 2 h reaction, the intensity of that peak was significantly reduced and B1 peak disappeared, while the B2 one was more pronounced. Besides, two other peaks emerged (B4 and B5), with the m/z values of 98.0 and 126.5, respectively. The mass ion spectrum of the former was similar to that of the A1 peak, assessed to Cy-one, while the second included the structure of the decarboxylated CHBA. With higher amount of PS (20% of the stoichiometric), the intensity of the peaks was greatly reduced and only the B2 and B4 were observed.

Only three peaks of some significance were detected in the effluent from 2-NA oxidation under all the conditions tested. At 5% of the stoichiometric PS and 10 min reaction time, the C1 and C2 peaks were already observed. Their MS spectra include m/z values of 158.2 and 156.1, respectively, whose corresponding assessed structures are given in Table 3.2.1. Peak C3 was identified as remaining 2-NA. Different PS dose or reaction time did not lead to any other detectable reaction byproduct.

Table 3.2.1 Assessed species from PS oxidation of NAs corresponding to Fig. 3.2.1.

Compound	Peak	Retention time(min)	m/z value	Assessed structure	Peak	Retention time(min)	m/z value	Assessed structure
CHA	peak A1	3.34	98.0	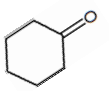	peak A3	7.12	188.3	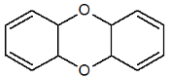
	peak A2	4.81	128.2	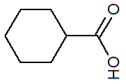 (CHA)	peak A4	8.30	209.3	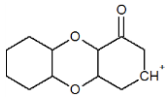
CHBA	peak B1	4.50	140.3	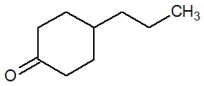	peak B5	4.23	126.5	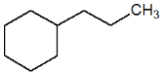
	peak B2	4.89	122.1	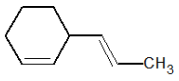	peak B6	9.88	153.3	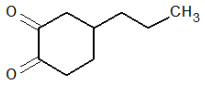
	peak B3	6.28	171.2	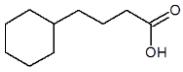 (CHBA)	peak B7	11.68	321.7	Unknown byproduct
	peak B4	3.35	98.0					
2-NA	peak C1	6.27	158.1	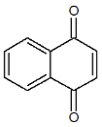	peak C3	7.64	172.3	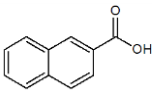 (2-NA)
	peak C2	6.70	156.1	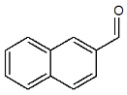				
1234-T-2-NA	peak D1	5.97	132.9	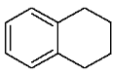	peak D7	9.63	176.8	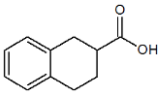 (1234-T-2NA)
	peak D2	6.17	129.8	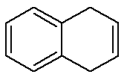	peak D8	7.99	157.8	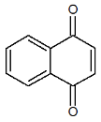
	peak D3	6.40	128.0	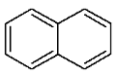	peak D9	8.39	162.0	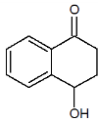
	peak D4	6.65	145.8	 isomers	peak D10	8.45	159.8	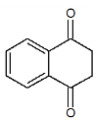 isomers
	peak D5	7.63	145.8	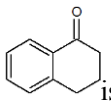 isomers	peak D11	8.74	159.7	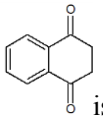 isomers

peak D6	7.74	145.9	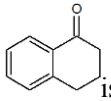 isomers	peak D12	7.79	148.5	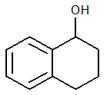

Oxidation of 1234-T-2-NA gave rise to more complex effluents, where at least 12 byproducts could be detected. The D1 peak included the m/z of 132.9, which can be assessed to decarboxylated 1234-T-2-NA, suggesting that decarboxylation is probably the initial step of the oxidation. The D2 and D3 peaks correspond to species giving MS spectra signals of 129.8 and 128 m/z, respectively. These species have similar structure as the one of D1 peak but with various numbers of shedding hydrogen atoms from the saturated hydrocarbon ring. The species associated to D4, D5 and D6 peaks yielded similar m/z values ≈ 146, suggesting that they are probably isomers. These species can correspond to decarboxylated 1234-T-2-NA with one oxygen atom added to the saturated ring to form a carbonyl structure. The D7 peak was identified as the remaining 1234-T-2-NA. Further reaction at longer time up to 2 h or at increasing PS dose up to 20% of the stoichiometry resulted in the disappearance of D1, D2, D4, D6 and D7 peaks and the emergence of new peaks (D8–D11) with quite similar m/z values around 160. They may correspond to related structures with two oxygen atoms added to the saturated ring of decarboxylated 1234-T-2-NA with different number of hydrogen atoms as shown in Table 3.2.1.

3.2.3.2 Discrimination of the reaction byproducts in the presence and absence of oxygen

As has been verified in the section 3.1 and reported by Xu et al (2016), oxygen plays an important role in the PS oxidation of NAs and the significance of this effect varies according to the structure of the target naphthenic acid. In that respect, it is quite important to discriminate the PS-oxidation byproducts in the presence and

absence of oxygen for a deeper insight of the possible reaction pathways.

In the case of CHA after 2 h of PS oxidation under inert atmosphere, only detectable levels of the A1 and A4 peaks were observed together with some other peaks from the back ground or column (Table S1 in supporting information). The A2 peak (remaining CHA) was quite significant compared with the obtained under air atmosphere, confirming the positive effect of oxygen for the breakdown of CHA. The contributions of HO• radicals has been demonstrated in PS oxidation systems especially at alkaline pH(Anipsitakis and Dionysiou 2004). The emergence of more oxygenated species (A4 peak) may be associated to HO• radicals attack.

In the case of CHBA, two peaks (B6 and B7) were detected after PS oxidation under oxygen-free conditions which did not appear when working in air atmosphere. The former included mass ion of 153.3 which can be interpreted as the decarboxylated CHBA with two oxygen atoms added, and the second must correspond to some condensation byproduct possessing a much higher m/z value (321.7) (Table 3.2.1).

No obvious differences were found between the TIC spectra of the 2-NA oxidation in presence and absence of oxygen, confirming the lower effect of oxygen toward aromatic ring-bearing NAs compared to saturated-ring ones. Regarding 1234-T-2-NA, the aforementioned species with two oxygen atoms added were not detected under oxygen-free conditions.

3.2.3.3 Formation of short-chain acids

Determination of the short-chain acids formed during the reaction gives important information on the ring-opening. Thus, the time-course of those acids produced upon the oxidation of NAs under air and inert atmosphere was followed. For that purpose, 40% of the stoichiometric PS amount was used in these

experiments and the reaction time was extended for 4 h. As can be observed in Fig. 3.2.2, the effluents resulting under air atmosphere contained short-chain acids ranging within 1-4 carbon atoms, including formic, acetic, oxalic and fumaric. For the NAs with saturated rings, namely CHA and CHBA, peak concentration of those organic acids were found and frankly low amounts of them remained after 4 h of reaction in agreement with the high mineralization achieved, as previously reported (Xu et al., 2016). This is an advantage of PS oxidation compared to Fenton-based systems, where some certain short-chain acids specially oxalic and acetic are quite refractory to further oxidation (Zazo et al., 2005), even at high temperature (Pliego et al., 2015). The peak values of fumaric acid appeared at the earlier stages of reaction, indicating that it is a primary product from the ring-opening of NAs or intermediates, which further evolves into lower molecular weight acids. The maximum observed for oxalic acid at low reaction times must be associated to the breakage of the side chain of the NAs. For the aromatic ring-bearing NAs (2-NAs and 1234-T-2-NA), the remaining amount of those acids was higher. On the other hand, lower amounts of short-chain acids were formed under inert atmosphere, due to the less effective breakdown of the starting NAs with the PS amount used in absence of dissolved oxygen (Xu et al., 2016). Moreover, fumaric acid was not detected under this condition, confirming the restrained ring-opening of the NAs structures.

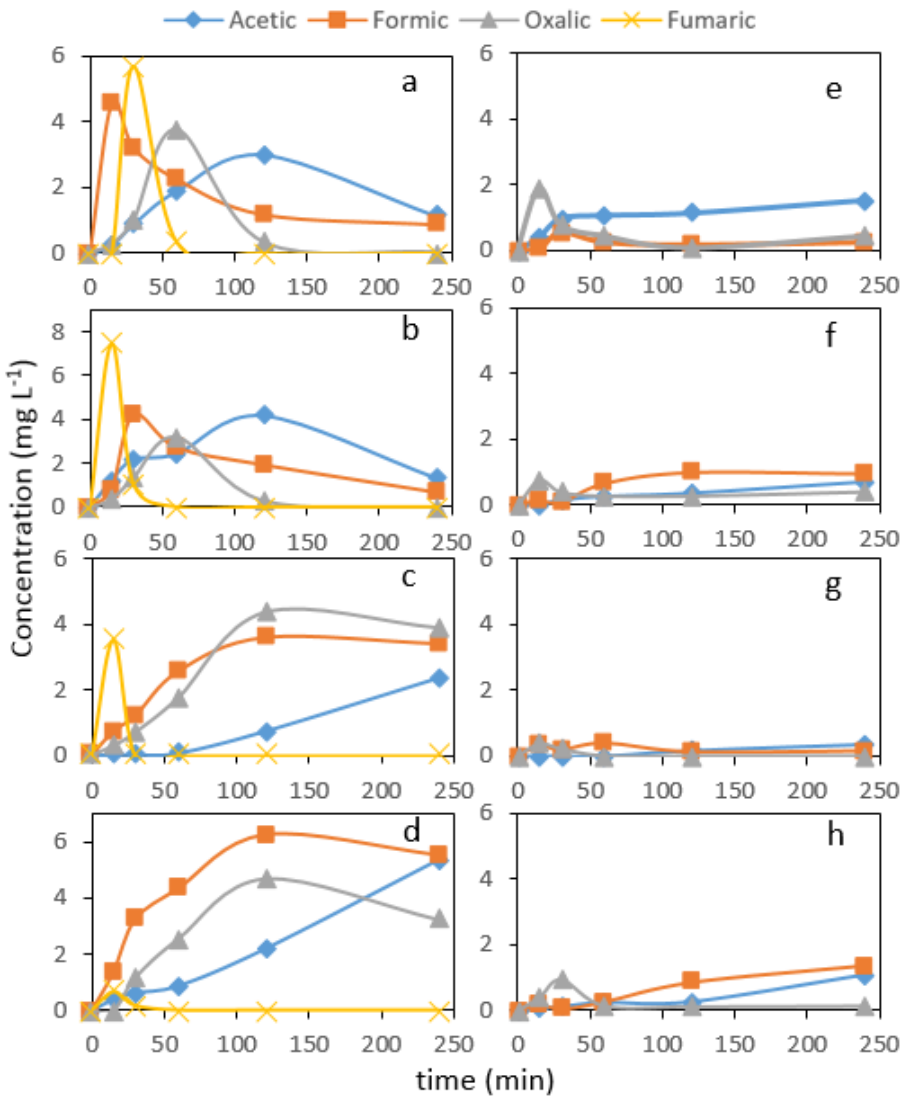

Fig. 3.2.2 Time-course of short-chain organic acids upon PS oxidation of NAs. (a) to (d) correspond, respectively, to CHA, CHBA, 2-NA and 1234-T-2-NA oxidation under air atmosphere; (e) to (h) are the same in oxygen-free conditions ([NA] = 50 mg L^{-1}; [PS] = 40% of the stoichiometric; T = 80 °C)

3.2.3.4 Proposed reaction pathways with and without O_2

3.2.3.4.1 Reaction pathways of CHA degradation

As indicated before, cyclohexanone was the main byproduct from thermally-activated PS oxidation of CHA. The formation of this compound suggests the

possible previous generation of cyclohexane from decarboxylation of CHA by the effect of $SO_4^{\bullet -}$ radicals as the primary degradation step (reaction 1)(Drzewicz et al. 2010, Madhavan et al. 1978). Subsequent hydrogen extraction from the cyclohexane ring would give rise to the corresponding organic radical ($Cy^{\bullet}$) (Drzewicz et al. 2010), which upon reaction with O_2 would produce oxygen-containing intermediate radicals ($CyO_2^{\bullet}$) with the effect of thermally-activated $SO_4^{\bullet -}$, also suggested by Drzewicz et al. (2010) in the UV/H_2O_2 breakdown of CHA.

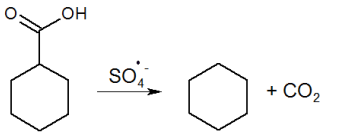

(1)

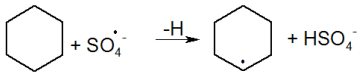

(2)

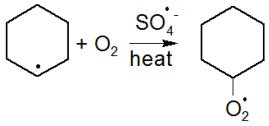

(3)

The $CyO_2^{\bullet}$ radical can degrade following a self-decay pathway described by reactions 4 and 5. The single oxygen-containing product ($CyO^{\bullet}$) from reaction 5 can undergo α-hydrogen shift and then react with more O_2 giving rise to Cy-one (reactions 6-8) (Bothe et al. 1978, Drzewicz et al. 2010).

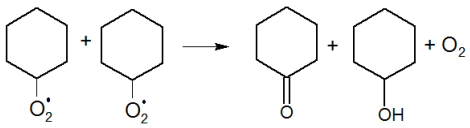

(4)

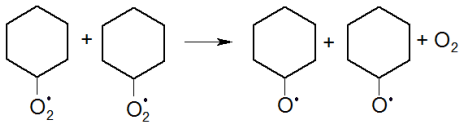

(5)

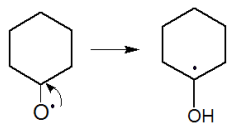

(6)

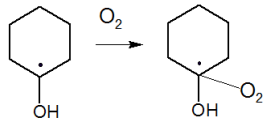

(7)

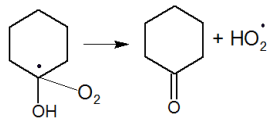

(8)

On the other hand, $CyO_2^{\bullet}$ can also react with cyclohexane to produce another $Cy^{\bullet}$ radical and cyclohexylhydroperoxide ($CyHO_2$) through reaction 9. $CyHO_2$ is quite reactive toward $CyO_2^{\bullet}$, as has been verified by Hermans et al. (2005), giving rise to $Cy^{\bullet}$ (reaction 10).

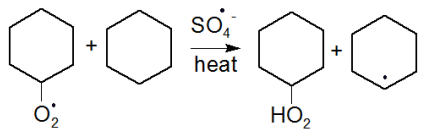

(9)

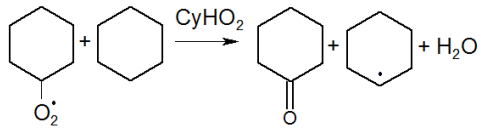

(10)

The time-course of Cy-one in PS oxidation of CHA in air atmosphere shows a rapid formation followed by a slower decay, except at the lowest PS dose tested, when the lack of oxidant hinders further degradation (Fig. 3.2.3). The rate of both formation and decay of Cy-one is consistently related with the amount of PS used.

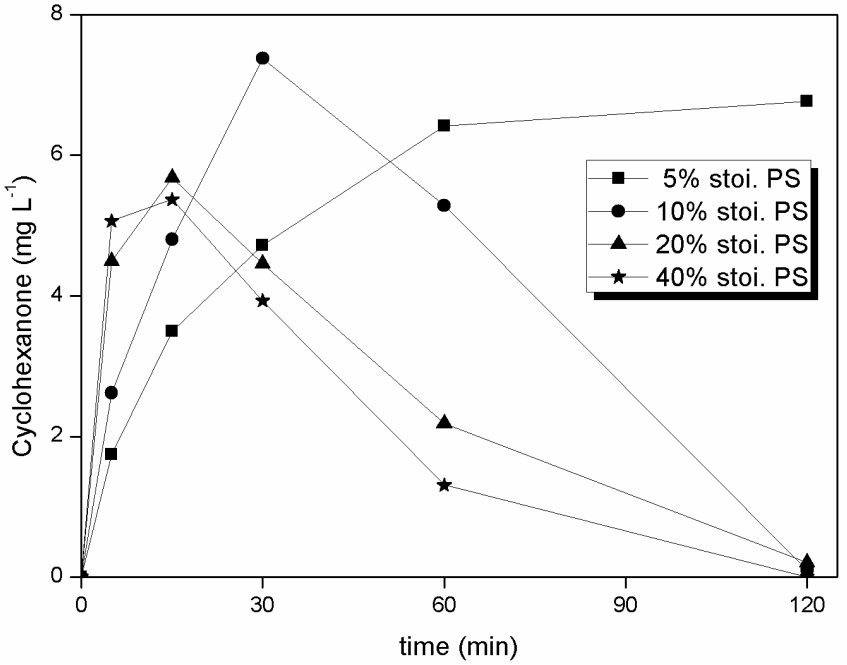

Fig. 3.2.3 Evolution of cyclohexanone upon PS oxidation of CHA in air atmosphere at different amounts of PS (% of the stoichiometric). $[CHA]_0$ = 100 mg L^{-1}; T = 80 °C, pH = 8.

With regard to the mechanism of ring cleavage, the scission may occur at the oxygen-bonded Carbon position (reaction 11) (Drzewicz et al. 2010). A more recent study postulated the formation of an intramolecular-endoperoxide-structured byproduct from the rearrangement of the dioxyl-structured Cy-one (reaction 12 and 13), a key intermediate in PS oxidation of organic species, with the positive effect of oxygen (Liu et al. 2016), which is more likely the case in the current study. The ring scission can occur at one of the carbon positions with C–O bond (reaction 14). Consequently, short-chain organic acids with one to four carbon atoms can be formed, as in fact detected by IC. After ring cleavage, breakdown proceeds toward mineralization.

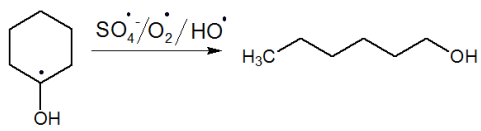

(11)

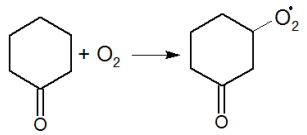

(12)

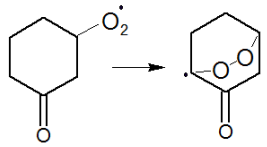

(13)

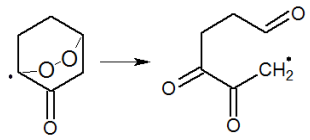

(14)

In addition to these breakdown reactions, condensation (oligomerization) may also occur, as supported by the appearance of higher molecular weight species (Table 3.2.1). For instance, the species giving m/z = 188.3 (peak A3) may result from hydrogen extraction of a Cy-one dimer (Scheme 3.2.1).

In absence of oxygen, less CHA was converted, as depicted in Fig. 3.2.1 being also detected Cy-one, which may result from attack of HO• radicals through a reaction mechanism similar to the proposed by Drzewicz et al. (2010). Instead of the species found under air atmosphere, the A4 peak was detected, which may correspond from two cyclohexane molecules with one oxygen atom added.

3.2.3.4.2 Degradation pathway of other NAs

Similarly to CHA, the initial degradation step of CHBA is decarboxylation as verified by the presence of the species with m/z = 126.5 (peak B5 of Table 3.2.1). This species can decay to cyclohexane and then be oxidized to Cy-one under air atmosphere. The decarboxylated CHBA can also be further oxidized to the corresponding cyclohexanone-like structure with m/z of 140.3 (peak B1) which is absent after reaction under inert atmosphere (Scheme 3.2.1).

The degradation of aromatic-ring 2-NA by PS most likely starts also with decarboxylation and then reaction with oxygen must occur to form the compound with m/z = 158.2 (peak C1). The species giving m/z = 156.1 (peak C2) may be the initial 2-NA without −OH. In the absence of oxygen, no different reaction pathway can be addressed in the case of this NA.

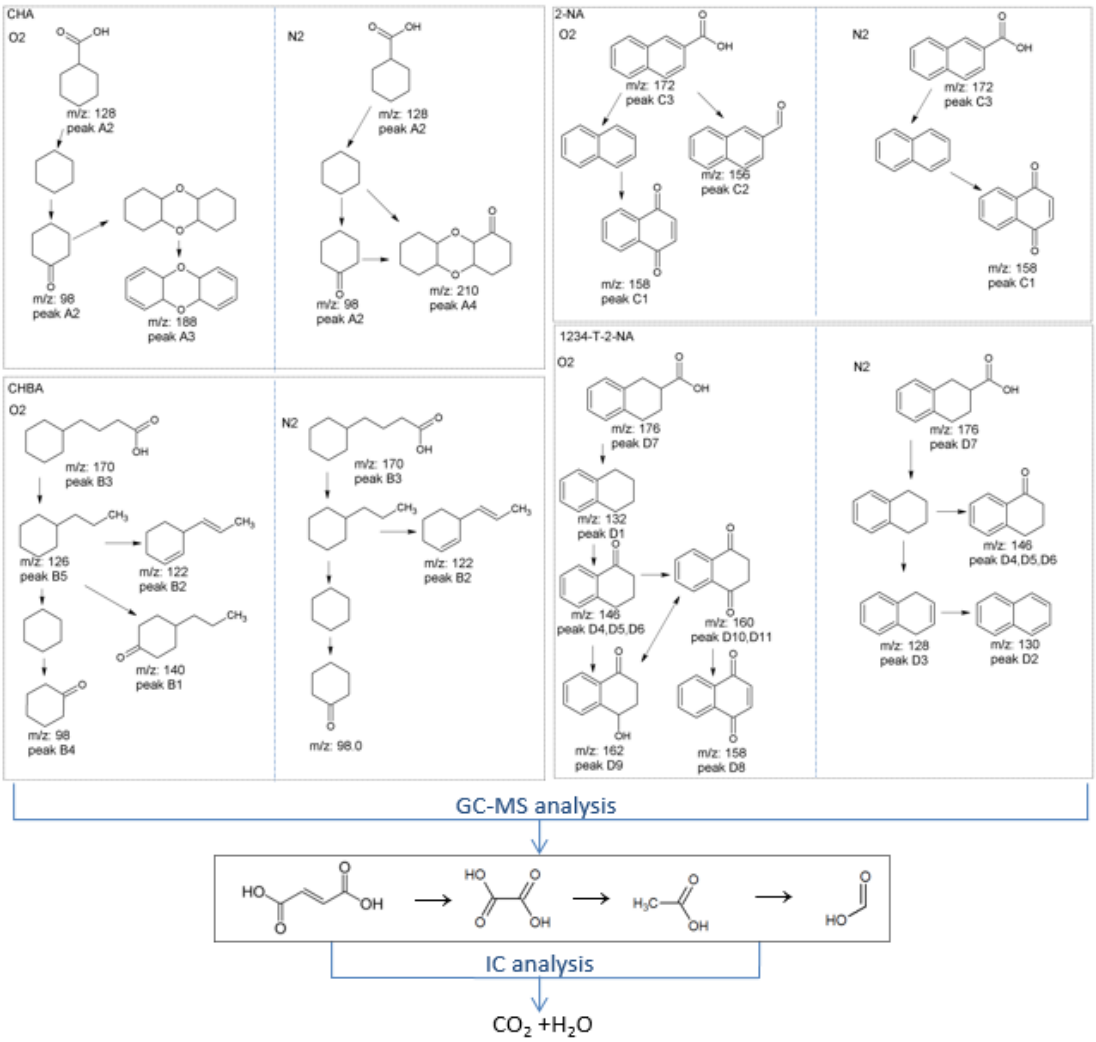

Scheme 3.2.1 Proposed reaction pathways for NAs oxidation by thermally-activated PS.

Regarding 1234-T-2-NA, the decarboxylation step gives rise to the species with m/z = 132.9 (peak D1) after which the single oxygen atom addition occurs to

form the cyclohexanone-structured compound (m/z = 145.8, peak D4). Another oxygen atom can also be added to form the detected compounds with m/z values from 157.8 to 162.0 with various hydrogen atom numbers. Under inert atmosphere, however, much less amount of oxygenated species was formed but more decarboxylated 1234-T-2-NA was detected, with m/z = 129.8 (peak D2) and 128.0 (peak D3).

The proposed reaction pathways are summarized in the Scheme 3.2.1.

3.2.3.5 Kinetic study

The kinetics of mineralization of NAs has been simply fitted to a pseudo-first order rate equation in the previous section (Xu et al. 2016). An obvious lag period of the early stage for the NAs' mineralization was observed especially at relatively high PS doses like 100% stoichiometric. That was probably because of the variation of the predominant reactive species and the emergence of certain intermediates with different reactivity along the course of the reaction. Thus, different TOC lumps can be assumed related with the susceptibility of the corresponding species to mineralization. Following this approach, a kinetic model is proposed to describe the time-course of TOC upon PS oxidation of NAs based on the reaction scheme below:

In presence of oxygen (air atmosphere):

$$\begin{array}{l} CO_2 \\ \uparrow k_2 \end{array}$$

$$TOC_A + SO_4^{\bullet -}/O_2^{\bullet} \xrightarrow{k_1} TOC_B + SO_4^{\bullet -}/O_2^{\bullet} \xrightarrow{k_3} CO_2 \qquad \text{(E1)}$$

$$SO_4^{\bullet -} + e^- \xrightarrow{k_s} SO_4^{2-} \qquad \text{(E2)}$$

$$TOC = TOC_A + TOC_B \qquad \text{(E3)}$$

The corresponding rate equations can be written:

$$-\frac{dTOC_A}{dt} = (k_1 + k_2)TOC_A[SO_4^{\bullet-}] \quad (E4)$$

$$\frac{dTOC_B}{dt} = k_1 TOC_A[SO_4^{\bullet-}] - k_3 TOC_B[SO_4^{\bullet-}] \quad (E5)$$

$SO_4^{\bullet-}$ decomposition has been reported to follow first-order kinetics (Furman et al. 2010):

$$-\frac{d[SO_4^{\bullet-}]}{dt} = k_S[SO_4^{\bullet-}] \quad (E6)$$

Under oxygen-free conditions (inert atmosphere):

$$TOC_{AN} + SO_4^{\bullet-} \xrightarrow{k_{S1}} TOC_{BN} + SO_4^{\bullet-} \xrightarrow{k_{S3}} CO_2 \quad (E7)$$

(CO_2 ↑ k_{S2})

$$SO_4^{\bullet-} + e^- \xrightarrow{k_{Ss}} SO_4^{2-} \quad (E8)$$

$$-\frac{dTOC_{AN}}{dt} = (k_{S1} + k_{S2})TOC_{AN}[SO_4^{\bullet-}] \quad (E9)$$

$$\frac{dTOC_{BN}}{dt} = k_{S1}TOC_{AN}[SO_4^{\bullet-}] - k_{S3}TOC_{BN}[SO_4^{\bullet-}] \quad (E10)$$

$$TOC_N = TOC_{AN} + TOC_{BN} \quad (E11)$$

$$-\frac{d[SO_4^{\bullet-}]}{dt} = k_{SS}[SO_4^{\bullet-}] \quad (E12)$$

Considering both the k_n and k_{Sn} (n = 1, 2, 3 and S) values in the presence and absence of oxygen respectively, the apparent enhancing contribution of oxygen in the PS-oxidation system can be expressed by:

$$k_{On} = k_n - k_{Sn} \quad (E13)$$

The experimental TOC vs. time data obtained at 80 °C with the stoichiometric PS dose in the presence and absence of oxygen were fitted to the corresponding

model and the values obtained for the rate constants are summarized in Table 3.2.2 with the corresponding correlation coefficients.

Table 3.2.2 Rate constants for the proposed kinetic models of PS oxidation of NAs with and without oxygen. Conditions: PS = 100% stoichiometry; T = 80 °C.

compounds	rate constants (L mg^{-1} min^{-1})				
	PS/O_2 co-contribution				
	k_1	k_2	k_3	k_S (min^{-1})	R^2
CHA	5.05×10^{-2}	2.10×10^{-3}	5.24×10^{-2}	6.83×10^{-3}	0.980
CHBA	7.94×10^{-2}	4.52×10^{-4}	7.96×10^{-2}	7.91×10^{-3}	0.990
2-NA	3.19×10^{-2}	6.28×10^{-5}	3.20×10^{-2}	8.75×10^{-3}	0.993
1234-T-2NA	4.94×10^{-2}	6.60×10^{-5}	4.97×10^{-2}	6.93×10^{-3}	0.992
	PS contribution (oxygen-free)				
	k_{S1}	k_{S2}	k_{S3}	k_{SS} (min^{-1})	R^2
CHA	1.71×10^{-2}	5.57×10^{-3}	2.28×10^{-2}	8.16×10^{-3}	0.993
CHBA	5.40×10^{-2}	3.32×10^{-4}	1.22×10^{-2}	1.35×10^{-2}	0.991
2-NA	8.89×10^{-3}	2.61×10^{-5}	1.04×10^{-2}	1.25×10^{-2}	0.993
1234-T-2NA	1.55×10^{-3}	9.68×10^{-4}	3.22×10^{-4}	9.85×10^{-3}	0.999
	O_2 contribution				
	k_{O1}	k_{O2}	k_{O3}	k_{OS} (min^{-1})	R^2
CHA	3.34×10^{-2}	-3.47×10^{-3}	2.96×10^{-2}	-1.35×10^{-3}	0.973
CHBA	2.54×10^{-2}	1.20×10^{-4}	6.74×10^{-2}	-5.59×10^{-3}	0.981
2-NA	2.30×10^{-2}	3.67×10^{-5}	2.16×10^{-2}	-3.75×10^{-3}	0.986
1234-T-2NA	4.79×10^{-2}	-9.61×10^{-3}	4.97×10^{-2}	-2.92×10^{-3}	0.991

As can be seen, the k_1 and k_{S1} values are always substantially higher than those of k_2 and k_{S2} respectively confirming that the starting NAs (TOC_A) evolves essentially to oxidation intermediates rather than direct mineralization, although this last is also possible as a minor contribution (Xu et al. 2016). Oxygen enhances the conversion of the starting NAs into oxidation intermediates (TOC_A to TOC_B) since the k_{O1} values are all positive. The negative values of k_{O2} in the oxidation of CHA and 1234-T-2-NA suggest some hindering effect of oxygen on the direct mineralization of these two NAs at the early stages. However, the final mineralization was enhanced as indicated by the positive values of k_{O3}. The

negative values of k_{os} confirm the reduced PS consumption in the presence of oxygen.

3.2.4 Conclusions

The byproducts of CHA oxidation by thermally-activated PS in the presence and absence of oxygen have been analyzed and reaction mechanisms are proposed. Decarboxylation appears in the initial step of PS oxidation of NAs. Cyclohexanone has been identified as a main intermediate of CHA oxidation under air atmosphere, while only trace amounts were found in oxygen-free conditions, due to the lower contribution of $HO^{\bullet}$ radicals. Similar cyclohexanone-like species were also detected in the cases of the other NAs tested but their significance was lower for the aromatic ring-bearing ones. This provides a possible explanation for the stronger effect of oxygen with the saturated ring-bearing NAs than with the aromatic ones. The kinetics of mineralization upon PS oxidation with and without oxygen was well described by analogous models based on TOC lumps. The values of the kinetic constants confirm the positive effect of oxygen on the rate of mineralization as well as on the PS consumption.

References

Anipsitakis, G.P. and Dionysiou, D.D. (2004) Radical generation by the interaction of transition metals with common oxidants. Environ Sci Technol 38(13), 3705-3712.

Bataineh, M., Scott, A., Fedorak, P. and Martin, J. (2006) Capillary HPLC/QTOF-MS for characterizing complex naphthenic acid mixtures and their microbial transformation. Anal Chem 78(24), 8354-8361.

Bothe, E., Schuchmann, M.N., Schulte-Frohlinde, D. and Sonntag, C.v. (1978) HO_2 elimination from α-hydroxyalkylperoxyl radicals in aqueous solution. Photochemistry and photobiology 28(4-5), 639-643.

Brown, L.D. and Ulrich, A.C. (2015) Oil sands naphthenic acids: A review of properties, measurement, and treatment. Chemosphere 127, 276-290.

Drzewicz, P., Afzal, A., El-Din, M.G. and Martin, J.W. (2010) Degradation of a model naphthenic acid, cyclohexanoic acid, by vacuum UV (172 nm) and UV (254 nm)/H_2O_2. The Journal of Physical Chemistry A 114(45), 12067-12074.

Drzewicz, P., Perez-Estrada, L., Alpatova, A., Martin, J.W. and Gamal El-Din, M. (2012) Impact of peroxydisulfate in the presence of zero valent iron on the oxidation of cyclohexanoic acid and naphthenic acids from oil sands process-affected water. Environ Sci Technol 46(16), 8984-8991.

Fang, G.-D., Dionysiou, D.D., Al-Abed, S.R. and Zhou, D.-M. (2013) Superoxide radical driving the activation of persulfate by magnetite nanoparticles: Implications for the degradation of PCBs. Appl. Catal. B-Environ. 129, 325-332.

Furman, O.S., Teel, A.L. and Watts, R.J. (2010) Mechanism of base activation of persulfate. Environ Sci Technol 44(16), 6423-6428.

Han, X., MacKinnon, M.D. and Martin, J.W. (2009) Estimating the in situ biodegradation of naphthenic acids in oil sands process waters by HPLC/HRMS. Chemosphere 76(1), 63-70.

Hermans, I., Nguyen, T.L., Jacobs, P.A. and Peeters, J. (2005) Autoxidation of cyclohexane: Conventional views challenged by theory and experiment. ChemPhysChem 6(4), 637-645.

Hong, P.A., Cha, Z., Zhao, X., Cheng, C.-J. and Duyvesteyn, W. (2013) Extraction of bitumen from oil sands with hot water and pressure cycles. Fuel Processing Technology 106, 460-467.

Kamaluddin, M. and Zwiazek, J.J. (2002) Naphthenic acids inhibit root water transport, gas exchange and leaf growth in aspen (Populus tremuloides) seedlings. Tree physiology 22(17), 1265-1270.

Kannel, P.R. and Gan, T.Y. (2012) Naphthenic acids degradation and toxicity mitigation in tailings wastewater systems and aquatic environments: a review. J Environ Sci Health A Tox Hazard Subst Environ Eng 47(1), 1-21.

Leung, S.S., MacKinnon, M.D. and Smith, R.E. (2003) The ecological effects of naphthenic acids and salts on phytoplankton from the Athabasca oil sands region. Aquatic Toxicology 62(1), 11-26.

Liang, X., Zhu, X. and Butler, E.C. (2011) Comparison of four advanced oxidation processes for the removal of naphthenic acids from model oil sands process water. J Hazard Mater 190(1-3), 168-176.

Liu, H., Bruton, T.A., Li, W., Buren, J.V., Prasse, C., Doyle, F.M. and Sedlak, D.L. (2016) Oxidation of benzene by persulfate in the presence of Fe (III)-and Mn (IV)-containing oxides: stoichiometric efficiency and transformation products. Environ Sci Technol 50(2), 890-898.

Madhavan, V., Levanon, H. and Neta, P. (1978) Decarboxylation by SO_4-radicals. Radiation Research 76(1), 15-22.

Martin, J.W., Barri, T., Han, X., Fedorak, P.M., El-Din, M.G., Perez, L., Scott, A.C. and Jiang, J.T. (2010) Ozonation of oil sands process-affected water accelerates microbial bioremediation. Environ Sci Technol 44(21), 8350-8356.

Melvin, S.D. and Trudeau, V.L. (2012) Toxicity of naphthenic acids to wood frog tadpoles (Lithobates sylvaticus). Journal of Toxicology and Environmental Health, Part A 75(3), 170-173.

Pliego, G., Zazo, J.A., Blasco, S., Casas, J.A. and Rodriguez, J.J. (2012) Treatment of highly polluted hazardous industrial wastewaters by combined coagulation–adsorption and high-temperature Fenton oxidation. Ind Eng Chem Res 51(7), 2888-2896.

Pliego G, Zazo JA, Garcia-Muñoz P, Munoz M, Casas JA, Rodriguez JJ. Trends in the intensification of the Fenton process for wastewater treatment: an overview. Crit Rev Environ Sci Technol 2015; 45: 2611-2692.

Rowland, S.J., Scarlett, A.G., Jones, D., West, C.E. and Frank, R.A. (2011) Diamonds in the rough: identification of individual naphthenic acids in oil sands process water. Environ Sci Technol 45(7), 3154-3159.

Scarlett, A., Reinardy, H., Henry, T., West, C., Frank, R., Hewitt, L. and Rowland, S. (2013) Acute toxicity of aromatic and non-aromatic fractions of naphthenic acids extracted from oil sands process-affected water to larval zebrafish. Chemosphere 93(2), 415-420.

Waldemer, R.H., Tratnyek, P.G., Johnson, R.L. and Nurmi, J.T. (2007) Oxidation of chlorinated ethenes by heat-activated persulfate: kinetics and products. Environ Sci Technol 41(3), 1010-1015.

Wan, Y., Wang, B., Khim, J.S., Hong, S., Shim, W.J. and Hu, J. (2014) Naphthenic acids in coastal sediments after the Hebei Spirit oil spill: a potential indicator for oil contamination. Environ Sci Technol 48(7), 4153-4162.

West, C.E., Jones, D., Scarlett, A.G. and Rowland, S.J. (2011) Compositional heterogeneity may

limit the usefulness of some commercial naphthenic acids for toxicity assays. Sci Total Environ 409(19), 4125-4131.

Xu, X., Pliego, G., Zazo, J.A., Casas, J.A. and Rodriguez, J.J. (2016) Mineralization of naphtenic acids with thermally-activated persulfate: The important role of oxygen. J Hazard Mater 318, 355-362.

Zazo, J., Casas, J., Mohedano, A. and Rodriguez, J. (2009) Semicontinuous Fenton oxidation of phenol in aqueous solution. A kinetic study. Water Res 43(16), 4063-4069.

Zhang, Y., Klamerth, N., Chelme-Ayala, P. and Gamal El-Din, M. (2016) Comparison of nitrilotriacetic acid and [S, S]-ethylenediamine-N, N'-disuccinic acid in UV-Fenton for the treatment of oil sands process-affected water at natural pH. Environ Sci Technol.

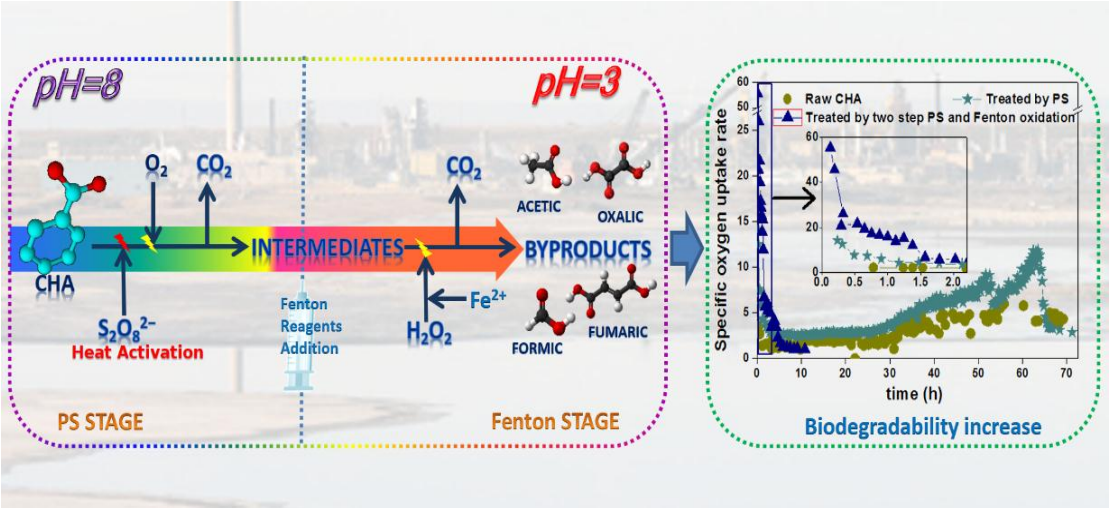

3-3

Two-step persulfate and Fenton oxidation of naphthenic acids in water

Oxidación sulfato y Fenton en dos estapas de ácidos nafténicos en agua

环烷酸溶液的过硫酸盐-芬顿联合氧化降解

3.3.1 Abstract

In this section, two-step persulfate (PS) and Fenton oxidation has been investigated for the mineralization of naphthenic acids (NAs) at 80 ^{o}C and circumneutral initial pH. The effects of PS and H_2O_2 doses, iron concentration, duration of the PS oxidation step and operating temperature have been assessed using cyclohexanoic acid (CHA, 50 mg L^{-1}) as the model compound. The combined treatment allowed up to ≈ 80% mineralization of CHA with using fairly low relative amounts of reagents (20 and 30% of the stoichiometric for PS and H_2O_2, respectively). A kinetic model combining both the PS and Fenton oxidation stages is proposed to describe the rate of TOC removal, where the values of rate constants and apparent activation energy are provided. The system was also successfully tested with other NAs including saturated ring as well as aromatic structures, namely cyclohexanebutyric acid (CHBA), 2-naphthoic acid (2-NA) and 1,2,3,4-tetrahydro-2-naphthoic acid (1234-T-2-NA). Treatment of the NAs tested by this system gave rise to easily biodegradable effluents which included mainly short-chain organic acids, as confirmed by ionic chromatography (IC), BOD_5/COD ratio and respirometric tests. The results show the potential application of this approach as a promising cost-effective solution for the treatment of NAs-bearing aqueous wastes.

3.3.2 Introduction

The previous sections demonstrated that oxygen is able to participate in the mineralization of NAs by the thermally-activated PS oxidation to result in high efficiency, as also reported in our previous work (Xu et al., 2016). Nonetheless, the PS-based approach has its own drawbacks for practical use like the introduction of copious sulfur element and high cost due to the PS consumption.

Fenton oxidation is one of the main AOP systems and has been recognized as a cost-effective solution for a number of industrial wastewaters (Bautista et al., 2008; Pignatello et al., 2006). Fenton process can also be intensified by increasing the temperature (i.e. high temperature Fenton, HTF) (Pliego et al., 2014; Zazo et al., 2010). However, this approach has been rarely attempted for NAs breakdown, due partially to the basic pH of the OSPWs containing NAs (Drzewicz et al., 2012; Liang et al., 2011) and also to the complexation of Fe by NAs which hinders the activity of Fe ion in the solution (Laredo et al., 2004). In fact, several efforts have been made to adapt the Fenton-based technology to a wider range of pH (Barona et al., 2015). Recently, Zhang et al. (2016a, b and c) used chelate-Fenton systems to treat CHA at basic condition. However, the scavenging effect of the chelate agents toward $HO^{\bullet}$ radicals represents a main drawback regarding H_2O_2 consumption and on the other hand it has to be considered the possible increase of toxicity derived from them and/or their degradation byproducts.

The reactions involved in PS oxidation yield important amounts of protons (Drzewicz et al., 2012; Xu et al., 2012), thus giving rise to strong decrease of pH. The as-generated OSPWs are commonly characterized by a moderately basic pH (≈ 8) and a temperature well above the ambient (≈ 80 ^{o}C) used in the oil sand extraction process (Hong et al., 2013; Kannel and Gan, 2012).

Therefore, a treatment based on thermally-activated PS oxidation followed Fenton to deal with NAs from OSPWs could achieve several objectives. The first step allows a significant mineralization of NAs (Xu et al., 2016) while reducing the pH to the optimum range for the Fenton process. The effluent from this step would also reduce the Fe-NA complexation, improving the following Fenton oxidation step. A convenient combination of those two AOPs could provide a high mineralization of NAs giving rise to a final effluent of lower toxicity and easily biodegradable at much lower expense by replacing PS with more cost-effective Fenton reagents without the need of acidifying agents.

The aim of this study is to assess the efficiency of this approach for the abatement of model NAs, namely cyclohexanoic acid (CHA), cyclohexanebutyric acid (CHBA), 2-naphthoic acid (2-NA) and 1,2,3,4-tetrahydro-2-naphthoic acid (1234-T-2-NA), which include naphthenic ring and aromatic structures. To that end, CHA was used as model compound to analyze the effect of the operating variables as well as the kinetics of TOC removal. Then, the effluents from the oxidation of all the four NAs tested were studied to address the improvement of biodegradability by the current approach.

3.3.3 Results and discussion

CHA mineralization by conventional Fenton oxidation was firstly checked at initial pH = 3 and 80 ^{o}C with 40 and 100% of the stoichiometric amount of H_2O_2 and 5 mg L^{-1} Fe^{2+}. The results are shown in Fig. 3.3.1 together with those obtained upon PS only and PS/H_2O_2 simultaneous oxidation at the same temperature and initial pH = 8, using 20 % of the stoichiometric amount.

Fairly poor mineralization (≈ 18%) was achieved by only Fenton oxidation even using H_2O_2 at 239 mg L^{-1} (i.e. 100% of the stoichiometric). Slow

decomposition of H_2O_2 was observed (≈ 25%, after 6 h of reaction) associated to a continuous reduction of the measured Fe concentration down to less than 1 mg L^{-1} whereas the pH was still at the optimum value for the Fenton process (≈ 3). That might be due to the complexation of Fe by CHA (Laredo et al., 2004). On the other hand, PS oxidation yielded 40% mineralization at 20% of the stoichiometric amount. Simultaneous PS/Fenton oxidation with PS and H_2O_2 at 20 and 40% of the stoichiometric, respectively, led to only slightly higher mineralization than the sole PS at the same dose (20%), in spite that certain synergetic effect has been reported by other authors in PS/H_2O_2 oxidation (Hilles et al., 2016; Liang et al., 2014).

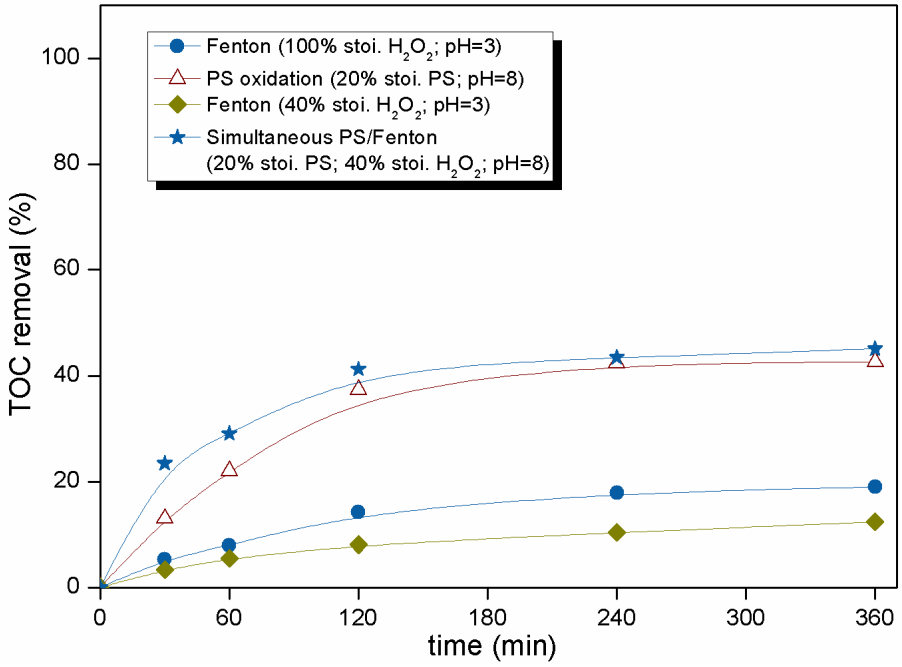

Fig. 3.3.1 CHA mineralization by various oxidation approaches (Fe^{2+} at 5 mg L^{-1} in Fenton; T = 80 °C).

3.3.3.1 Two-step PS and Fenton oxidation

Based on the important pH reduction caused by PS oxidation, a combination of PS and subsequent Fenton oxidation was investigated. The amount of PS as well

as the reaction time in the PS oxidation step will affect to the pH and composition of the resulting effluent which enters the following Fenton oxidation step. Different experiments were performed using 1, 5, 10 and 20% of the stoichiometric PS with CHA at 50 mg L^{-1} and 2 h reaction time, followed by Fenton oxidation with 95.6 mg L^{-1} of H_2O_2 (40% of the stoichiometric) and 5 mg L^{-1} Fe^{2+}.

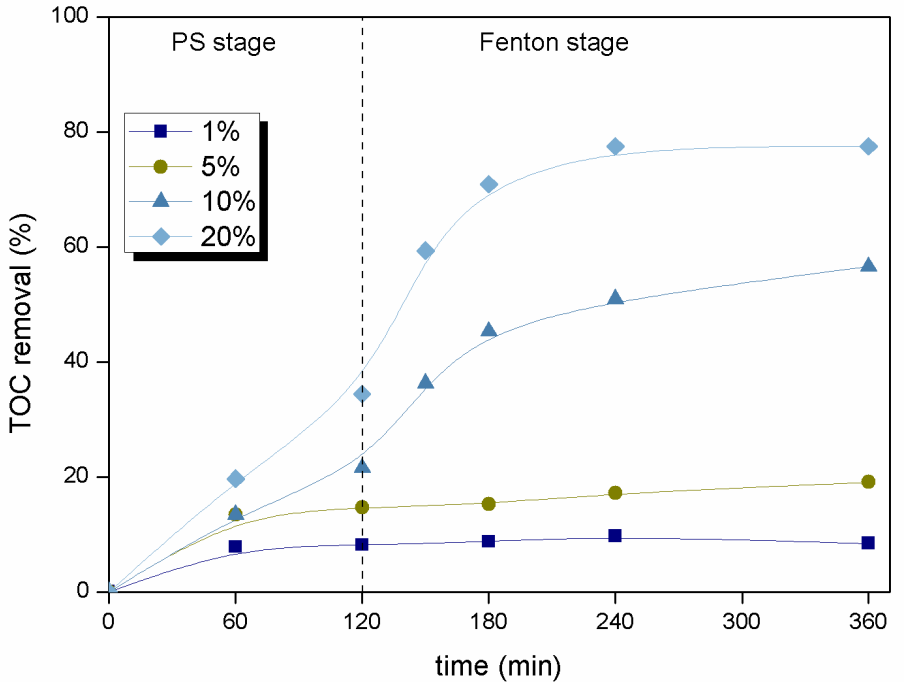

Fig. 3.3.2 Two-step PS(2 h)-Fenton(4 h) oxidation of CHA (50 mg L^{-1}) at 80 °C with different PS amounts (% of the stoichiometric). Fenton step with H_2O_2 at 40% of the stoichiometric and Fe^{2+} at 5 mg L^{-1}.

The results are shown in Fig. 3.3.2, where it can be seen the important effect of increasing the PS dose within the range tested. Below 10% of the stoichiometric, the subsequent Fenton step has no significant effect. Beyond that PS dose, further Fenton oxidation becomes increasingly efficient while effective H_2O_2 decomposition was observed and the measured Fe concentration remained stable in the vicinity of 5 mg L^{-1}. This can be explained by the pre-degradation extent of CHA so that iron naphthenates are not formed, but also by the fact that the pH of

the effluent from the PS step approaches to the optimum for Fenton oxidation (≈ 3) as the PS dose is increased. In fact, PS oxidation alone at higher dose of around 35% of the stoichiometric allows achieving 80% mineralization of CHA (Xu et al., 2016). Now, the combination with a subsequent Fenton treatment provides a way of reducing the PS needs to one-half by using much cheaper Fenton reagents while still maintaining close to that mineralization extent. The remaining TOC in the current system corresponds to short-chain organic acids of very low significance in terms of toxicity. The combined system substantially improves the TOC removal achieved by PS oxidation alone at the same PS dose (see Fig. 3.3.1). It is true that the reduction of the PS amount is accompanied by a complementary addition of H_2O_2 to accomplish further Fenton oxidation, so the amount of H_2O_2 must be conveniently adjusted to minimize total reagent consumption.

Fig. 3.3.3 shows the results obtained with different H_2O_2 doses expressed as percent of the theoretical stoichiometric amount relative to initial CHA. The PS amount in the previous step was always 20% of the stoichiometric. As can be seen, the extent of mineralization in the Fenton step increased significantly with the H_2O_2 dose up to around 30% of the stoichiometric and then the remaining TOC (corresponding mostly to short-chain organic acids) seems refractory to Fenton oxidation. Increasing the Fe^{2+} dose above 5 mg L^{-1} neither showed any significant effect on the Fenton step.

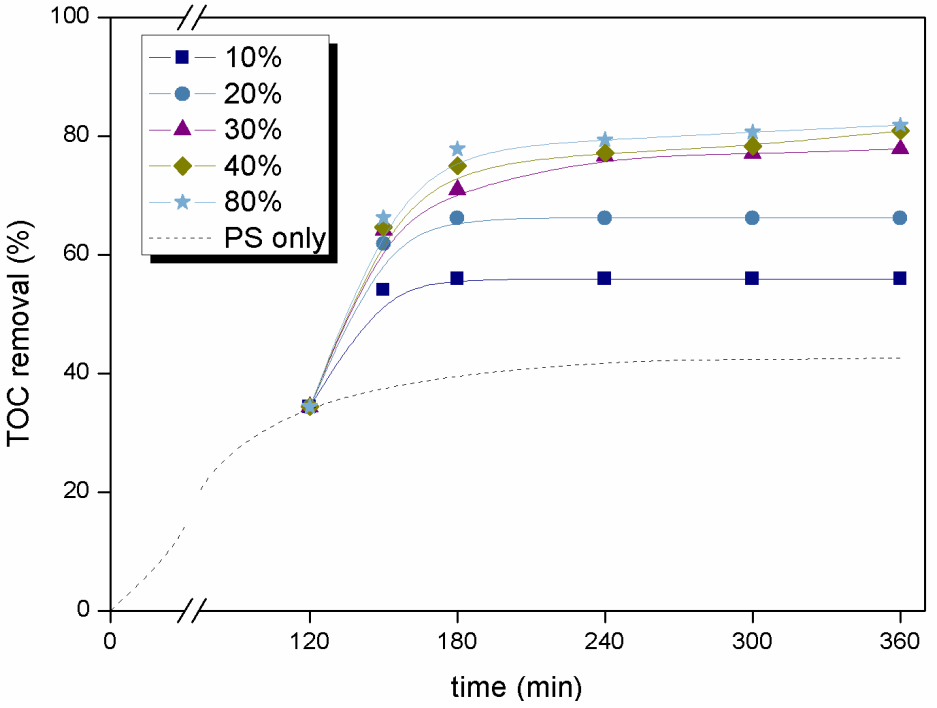

Fig. 3.3.3 Two-step PS (120 min)-Fenton oxidation of CHA (50 mg L^{-1}) at 80 ºC with different H_2O_2 amounts (% of the stoichiometric) in the Fenton step. PS at 20% of stoichiometric and Fe^{2+} at 5 mg L^{-1}.

The duration of the PS step was also varied since it can affect to the extent of CHA breakdown in that stage and consequently to the evolution of TOC upon further Fenton oxidation. Fig. 3.3.4 shows the results obtained upon different time durations for the PS reaction. As can be seen, the overall TOC removal of the combined system decreased significantly when the PS oxidation step lasted less than 1.5-2 h.

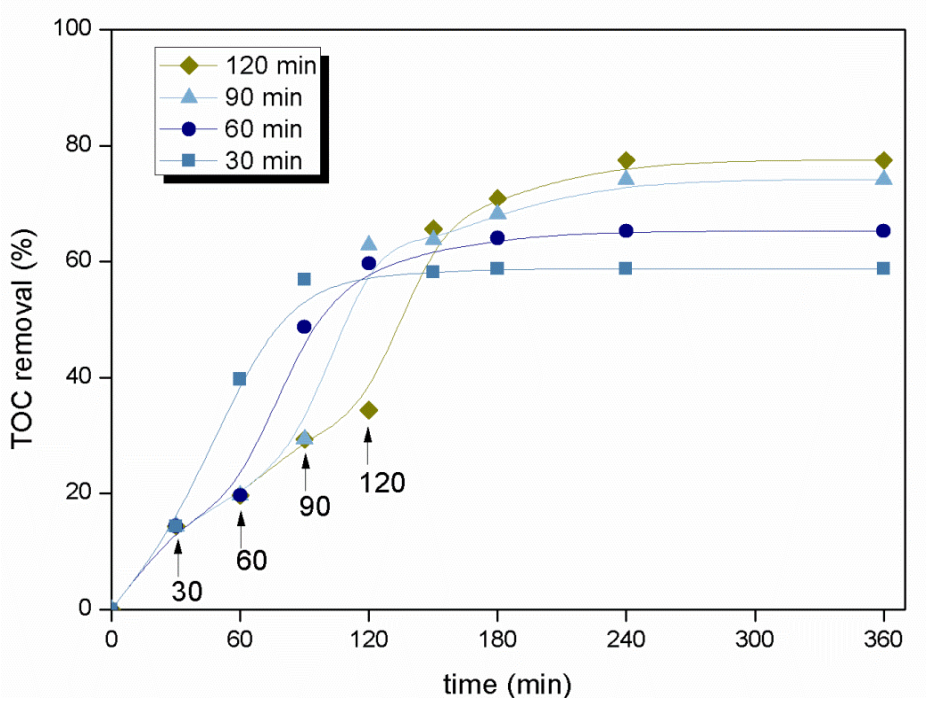

Fig. 3.3.4 Two-step PS and Fenton oxidation of CHA (50 mg L^{-1}) at 80 °C with different PS step durations. PS and H_2O_2 at 20 and 40% of the stoichiometric, respectively.

Finally, the effect of initial pH was studied within the range of 3 to 12, using 20% of the stoichiometric amount of PS in the first step, and 40% of the stoichiometric H_2O_2 with 5 mg L^{-1} Fe^{2+} in the sequent Fenton. As can be observed in Fig. 3.3.5, the initial pH had no significant effect on CHA mineralization, given the fact that the pH evolved always to around 3 in the PS oxidation step. Therefore, this two-step PS and Fenton system does not need any artificial correction of the initial pH of the wastewater to be treated.

Summarizing, the combined PS and Fenton system shows significant advantage compared to the only thermally-activated PS and to Fenton oxidation. It mineralizes close to 80% of CHA (50 mg L^{-1}) working at 80 °C (thermally-activated PS) with PS and H_2O_2 at 20 and 30% of the stoichiometric amount, respectively. That represents ≈ 335 mg L^{-1} of sodium PS and 75 mg L^{-1} of H_2O_2 (plus 5 mg L^{-1} Fe^{2+}) in terms of reagents consumption. Fenton alone is far from achieving that

objective even at high H_2O_2 doses (100% of the stoichiometric) whereas PS oxidation by itself would require around 35% of the stoichiometric amount, i.e. ≈ 586 mg L^{-1} of sodium PS. Therefore, about 251 mg L^{-1} sodium PS are substituted by ≈ 75 mg L^{-1} of H_2O_2 in the combined treatment. At average industrial prices of around 1100 \$ t^{-1} for the former, 250 \$ t^{-1} (35% solution) for H_2O_2 and 46 \$ t^{-1} for $FeSO_4 \cdot 7H_2O$, the combined treatment system means a much lower cost in terms of reagent consumption (reduced by ≈ 80% for the Fenton oxidation step and 35% for the overall cost) and also has the additional advantage of significantly lower sulfate and sodium concentration in the final effluent.

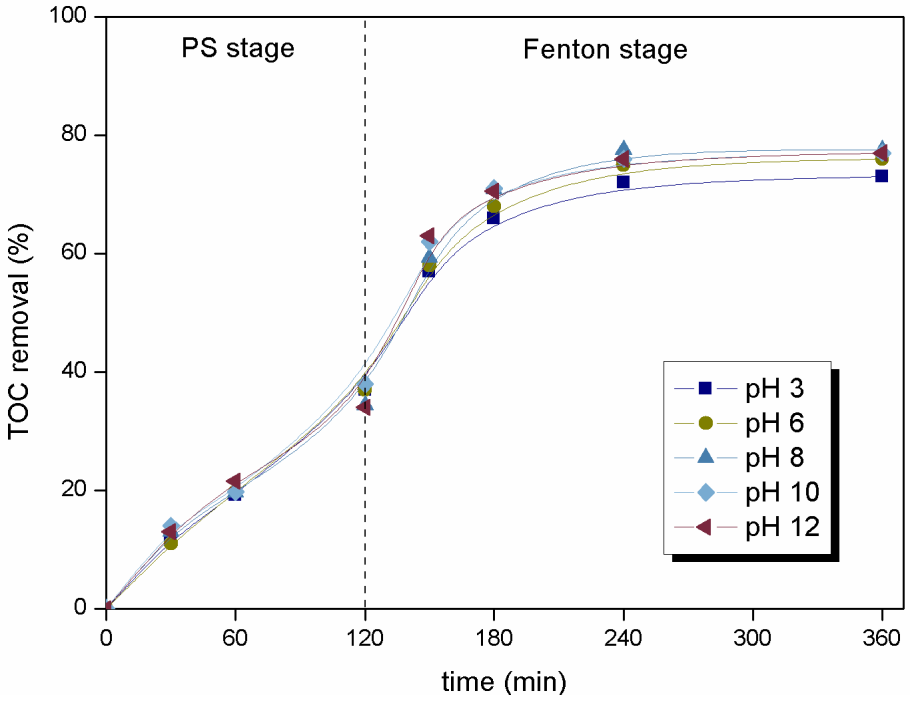

Fig. 3.3.5 The effect of initial pH.

3.3.3.2 Kinetic analysis

The rates of PS and H_2O_2 decomposition in the two steps, respectively, can be expressed by first-order kinetics:

$$-\frac{dC_{PS}}{dt} = k_{PS}C_{PS} \qquad (E1)$$

$$-\frac{dC_{H_2O_2}}{dt} = k_{H_2O_2} C_{H_2O_2} \quad \text{(E2)}$$

where C_{PS} and $C_{H_2O_2}$ represent the concentrations of PS and H_2O_2, respectively and k_{PS} and $k_{H_2O_2}$ the corresponding rate constants.

Oxygen can be considered in excess with respect to the reactants at the working conditions, so that its effect can be seen as invariable during the PS stage. For TOC removal, the following equation is proposed:

$$-\frac{dC_{TOC}}{dt} = k_1 C_{TOC} C_{PS} + k_2 C_{TOC}^2 C_{H_2O_2} \quad \text{(E3)}$$

where C_{TOC} is the concentrations of TOC, and k_1 and k_2 are the apparent rate constants of mineralization of the species tested in the PS and Fenton oxidation steps, respectively. Mineralization of NAs with PS has been well described by a first-order rate equation respect to TOC in a previous work (Xu et al., 2016) whereas second-order dependence has been used in the literature for phenol mineralization upon Fenton oxidation (Bautista et al., 2008). Scientist 3.0 software was used to fit the experimental data to equation (E3).

The results are shown in Fig. 3.3.6, where fairly good fitting can be observed. The values of the corresponding apparent rate constants are listed in Table 3.3.1 together with the correlation coefficients. A difference of two orders of magnitude among the rate constants at 60 and 97 ^{o}C can be observed, suggesting that the system is quite temperature-dependent. The Arrhenius plots are depicted in Fig. 3.3.7. A value of 115 kJ mol^{-1} (r^2 = 0.998) was obtained for the apparent activation energy of the PS oxidation step and 87 kJ mol^{-1} for the Fenton one (in this case, the value of the rate constant at 60 ^{o}C was not considered since desirable pH for Fenton was not achieved working at that temperature).

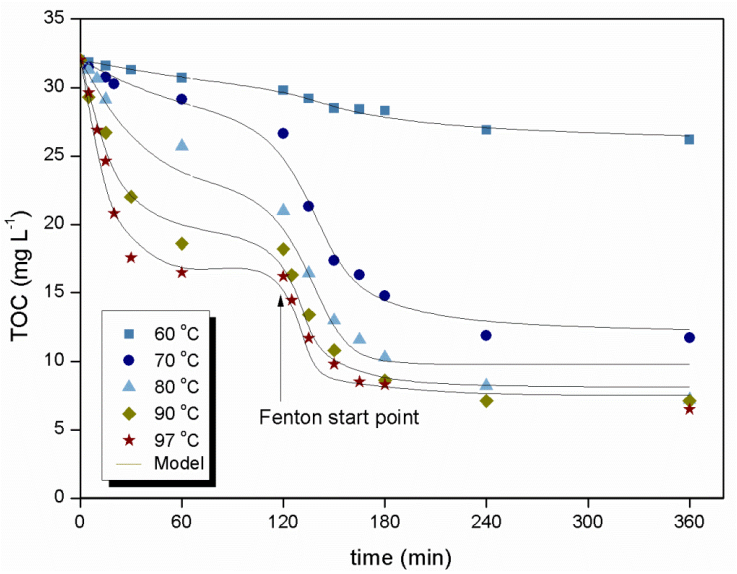

Fig. 3.3.6 Experimental (points) and predicted (lines) TOC values upon reaction time at different temperatures.

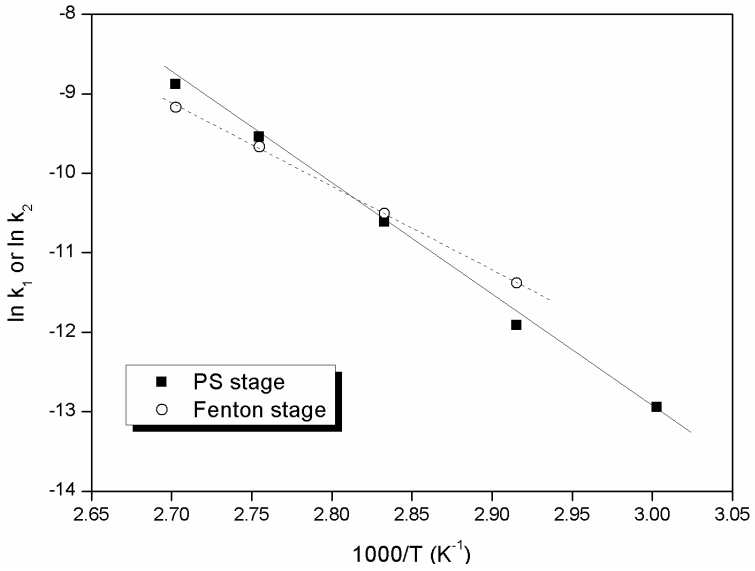

Fig. 3.3.7 Arrhenius plots for the PS and Fenton mineralization of CHA.

3.3.3.3 Degradation of other NAs

Other individual NAs, namely CHBA, 2-NA and 1234-T-2-NA, as well as a mixture of them (including CHA), were tested. These NAs include saturated-ring

as well as aromatic structures. The amounts of PS and H_2O_2 used for the treatment of the NAs mixture were calculated according to the proportionof each NA (equally in volumn). As can be seen from Fig. 3.3.8, the mineralization efficiency was significantly improved after the addition of Fenton reagent in all cases. The corresponding rate constants are collected in Table 3.3.2.

Table 3.3.1 Apparent rate constants of CHA mineralization upon PS and Fenton oxidation under different working temperatures. PS and H_2O_2 at 20 and 40% of the stoichiometric, respectively; Fe^{2+} at 5 mg L^{-1}.

T	PS stage				Fenton stage			
(°C)	$k_1 \times 10^5$ L mg^{-1} min^{-1}	r^2	$k_{PS} \times 10^2$ min^{-1}	r^2	$k_2 \times 10^5$ L^2 mg^{-2} min^{-1}	r^2	$k_{H_2O_2} \times 10^2$ min^{-1}	r^2
97	13.9 ±3.22	0.992	7.98 ±0.43	0.995	10.4 ±2.47	0.978	20.4 ±2.46	0.999
90	7.19 ±1.57	0.998	4.56 ±0.10	0.999	6.33 ±2.54	0.972	12.6 ±2.91	0.999
80	2.46 ±1.25	0.998	1.56 ±0.12	0.993	2.74 ±0.54	0.988	4.18 ±0.61	0.975
70	0.669 ±0.32	1.000	0.798 ±0.04	0.998	1.14 ±0.61	0.998	2.46 ±0.35	0.967
60	0.239 ±0.15	1.000	0.521 ±0.02	0.999	0.065 ±0.04	1.000	1.41 ±0.22	0.965

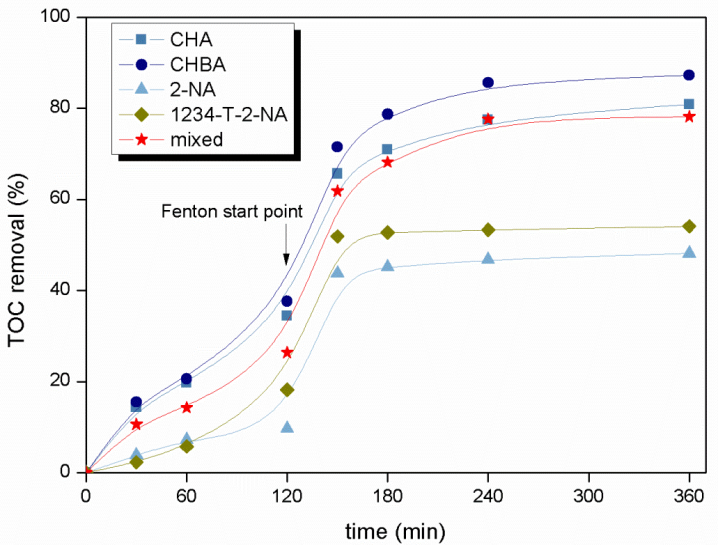

Fig. 3.3.8 Mineralization of various individual and mixed NAs.

Regarding the NAs mixture, it is remarkable that the extent of mineralization was close to the observed for the most reactive ones, suggesting some kind of synergistic effect which requires further research given its importance to cope

with the complexity of real OSPWs.

Table 3.3.2 Apparent rate constants for the individual and mixed NAs upon PS and Fenton mineralization with PS and H_2O_2 at 20 and 40% of the stoichiometric, respectively (Fe^{2+} at 5 mg L^{-1}; T = 80 °C).

	PS stage				Fenton stage			
NAs	$k_1 \times 10^5$ L mg^{-1} min^{-1}	r^2	$k_{PS} \times 10^2$ min^{-1}	r^2	$k_2 \times 10^5$ L^2 mg^{-2} min^{-1}	r^2	$k_{H_2O_2} \times 10^2$ min^{-1}	r^2
CHBA	2.91 ±0.23	0.998	1.84 ±0.16	0.991	5.51 ±1.54	0.976	4.22 ±0.58	0.992
2-NA	0.482 ±0.12	1.000	1.13 ±0.14	0.986	7.79 ±0.38	1.000	5.29 ±0.64	0.986
1234-T-2-NA	0.699 ±0.25	1.000	1.02 ±0.17	0.987	6.31 ±0.32	0.999	5.12 ±0.59	0.987
Mixed	1.50 ±0.22	0.999	1.58 ±0.19	0.985	5.95 ±1.58	0.987	4.98 ±0.71	0.980

3.3.3.4 Evolution of the NAs and oxidation byproducts upon two-step PS and Fenton oxidation

Fig. 3.3.9 provides the time-course of NAs upon oxidation by thermally-activated PS with 20% of the stoichiometric amount. As can be observed, that PS dose was enough to achieve complete conversion of the four model NAs tested. Moreover, the results show that the aromatic ring-bearing NAs, namely 2-NA and 1234-T-2-NA, are more resistant to oxidation than the saturated ring-bearing ones (CHA and CHBA).

Several oxidation by-products were detected, mainly short-chain organic acids from the ring-opening as indicated in section 3.2. In all cases, fumaric acid appears as the primary product from the ring-opening and evolves to formic, acetic and oxalic acid, the two latest being refractory to Fenton oxidation under the operating conditions of the experiments. Apart from those organic acids, there are also some cyclohexanone-structured species identified in section 3.2, as well as trace amount of intermediates, which could not be quantifiable by the currently available identification approaches.

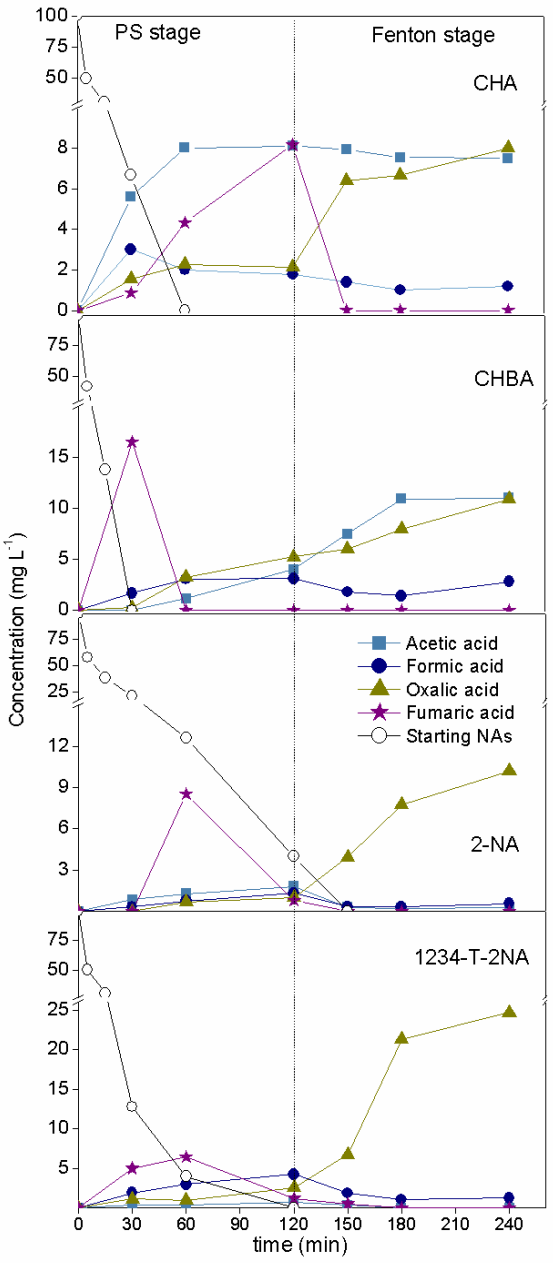

Fig. 3.3.9 Time-course of the starting NAs and short-chain acids upon the two-step PS(2 h) and Fenton oxidation of NAs. $[NAs]_0$ = 100 mg L^{-1}; [PS] = 20% of the stoichiometric; $[H_2O_2]$ = 40 % of the stoichiometric; $[Fe^{2+}]$ = 5.0 mg L^{-1}; pH_0 = 8; T = 80 ºC.

Fig. 3.3.10 shows the carbon balance throughout the two-step treatment. As can be observed, a large proportion of unidentified organic matter (measured as TOC) was found in the earlier oxidation stages (PS step) in all cases, decreasing gradually as oxidation proceeds upon the Fenton step. Those unidentified species are assessed to oligomeric compounds resulting from the condensation of ring radicals. The nature of those species is related to the starting NA, which also affects to the final breakdown. In the case of the two saturated ring-bearing NAs tested, those compounds appear quite easily oxidized by Fenton, achieving final mineralization percentages up to 80 and 91% for CHA and CHBA after the 6 h of the experiments, where the final identified carbon mass was 85 and 97%, respectively. On the opposite, in the case of the aromatic ring-bearing NAs, the oligomeric byproducts are more refractory, giving rise to significantly lower mineralization (48 and 51% for 2-NA and 1234-T-2-NA, respectively). Thus, only 51 and 63% of carbon could be identified after oxidation. Therefore, it is important to assess the biodegradability of the remaining matter in order to learn on its potential behavior in a further biological treatment.

3.3.3.5 Biodegradability

Fig. 3.3.11 shows the evolution of the BOD_5 and COD values as well as the BOD_5/COD ratio upon the oxidative treatments of the NAs. The amount of PS used was 20% of the stoichiometric and the reaction conditions in the two-step PS/Fenton oxidation were similar to those of the experiments of Fig. 3.3.10. It can be seen that COD values decreased upon the treatment due to oxidation. Looking at the BOD_5/COD ratio, the starting NAs tested yield quite different values, being particularly low in the case of the aromatic ring-bearing ones (2-NA and 1234-T-2-NA). PS oxidation at 20% of the stoichiometric amount led to a significantly better biodegradability, which was then improved upon the application of the further Fenton treatment.

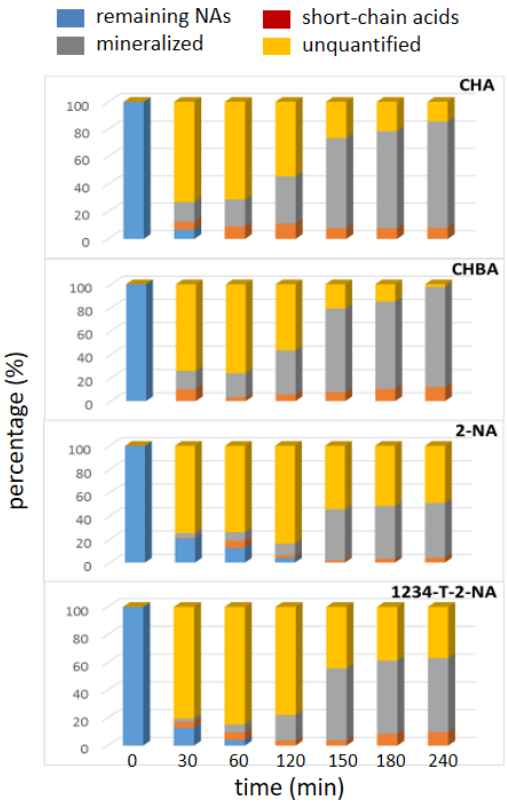

Fig. 3.3.10 Carbon balance upon the two-step PS(2 h) and Fenton oxidation. [PS] = 20% of the stoichiometric; [H_2O_2] = 40 % of the stoichiometric; [Fe^{2+}] = 5.0 mg L^{-1}; pH_0 = 8; T = 80 ºC.

The respirometric profiles serve to learn on the behavior of the oxidation effluents upon further biological treatment (Polo et al., 2011; Sanchis et al., 2014). Since fairly low TOC remains after the two-step oxidation approach using the aforementioned doses of reactants (PS at 20% of the stoichiometric amount, H_2O_2 at 40 % of the stoichiometric and Fe^{2+} at 5.0 mg L^{-1}), now only 20% of the stoichiometric amount of H_2O_2 was used in the Fenton stage. The results of the respirometric tests with the starting NAs (100 mg L^{-1}) and the effluents from PS oxidation alone and PS+Fenton are depicted in Fig. 3.3.12 (for the saturated-ring bearing ones) and 3.3.13 (for the aromatic ones).

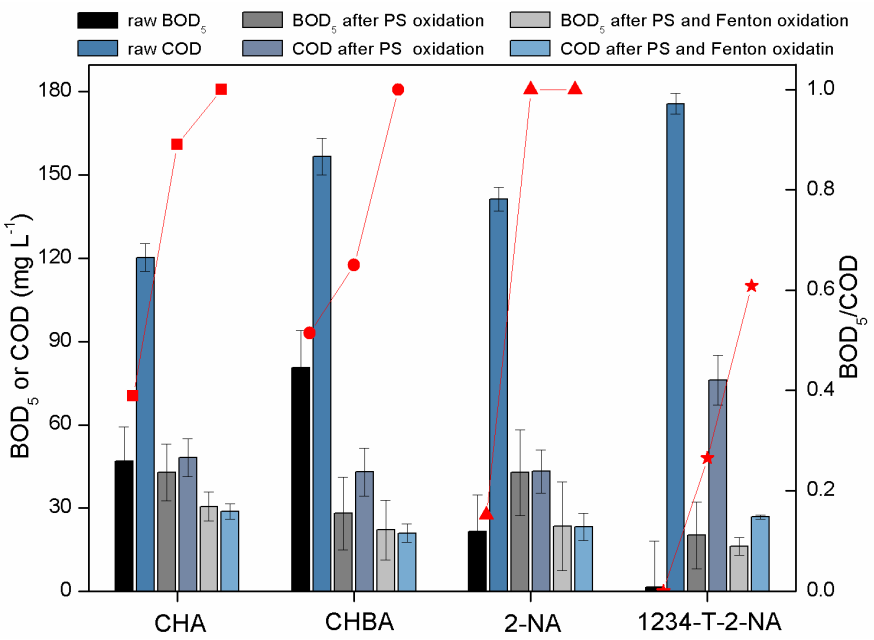

Fig. 3.3.11 BOD_5 and COD values of NAs after reactions at different conditions (bars) and the corresponding BOD_5/COD values (line+symbols).

Relatively slow sludge respiration of the raw CHA was observed throughout the respirometric test especially within the starting stages (inserted graph in Fig. 3.3.12) with less than 15% of TOC consumed at the end of 72 h, confirming its bio-recalcitrant character, in agreement with the literature (Kannel and Gan, 2012) and consistently with the previous value of the BOD_5/COD ratio. However, no obvious toxic effect of this compound can be inferred from the Microtox ecotoxicity values (EC50 > 10 mg L^{-1}). In fact, some moderate increase of the microbial activity was observed after around 30 h. The frequently reported high ecotoxicity of NAs mainly comes from their structural complexity with various functional groups (Brown and Ulrich, 2015; Clemente and Fedorak, 2005). In the current case, however, CHA is one of the most basic model NAs, which does not include aromatic structures, so it is not highly ecotoxic toward the microorganisms used for the ecotoxicity tests. Regarding the effluent from thermally-activated PS oxidation of CHA, the respirometric test showed obvious activity at the beginning with a sharp decline of SOUR within the first 2 hours (corresponding insert graph in Fig. 3.3.12),

indicating a fast consumption of some readily biodegradable intermediates. The microbial activity was then maintained at slow SOUR and after around 25 h an increased microbial activity was observed, which dramatically decreased at ≈ 65 h, suggesting the recalcitrant character of the degradation byproducts at that point of the respirometric test. With the effluents from the oxidative treatments much higher microbial activity can be seen within the initial period of the respirometric tests, but then fairly low values of SOUR were measured given the strong reduction of TOC.

With regard to CHBA, some higher respirometric intensity was registered within the starting period with the effluents from both the thermally-activated PS and the two-step PS and Fenton treatments. However, with the former, no more data could be recorded after a sharp increase of SOUR at around 10 h, suggesting some toxic incidence on the microorganisms since about 60% of the initial TOC was still remaining so that a lack of available carbon source cannot be postulated.

In the case of the aromatic-ring-bearing NAs (2-NA and 1234-T-2-NA), the effluents from the two-step oxidation always showed the best biodegradability within the starting hours, compared with the thermally-activated PS-treated and the original NAs (Fig. 3.3.13). The two-step oxidation effluents from those species show almost complete decline, most probably due to the almost complete degradation of the TOC remaining after the oxidative treatment. This is consistent with the high value of the BOD_5/COD ratio (≈ 1) of that effluent.

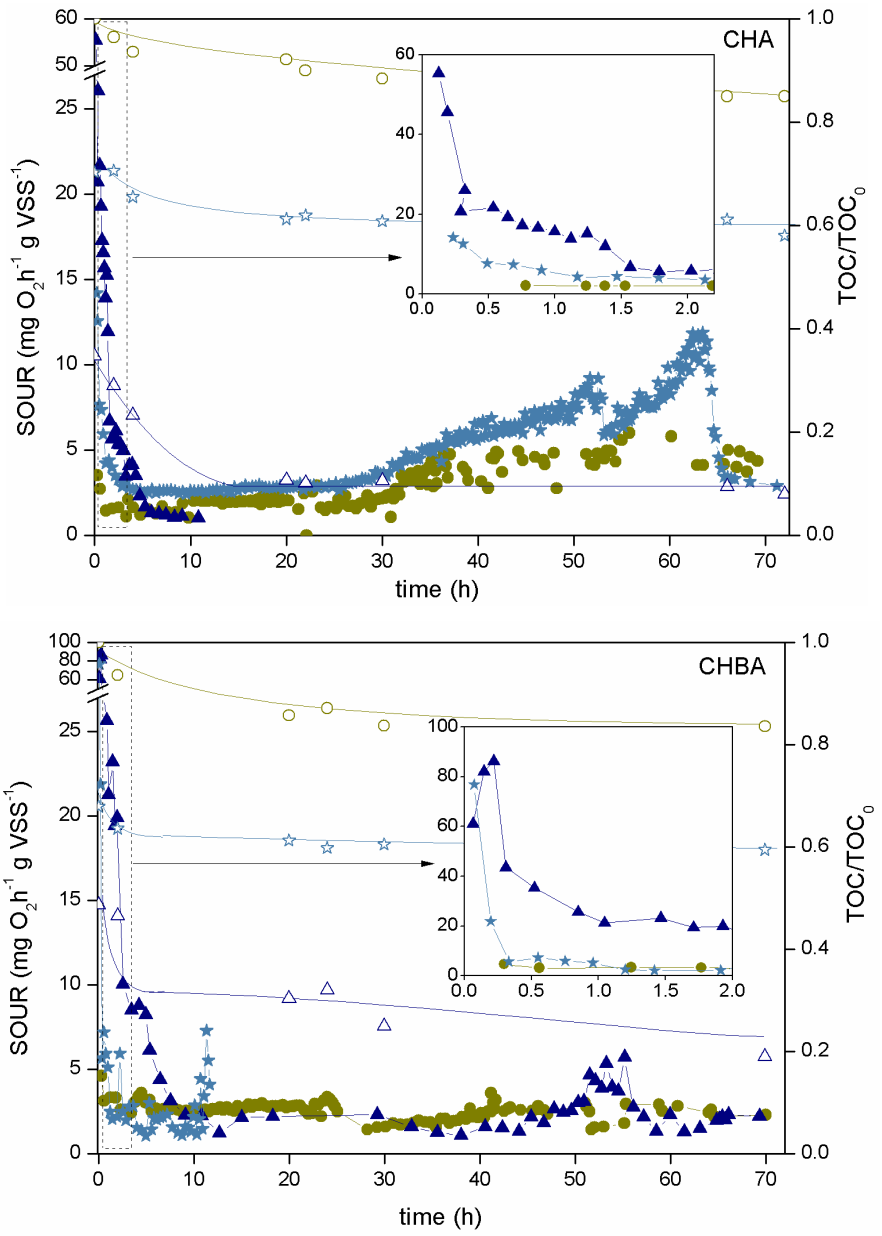

Fig. 3.3.12 Time-course of SOUR (solid symbols) and TOC (opened symbols) upon respirometric tests with the starting CHA and CHBA and the effluents from the oxidation treatments. Initial NAs (circle), NAs after thermally-activated PS oxidation (star) and two-step PS(2 h) and Fenton(2 h) oxidation (triangle). The inset figures show the profiles within the earlier stages.

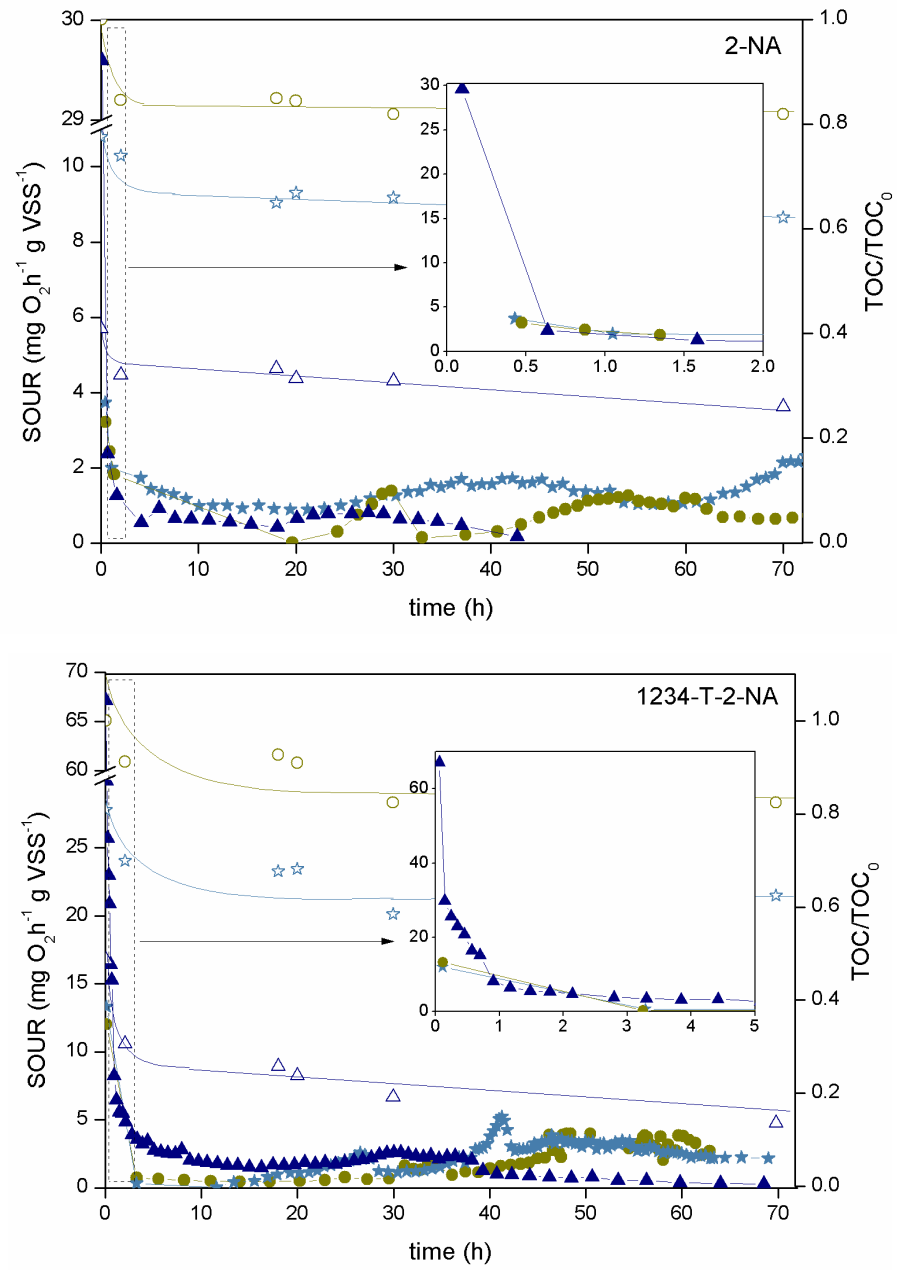

Fig. 3.3.13 Time course of SOUR (solid symbols) and TOC (opened symbols) upon respirometric tests with the starting 2-NA and 1234-T-2-NA and the effluents from the oxidation treatments. Symbols as in Fig. 3.3.12.

3.3.4 Conclusions

Two-step PS and Fenton oxidation provides a promising cost-effective approach for the degradation of NAs. About 80% TOC reduction was achieved from

CHA (50 mg L^{-1}) with 20 and 30% of the stoichiometric amount of PS and H_2O_2, respectively. This system is much more effective than Fenton oxidation alone and allows reducing the reagent cost with respect to single PS-oxidation while introducing less sulfate in the final effluent. Other individual NAs and their mixture were also tested and high mineralization efficiencies were achieved as well. A simple and practical kinetic model has been proposed, which describes fairly well the time-course of TOC. Values of the rate constants are provided. For CHA mineralization, 115 and 87 kJ mol^{-1} were obtained as representative values of the apparent activation energy for the PS and Fenton oxidation steps, respectively. The remaining TOC corresponded to short-chain organic acids easily biodegradable as demonstrated by IC, BOD_5/COD ratio and respirometric tests.

References

Barona JF, Morales DF, González-Bahamón LF, Pulgarín C, Benítez LN. Shift from heterogeneous to homogeneous catalysis during resorcinol degradation using the solar photo-Fenton process initiated at circumneutral pH. Applied Catalysis B: Environmental 2015; 165: 620-627.

Bautista P, Mohedano A, Casas J, Zazo J, Rodriguez J. An overview of the application of Fenton oxidation to industrial wastewaters treatment. Journal of Chemical Technology and Biotechnology 2008; 83: 1323-1338.

Brown LD, Ulrich AC. Oil sands naphthenic acids: A review of properties, measurement, and treatment. Chemosphere 2015; 127: 276-290.

Chou Y-C, Lo S-L, Kuo J, Yeh C-J. Microwave-enhanced persulfate oxidation to treat mature landfill leachate. Journal of hazardous materials 2015; 284: 83-91.

Clemente JS, Fedorak PM. A review of the occurrence, analyses, toxicity, and biodegradation of naphthenic acids. Chemosphere 2005; 60: 585-600.

Drzewicz P, Perez-Estrada L, Alpatova A, Martin JW, El-Din MG. Impact of Peroxydisulfate in the Presence of Zero Valent Iron on the Oxidation of Cyclohexanoic Acid and Naphthenic Acids from Oil Sands Process-Affected Water. Environmental Science & Technology 2012; 46: 8984-8991.

Hilles AH, Amr SSA, Hussein RA, El-Sebaie OD, Arafa AI. Performance of combined sodium persulfate/H 2 O 2 based advanced oxidation process in stabilized landfill leachate treatment. Journal of Environmental Management 2016; 166: 493-498.

Hong PA, Cha Z, Zhao X, Cheng C-J, Duyvesteyn W. Extraction of bitumen from oil sands with hot water and pressure cycles. Fuel Processing Technology 2013; 106: 460-467.

Kannel PR, Gan TY. Naphthenic acids degradation and toxicity mitigation in tailings wastewater systems and aquatic environments: a review. J Environ Sci Health A Tox Hazard Subst Environ Eng 2012; 47: 1-21.

Laredo GC, López CR, Alvarez RE, Cano JL. Naphthenic acids, total acid number and sulfur content profile characterization in Isthmus and Maya crude oils. Fuel 2004; 83: 1689-1695.

Liang C, Guo Y-Y, Pan Y-R. A study of the applicability of various activated persulfate processes for the treatment of 2, 4-dichlorophenoxyacetic acid. International Journal of Environmental Science and Technology 2014; 11: 483-492.

Liang X, Zhu X, Butler EC. Comparison of four advanced oxidation processes for the removal of naphthenic acids from model oil sands process water. J Hazard Mater 2011; 190: 168-76.

Pignatello JJ, Oliveros E, MacKay A. Advanced oxidation processes for organic contaminant

destruction based on the Fenton reaction and related chemistry. Critical reviews in environmental science and technology 2006; 36: 1-84.

Pliego G, Zazo JA, Blasco S, Casas JA, Rodriguez JJ. Treatment of highly polluted hazardous industrial wastewaters by combined coagulation–adsorption and high-temperature Fenton oxidation. Industrial & Engineering Chemistry Research 2012; 51: 2888-2896.

Pliego G, Zazo JA, Casas JA, Rodriguez JJ. Fate of iron oxalates in aqueous solution: The role of temperature, iron species and dissolved oxygen. Journal of Environmental Chemical Engineering 2014; 2: 2236-2241.

Polo A, Tobajas M, Sanchis S, Mohedano A, Rodriguez J. Comparison of experimental methods for determination of toxicity and biodegradability of xenobiotic compounds. Biodegradation 2011; 22: 751-761.

Sanchis S, Polo A, Tobajas M, Rodriguez J, Mohedano A. Coupling Fenton and biological oxidation for the removal of nitrochlorinated herbicides from water. Water research 2014; 49: 197-206.

Xu X-Y, Zeng G-M, Peng Y-R, Zeng Z. Potassium persulfate promoted catalytic wet oxidation of fulvic acid as a model organic compound in landfill leachate with activated carbon. Chemical engineering journal 2012; 200: 25-31.

Xu X, Pliego G, Zazo JA, Casas JA, Rodriguez JJ. Mineralization of naphtenic acids with thermally-activated persulfate: The important role of oxygen. Journal of Hazardous Materials 2016; 318: 355-362.

Zazo JA, Pliego G, Blasco S, Casas JA, Rodriguez JJ. Intensification of the Fenton process by increasing the temperature. Industrial & Engineering Chemistry Research 2010; 50: 866-870.

Zhang, Y., Klamerth, N., Chelme-Ayala, P. and Gamal El-Din, M. (2016a) Comparison of nitrilotriacetic acid and [S, S]-ethylenediamine-N, N'-disuccinic acid in UV-Fenton for the treatment of oil sands process-affected water at natural pH. Environ Sci Technol.

Zhang, Y., Klamerth, N. and El-Din, M.G. (2016b) Degradation of a model naphthenic acid by nitrilotriacetic acid–modified Fenton process. Chem Eng J 292, 340-347.

Zhang, Y., Klamerth, N., Messele, S.A., Chelme-Ayala, P. and El-Din, M.G. (2016c) Kinetics study on the degradation of a model naphthenic acid by ethylenediamine-N, N'-disuccinic acid-modified Fenton process. J Hazard Mater 318, 371-378.

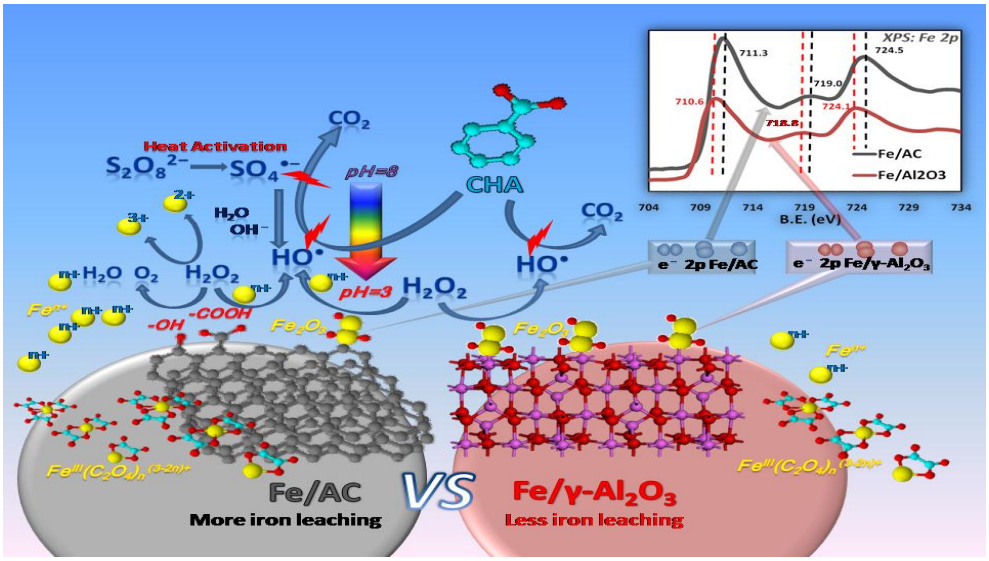

3-4

Cyclohexanoic acid breakdown by two-step persulfate and heterogeneous Fenton-like oxidation with Fe catalysts supported on activated carbon and γ-alumina

Degradación de ácido ciclohexanoico por oxidación en dos etapas mediante persulfato y Fenton heterogéneo con catalizadores de Fe sobre carbón activo y γ-alúmina

过硫酸盐-非均相类芬顿（活性炭和γ-氧化铝为催化剂）两步法降解环己酸

3.4.1 Abstract

This section reports on the application of a two-step treatment consisting of persulfate(PS) and heterogeneous Fenton-like oxidation for the breakdown of cyclohexanoic acid (CHA, 50 mg L^{-1}) as the model naphthenic acid (NA) at circumneutral initial pH (≈ 8). Home-made activated carbon and γ-alumina-supported iron (Fe/AC and Fe/γ-Al_2O_3) catalysts were tested for the Fenton-like step, namely Catalytic Wet Peroxide Oxidation (CWPO). The effect of H_2O_2 dose and temperature was checked, as well as the stability of the catalysts, related with iron loss by leaching. The catalysts were characterized before and after reaction by 77 k N_2 adsorption-desorption, TXRF and XPS analysis. No significant differences were observed in terms of TOC reduction (mineralization) between the Fe/AC and Fe/Al_2O_3 catalysts. Nevertheless, the former showed a lower stability as the result of higher iron lixiviation, as well as more ineffective consumption of H_2O_2. The amount of oxalic acid formed, the low pH value of the solution after the PS pretreatment and the different metal-support interaction between the catalysts tested are experimentally demonstrated to be responsible for iron leaching.

3.4.2 Introduction

The previous section showed the efficiency of the two-step PS and Fenton oxidation for the breakdown of model NAs. This combined system allowed reducing the PS needs upon partial substitution by H_2O_2, giving rise to lower reagents cost while maintaining closely high TOC removal. However, some drawbacks of the homogeneous Fenton approach cannot be ignored, these consisting mainly in the continuous iron loss with the effluent and the subsequent need of dealing with the sludge resulting from $Fe(OH)_3$ precipitation.

To avoid this problem, heterogeneous Fenton-like, namely catalytic wet peroxide oxidation (CWPO) has been proposed. The most commonly used catalysts for that purpose are based on Fe as active phase, supported on different materials, such as activated carbon (AC) (Zazo et al., 2006) and alumina (Al_2O_3) (Bautista et al., 2010; Munoz et al., 2013a) or pillared clays (Herney-Ramirez et al., 2010). AC has been studied also as catalyst itself for H_2O_2 decomposition upon thermal-activation (Domínguez et al., 2013). Regarding γ-Al_2O_3, the corresponding Fe catalysts proved to be more stable than the Fe/AC ones (Munoz et al., 2013b).

Leaching of the metallic phase is one of the main causes of catalyst decay limiting potential application. Previous investigations showed that oxalic acid resulting from the oxidation of organic pollutants is a main responsible of that iron leaching (Zazo et al., 2006). Besides, the metal-support interactions are also crucial. Metals can connect directly to the different sites on the carbon surface or corresponding surface groups (Efremenko and Sheintuch, 2003; Wildgoose et al., 2006), while they tend to connect with γ-Al_2O_3 in a particular pentacoordinated manner to form a relatively strong link (Kwak et al., 2009). However, there is still a lack of available information on the comparison between these two commonly used supports in iron catalysts for CWPO.

In the current section, a two-step PS and heterogeneous Fenton-like oxidation system is investigated for the breakdown of CHA, as the model NA in aqueous phase. Home-made Fe/AC and Fe/γ-Al_2O_3 are tested as catalysts for the Fenton-like step, making a comparison of their performance in terms of activity and stability.

3.4.3 Results and discussion

3.4.3.1 Heterogeneous Fenton oxidation process

The two-step PS and heterogeneous Fenton-like oxidation of CHA (50 mg L^{-1}) was carried out with 20% of the stoichiometric amount of PS in a first 2h-step followed by heterogeneous Fenton oxidation with different amounts of H_2O_2 for another 4 h, using 250 mg L^{-1} of the catalysts tested. The working temperature was 80 ^oC in both steps.

Fig. 3.4.1 shows the results obtained. As can be seen, PS oxidation under the above conditions allowed around 40% TOC reduction and the later CWPO step gave rise to significant further mineralization, depending on the H_2O_2 amount and the catalyst used. Previous adsorption tests (in the absence of H_2O_2) were carried out with the effluent from the PS oxidation step and no significant TOC reduction was found under the 80 ^oC working temperatures so that the contribution of that phenomenon can be neglected. In the PS oxidation step, PS gives rise to $SO_4^{\bullet-}$ radicals which can efficiently mineralize CHA with the positive effect of $O_2^{\bullet-}/HO_2^{\bullet}$ radicals derived from dissolved oxygen, as reported before in this Thesis and in our previous work (Xu et al., 2016). Those radicals allow the pre-degradation of CHA and also an important release of protons causing pH reduction (≈ 3). This pH is optimum for the following Fenton step where the $HO^{\bullet}$ radicals generated from H_2O_2 allow the further mineralization of CHA.

Looking at the two catalysts, the AC-supported yielded faster and higher mineralization. That can be attributed to the faster HO• generation from H_2O_2 decomposition in the former system, due in part to higher iron leaching, since about 3 mg L^{-1} were analyzed in the liquid phase with Fe/AC vs no more than 0.3 mg L^{-1} with Fe/γ-Al_2O_3. Therefore, with the former, there must be some significant homogeneous contribution. The extent of mineralization at the end of the experiment becomes quite similar with both catalysts, except at the lowest H_2O_2 dose tested. With the highest one (80% of the stoichiometric) around 80% TOC reduction was achieved, fairly similar to the obtained with the combined PS + homogeneous Fenton system previously (see section 3.3) (Xu et at., 2017). Looking at the kinetics, the approach using the Fe/AC catalyst showed closer to this last.

As observed in Fig. 3.4.1, increasing the H_2O_2 dose improves TOC reduction, although above 30% of the stoichiometric that effect becomes of lower relative significance. The remaining TOC corresponded to short chain organic acids, including fumaric, oxalic, formic and acetic as reported in the previous PS-homogeneous Fenton treatment. Obvious iron leaching was found after the reaction in all the cases with the AC-supported catalyst opposite to the observed with the γ-Al_2O_3 one.

Two other working temperatures were tested (60 and 97 ^oC) and the results are shown in Fig. 3.4.2. The rate and extent of mineralization were significantly lower at the lowest temperature tested. However, when comparing with the results of Fig. 3.4.1, it can be seen that increasing the temperature from 80 to 97 ^oC has no significant and even some small negative effect on the extent of mineralization, which can be due to enhanced radical scavenging at the highest temperature(Rivas et al., 2004). H_2O_2 decomposed more rapidly at that temperature, especially in Fe/AC system where it was consumed completely within 30 min after added (Fig. 3.4.2). On the other hand, no significant difference of iron leaching was found

between 80 and 97 ºC. These results indicate that increasing the temperature does not provoke higher iron leaching within the range tested. Dramatic decrease of mineralization at 60 ºC occurs in both the PS and CWPO steps. In the former, 60ºC is too low for PS activation and the decreased efficiency of that step leads to a lower pH decrease, so that the start of CWPO the pH was in this case around 4.5, above the optimum for Fenton-based oxidation.

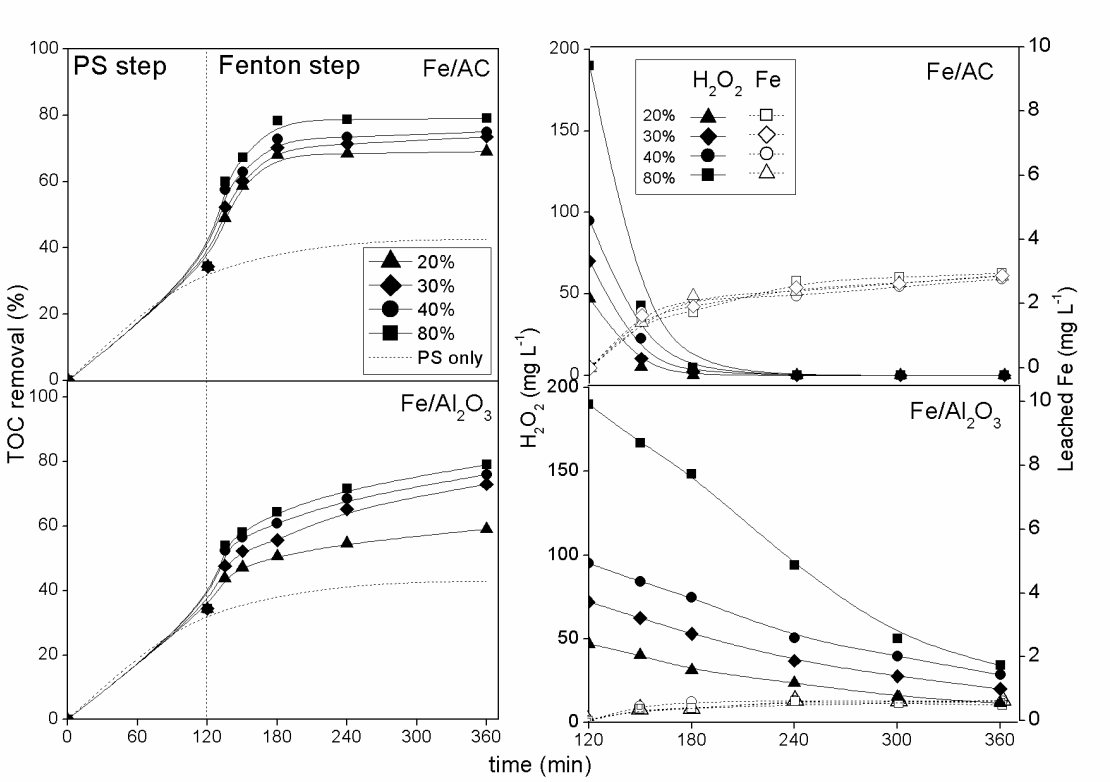

Fig. 3.4.1 Time-course of TOC, H_2O_2 and leached Fe upon the two-step PS(2 h) and CWPO(4h) with the catalysts tested at different H_2O_2 doses (% of the stoichiometric). [PS] = 20% of the stoichiometric, [catalysts] = 250 mg L^{-1}, pH_0 = 8, T = 80 ºC.

Finally, the remaining concentrations of organic acids at the end of the experiments confirm the recalcitrant character of acetic and most in particular oxalic acid to Fenton-based oxidation even at high temperature. Formation of iron(III)-oxalate complex prevents further mineralization (Pliego et al., 2014b; Zazo et al., 2006).

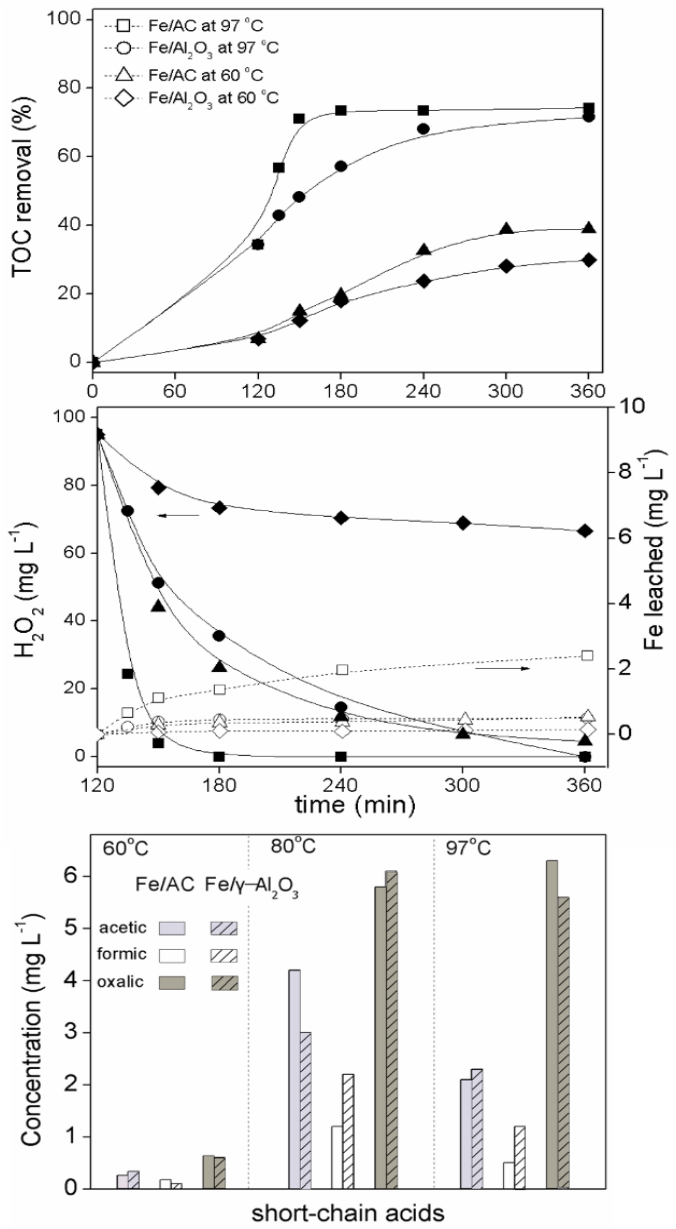

Fig. 3.4.2 Time-course of TOC, H_2O_2 and leached Fe (open symbols) and final concentrations of short-chain organic acids upon PS(2 h)-CWPO(4 h) with the catalysts tested at different temperatures. (PS and H_2O_2 at 20 and 40% of the stoichiometric, [catalysts] = 250 mg L^{-1}, pH_0 = 8, T = 80 °C.

3.4.3.2 Kinetics

The following second-order equation has been used to describe the kinetics of CHA mineralization upon AC-supported Fenton oxidation(Zazo et al., 2005):

$$-\frac{d[TOC]}{dt} = k_1[TOC]^2[H_2O_2]$$

and first-order for the γ-Al_2O_3 one(Munoz et al., 2013b):

$$-\frac{d[TOC]}{dt} = k_1[TOC][H_2O_2]$$

while the evolution of H_2O_2 follows the first-order(Munoz et al., 2013b):

$$-\frac{d[H_2O_2]}{dt} = k_2[H_2O_2]$$

Fitting of the experimental values of TOC and H_2O_2 concentration upon reaction time with the Fe/AC and Fe/γ-Al_2O_3 catalysts at different H_2O_2 doses and temperatures provided the values of the kinetics constants summarized in Table 3.4.1, which confirm the higher activity of the Fe/AC catalyst. The values of the regression coefficient are of good fitting, which can be seen from the curves of Figure 3.4.2 (branches corresponding to the heterogeneous Fenton step, beyond 2 h).

Table 3.4.1 Values of the rate constant for CHA mineralization and H_2O_2 decomposition upon heterogeneous Fenton oxidation catalyzed by Fe/AC and Fe/γ-Al_2O_3 at different conditions.

H_2O_2 (% stoi.)	T (ºC)	Fe/AC				Fe/γ-Al_2O_3			
		$k_1 \times 10^5$ L mg^{-1} min^{-1}	R^2	$k_2 \times 10^2$ min^{-1}	R^2	$k_1 \times 10^6$ L^2 mg^{-2} min^{-1}	R^2	$k_2 \times 10^3$ min^{-1}	R^2
20	80	2.26±0.50	0.99	5.34±0.14	0.99	3.97±1.59	0.99	5.82±0.36	0.99
30	80	2.98±0.66	0.98	5.59±0.53	0.97	4.33±1.70	0.99	5.03±0.21	0.99
	60	0.31±0.08	0.99	2.19±0.14	0.98	0.68±0.21	0.99	1.95±0.26	0.99
40	80	3.57±0.74	0.99	5.67±0.29	0.99	5.09±0.13	0.99	4.86±0.17	0.99
	97	5.85±0.67	0.98	9.27±0.32	0.99	8.58±1.87	0.99	17.6±0.71	0.99
80	80	5.53±0.76	0.99	6.23±0.40	0.99	5.83±0.68	0.99	5.96±0.22	0.99

3.4.3.3 Effect of chloride

The effect of chloride ion was considered, since the OSPWs contain in general fairly high concentrations of that species (Drzewicz et al., 2012) which has been claimed a potential scavenger of HO• radicals (Buxton et al., 1988; Grebel et al., 2010; Liao et al., 2001). Some small negative effect on PS oxidation of NAs has been reported in section 3.1 of this Thesis and our previous work (Xu et al., 2016). In the current study, sodium chloride was added at 10 g L^{-1} to analyze its effect on the PS-Fenton oxidation of CHA using 20% of the stoichiometric PS amount and 40% of the stoichiometric H_2O_2 with 250 mg L^{-1} catalysts for the heterogeneous Fenton stage. Under these conditions, despite similar H_2O_2 decomposition (compared to that without scavenger) TOC removal was reduced by around 20% with both catalysts after 6 h of reaction, confirming the scavenging effect of chloride. It has been reported that chloride might even provoke the formation of organochlorinated species upon advanced oxidation (Drzewicz et al., 2012). Therefore, the effect of chloride needs to be taken into account regarding the potential application of the current PS-CWPO approach as has been reported for other AOP systems (Buxton et al., 1988; Grebel et al., 2010; Liao et al., 2001).

3.4.3.4 Stability of the catalysts

Reusability is an important factor for evaluating the potential application of a catalyst. The catalysts tested were separated and dried after reaction, and then the oxidation process was repeated with 40% of the stoichiometric H_2O_2. As shown in Fig. 3.4.3, the extent of mineralization decreased more significantly upon successive uses in the case of the AC-supported catalyst. This must be due to the higher iron loss by leaching. About 60% mineralization was still achieved after 7 uses, with 77.6% and 44.3% overall iron loss from the Fe/AC and Fe/γ-Al_2O_3 catalysts, respectively. These results prove a somewhat better stability of the γ-

Al_2O_3-supported catalyst.

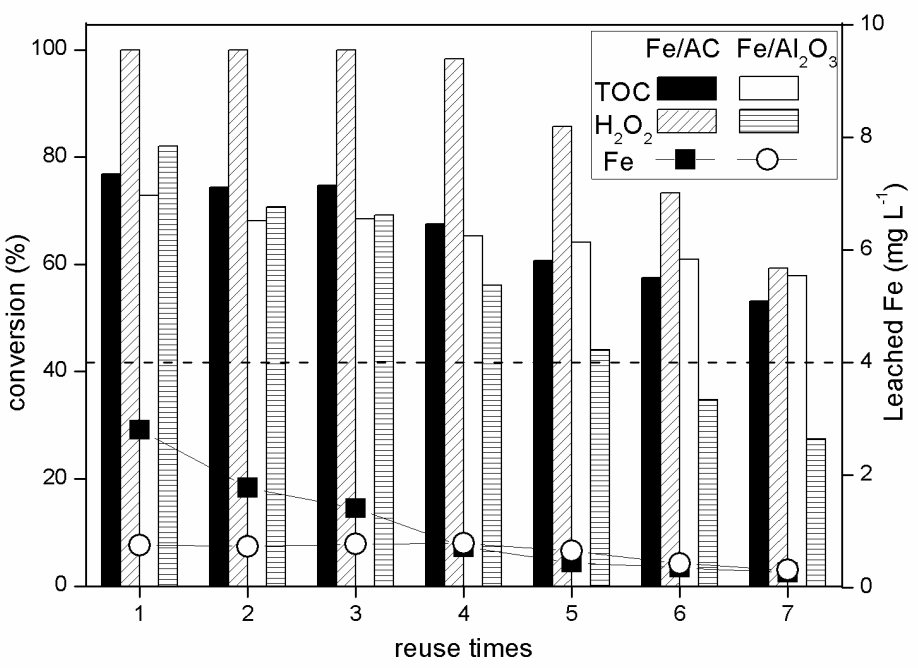

Fig. 3.4.3 Performance of the catalysts tested upon successive application in the two-step PS(2 h) and CWPO(4 h) of CHA. Mineralization of CHA achieved by PS oxidation with 20% of the stoichiometric is shown by the dash line (42.0%). ([H_2O_2] = 40% of the stoichiometric, [catalysts] = 250 mg L^{-1}, pH_0 = 8, T = 80 ^oC)

On the other hand, it can be seen in Fig. 3.4.3 that less significant differences were observed on CHA mineralization than for H_2O_2 consumption between the two catalysts upon successive uses and, opposite to TOC reduction, H_2O_2 conversion decreased more rapidly in the case of the γ-Al_2O_3-supported one. This can be explained by the fact that AC promotes in some extent H_2O_2 decomposition into H_2O_2 and O_2 with no effect on mineralization (Rey et al., 2016). Also, the parasite scavenging of $HO^{\bullet}$ radicals can be more pronounced in the case of Fe/AC due to the higher iron concentration in the liquid phase (Pliego et al., 2014a). Therefore, the Fe/γ-Al_2O_3 catalyst provide more efficient consumption of H_2O_2.

With regard to iron leaching, it has been reported that oxalic acid formed as

oxidation byproduct is a main responsible (Zazo et al., 2006; Zazo et al., 2016). Experiments were carried out to further explore the effect of oxalic acid on iron leaching under the conditions of the current study. To that end, the impact of oxalic acid on the two catalysts were checked by adding 0 – 10 mg L^{-1} to aqueous (distilled water) suspensions of them and stirring for 6 h at 80 ^{o}C and pH = 3. Blank experiments at that pH without oxalic acid yielded 0.64 and 0.09 mg L^{-1} of iron leached from the Fe/AC and Fe/γ-Al_2O_3 catalysts, respectively (Fig. 3.4.4), whereas no iron leaching was observed at pH = 8. This demonstrates that the acidity of the solution has some partial effect on iron leaching, being that more accused for the AC-supported catalyst.

On the other hand, increasing the oxalic acid concentration enhances iron leaching, confirming its significant impact (Fig. 3.4.4). However, very significant differences are observed between the two catalysts. Linear correlation is found among iron leached vs. oxalic acid concentration, showing the AC-supported one much lower stability(Fig. 3.4.4, inset graph) with the slope 16 times higher than the γ-Al_2O_3-supported. Therefore, the specific metal-support interaction must play an important role in that respect.

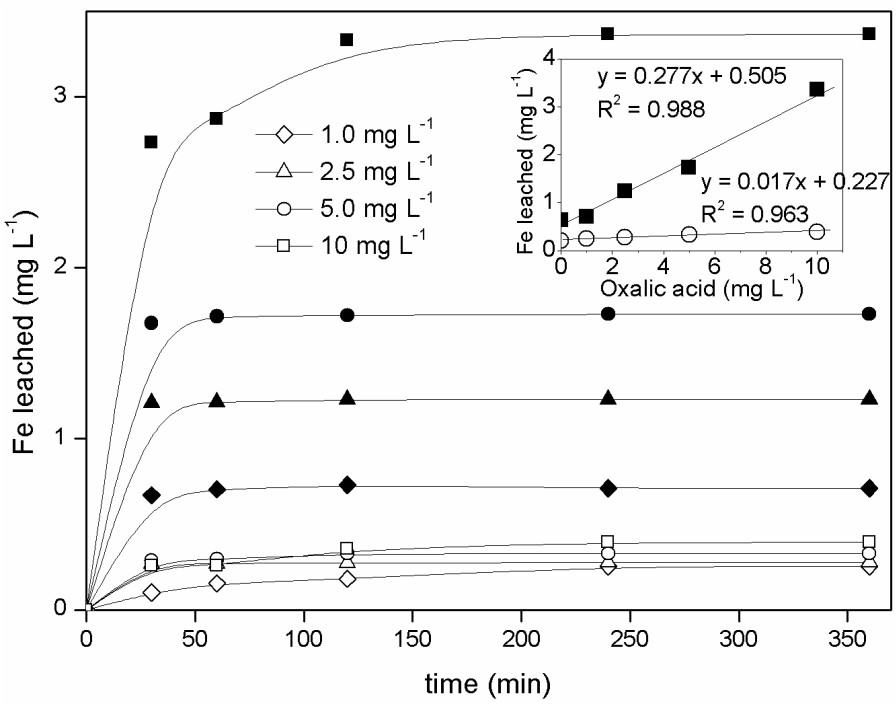

Fig. 3.4.4 Effect of oxalic acid on iron leaching from the Fe/AC (solid symbols) and Fe/γ-Al_2O_3 (open symbols) catalysts. pH = 3, T=80 ºC.

3.4.3.5 Characterization of the fresh and used catalysts

To learn more on the causes of deactivation of the catalysts tested, they have been characterized by different techniques before and after use in CWPO.

The 77 K N_2 adsorption-desorption isotherms are shown in Fig. 3.4.5. As expected, the Fe/AC catalyst showed much higher adsorption than the Fe/γ-Al_2O_3 one, given the higher BET surface area of the activated carbon support, which is an essentially microporous solid while γ-Al_2O_3 is basically mesoporous. No significant changes are observed in the used catalysts respect to the corresponding fresh ones as confirmed by the representative values of the porous texture summarized in Table 3.4.2.

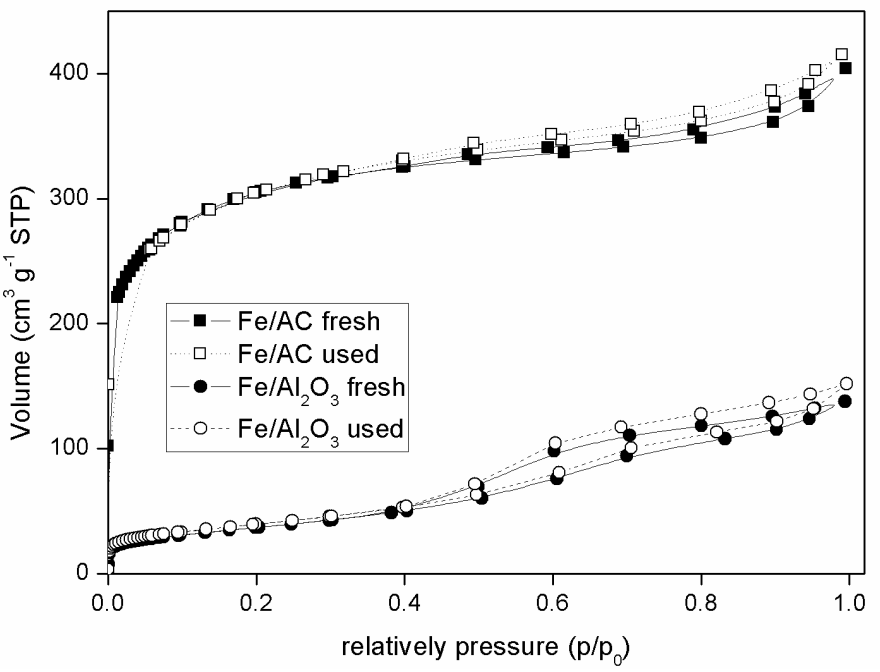

Fig. 3.4.5 77K N_2 adsorption-desorption isotherms of the fresh and used catalysts.

Table 3.4.2 Characteristics of the porous texture of the fresh and used catalysts.

Catalysts		S_{BET} (m^2 g^{-1})	S_{Micro} (m^2 g^{-1})	V_{Total} (cm^3 g^{-1})	V_{Micro} (cm^3 g^{-1})
Fe/AC	fresh	1026	903	0.62	0.43
	used	1011	845	0.64	0.41
Fe/γ-Al_2O_3	fresh	133	≈ 0	0.21	≈ 0
	used	139	≈ 0	0.23	≈ 0

The fresh and used catalysts were characterized also by XPS and the corresponding profiles are shown in Fig. 3.4.6. Table 3.4.3 summarizes the information on the nature and relative amounts of surface oxygen groups (SOGs) assessed from the O 1 s spectra. In the fresh and used AC-supported catalysts, four symmetric peaks at binding energy values of 530.0, 531.5, 532.9 and 534 eV were obtained from deconvolution of the spectra. Those groups were assessed to the oxygen of the inorganic matter, C=O bonds associated to carbonyl or quinone groups, C–O bonds of phenol, anhydride or ether groups and carboxylic acid

(COOH) groups, respectively, following the criteria used in the literature(Moreno-Castilla et al., 1995; Rey et al., 2016). An additional symmetric peak at 536.0 eV can be observed in the used catalyst, simply assessed to the adsorbed water(Darmstadt et al., 1994; Rey et al., 2016).

Table 3.4.3 SOG assessment from deconvolution of the O 1s region of the XPS.

Peak position (eV)	Estimated SOGs	Proportion (%)	
Fe/AC		Fresh	used
530	O–Fe; O–In[a]	42.9	4.0
531.5	C=O	45.9	44.5
532.9	C–O	3.2	13.2
534	COOH	8.1	25.0
536	Ads. water	n.d.	13.3
Fe/γ-Al_2O_3			
530.4	Fe/Al_2O_3	75.7	32.7
531.3	S–O	n.d.	8.5
531.5	O–H	n.d.	33.5
531.95	Fe_2O_3	24.3	25.3

[a]In: Inorganic impurities from the ash content in AC supports.

n.d.: not deconsulved.

The CWPO process significantly decreased the proportion of inorganic oxygen bonds like Fe–O on the surface of the Fe/AC catalysts, consistently with the iron leaching. The content of carboxylic acid groups was clearly increased. Those groups have been claimed as the sites for ineffective decomposition of H_2O_2(Rey et al., 2016). Regarding to the alumina-supported catalyst, the symmetric peaks at 530.4 and 531.95 eV are associated with the oxygen bonds of Fe/γ-Al_2O_3(Paparazzo, 1987) and Fe_2O_3(Lee et al., 1995), respectively. One more peak at 531.3 eV in the used catalyst may correspond to sulfur-oxygen (S-O) bonds of adsorbed sulfate remaining from the PS step(Terlingen et al., 1993).

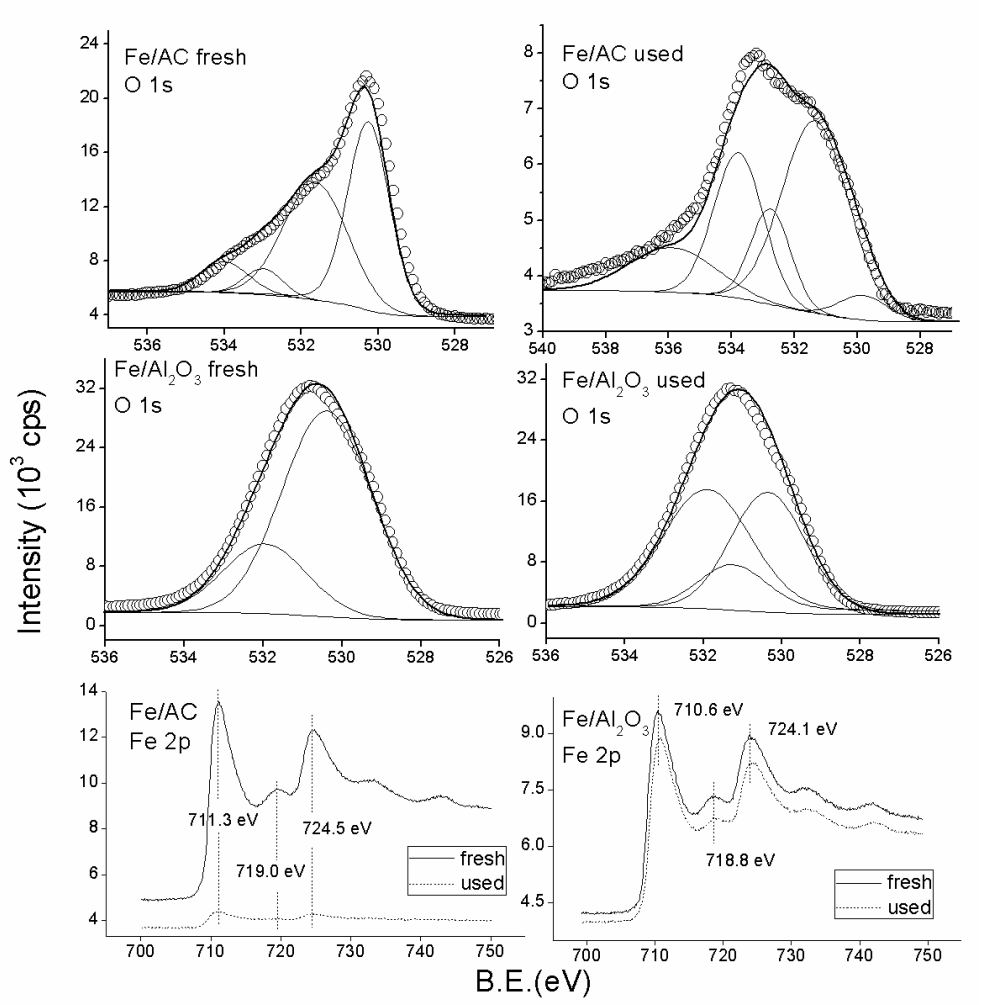

Fig. 3.4.6 O 1s, Al 2p and Fe 2p XPS profiles of the fresh and used catalysts.

The results of the TXRF analyses showed that the percentage of Fe in the Fe/AC and Fe/γ-Al_2O_3 used catalysts decreased to 3.09% and 3.67%, respectively versus the original 4%, showing the higher iron loss from the former. This can also be confirmed by the significantly decreased Fe 2 p region of the XPS spectra of Fe/AC after use (Fig. 3.4.6). In addition, it can be observed that the bonding energy of the characteristic peaks of the Fe 2 p spectra of the two catalysts varied slightly from 711.3, 719.0 and 724.5 eV for the AC-supported catalyst(Rey et al., 2016) to 710.6, 718.8 and 724.1 eV, respectively, for the γ-Al_2O_3 one(Munoz et al., 2013b). This must be due to the different metal-support interaction between the two catalysts. The electrons in the 2 p orbital of Fe borne on the two catalysts suffer

distinctive interactions like coulomb force, so that the corresponding stability toward X-ray excitation differs, resulting in the displacement of Fe 2p binding energy(Liu, 2011; Tauster et al., 1978). That provides some evidence for the difference of the metal-support interaction of these two catalysts.

3.4.4 Conclusions

In the current section, two-step PS and CWPO was applied for the breakdown of CHA using home-made Fe/AC and Fe/γ-Al_2O_3 catalysts (250 mg L^{-1}) at 80 ^oC. Over 75% final TOC removal can be achieved by both of the catalysts using 20 and 30% of the stoichiometric amount of PS and H_2O_2, respectively. The AC-supported catalyst yielded a higher rate than the γ-Al_2O_3 one. However, the former gave a less effective H_2O_2 consumption due to the presence of some oxygen surface groups confirmed by XPS analyses. Also, it suffered higher iron leaching because of weaker metal-support interaction. Other factors like the concentration of oxalic acid and the acidity of the solution were also responsible for the iron loss from the catalysts.

References

Bautista P, Mohedano A, Menéndez N, Casas JA, Rodríguez JJ. Catalytic wet peroxide oxidation of cosmetic wastewaters with Fe-bearing catalysts. Catal Today 2010; 151: 148-152.

Buxton GV, Greenstock CL, Helman WP, Ross AB. Critical review of rate constants for reactions of hydrated electrons, hydrogen atoms and hydroxyl radicals ($^{\bullet}OH/^{\bullet}O^{-}$ in aqueous solution. J Phys Chem Ref Data 1988; 17: 513-886.

Darmstadt H, Roy C, Kaliaguine S. ESCA characterization of commercial carbon blacks and of carbon blacks from vacuum pyrolysis of used tires. Carbon 1994; 32: 1399-1406.

Domínguez C, Quintanilla A, Ocón P, Casas J, Rodriguez J. The use of cyclic voltammetry to assess the activity of carbon materials for hydrogen peroxide decomposition. Carbon 2013; 60: 76-83.

Drzewicz P, Perez-Estrada L, Alpatova A, Martin JW, El-Din MG. Impact of Peroxydisulfate in the Presence of Zero Valent Iron on the Oxidation of Cyclohexanoic Acid and Naphthenic Acids from Oil Sands Process-Affected Water. Environ Sci Technol 2012; 46: 8984-8991.

Efremenko I, Sheintuch M. Carbon-supported palladium catalysts. Molecular orbital study. J Catal 2003; 214: 53-67.

Grebel JE, Pignatello JJ, Mitch WA. Effect of halide ions and carbonates on organic contaminant degradation by hydroxyl radical-based advanced oxidation processes in saline waters. Environ Sci Technol 2010; 44: 6822-6828.

Herney-Ramirez J, Vicente MA, Madeira LM. Heterogeneous photo-Fenton oxidation with pillared clay-based catalysts for wastewater treatment: a review. Appl. Catal. B-Environ. 2010; 98: 10-26.

Kwak JH, Hu J, Mei D, Yi C-W, Kim DH, Peden CH, et al. Coordinatively unsaturated Al^{3+} centers as binding sites for active catalyst phases of platinum on γ-Al_2O_3. Science 2009; 325: 1670-1673.

Lee Y-S, Kim H-T, Yoo K-O. Effect of ferric oxide on the high-temperature removal of hydrogen sulfide over ZnO-Fe_2O_3 mixed metal oxide sorbent. Ind Eng Chem Res 1995; 34: 1181-1188.

Liao C-H, Kang S-F, Wu F-A. Hydroxyl radical scavenging role of chloride and bicarbonate ions in the H_2O_2/UV process. Chemosphere 2001; 44: 1193-1200.

Liu JJ. Advanced electron microscopy of metal–support interactions in supported metal catalysts. ChemCatChem 2011; 3: 934-948.

Moreno-Castilla C, Ferro-Garcia M, Joly J, Bautista-Toledo I, Carrasco-Marin F, Rivera-Utrilla J. Activated carbon surface modifications by nitric acid, hydrogen peroxide, and ammonium peroxydisulfate treatments. Langmuir 1995; 11: 4386-4392.

Munoz M, de Pedro ZM, Casas JA, Rodriguez JJ. Chlorophenols breakdown by a sequential hydrodechlorination-oxidation treatment with a magnetic Pd–Fe/γ-Al_2O_3 catalyst. Water research 2013a; 47: 3070-3080.

Munoz M, de Pedro ZM, Menendez N, Casas JA, Rodriguez JJ. A ferromagnetic γ-alumina-supported iron catalyst for CWPO. Application to chlorophenols. Appl. Catal. B-Environ. 2013b; 136: 218-224.

Paparazzo E. XPS and auger spectroscopy studies on mixtures of the oxides SiO_2, Al_2O_3, Fe_2O_3 and Cr_2O_3. Journal of electron spectroscopy and related phenomena 1987; 43: 97-112.

Pliego G, Xekoukoulotakis N, Venieri D, Zazo JA, Casas JA, Rodriguez JJ, et al. Complete degradation of the persistent anti-depressant sertraline in aqueous solution by solar photo-Fenton oxidation.J Chem Technol Biot 2014a; 89: 814-818.

Pliego G, Zazo JA, Casas JA, Rodriguez JJ. Fate of iron oxalates in aqueous solution: The role of temperature, iron species and dissolved oxygen. J Environ Chem Eng 2014b; 2: 2236-2241.

Rey A, Hungria A, Duran-Valle C, Faraldos M, Bahamonde A, Casas J, et al. On the optimization of activated carbon-supported iron catalysts in catalytic wet peroxide oxidation process. Appl. Catal. B-Environ. 2016; 181: 249-259.

Rivas F, Navarrete V, Beltran F, Garcıa-Araya J. Simazine Fenton's oxidation in a continuous reactor. Appl. Catal. B-Environ. 2004; 48: 249-258.

Tauster S, Fung S, Garten R. Strong metal-support interactions. Group 8 noble metals supported on titanium dioxide. J Am Chem Soc 1978; 100: 170-175.

Terlingen JG, Feijen J, Hoffman AS. Immobilization of surface active compounds on polymer supports using glow discharge processes: 1. Sodium dodecyl sulfate on poly (propylene). J Colloid Interf Sci 1993; 155: 55-65.

Wildgoose GG, Banks CE, Compton RG. Metal nanoparticles and related materials supported on carbon nanotubes: methods and applications. Small 2006; 2: 182-193.

Xu X, Pliego G, Zazo JA, Casas JA, Rodriguez JJ. Mineralization of naphtenic acids with thermally-activated persulfate: The important role of oxygen. J Hazard Mater 2016; 318: 355-362.

Zazo J, Casas J, Mohedano A, Gilarranz M, Rodriguez J. Chemical pathway and kinetics of phenol oxidation by Fenton's reagent. Environ Sci Technol 2005; 39: 9295-9302.

Zazo JA, Casas JA, Mohedano AF, Rodríguez JJ. Catalytic wet peroxide oxidation of phenol with a Fe/active carbon catalyst. Appl. Catal. B-Environ. 2006; 65: 261-268.

Zazo JA, Pliego G, García-Muñoz P, Casas JA, Rodriguez JJ. UV-LED assisted catalytic wet peroxide oxidation with a Fe (II)-Fe (III)/activated carbon catalyst. Appl. Catal. B-Environ. 2016; 192: 350-356.

CHAPTER IV/ CAPÍTULO IV/卷四

CONCLUSIONS AND OUTLOOK

CONCLUSIONES Y PERSPECTIVAS

结论与展望

Conclusions

1. Thermally-activated persulfate oxidation at 80 ^{o}C has proved to be effective for the removal of NAs from water at the circumneutral pH of the original solutions (≈ 8). Complete mineralization was achieved at frankly substoichiometric amounts of PS with all the NAs tested, which included saturated and aromatic ring-bearing species, namely CHA, CHBA, 2-NA and 1234-T-2-NA. This can be explained by the important role of oxygen, which was experimentally demonstrated, so that the oxidation reactions were reformulated to include the contribution of O_2. The system was more effective toward the saturated-ring species than the aromatic ones.

2. The kinetics of mineralization of the NAs tested was fairly well described by simple pseudo-first order rate equations. The values of the rate constant normalized to the PS dose at 80 ^{o}C were between 0.062–0.099 h^{-1}, following the order: CHBA > 1234-T-2-NA > CHA > 2-NA. Fairly similar values of activation energy (≈ 100 kJ moL^{-1}) were obtained.

3. Sulfate and hydroxyl radicals were verified as the main reactive species for NAs breakdown, with the former being the dominant one. Only certain small negative effect of chloride and almost negligible of bicarbonate were observed. Dissolved oxygen plays a very important role in this system through the formation of the $O_2^{\bullet -}/HO_2^{\bullet}$ radicals which may promote the transformation of NAs into the corresponding organic radicals.

4. Reaction mechanisms of the tested NAs in the thermally-activated PS oxidation with and without oxygen were postulated based on the identification of intermediates and reaction byproducts. Decarboxylation is proved to be the first step of PS oxidation of NAs. Dissolved oxygen promotes the formation of

cyclohexanone-structured intermediates among the main byproducts from each model NAs, as inferred by the significantly lower presence of those species under inert atmosphere conditions. Lower amounts of those compounds were observed from the aromatic NAs than from the saturated ring-bearing ones, indicative of a weaker effect of oxygen in the case of the former.

5. Kinetic models for the mineralization of the NAs tested are provided with the consideration of the susceptibility of the initial compounds and the corresponding intermediates. The contribution of oxygen is found to be positive for the transformation of the easily degradable TOC into more recalcitrant one as well as for the final mineralization efficiency and for persulfate saving.

6. Two-step PS and Fenton oxidation provides a promising approach for the degradation of NAs. About 80% TOC reduction was achieved from CHA (50 mg L^{-1}) with 20 and 30% of the stoichiometric amount of PS and H_2O_2, respectively. The remaining TOC corresponded to short-chain organic acids easily biodegradable as demonstrated by respirometric tests. This system is much more effective than Fenton oxidation alone and allows reducing the reagent cost with respect to single PS-oxidation while introducing less sulfate in the final effluent. The presence of chloride has to be considered for practical use since it showed a detrimental scavenging effect, affecting to the Fenton step. The other individual NAs and their mixtures were also tested and high mineralization efficiencies were achieved as well. A simple and practical kinetic model has been proposed, which describes fairly well the time-course of TOC. Values of the rate constants are provided. For CHA mineralization, 115 and 87 kJ mol^{-1} were obtained as representative values of the apparent activation energy for the PS and Fenton oxidation steps, respectively.

7. The two-step PS and Fenton system significantly improved the biodegradability (BOD_5/COD) of the effluents with respect to the starting NAs.

Furthermore, the respirometric tests provided available information on the time-course of the biodegradability upon the bio-respiration. Final mineralization of 95%, 85%, 70% and 82% was achieved by respirometric tests of the samples from the PS and Fenton two-step oxidation of CHA, CHBA, 2-NA and 1234-T-2-NA, respectively. The amount of PS and H_2O_2 used was only 20% of the stoichiometric.

8. Efficient mineralization of CHA was also achieved by the tow-step PS and heterogeneous Fenton oxidation (CWPO), this last catalyzed by home-made Fe/AC and Fe/γ-Al_2O_3. This approach allowed similar mineralization (over 75%) as in the previous one (PS-homogeneous Fenton) under the same reagents doses but with less iron loss. The Fe/γ-Al_2O_3 catalyst showed somewhat lower activity (oxidation rate) but a more efficient H_2O_2 consumption and higher stability due to the significantly lower Fe leaching than the Fe/AC one. Certain positions on the carbon surface were inferred to cause some inefficient decomposition of H_2O_2 to H_2O and O_2, which did not occur in the case of Fe/γ-Al_2O_3. The concentration of oxalic acid and the pH of the solution affect to the iron leaching of the catalysts. The significant difference of iron leaching between the two catalysts under similar operating conditions suggests that metal-support interactions are also determining with regard to the stability.

Outlook

This Thesis proposes several efficient AOP approaches for the treatment of model NAs, including PS oxidation, two-step PS and Fenton (both conventional and heterogeneous) with the new knowledge of the relevant reaction mechanisms and kinetics. Based on the results, further research should regard:

Deeper understanding of those proposed oxidation processes for NAs is needed, on the basis of more detailed identification and quantification of the reaction intermediates. That would serve to clarify the reaction mechanisms. Proper detection approaches like spectroscopic ones can be modified and used to provide more direct evidence on the effects of the reactive radical species.

Since the investigations carried out in this Thesis are all with model NAs, the potential application of the treatment systems should be further tested with real oil-containing wastewaters from oil-shales and tar-sand processing operations (OSPWs).

Conclusiones

1. La oxidación mediante persulfato (PS) térmicamente activado a 80 ^{o}C se ha mostrado como una alternativa eficaz para la degradación de ácidos nafténicos (ANs) en agua, sin necesidad de modificar el pH inicial (≈ 8) de la disolución. Se ha conseguido la mineralización de los ANs estudiados, entre los que se incluyen estructuras cíclicas saturadas (CHA y CHBA) y aromáticas (2-NA y 1234-T-2-NA), con dosis de persulfato muy por debajo de la estequiométrica, lo que se explica por el efecto del oxígeno disuelto. Las correspondientes reacciones de oxidación se han reformulado para incluir la contribución del oxígeno. La estructura de los ANs constituye un factor importante para su degradación mediante este procedimiento, que resulta más efectivo en el caso de las estructuras cíclicas saturadas.

2. La mineralización de los ANs ensayados se describe adecuadamente mediante una cinética de pseudo-primer orden. Los valores de las constantes de velocidad a 80 ^{o}C, normalizados con la dosis de PS, varían entre 0,062 y 0,099 h^{-1}, siguiendo el orden: CHBA > 1234-T-2-NA > CHA > 2-NA. La energía de activación aparente tiene en todos los casos un valor en torno a 100 kJ mol^{-1}.

3. Los radicales sulfato e hidroxilo son las principales especies responsables de la degradación de los ANs, siendo el primero de ellos la predominante. Además, el oxígeno disuelto juega un papel relevante en este sistema, a través de la formación de radicales $O_2^{\bullet -}/HO_2^{\bullet}$, que pueden promover la transformación de los ANs en los correspondientes radicales orgánicos. Por otro lado, se ha observado un cierto efecto negativo por la presencia de cloruro, mientras que dicho efecto resulta prácticamente despreciable en el caso del bicarbonato.

4. Se han propuestos mecanismos de oxidación con PS para cada uno de los ANs ensayados, en presencia y ausencia de oxígeno, basados en la identificación

de los intermedios y productos de reacción. En todos los casos, la descarboxilación constituye la primera etapa del proceso. El oxígeno disuelto promueve la formación de intermedios con estructura tipo ciclohexanona, hecho soportado por la escasa presencia de estos compuestos en los experimentos realizados en atmósfera inerte. La concentración de este tipo de intermedios fue muy inferior en el caso de los ANs con estructuras aromáticas, lo que indica una menor influencia del oxígeno disuelto en la oxidación de este grupo de ANs.

5. Se ha descrito la cinética de mineralización de los ANs ensayados, teniendo en cuenta la susceptibilidad de los mismos y de sus intermedios a la oxidación, de forma que se establecen dos categorías de compuestos, en términos de COT, atendiendo a dicha susceptibilidad. Se confirma el efecto positivo del oxígeno en la mineralización, así como en el alcance final de la misma y en el ahorro de PS.

6. El tratamiento combinado PS–Fenton constituye una prometedora alternativa para la degradación de ANs. Se alcanza una reducción de COT en torno al al 80% en el caso del CHA (50 mg L^{-1}) con un 20 y un 30% de la dosis estequiométrica de PS y H2O2, respectivamente. La materia orgánica residual corresponde a ácidos orgánicos de cadena corta, cuya alta biodegradabilidad se ha demostrado mediante ensayos respirométricos. Este sistema combinado resulta mucho más eficiente que la oxidación Fenton y permite reducir los costes de reactivos en comparación con la oxidación con PS, minimizando la concentración de sulfato en el efluente. Se ha tenido en cuenta la presencia de cloruro, dado su capacidad secuestrante de radicales, que afecta fundamentalmente a la etapa Fenton. De forma análoga, se han realizado ensayos con los demás ANs, así como con mezclas de los mismos, en los que se han alcanzado también altos niveles de mineralización. Se ha propuesto un modelo cinético simple y práctico, que describe bien la evolución del COT, y se han obtenido los valores de las constantes de velocidad. Para el CHA se obtuvieron valores de la energía de activación

aparente de 115 y 87 kJ mol^{-1} para las etapas de oxidación con PS y Fenton, respectivamente.

7. El tratamiento en dos etapas mejoró sustancialmente la biodegradabilidad (DBO_5/DQO) del efluente, con respecto a la de los ANs de partida. Además, los ensayos respirométricos proporcionaron información adicional sobre la evolución esperada de la biodegradabilidad a lo largo de un tratamiento biológico aerobio convencional. Se alcanzaron porcentajes de mineralización del 95, 85, 70 y 82% en los ensayos respirométricos con los efluentes de la oxidación de CHA, CHBA, 2-NA and 1234-T-2-NA, respectivamente, por el sistema combinado PS/Fenton, con el 20 % de la dosis estequiométrica de cada uno de los reactivos.

8. Se ha investigado también un tratamiento combinado, a base de oxidación con PS, seguida de Fenton heterogéneo, empleando, para esta segunda etapa, catalizadores preparados en el laboratorio, a base de hierro soportado sobre carbón activo o γ-alúmina (Fe/CA y Fe/γ-Al_2O_3). Mediante este sistema se alcanzaron niveles de mineralización próximos a los anteriores (alrededor del 75% en el caso del CHA), con las mismas concentraciones de PS y H_2O_2, pero minimizando las pérdidas de hierro. De los dos catalizadores ensayados, el de Fe/γ-Al_2O_3 mostró una menor actividad (velocidad de mineralización) si bien resultó ser más eficiente en relación con el consumo de H_2O_2, lo que se explica por la descomposición del reactivo en H_2O y O_2 sobre la superficie del carbón, inexistente o mucho menos significativa en el caso del catalizador de Fe/γ-Al_2O_3. Este último mostró, además, una estabilidad muy superior, con muy baja γ-Al_2O_3.

Perspectivas

La presente Tesis propone varias alternativas basadas en procesos avanzados de oxidación (PAOs), para el tratamiento de ácidos nafténicos en agua. Dichas opciones incluyen, oxidación con persulfato y su combinación con el proceso Fentos, homogéneo como heterogéneo. Los resultados aportan nuevo conocimiento tanto a las reacciones químicas y sus mecanismos como a la cinética de los procesos estudiados.

Un conocimiento más en profundidad de las reacciones implicadas constituye parte de las tareas futuras, para lo que se requiere una identificación más detallada y cuantitativa de los intermedios y productos de degradación de estos ácidos nafténicos. Para ello habrán de adaptarse protocolos analíticos más desarrollados para este tipo de compuestos, basados en el empleo de técnicas de alta resolución.

En la investigación llevada a cabo en esta Tesis se han empleado ácidos nafténicos modelo, con distintas estructuras. Evidentemente, el análisis de la aplicación potencial de estas tecnologías requiere estudios posteriores con aguas reales, como las resultantes de los procesos de extracción de arenas y pizarras bituminosas y fracturación hidráulica.

Supporting information

Table S1. Mass spectra of the oxidation effluents.

Compound	Peak	Mass spectra
CHA	peak A1	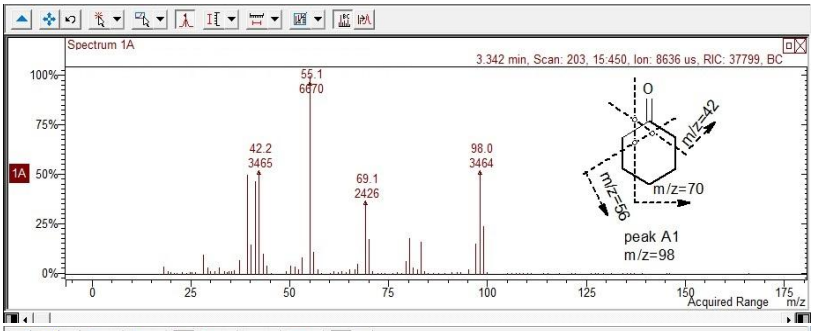
	peak A2	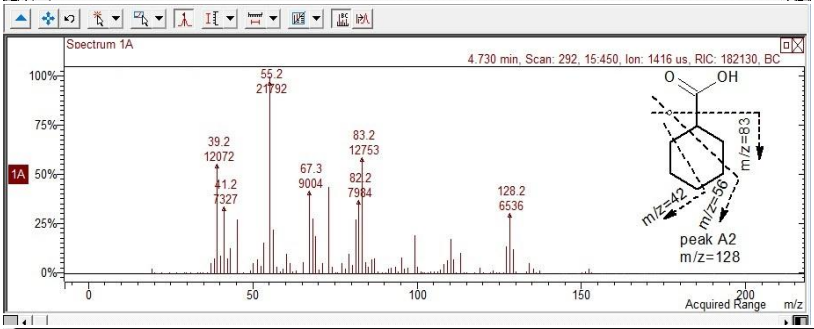
	peak A3	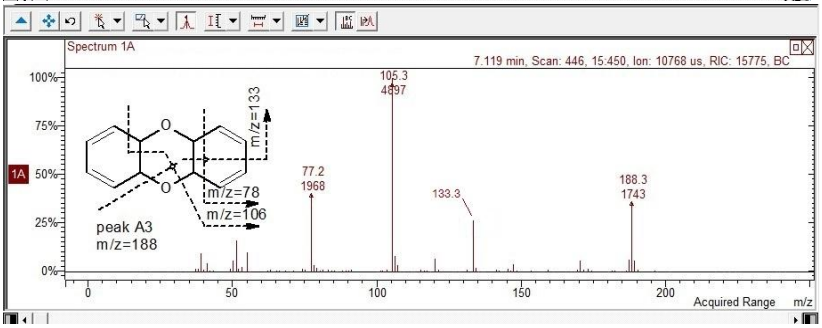
	peak A4	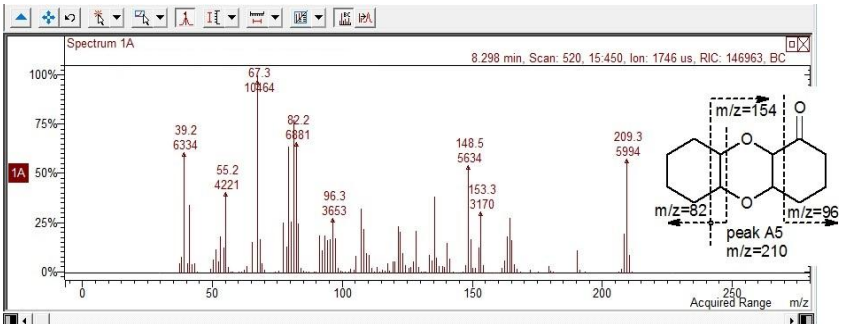

CHBA

peak B1

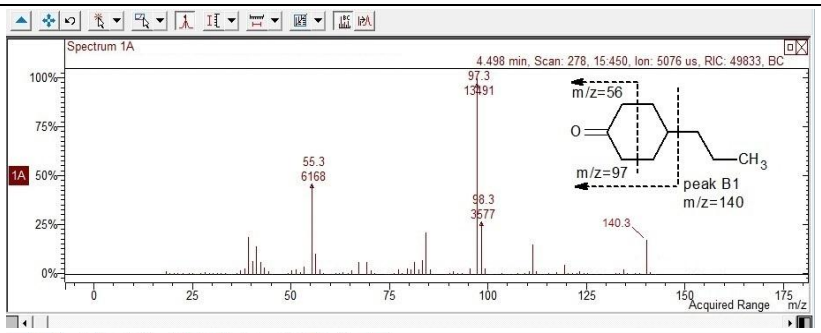

peak B2

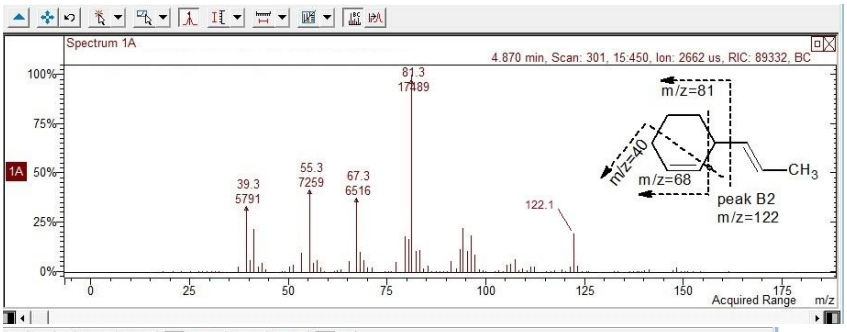

peak B3

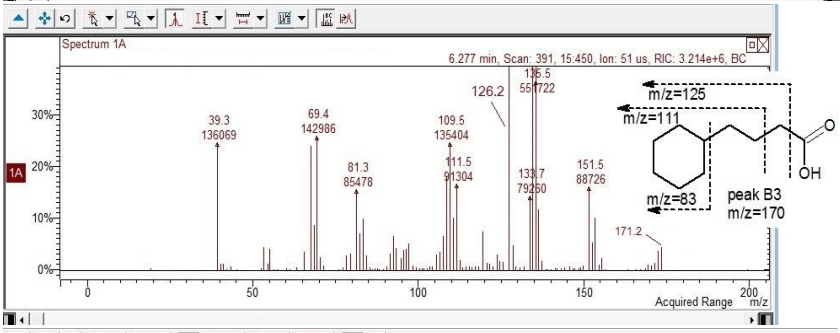

peak B4

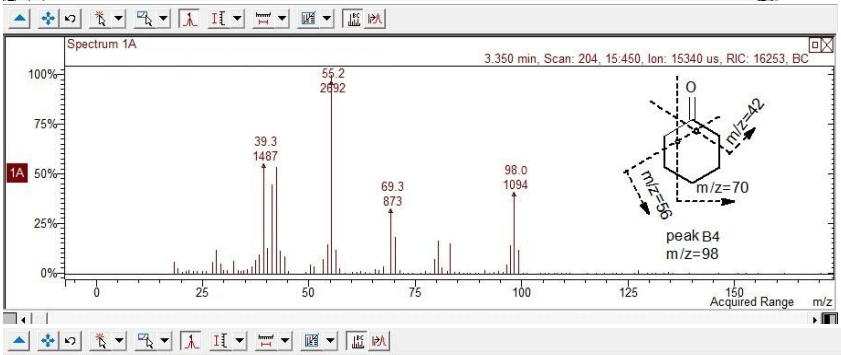

peak B5

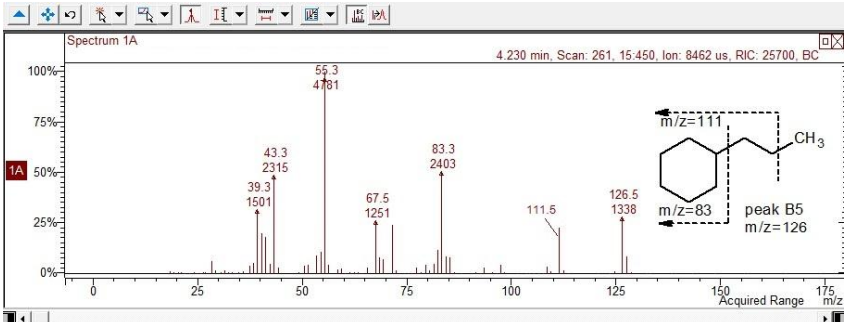

peak B6

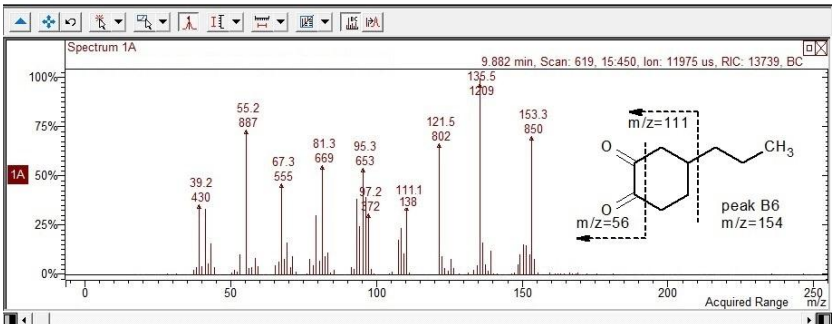

peak B7

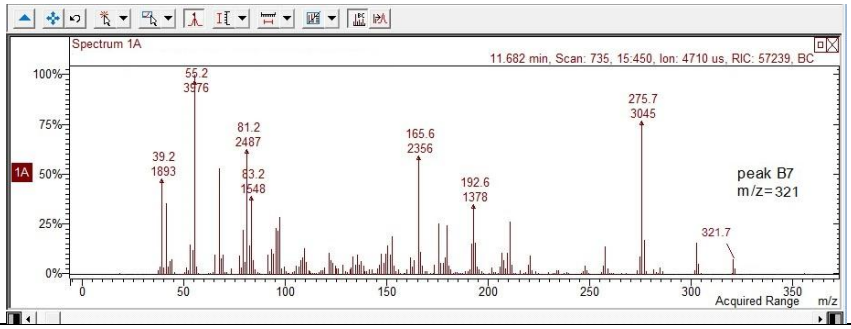

2-NA

peak C1

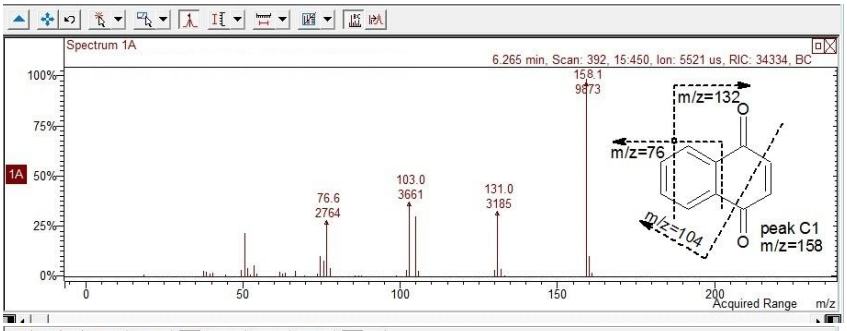

peak C2

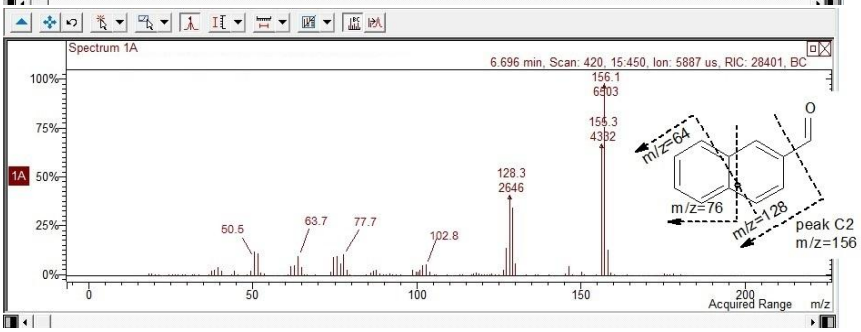

peak C3

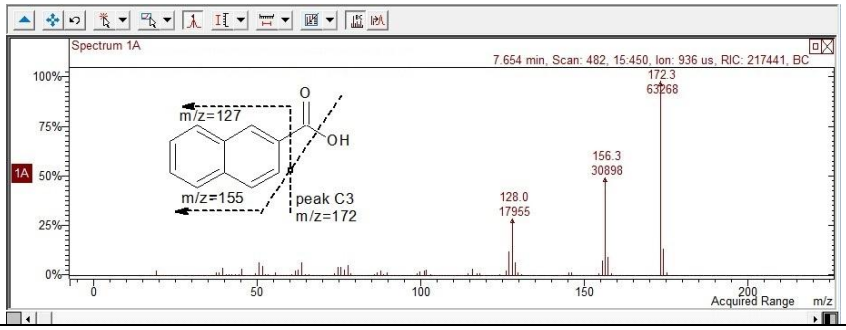

1234-T-2-NA

peak D1

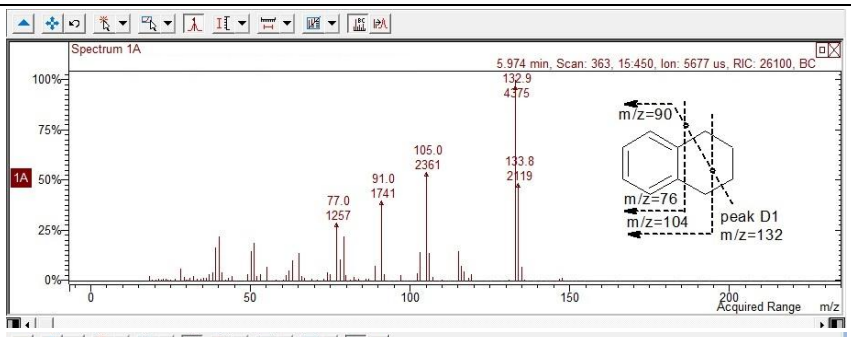

peak D2

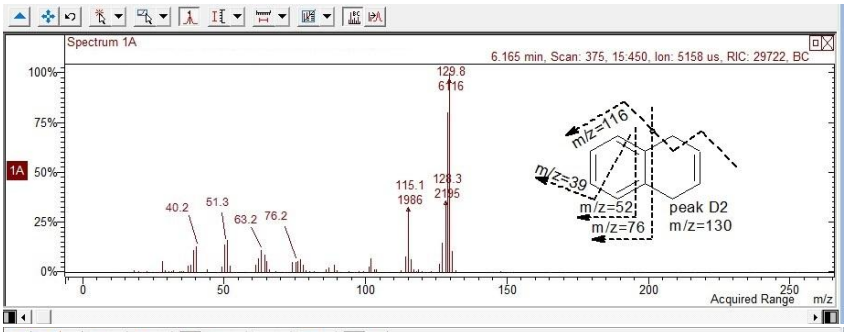

peak D3

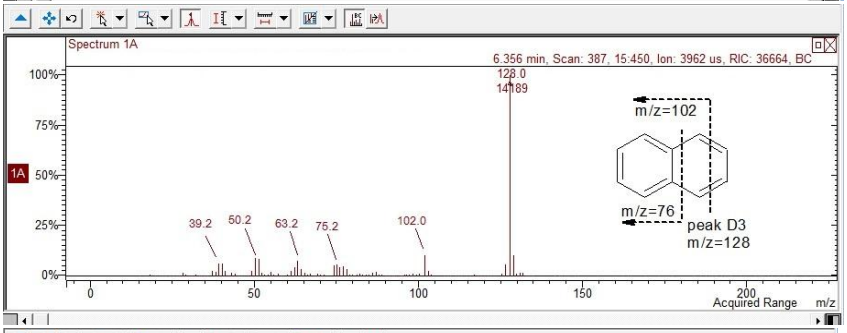

peak D4

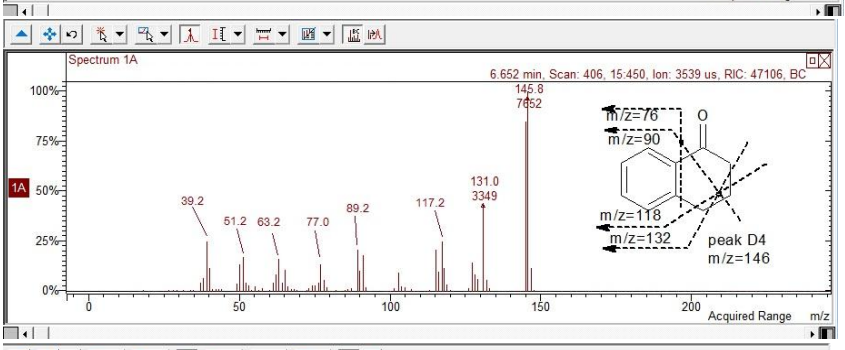

peak D5

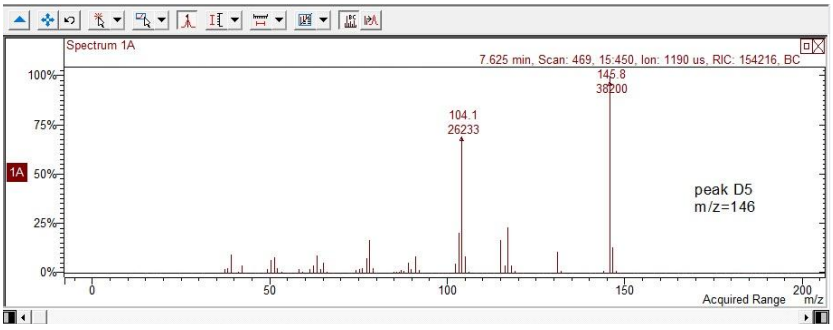

peak D6

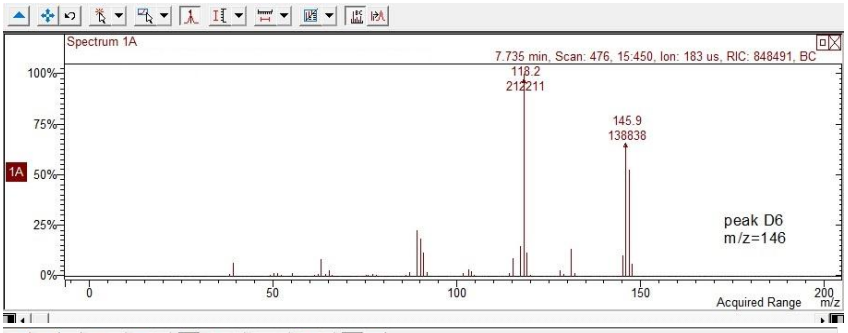

peak D7

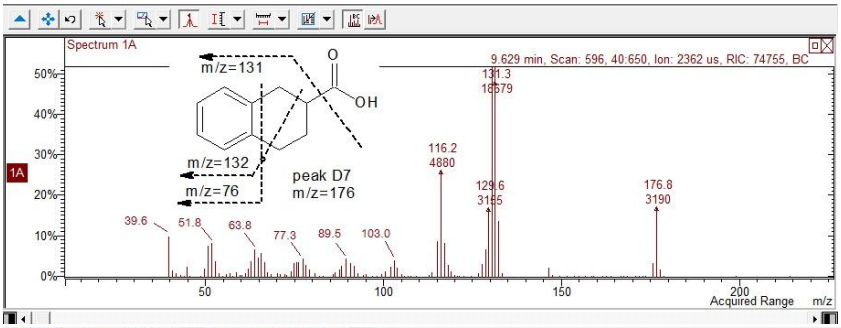

peak D8

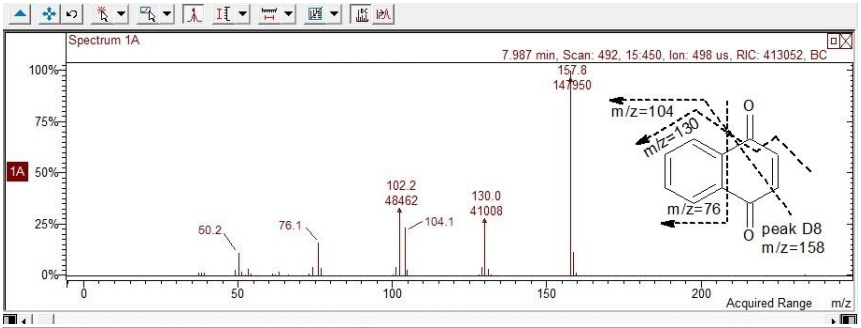

peak D9

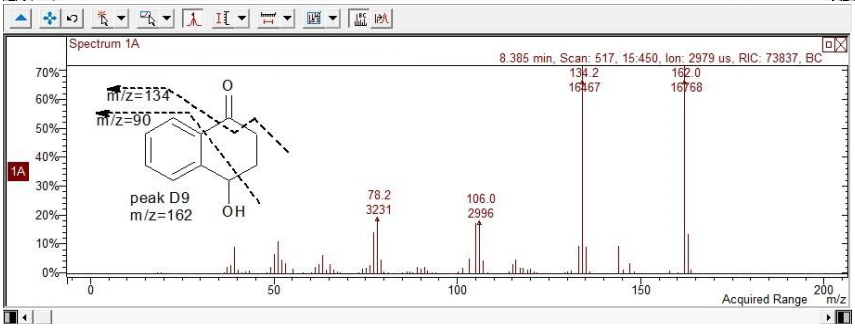

peak D10

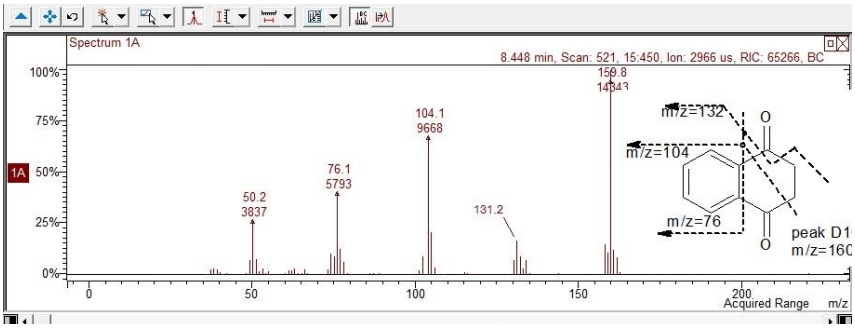

peak D11	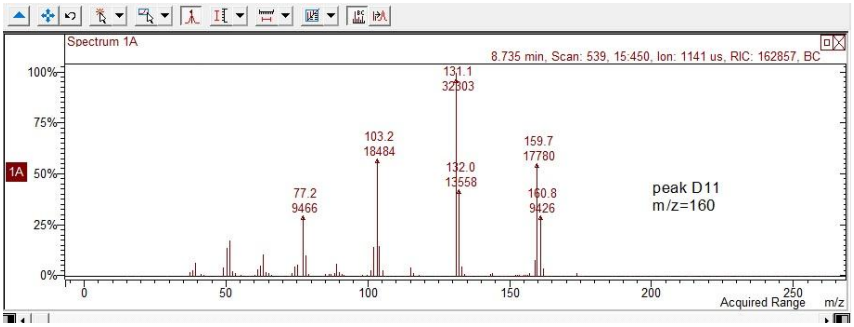
peak D12	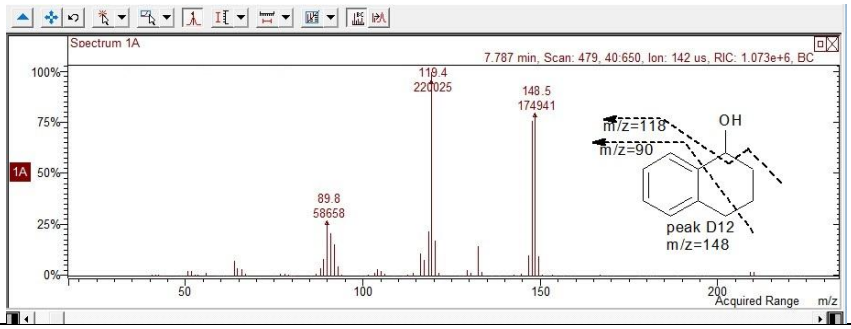
peak back ground	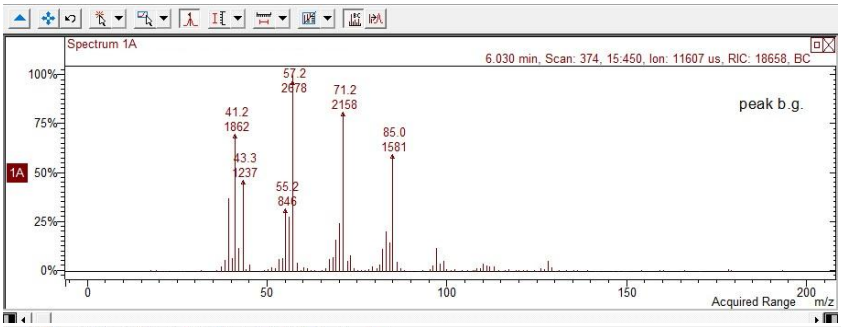
Peak column	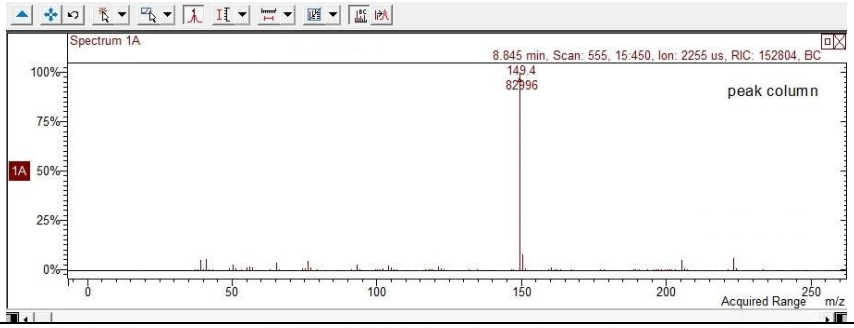

Note: For Section 3.2, Chapter III.

Published and submitted articles

Journal of Hazardous Materials 318 (2016) 355–362

Contents lists available at ScienceDirect

Journal of Hazardous Materials

journal homepage: www.elsevier.com/locate/jhazmat

Mineralization of naphtenic acids with thermally-activated persulfate: The important role of oxygen

Xiyan Xu, Gema Pliego, Juan A. Zazo, Jose A. Casas, Juan J. Rodriguez *

Chemical Engineering Section, University Autonoma of Madrid, Crta. Colmenar km 15, 28049 Madrid, Spain

HIGHLIGHTS

- Complete mineralization of NAs was achieved with substoichiometric persulfate.
- Dissolved oxygen played an important role as experimentally verified.
- The normalized rate constants of mineralization (k_n) are obtained.
- The radical mechanism is analyzed.
- The effect of chloride and bicarbonate as potential scavengers is investigated.

GRAPHICAL ABSTRACT

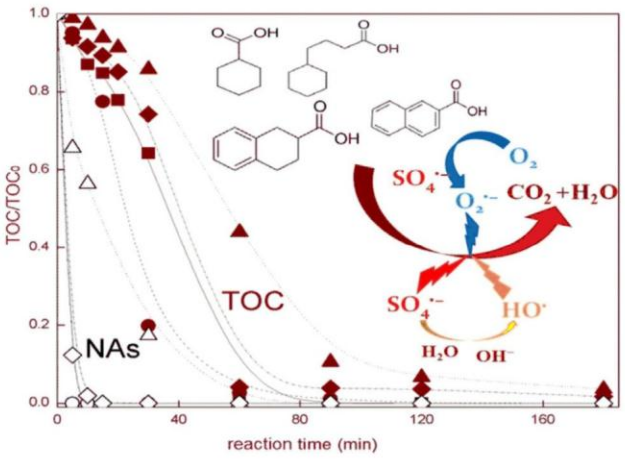

ARTICLE INFO

Article history:
Received 14 May 2016
Received in revised form 3 July 2016
Accepted 5 July 2016
Available online 6 July 2016

Keywords:
Naphthenic acids
Persulfate oxidation
Oxygen oxidation
Mineralization
Radical reaction

ABSTRACT

This study reports on the mineralization of model naphtenic acids (NAs) in aqueous solution by catalyst-free thermally-activated persulfate (PS) oxidation. These species are found to be pollutants in oil sands process-affected waters. The NAs tested include saturated-ring (cyclohexanecarboxylic and cyclohexanebutyric acids) and aromatic (2-naphthoic and 1,2,3,4-tetrahydro-2-naphthoic acids) structures, at 50 mg L^{-1} starting concentration. The effect of PS dose within a wide range (10–100% of the theoretical stoichiometric) and working temperature (40–97 °C) was investigated. At 80 °C and intitial pH = 8 complete mineralization of the four NAs was achieved with 40–60% of the stoichiometric PS dose. This is explained because of the important contribution of oxygen, which was experimentally verified and was found to be more effective toward the NAs with a single cyclohexane ring than for the bicyclic aromatic-ring-bearing ones. The effect of chloride and bicarbonate was also checked. The former showed negative effect on the degradation rate of NAs whereas it was negligible or even positive for bicarbonate. The rate of mineralization was well described by simple pseudo-first order kinetics with values of the rate constants normalized to the PS dose within the range of 0.062–0.099 h^{-1}. Apparent activation energy values between 93.7–105.3 kJ mol^{-1} were obtained.

1. Introduction

Exploitation of non-conventional gas and oil resources has to deal with important challenges [1,2]. Increasing attention has been

* Corresponding author.
E-mail address: juanjo.rodriguez@uam.es (J.J. Rodriguez).

http://dx.doi.org/10.1016/j.jhazmat.2016.07.009
0304-3894/

paid to the environmental impact of naphthenic acids (NAs) from oil sands process-affected water (OSPW). These species appear also in other industries such as wood preservatives and paint additives [3–5]. In general terms, NAs refer to carboxylic acids found in crude oil. The predominant species correspond to alkyl-substituted cycloaliphatic structures and also aromatic rings are present in some minor components but of significant environmental concern [5,6]. NAs have been reported as extremely persistent in the tailing ponds with in-situ degradation half-life higher than ten years [7]. Moreover, they have been observed to be of great hazard toward several testing organisms due to its acute toxicity associated to their complex structure and their transformation into oxy-NAs induced by oxygen-containing species upon long time retention in aquatic systems [8].

Some non-destructive methods, like adsorption, allow successful removal from the aqueous phase but transferring the NAs to the solid adsorbent which then has to be conveniently treated or disposed [9–11]. Biological treatments have proved to be cost-effective for partially reducing the toxicity of NAs [12], but complete decomposition of certain portion of recalcitrant NAs cannot be achieved by biodegradation [13]. Advanced oxidation processes (AOPs) have been widely investigated for the breakdown of many recalcitrant compounds due to their broad applicability [14–16]. AOPs are based on the action of the hydroxyl radical as main oxidizing species with a high redox potential ($E_0 = 2.8$). Meanwhile, sulfate radical-based AOPs exhibit competitive oxidation capacity ($E_0 = 2.5–3.1$) [17] for the degradation of different kinds of pollutants [18,19]. The generation of hydroxyl or sulfate radicals in advanced oxidation systems are commonly induced by metal catalysts [20], or energy sources, including thermal [21], light [22,23] and electrical [24]. Thermally-activated decomposition of persulfate (PS) gives rise to sulfate radicals according to Reaction (1):

$$S_2O_8^{2-} + \text{heat} \rightarrow 2SO_4^{\bullet-} \quad (1)$$

Besides, mechanistic studies have shown that hydroxyl radicals, generated from the interaction of PS and hydroxide ions and/or water (Reactions (2) and (3)), could also participate in the breakdown of target pollutants [25].

$$SO_4^{\bullet-} + OH^- \rightarrow SO_4^{2-} + HO^{\bullet} \quad (2)$$

$$SO_4^{\bullet-} + H_2O \rightarrow SO_4^{2-} + HO^{\bullet} + H^+ \quad (3)$$

In recent years, several evidences have been reported that oxygen acts positively in PS-based oxidation systems at ambient conditions in the presence of various catalysts by transforming into reactive $O_2^{\bullet-}/HO_2^{\bullet}$ [26–28]. However, the stoichiometric contribution of oxygen as an oxidant in the PS-based systems for the mineralization of the target pollutants has not been documented in those literatures.

The mineralization ability of PS-based systems has been investigated with different organic contaminants. Complete [25] as well as partial [23,29] TOC removal has been reported. Kinetic studies of PS oxidation activated by different approaches confirm that several reactive species play a role in the mineralization process. As indicated before, those species include sulfate/hydroxyl radicals, but also PS ions and/or other intermediates. Models, such as those based on competitive reactions with steady-state approximation, have been used to describe the kinetics of PS oxidation [30–32]. In principle, the evolution of target pollutants can be described by a pseudo-first-order rate equation [33] and the values of the apparent rate constant and the corresponding normalized rate constants can be used to compare among different systems at a level of generality [34] so that they can provide information on the suitability of AOP methods toward given target pollutants. However, the apparent rate constants referred to specific compounds obviously serve only to describe the rate of disappearance of those species whereas TOC-based kinetic studies are needed to learn on the rate of mineralization. So far, there is a lack of information on that respect in the literature.

Because of the well-known stability of PS, remote/localized or even direct heating activation of PS could be used in several in situ thermal remediation (ISTR) technologies. Increasing the temperature will not only promote the decomposition of PS to sulfate radicals, but also would favor the activation of other related radicals [33]. Therefore, the application of ISTR with PS oxidation approach making use of the processing temperature of OSPWs, well above the ambient, is of promising potential for the abatement of NAs from those effluents [35].

A few hydroxyl or sulfate radical-based AOPs using different activation approaches have been checked for the degradation of NAs, such as UV/H_2O_2, UV/$S_2O_8^{2-}$ and Zero Valent Iron (ZVI) catalyze [6,22,36]. The generated hydroxyl radicals attack the 4 position of the hydrocarbon rings of cyclohexanoic acid and the α position of aliphatic chain [36], while the sulfate radicals provoke the decarboxylation of target pollutants [37]. Fenton, that is one of the main hydroxyl radical generating systems, has not been successfully used in NAs abatement, because of the basic pH (around 8) of the OSPW containing those species [38], whereas Fenton oxidation is strictly pH dependent (pH ≈ 3.5). Opposite to that, PS-based oxidation systems have proved to be effective for the degradation of pollutants within a wide pH range [25,39]. PS oxidation not relying on the action of radicals from PS has also been reported recently. Zhang et al. [23] investigated the degradation of 2,4-dichlorophenol with PS activated with CuO.

In the current work, the mineralization of four NAs (with and without aromatic rings) by catalyst-free thermally-activated PS oxidation is investigated and the corresponding constants are given. The NAs used as target pollutants include cyclohexanecarboxylic acid (CHA), cyclohexanebutyric acid (CHBA), 2-naphthoic acid (2-NA) and 1,2,3,4-tetrahydro-2-naphthoic acid (1234-T-2-NA). The two former are saturated-ring structures while the last are aromatic ring-bearing bicyclic ones. The role of oxygen is studied, as well as the effect of potential scavenging ions, like chloride and bicarbonate commonly found in OSPWs.

2. Material and methods

The NAs tested (CHA, CHBA, 2-NA and 1234-T-2-NA, see Fig. S1 in Supporting information) were purchased from Sigma-Aldrich (purity ≥98%). PS oxidation experiments were carried out in 100 mL glass batch reactors placed in a constant-temperature water bath with a shacking frequency equivalent to 200 rpm. Given amounts of PS and/or other reagents (scavengers or salts) were added into the reactors containing 50 mL of 50 mg L^{-1} NAs aqueous solution (0.39, 0.29, 0.29 and 0.28 mM of CHA, CHBA, 2-NA and 1234-T-2-NA respectively). Previous to the addition of PS, the reactors were preheated for 15–30 min to make sure that the reactions were initiated at the testing temperature (40–97 ± 1 °C). The degradation of the starting compounds during the preheating stage was always negligible in all the cases. Tests in inert atmosphere were also carried out, using an inert atmosphere chamber with the NAs samples and PS solutions previously bubbled by N_2 for 30 min. All the experiments were performed by duplicate and the differences were always lower than 5%. The theoretical stoichiometric dose of PS for complete oxidation of CHA, CHBA, 2-NA and 1234-T-2-NA was calculated from the reactions:

$$\text{CHA}: C_7H_{12}O_2 + 36SO_4^{\bullet-} + 12H_2O \rightarrow 7CO_2 + 36SO_4^{2-} + 36H^+ \quad (4)$$

$$\text{CHBA}: C_{10}H_{18}O_2 + 54SO_4^{\bullet-} + 18H_2O \rightarrow 10CO_2 + 54SO_4^{2-} + 54H^+ \quad (5)$$

$$\text{2-NA}: C_{11}H_8O_2 + 48SO_4^{\bullet-} + 20H_2O \rightarrow 11CO_2 + 48SO_4^{2-} + 48H^+ \quad (6)$$

$$\text{1234-T-2-NA}: C_{11}H_{12}O_2 + 52SO_4^{\bullet-} + 20H_2O \rightarrow 11CO_2 + 52SO_4^{2-} + 52H^+ \quad (7)$$

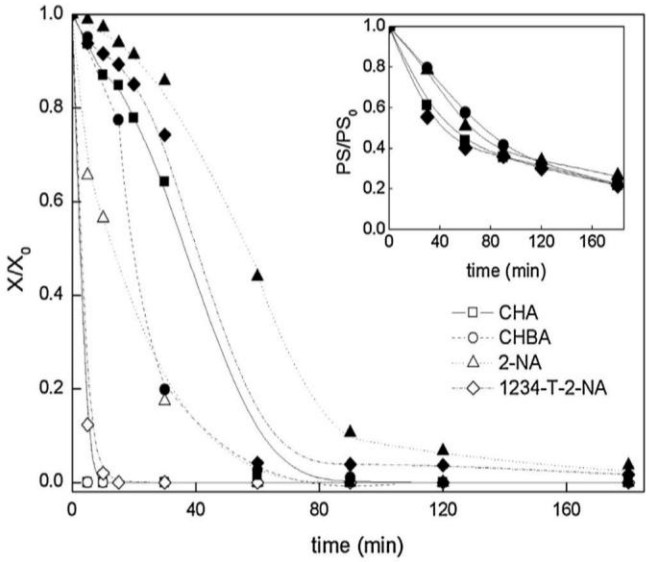

Fig. 1. Time course of NAs (open symbols) and TOC (solid symbols) upon thermally-activated PS oxidation. [NAs] = 50 mg L^{-1}, T = 80 °C, pH = 8, PS at the corresponding stoichiometric dose.

The samples were cooled in water bath to room temperature after reaction and analyzed immediately. The concentrations of CHA and CHBA were measured by Gas Chromatography with Flame Ionization Detector (GC-FID) in a GC 3900 Varian provided with a 30 mm length × 0.25 mm i.d. capillary column (CP-Wax 52 CB, Varian) using nitrogen as carrier gas. For CHA, the initial oven temperature was set at 70 °C and then increased up to 240 °C at a rate of 30 °C min^{-1}. For CHBA, the only difference was lowering the heating rate to 20 °C min^{-1}. The concentrations of 2-NA and 1234-T-2-NA were determined by high-performance liquid chromatography (HPLC; Varian Pro-Start 240) with a UV detector and Microsorb C18 5 μm column (250 × 4.6 mm) as stationary phase. Acetonitrile and 4 mM H_2SO_4 (1/1) were used as mobile phase at an injection rate of 1 mL min^{-1} with the oven temperature set at 60 °C. Total organic carbon (TOC) was measured by a TOC analyzer (Shimadzu, mod. TOC VSCH). PS concentration was determined by a spectrophotometric method based on a modification of the iodometric titration analysis [40].

3. Results and discussion

Fig. 1 shows the evolution of the four NAs tested upon reaction time using the corresponding stoichiometric amount of PS at 80 °C and initial pH = 8. Blank experiments were performed under the same conditions in absence of PS where the degradation of the NAs tested was always negligible, thus confirming the thermal stability of those compounds already reported in the literatures [6,22]. The two NAs containing a single cyclohexane ring (CHA and CHBA) were converted in a fairly short time in the presence of PS, most in particular CHBA, whereas the disappearance of the aromatic ring-bearing bicyclic NAs required some more time, especially in the case of the binuclear aromatic 2-NA, although complete conversion was also achieved in less than 1.5 h. The disappearance of the starting NAs consumed fairly low relative amounts of PS as can be seen from its evolution, also depicted in Fig. 1.

To learn more on the degradation of the NAs, the evolution of TOC upon reaction time was also followed and is included in Fig. 1. As expected, the mineralization of NAs was slower than its disappearance since intermediate reaction byproducts are formed along the oxidation process. The reactive radical species attack certain positions of the naphthenic and aromatic rings of NAs giving rise to ring opening which leads to the formation of short-chain carboxylic acids further oxidized to CO_2 and H_2O [6,36]. Complete mineralization was finally achieved in all the cases although upon significantly different reaction times following the same order observed for the disappearance of the starting NAs. TOC reduction takes place from the beginning of the oxidation process suggesting that some extent of direct mineralization of the starting NAs may not be discarded although proceeding at a slower rate as inferred from the lower slope of the initial stage of the TOC curves. The evolution of TOC has been fitted to a simple pseudo-first order rate equation and the corresponding values of the rate constants are given in Table 1. In each case, separate values for the initial stage and the rest of the TOC curve have been calculated, showing significant differences among both regions as expected from the shape of the curves. Overall values are also included in Table 1, together with the corresponding correlation coefficients which confirm the significantly poorer fitting of the data when considering a sole rate equation for the whole TOC curve.

3.1. Effect of PS dose

Different relative amounts of PS were tested, varying from 10 to 80% of the corresponding theoretical stoichiometric dose and the results in terms of mineralization are depicted in Fig. 2. Some differences are observed among the four NAs tested at equivalent PS doses. However, it is interesting that complete mineralization of the four was achieved with PS doses well below the stoichiometric (40% for CHA and CHBA, 50% for 1234-T-2-NA and 60% for 2-NA). The mineralization of non-aromatic NAs consumes less PS than the aromatic ones. These doses are lower than the previously reported in the literatures [22,41], thus allowing a more favorable view on the potential application.

Opposite to the observed at 100% and 80% of the stoichiometric PS dose, the kinetics of mineralization under strongly substoichiometric conditions (10%–60%) can be well described in all the cases by a sole rate equation covering the overall TOC vs. time curve with correlation coefficients between 0.95–0.99 (Table 2).

The values of the pseudo-first order rate constant at different initial PS/NAs molar ratios are plotted in Fig. 3. Reasonably good linear fits were obtained, with the corresponding slopes providing the values of normalized rate constants which serve to compare the reactivity of the NAs tested. Those values (k_n) are included in Fig. 3 together with the correlation coefficients. Looking at the k_n values, the reactivity of the four NAs tested are of the same order, differing less than two-fold between the most (CHBA) and the least (2-NA) reactive species. A conclusive structure-to-reactivity relationship cannot be established at this point since the susceptibility to mineralization does not depend exclusively on the starting compound but also on the intermediate oxidation byproducts, being k_n a lumped parameter in that respect, which, anyway, provides useful practical information.

3.2. Effect of the temperature

Experiments were carried out at different temperatures (40, 60, 80, and 97 °C) with PS at 40% of the stoichiometric. The results are shown in Fig. 4, where it can be seen that the oxidation process must work at least around 80 °C to be effective at that low PS dose. At that temperature, more than 90% mineralization of the single-cyclohexane-ring-NAs tested was achieved after 4 h while the bicyclic aromatic ring-bearing ones required substantially higher reaction time. Below 80 °C, TOC reduction was very slow in all cases. Extending the reaction time up to 1 d, complete mineralization of CHA and CHBA was achieved at 60 °C while it still was fairly low in the cases of 2-NA and 1234-T-2-NA (23.6 and 27.7% respectively). At 40 °C, less than 10% TOC removal was

Table 1
Mineralization rate constants of NAs with the stoichiometric dose of PS: T = 80 °C, pH = 8.

NAs	Stage 1			Stage 2		Overall	
	$k_{TOC'_1}$ (h^{-1})	R^2	stage 1 duration (min)	$k_{TOC'_2}$ (h^{-1})	R^2	$k_{TOC'}$ (h^{-1})	R^2
CHA	0.72 ± 0.06	0.98	20	6.20 ± 0.65	0.96	4.09 ± 0.81	0.80
CHBA	1.05 ± 0.11	0.97	20	4.07 ± 0.37	0.99	3.64 ± 0.30	0.80
2-NA	0.32 ± 0.02	0.97	30	1.71 ± 0.19	0.96	0.98 ± 0.13	0.87
1234-T-2-NA	0.76 ± 0.06	0.98	20	3.49 ± 0.23	0.96	1.84 ± 0.33	0.86

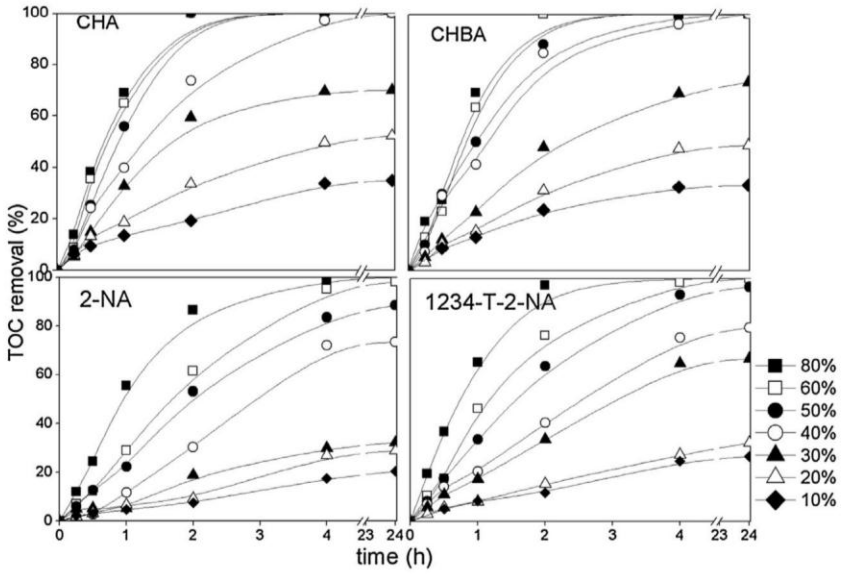

Fig. 2. TOC evolution upon reaction time at different PS doses (% of the stoichiometric).

Table 2
Mineralization rate constants of NAs under different conditions.

Percentage of stoich. dose (%)		CHA		CHBA		2-NA		1234-T-2-NA	
	T (°C)	$k_{TOC'} \times 10$ (h^{-1})	R^2	$k_{TOC'}$ (h^{-1})	R^2	$k_{TOC'} \times 10$ (h^{-1})	R^2	$k_{TOC'} \times 10$ (h^{-1})	R^2
10	80	0.95 ± 0.05	0.98	0.10 ± 0.01	0.95	0.02 ± 0.001	0.95	0.58 ± 0.04	0.98
20	80	1.66 ± 0.10	0.97	0.19 ± 0.02	0.97	0.77 ± 0.09	0.95	0.95 ± 0.07	0.98
30	80	3.87 ± 0.35	0.98	0.39 ± 0.02	0.99	1.60 ± 0.09	0.99	2.62 ± 0.19	0.98
40	40	0.16 ± 0.01	0.98	0.07 ± 0.007	0.96	0.11 ± 0.01	0.95	0.05 ± 0.001	0.99
	60	0.77 ± 0.08	0.95	0.35 ± 0.04	0.97	0.55 ± 0.05	0.95	0.20 ± 0.01	0.99
	80	6.55 ± 0.48	0.95	0.84 ± 0.07	0.97	3.29 ± 0.44	0.95	4.17 ± 0.42	0.95
	97	40.5 ± 7.03	0.98	18.9 ± 1.75	0.96	16.3 ± 1.39	0.98	9.19 ± 0.47	0.99
50	80	8.23 ± 0.93	0.96	1.20 ± 0.08	0.98	4.63 ± 0.31	0.98	6.86 ± 0.55	0.97
60	80	10.6 ± 1.06	0.98	1.38 ± 0.08	0.98	7.50 ± 0.37	0.98	9.85 ± 0.76	0.95

achieved after one-day reaction time in all the cases since PS conversion remained also below that percentage. The starting colorless solution of the aromatic NAs turned to dark brown, suggesting that although 40 °C is too low for the mineralization, certain transformation seems to be induced. At 97 °C, the TOC abatement was dramatically accelerated (Fig. 4 and Table 2). However, complete mineralization was never achieved at this PS dose (40% of the stoichiometric), although PS was completely converted within 1 h. Opposite to that, at 80 °C complete mineralization appears more likely (in particular for the non-aromatic NAs) since the corresponding curves did not reach a saturation level as it was the case at 97 °C. This high-temperature-caused efficiency decline has been previously reported in PS oxidation [21,42]. Increasing the temperature accelerates the release of sulfate radicals leading to a faster breakdown of NAs, but the scavenging effect of those radicals can also be accelerated due to the higher concentration [25].

The values of the mineralization first-order rate constants at different temperatures are collected in Table 2, confirming the important effect of temperature above 60 °C. Table 3 summarizes the values of apparent activation energy calculated from the Arrhenius equation. As can be seen, they fall within a fairly narrow range in the vicinity of 100 kJ mol^{-1} for all the NAs tested.

Table 3
Apparent activation energy of NAs mineralization.

NAs	Ea (kJ mol^{-1})	R^2
CHA	96.2 ± 0.7	0.99
CHBA	100.9 ± 0.6	0.98
2-NA	93.7 ± 0.7	0.99
1234-T-2-NA	105.3 ± 1.9	0.97

3.3. The role of oxygen

The results obtained under substoichiometric PS doses suggest that sulfate radicals must not be the only reactive species to

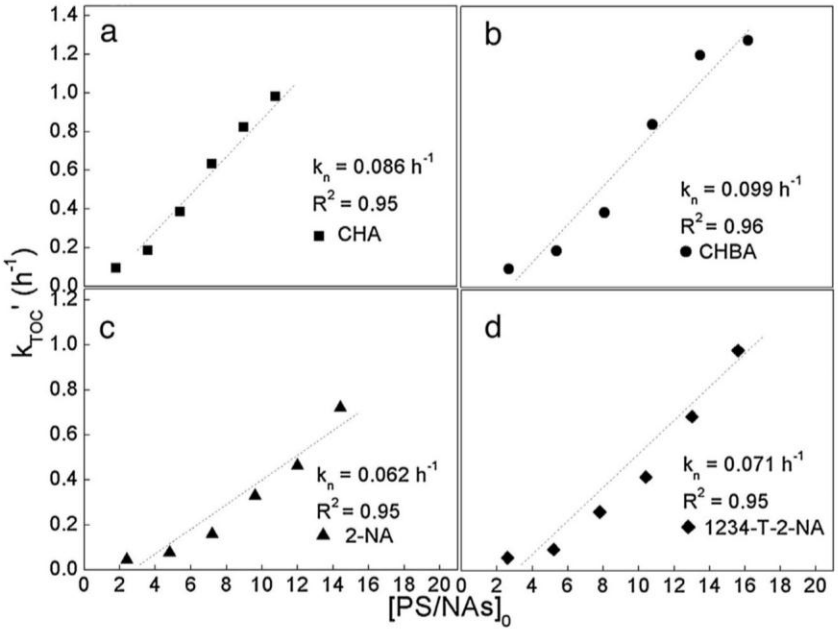

Fig. 3. Values of the pseudo-first order rate constant of NAs mineralization at different initial PS/NAs molar ratios.

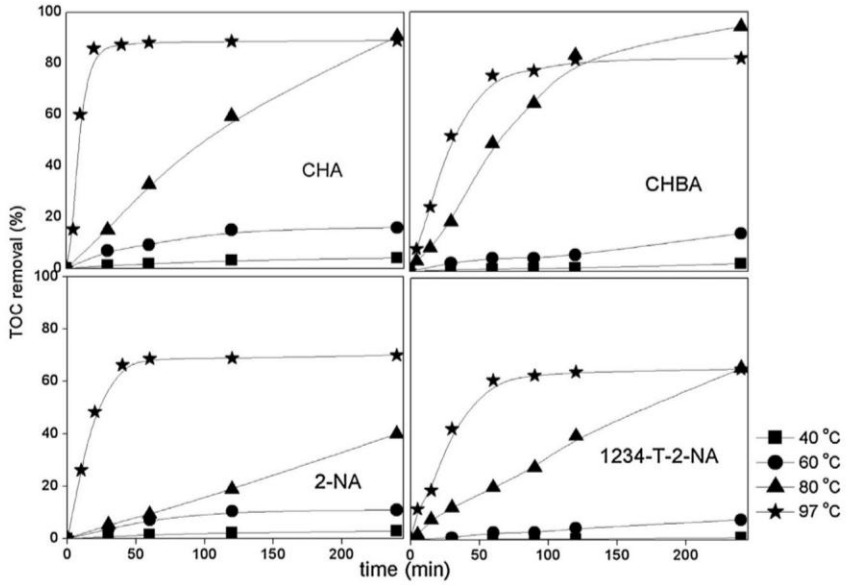

Fig. 4. Effect of temperature on the mineralization of the NAs tested with PS at 40% of the stoichiometric.

degrade NAs but some other must also contribute. In fact it has been reported that PS gives rise to other active species in addition to sulfate radicals in AOP systems [21,43,44]. PS might react with water or even hydroxide ions in alkaline conditions generating hydroxyl radicals (Reactions (2) and (3)) [43]. Consistently with those reactions, an important decrease of pH (from 8 to 2–4) was observed in all of our experiments in agreement with other authors [43]. However, those hydroxyl radicals result from sulfate ones so that there is no net gain in the stoichiometry towards mineralization and the same occurs with other potentially oxidant species whose occurrence is consequent to PS decomposition or reaction. Therefore, the extra oxidation ability observed with respect to the theoretically expected from PS and PS-derived oxidant species must have other origin. In that respect, oxygen appears the most likely candidate for that extra capacity. Oxygen takes part in catalytic wet air oxidation but that technology operates under fairly different conditions than those of thermally-activated PS oxidation. On the other hand, this last does not use any metallic catalyst capable of activating the oxygen molecule. To investigate the possible role of oxygen, runs under O_2 free conditions were carried out as described before (Materials and methods). The results (depicted in Fig. 5) differ significantly from the obtained in the previous regular experiments carried out in presence of oxygen (Fig. 1). The mineralization proceeds now at lower rate and the extent of mineralization after 4 h of reaction is also lower. Fig. 6 shows the TOC removal vs. PS converted in the presence and absence of oxygen. As can be seen, the system is significantly more efficient in the presence of oxygen where the TOC abatement clearly exceeds the maximum expected from the stoichiometry of Reactions ((4)–(7)). Fang et al. [45] found that the $O_2^{\bullet-}$ radicals derived from oxygen could enhance the generation of $SO_4^{\bullet-}$ radicals from PS when investigating the degradation of PCBs with magnetite nanoparticles as catalyst. Very recently,

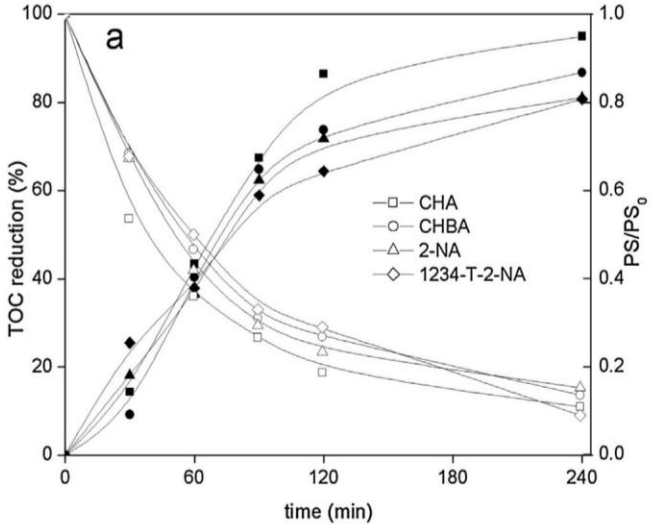

Fig. 5. Time course of TOC (solid symbols) and PS (open symbols) upon thermally-activated PS oxidation of the NAs tested under oxygen-free conditions (PS at the stoichiometric dose).

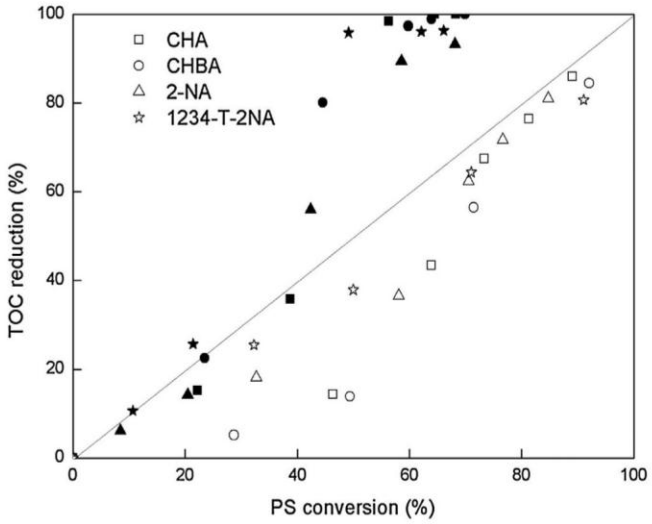

Fig. 6. TOC removal vs. PS converted in presence (solid symbols) and absence (open symbols) of oxygen (PS initially at the stoichiometric dose according to Reactions (4)–(7)).

detailed reaction mechanisms of benzene oxidation with PS in the presence of solid catalysts have been established including the contribution of oxygen [28]. A hydroxylcyclohexadienyl (HCHD) radical formed acted as a key intermediate which tent to react with oxygen to accelerate the ring-opening process. The current work further verifies quantitatively in terms of mineralization extent that oxygen is not only able to accelerate the PS oxidation process but also acts as an important oxidant enhancing mineralization in thermally-activated catalyst-free systems. The reaction between NAs and sulfate/hydroxyl radicals might give rise to the corresponding organic radicals (Reactions (8) and (9)) [28,45] that tend to react with oxygen to generate $O_2^{\bullet-}/HO_2^{\bullet}$ (Reactions (10) and (11)) [26,46], which have been recognized as reactive species in PS-based oxidation [27].

$$SO_4^{\bullet-} + R-H \rightarrow HSO_4^- + {}^{\bullet}R \quad (8)$$

$$HO^{\bullet} + R-H \rightarrow H_2O + {}^{\bullet}R \quad (9)$$

$$ {}^{\bullet}R + O_2 \rightarrow R^+ + O_2^{\bullet-} \quad (10)$$

$$O_2^{\bullet-} + H^+ \leftrightarrow HO_2^{\bullet} \quad (11)$$

The enhanced efficiency of the system under available oxygen is more noticeable as oxidation proceeds which can be explained by the increasing contribution of Reaction (11) at lower pH. Also in the earlier stages, at higher PS concentration, self-scavenging reactions are more likely.

According to the results so far, the reaction of PS oxidation can be rewritten to take into account the contribution of oxygen:

CHA:

$$C_7H_{12}O_2 + (36-4n)SO_4^{\bullet-} + nO_2 + (12-2n)H_2O \rightarrow 7CO_2 + (36-4n)SO_4^{2-} + (36-4n)H^+, (0 \le n \le 6) \quad (12)$$

CHBA:

$$C_{10}H_{18}O_2 + (54-4n)SO_4^{\bullet-} + nO_2 + (18-2n)H_2O \rightarrow 10CO_2 + (54-4n)SO_4^{2-} + (54-4n)H^+, (0 \le n \le 9) \quad (13)$$

2-NA:

$$C_{11}H_8O_2 + (48-4n)SO_4^{\bullet-} + nO_2 + (20-2n)H_2O \rightarrow 11CO_2 + (48-4n)SO_4^{2-} + (48-4n)H^+, (0 \le n \le 10) \quad (14)$$

1234-T-2-NA:

$$C_{11}H_{12}O_2 + (52-4n)SO_4^{\bullet-} + nO_2 + (20-2n)H_2O \rightarrow 11CO_2 + (52-4n)SO_4^{2-} + (52-4n)H^+, (0 \le n \le 10) \quad (15)$$

According to those reactions and our experimental results, the nature of the target compound is of great importance regarding the contribution of oxygen in thermally-activated PS oxidation. The system is, in that sense, especially more reactive toward saturated rings than to aromatic ones.

To learn more on the radical mechanism involved, some quenching experiments were carried out with 1234-T-2-NA, selected because it contains both naphthenic and aromatic ring. TBA and EtOH were used as quenching agents at 500/1 alcohol/PS molar ratio [18,39,43,47,48]. According to the different reaction rates between alcohols and free radicals, the generation of sulfate and hydroxyl radicals can be readily proved by the comparison of the inhibiting effect of scavengers toward our tested systems (Fig. 7). Furthermore, TBA was added into the system at different times. The rate of 1234-T-2-NA disappearance increased as the TBA addition was retarded, as can be seen in Fig. 7, suggesting that the formation of hydroxyl radicals (and thus their contribution) occurs mainly in the early stages.

It has been reported in the literature that the role of hydroxyl radicals in PS oxidation systems varies according to the reaction conditions, most in particular the pH of the medium [25,39]. More hydroxyl radicals are believed to be formed by increasing pH. However, a decrease of efficiency has been reported above pH 9 [25]. The reason is controversial, but one explanation is that reaction between hydroxyl and persulfate radicals might occur giving rise to relatively less reactive radicals. In our case, the initial pH of the NAs solutions was always set at 8 (the common pH of OSPW). At that pH, the contribution of hydroxyl radicals must be appreciable but quite limited compared with that of sulfate ones (Fig. 7).

Spectroscopic studies by EPR can contribute to better elucidate the radical mechanism involved in persulfate as well as other oxidation processes. However, much effort needs still to be done in the future to allow identifying the wide diversity of short-lived species in such complex reaction media. In a recent paper, C. Zhu et al. [49] have used EPR spectroscopy with DMPO as a spin-trapping agent

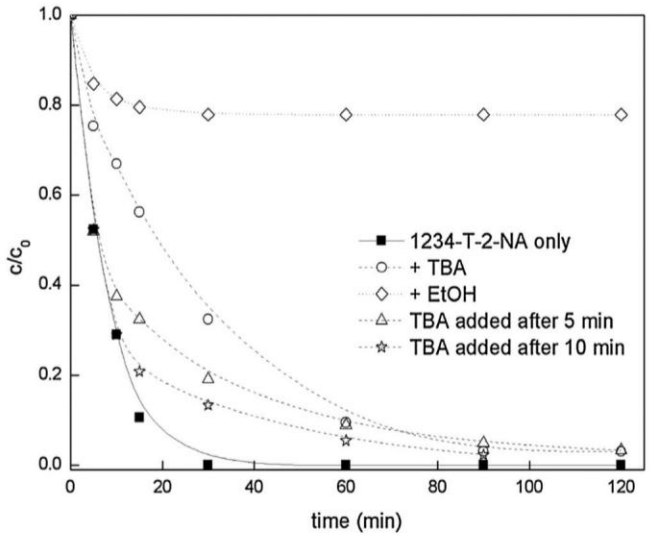

Fig. 7. Effect of scavengers on the degradation of 1234-T-2-NA (Scavenger/NA molar ratios = 500/1, PS at 40% of the stoichiometric).

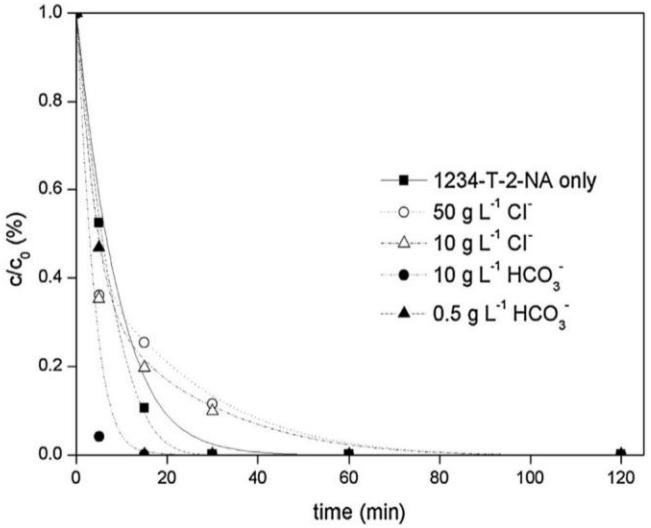

Fig. 8. Effect of Cl^- and HCO_3^- on the degradation of 1234-T-2-NA upon PS oxidation (PS at 40% of the stoichiometric, T = 80 °C).

to detect free radicals in the zero-valent iron-activated persulfate degradation of DDT. They could follow by this the generation of sulfate and hydroxyl radicals upon the reaction. Zhong et al. [50] found a more complex EPR spectrum, including a carbon-centered radical in addition to the sulfate and hydroxyl ones, for a reaction medium from 1,4-dioxane degradation upon persulfate activation by iron filings.

3.4. Effect of chloride and bicarbonate

OSPW in general contain fairly high concentrations of chloride as well as bicarbonate, both being potential scavengers [6]. Some authors have found that the effects of chloride and bicarbonate on PS oxidation systems relies on several factors such as the pH, the activation source and the type of target compounds [51,52]. For example, it has been reported that enhancement rather than inhibition of thermally-activated PS oxidation was observed in the presence of chloride using *p*-nitrosodimethylaniline as the target molecule, while no significant effect of bicarbonate ions was found [52].

To learn on the effect of those ions on the breakdown of 1234-T-2-NAs by PS oxidation, experiments were conducted at 80 °C with different concentrations of them, using 40% of the stoichiometric PS dose. The results obtained are shown in Fig. 8, where it can be observed only some small negative effect of chloride. Complex reactions are involved in the interaction between chloride ion and sulfate/hydroxyl radicals. Species like $Cl^{\bullet}$, $Cl_2^{\bullet-}$, $ClHO^{\bullet-}$ can be generated which are believed to be less reactive than sulfate or hydroxyl radicals [30,51,52]. Moreover, $Cl^{\bullet}$ can even provoke the formation of chloro-NA according to previous researches [6]. Therefore, the effect of chloride needs to be considered in practical application of oxidation processes in general. Regarding the impact of bicarbonate ions, it has been reported that $HCO_3^{\bullet}$ might be generated from the reaction between HCO_3^- and sulfate radicals giving rise to some changes of the redox potential [52].

4. Conclusions

Oxidation with thermally-activated PS at 80 °C allowed achieving complete mineralization of the naphthenic acids tested with frankly substoichiometric amount of PS. The rate of TOC removal was well described by a simple pseudo-first order rate equation. The values of the normalized rate constants (k_n) followed the order: CHBA > 1234-T-2-NA > CHA > 2-NA. Fairly similar values of activation energy, in the vicinity of 100 kJ moL^{-1}, were obtained. Oxygen was found to play an important role in the mineralization process and the system showed to be more effective toward the saturated-ring species than for the aromatic ones. Sulfate and hydroxyl radicals were verified to be the reactive species for NAs breakdown, with the former being by far the dominant ones. The impact of chloride and bicarbonate as potential scavengers was also analyzed. Only certain small negative effect of chloride was observed. The results allow learning on the potential application of this process to the treatment of oil sands process-affected waters (OSPWs).

Acknowledgements

Spanish MINECO is gratefully acknowledged for the financial support through the project CTQ2013-41963-R. We are also grateful to the Chinese Scholarship Council (CSC) for supporting the Ph.D. program of Xiyan Xu (CSC, File No. 201308410047).

Appendix A. Supplementary data

Supplementary data associated with this article can be found, in the online version, at http://dx.doi.org/10.1016/j.jhazmat.2016.07.009.

References

[1] D. Schindler, Tar sands need solid science, Nature 468 (2010) 499–501.
[2] G. Zeng, M. Chen, Z. Zeng, Shale gas: surface water also at risk, Nature 499 (2013), 154–154.
[3] D. Jones, A.G. Scarlett, C.E. West, S.J. Rowland, Toxicity of individual naphthenic acids to *Vibrio fischeri*, Environ. Sci. Technol. 45 (2011) 9776–9782.
[4] R.P. Rodgers, A.M. McKenna, Petroleum analysis, Anal. Chem. 83 (2011) 4665–4687.
[5] B. Wang, Y. Wan, Y. Gao, M. Yang, J. Hu, Determination and characterization of oxy-naphthenic acids in oilfield wastewater, Environ. Sci. Technol. 47 (2013) 9545–9554.
[6] P. Drzewicz, L. Perez-Estrada, A. Alpatova, J.W. Martin, M. Gamal El-Din, Impact of peroxydisulfate in the presence of zero valent iron on the oxidation of cyclohexanoic acid and naphthenic acids from oil sands process-affected water, Environ. Sci. Technol. 46 (2012) 8984–8991.
[7] X. Han, M.D. MacKinnon, J.W. Martin, Estimating the in situ biodegradation of naphthenic acids in oil sands process waters by HPLC/HRMS, Chemosphere 76 (2009) 63–70.
[8] X. Zhang, S. Wiseman, H. Yu, H. Liu, J.P. Giesy, M. Hecker, Assessing the toxicity of naphthenic acids using a microbial genome wide live cell reporter array system, Environ. Sci. Technol. 45 (2011) 1984–1991.

[9] A. Janfada, J.V. Headley, K.M. Peru, S. Barbour, A laboratory evaluation of the sorption of oil sands naphthenic acids on organic rich soils, J. Environ. Sci. Health A 41 (2006) 985–997.
[10] J.-L. Gong, B. Wang, G.-M. Zeng, C.-P. Yang, C.-G. Niu, Q.-Y. Niu, W.-J. Zhou, Y. Liang, Removal of cationic dyes from aqueous solution using magnetic multi-wall carbon nanotube nanocomposite as adsorbent, J. Hazard. Mater. 164 (2009) 1517–1522.
[11] S. Iranmanesh, T. Harding, J. Abedi, F. Seyedeyn-Azad, D.B. Layzell, Adsorption of naphthenic acids on high surface area activated carbons, J. Environ. Sci. Health A 49 (2014) 913–922.
[12] T. Siddique, P.M. Fedorak, J.M. Foght, Biodegradation of short-chain *n*-alkanes in oil sands tailings under methanogenic conditions, Environ. Sci. Technol. 40 (2006) 5459–5464.
[13] E. Quagraine, H. Peterson, J. Headley, In situ bioremediation of naphthenic acids contaminated tailing pond waters in the Athabasca oil sands region—demonstrated field studies and plausible options: a review, J. Environ. Sci. Health A 40 (2005) 685–722.
[14] R. Andreozzi, V. Caprio, A. Insola, R. Marotta, Advanced oxidation processes (AOP) for water purification and recovery, Catal. Today 53 (1999) 51–59.
[15] J.J. Pignatello, E. Oliveros, A. MacKay, Advanced oxidation processes for organic contaminant destruction based on the Fenton reaction and related chemistry, Crit. Rev. Environ. Sci. Technol. 36 (2006) 1–84.
[16] G. Pliego, J.A. Zazo, J.A. Casas, J.J. Rodriguez, Case study of the application of Fenton process to highly polluted wastewater from power plant, J. Hazard. Mater. 252 (2013) 180–185.
[17] P. Neta, R.E. Huie, A.B. Ross, Rate constants for reactions of inorganic radicals in aqueous solution, J. Phys. Chem. Ref. Data 17 (1988) 1027–1284.
[18] X.-Y. Xu, G.-M. Zeng, Y.-R. Peng, Z. Zeng, Potassium persulfate promoted catalytic wet oxidation of fulvic acid as a model organic compound in landfill leachate with activated carbon, Chem. Eng. J. 200 (2012) 25–31.
[19] Y. Yang, J.J. Pignatello, J. Ma, W.A. Mitch, Comparison of halide impacts on the efficiency of contaminant degradation by sulfate and hydroxyl radical-based advanced oxidation processes (AOPs), Environ. Sci. Technol. 48 (2014) 2344–2351.
[20] J. Zazo, J. Casas, A. Mohedano, J. Rodriguez, Catalytic wet peroxide oxidation of phenol with a Fe/active carbon catalyst, Appl. Catal. B 65 (2006) 261–268.
[21] Y.-C. Lee, S.-L. Lo, P.-T. Chiueh, Y.-H. Liou, M.-L. Chen, Microwave-hydrothermal decomposition of perfluorooctanoic acid in water by iron-activated persulfate oxidation, Water Res. 44 (2010) 886–892.
[22] X. Liang, X. Zhu, E.C. Butler, Comparison of four advanced oxidation processes for the removal of naphthenic acids from model oil sands process water, J. Hazard. Mater. 190 (2011) 168–176.
[23] D. Zhou, L. Chen, C. Zhang, Y. Yu, L. Zhang, F. Wu, A novel photochemical system of ferrous sulfite complex: kinetics and mechanisms of rapid decolorization of Acid Orange 7 in aqueous solutions, Water Res. 57 (2014) 87–95.
[24] S. Yuan, P. Liao, A.N. Alshawabkeh, Electrolytic manipulation of persulfate reactivity by iron electrodes for trichloroethylene degradation in groundwater, Environ. Sci. Technol. 48 (2013) 656–663.
[25] J. Criquet, N.K.V. Leitner, Degradation of acetic acid with sulfate radical generated by persulfate ions photolysis, Chemosphere 77 (2009) 194–200.
[26] G. Fang, J. Gao, D.D. Dionysiou, C. Liu, D. Zhou, Activation of persulfate by quinones: free radical reactions and implication for the degradation of PCBs, Environ. Sci. Technol. 47 (2013) 4605–4611.
[27] M.M. Ahmed, S. Chiron, Solar photo-Fenton like using persulphate for carbamazepine removal from domestic wastewater, Water Res. 48 (2014) 229–236.
[28] H. Liu, T.A. Bruton, W. Li, J. Van Buren, C. Prasse, F.M. Doyle, D.L. Sedlak, Oxidation of benzene by persulfate in the presence of Fe (III)-and Mn (IV)-containing oxides: stoichiometric efficiency and transformation products, Environ. Sci. Technol. (2015).
[29] Y.-T. Lin, C. Liang, J.-H. Chen, Feasibility study of ultraviolet activated persulfate oxidation of phenol, Chemosphere 82 (2011) 1168–1172.
[30] K.-C. Huang, R.A. Couttenye, G.E. Hoag, Kinetics of heat-assisted persulfate oxidation of methyl tert-butyl ether (MTBE), Chemosphere 49 (2002) 413–420.
[31] H.-S. Son, S.-B. Choi, E. Khan, K.-D. Zoh, Removal of 1,4-dioxane from water using sonication: effect of adding oxidants on the degradation kinetics, Water Res. 40 (2006) 692–698.
[32] F. Vicente, A. Santos, A. Romero, S. Rodriguez, Kinetic study of diuron oxidation and mineralization by persulphate: effects of temperature, oxidant concentration and iron dosage method, Chem. Eng. J. 170 (2011) 127–135.
[33] R.H. Waldemer, P.G. Tratnyek, R.L. Johnson, J.T. Nurmi, Oxidation of chlorinated ethenes by heat-activated persulfate: kinetics and products, Environ. Sci. Technol. 41 (2007) 1010–1015.
[34] R.H. Waldemer, P.G. Tratnyek, Kinetics of contaminant degradation by permanganate, Environ. Sci. Technol. 40 (2006) 1055–1061.
[35] P.A. Hong, Z. Cha, X. Zhao, C.-J. Cheng, W. Duyvesteyn, Extraction of bitumen from oil sands with hot water and pressure cycles, Fuel Process. Technol. 106 (2013) 460–467.
[36] P. Drzewicz, A. Afzal, M.G. El-Din, J.W. Martin, Degradation of a model naphthenic acid cyclohexanoic acid, by vacuum UV (172 nm) and UV (254 nm)/H_2O_2, J. Phys. Chem. A 114 (2010) 12067–12074.
[37] V. Madhavan, H. Levanon, P. Neta, Decarboxylation by SO_4-radicals, Radiat. Res. 76 (1978) 15–22.
[38] P.R. Kannel, T.Y. Gan, Naphthenic acids degradation and toxicity mitigation in tailings wastewater systems and aquatic environments: a review, J. Environ. Sci. Health A 47 (2012) 1–21.
[39] C. Liang, Z.-S. Wang, C.J. Bruell, Influence of pH on persulfate oxidation of TCE at ambient temperatures, Chemosphere 66 (2007) 106–113.
[40] C. Liang, C.-F. Huang, N. Mohanty, R.M. Kurakalva, A rapid spectrophotometric determination of persulfate anion in ISCO, Chemosphere 73 (2008) 1540–1543.
[41] S. Rodriguez, L. Vasquez, D. Costa, A. Romero, A. Santos, Oxidation of Orange G by persulfate activated by Fe (II), Fe (III) and zero valent iron (ZVI), Chemosphere 101 (2014) 86–92.
[42] Y.-C. Lee, S.-L. Lo, P.-T. Chiueh, D.-G. Chang, Efficient decomposition of perfluorocarboxylic acids in aqueous solution using microwave-induced persulfate, Water Res. 43 (2009) 2811–2816.
[43] G.P. Anipsitakis, D.D. Dionysiou, Radical generation by the interaction of transition metals with common oxidants, Environ. Sci. Technol. 38 (2004) 3705–3712.
[44] O.S. Furman, A.L. Teel, R.J. Watts, Mechanism of base activation of persulfate, Environ. Sci. Technol. 44 (2010) 6423–6428.
[45] G.-D. Fang, D.D. Dionysiou, S.R. Al-Abed, D.-M. Zhou, Superoxide radical driving the activation of persulfate by magnetite nanoparticles: implications for the degradation of PCBs, Appl. Catal. B 129 (2013) 325–332.
[46] G.R. Peyton, The free-radical chemistry of persulfate-based total organic carbon analyzers, Mar. Chem. 41 (1993) 91–103.
[47] G.P. Anipsitakis, D.D. Dionysiou, Degradation of organic contaminants in water with sulfate radicals generated by the conjunction of peroxymonosulfate with cobalt, Environ. Sci. Technol. 37 (2003) 4790–4797.
[48] G.P. Anipsitakis, D.D. Dionysiou, M.A. Gonzalez, Cobalt-mediated activation of peroxymonosulfate and sulfate radical attack on phenolic compounds. Implications of chloride ions, Environ. Sci. Technol. 40 (2006) 1000–1007.
[49] C. Zhu, G. Fang, D.D. Dionysiou, C. Liu, J. Gao, W. Qin, D. Zhou, Efficient transformation of DDTs with persulfate activation by zero-valent iron nanoparticles: a mechanistic study, J. Hazard. Mater. 316 (2016) 232–241.
[50] H. Zhong, M.L. Brusseau, Y. Wang, N. Yan, L. Quig, In-situ activation of persulfate by iron filings and degradation of 1,4-dioxane, Water Res. 83 (2015) 104–111.
[51] L.R. Bennedsen, J. Muff, E.G. Søgaard, Influence of chloride and carbonates on the reactivity of activated persulfate, Chemosphere 86 (2012) 1092–1097.
[52] C. Liang, Z.-S. Wang, N. Mohanty, Influences of carbonate and chloride ions on persulfate oxidation of trichloroethylene at 20 °C, Sci. Total Environ. 370 (2006) 271–277.

Submitted articles

An overview on the application of advanced oxidation processes for the removal of naphthenic acids from water

Xiyan Xu; Gema Pliego; Juan A. Zazo; Shibo Sun; Patricia Garc á-Mu ñoz; Li He; Jose A. Casas; Juan J. Rodriguez

ABSTRACT: *Although the exploitation of new energy sources like oil sand or shale may efficiently relieve the urgency of energy shortage, it would also cause significant environmental adverse impacts since huge volumes of oil-containing wastewaters are produced yearly worldwide due to those activities. Naphthenic acids (NAs) are the main harmful components of the oil shale fracking process and the oil sands process-affected waters (OSPWs), which are reported to be bio-recalcitrant due to their structural complexity and toxicity. Identification techniques, are being continuously improved to deal with the growing analytical needs for the traditional NAs and the emerging ones like oxy-, aromatic and diamondoid NAs. Meanwhile, treatment approaches have been investigated in the past decades addressed to implement technical solutions. Advanced oxidation processes (AOPs) are among the most studied. Different oxidizing agents, like ozone, hydrogen peroxide and persulfate, among other, have been used, giving rise to a diversity of specific techniques. The current work presents an updated overview of those techniques in their application for the abatement of NAs from water.*

KEYWORDS: Naphthenic acids; Advanced oxidation processes; Oil sands process-affected water; Identification techniques; Ozonation; Fenton; Persulfate oxidation.

1 Introduction

In the last two decades, there has been an increasing interest on the exploitation of non-conventional oil resources in the context of the growing energy demand (Gautier et al., 2009; Hughes, 2013). Oil sands (tar sands) or, more technically, bituminous sands and shales, are available non-conventional oil deposits, from which important amounts are refined nowadays (Kannel and Gan, 2012; Wang et al., 2015b). Taking the Alberta's oil sands in Canada for instance, over 1 million barrels of oil were produced daily in 2006 and it has been estimated to reach up to 3 million per day by 2020 (Schindler, 2010). In spite of the intermittent variation of oil prices due to different mixed reasons,

continuous exploration of new sources is a growing activity (Baffes et al., 2015; Tokic, 2015). The fast development of non-conventional oil refining industry brings not only more available energy supply and the corresponding potential economic benefits, but also concerning environmental impacts.

Amid 2–5 volumes of water are needed per unit volume of oil in the exploitation of oil or tar sands (Schindler, 2010). Those so-called oil sand process-affected waters (OSPWs) ultimately converge into tailing ponds. The area occupied by these ponds in Alberta was around 130 km^2 in 2009 (Kean, 2009) which denotes the magnitude of the problem. OSPWs have been demonstrated to be toxic and able to cause malformation of aquatic organisms and even affect people downstream the oil sand fields (Schindler, 2010).

Naphthenic acids (NAs) have been found as series of the emblematic toxic and recalcitrant organic compounds in OSPWs. Increasing research is being addressed toward their identification (Headley et al., 2016), toxicity assessment (Clemente and Fedorak, 2005) and treatment methods (Brown and Ulrich, 2015; Headley and McMartin, 2004) for the sake of providing useful knowledge to control the environmental impact of those species. The current review presents a summary of the properties of NAs, the available techniques for their analysis and the potential solutions for their abatement, with special emphasis on the application of advanced oxidation processes (AOPs).

2 Naphthenic acids

2.1 Chemical structure

The term naphthenic acids refers to a group of organic acids consisting in saturated alkyl-substituted acyclic and cycloaliphatic carboxylic structures, represented by a common formula of $C_nH_{2n+m}O_2$, where “n” stands for the number of carbon atoms and “m” is zero or a negative integer specifying the homologous series through hydrogen atoms deficiency with respect to saturated structures (Brown and Ulrich, 2015; Clemente and Fedorak, 2005). The diverse combination manners of the hydrocarbon rings and branches of the side chains determines the complexity of NAs (Grewer et al., 2010b; Johnson et al., 2011; Rowland et al., 2012). However, the above expression serves only to describe the “classic” NAs but does not afford the intricacy of all the transformed or derived NAs found in the OSPWs tailing ponds. For this reason, more complicated formulas have been suggested, like $C_nH_{2n+m}O_aN_bS_c$, including more oxygen as well as the possible formation of nitrogen- and sulfate-bearing groups during the long-term retention in the tailing ponds (Pereira et al., 2013a; Quinlan and Tam, 2015). Instead of the oxygen number “a” being 2 in the “classic” NAs, oxy-NAs with more oxygen (a=3, 4 or 5) in the structure are found as the intermediates frequently identified in the matured tailings or after the aerobic microbial biodegradation of OSPW

(Bataineh et al., 2006; Han et al., 2009; Han et al., 2008; Hindle et al., 2013; Islam et al., 2014; Wang et al., 2013a).

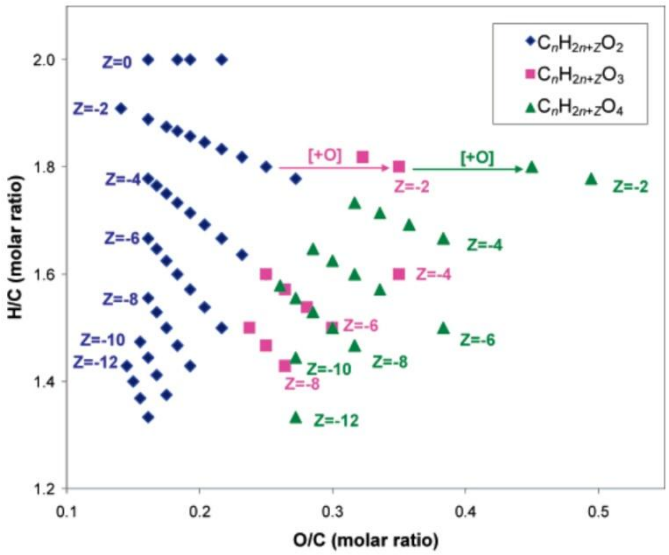

FIGURE 1 HPLC/QTOF-MS derived Van Krevelen diagram showing parent NA species and their oxidation byproducts in Syncrude tailing wastewaters. (reprinted with permission from Bataineh et al., (2006). Copyright (2006) American Chemical Society)

Oxy-NAs were firstly reported by Bataineh et al from the OSPWs of Syncrude Canada Ltd. postulated as possible byproducts of biodegradation (Bataineh et al., 2006) (Figure 1). Wang et al. (2013a) determined the NAs components from the oilfield wastewater in Hebei province and the oil sands extraction plants in the Xinjiang province of China. A great diversity of NAs within a wide range of carbon atoms (from 5 to 41) were identified, including fairly considerable proportions of oxy-NAs (in terms of O_a-NAs or (OH)-NAs) with "m" ranging from -14 to 0.

The differences found in the oxy-NAs proportions among various kinds of industrial OSPWs were attributed to the particular pretreatment or storage conditions. These compounds have been claimed as biodegradation intermediates (Islam et al., 2014) during the long-term storage in the tailing ponds (Grewer et al., 2010b; Han et al., 2009). The evolution of oxy- and aromatic NAs was followed in a wastewater treatment plant in north China which included physicochemical and biological processes (Wang et al., 2015a). The changes in the relative proportion of those species provided information on the biodegradation of NAs and on the observed seasonal differences in terms of removal efficiency.

The structural characteristics of aromatic ring-bearing NAs have also been considered in relation with their similarity with some estrogens and the corresponding potential disturbance toward living organisms (Rowland et al., 2011b; Johnson et al., 2012; Jones et al., 2012; Johnson et al., 2013; Reinardy et al., 2013). Scarlett et al. (2013) tested the impact of aromatic ring-bearing NAs toward *larval zebrafish* and LC_{50} values of 5 – 8 mg L^{-1} were determined for acute toxicity. Johnson et al. (2013)

investigated the ability of P. putida KT2440 to degrade different alkyl-branched aromatic NAs with n-BPBA. Those compounds were readily degraded within several days via beta-oxidation of the alkanoic acid side chain. However, this degradation was significantly inhibited by increasing the concentration of n-BPBA. Anaerobic biodegradation of polycyclic aromatic NAs was recently studied and 40% conversion upon 260 days was reported, being identified 2-Naphthoic acid as one of the main byproducts (Folwell et al., 2016).

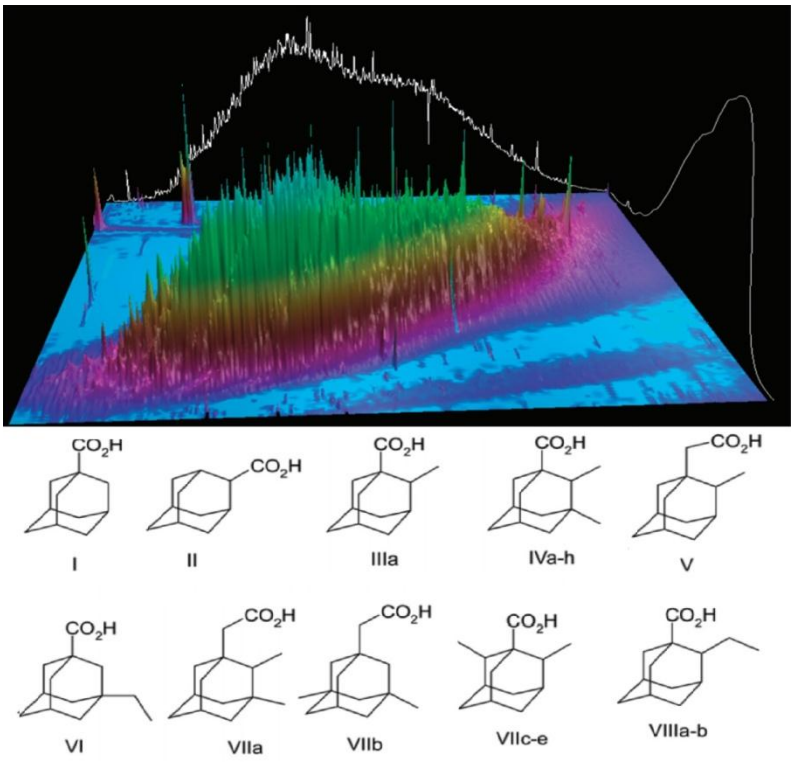

FIGURE 2 Total ion current chromatogram of OSPW NAs (methyl esters) examined by GCxGC-ToF-MS illustrating high chromatographic resolution by GCxGC compared with GCMS (white line on black background) together with the structures of some of the diamondoid acids identified. (reprinted with permission from Rowland et al., (2011a). Copyright (2011) American Chemical Society)

A group of special tricyclic diamondoid NAs structures have also been detected as biodegradation byproducts in OSPWs (Wang et al., 2006; Rowland et al., 2011a; Rowland et al., 2012) (Figure 2). These adamantine structures have been proved to be persistent and their adverse environmental effect has been analyzed in the literature (Jones et al., 2011; Dissanayake et al., 2016). In-vivo exposure for mussels were carried out in the presence of two diamondoid acids with varying degrees of genotoxicity displayed to hemocytes at a concentration of 30 μmol L^{-1} (Dissanayake et al., 2016).

2.2 Physical properties

Oil sand containing NAs is a mixture of clay, sand, water and bitumen (Barrow et al., 2010). The appearance of NAs in aquatic solution is viscous and the color varies

from light yellow to dark amber according to the components, showing high volatility with a musty hydrocarbon-like smell (Brient et al., 1995). The tailing pond of OSPWs possess weak alkaline pH, in the vicinity of 8 (Schramm et al., 2000). As kind of weak acids, NAs with dissociation constants (pKa) around 5−6 can be well dissolved in mild alkaline solutions, like OSPWs, but show poor solubility in acidic or neutral conditions (Drzewicz et al., 2012). High solubility of NAs in organic solvents has also been reported (Armstrong, 2008). The boiling point of individual NAs ranges from 250 to 300 ^{o}C, which must be considered for analysis since some of the available identification approaches include evaporation, like in gas chromatography. In alkaline aqueous solutions, NAs always exist in the ionized form and can be associated to metal ions as the corresponding metal salts (Brient et al., 1995).

2.3 Toxicity

NAs have been frequently reported among the most toxic components of OSPWs (Schramm et al., 2000; Madill et al., 2001; Biryukova et al., 2007; Frank et al., 2008; Toor et al., 2013; Mahdavi et al., 2015). There are numerous studies focusing on the toxicity of NAs toward various organisms covering almost the entire biological taxonomy both aquatic and terrestrial, including microorganisms (Dokholyan and Magomedov, 1984; Leung et al., 2001; Leung et al., 2003; Hayes, 2007; West et al., 2011), plants (Wort and Patel, 1970; Kamaluddin and Zwiazek, 2002) and animals (Myhre and Fonnum, 2001; Melvin and Trudeau, 2012; Tollefsen et al., 2012).

So far, no conclusive structure-toxicity relationship has been established for NAs. However, it has been determined that, in general, NAs with more carbon atoms and cyclic structures are more harmful, while branched chains imply less toxicity (Kannel and Gan, 2012). Previous reviews summarized the toxic properties of NAs in various aspects (Clemente and Fedorak, 2005; Kannel and Gan, 2012). Recently, Marentette et al. (2015) comprehensively examined the toxicity of extracted NAs fraction components (NAFCs) from fresh and aged OSPW as well as commercial ones toward the fathead minnow embryonic survival, growth and deformities. Both NAFC and commercial NA mixtures reduced hatch success, with NAFCs from OSPW showing less toxicity (EC_{50} = 5–12 mg L^{-1}) than the commercial NAs (≈2 mg L^{-1}) tested.

3. Analysis of NAs

The structural features of NAs demand the development of high resolution (semi-)quantitative analytical methods beyond the classical well-stablished techniques. Clemente and Fedorak (2005) reported an standard method for the determination of NAs, based on Fourier transform infrared spectroscopy (FTIR) after acidification, dichloromethane extraction and concentration of the sample. Other analytical procedures of higher resolution have been developed more recently, but a universally

accepted analytical approach is not available so far (Brown and Ulrich, 2015). Different mass spectrometry (MS)-based techniques have been used, like time-of-flight MS (ToF-MS) (Hao et al., 2005; Bataineh et al., 2006; Rowland et al., 2011a; Rowland et al., 2012; Hindle et al., 2013; Wang et al., 2013a; Brunswick et al., 2016), Linear trap quadropole MS (LTQ-Orbitrap-MS) (Pereira et al., 2013a; Pereira et al., 2013b) or Fourier transform ion cyclotron resonance MS (FT-ICR-MS) (Purcell et al., 2006; Da Campo et al., 2009; Headley et al., 2013; Dias et al., 2014; Ortiz et al., 2014; Rowland et al., 2014; Barrow et al., 2015). Other techniques, like FTIR (Luna et al., 2008; Scott et al., 2008a; Grewer et al., 2010a), synchronous fluorescence spectroscopy (SFS) (Kister et al., 1996; Kavanagh et al., 2009; Martin et al., 2014; Bauer et al., 2015; Klamerth et al., 2015) or Flame ionization (FID) detection (Pollard et al., 1992; Jones et al., 2001; Vaiopoulou et al., 2015) have been also successfully applied for NAs when specific structural analysis is not required. FTIR serves to determine not only NAs but also a total signal of various detectable characteristic bonds that may not correspond to NAs (Grewer et al., 2010b). SFS has been used to analyze the OSPW from Syncrude Canada Ltd. operations in Alberta (Kavanagh et al., 2009). In general, it is necessary to consider the structural particularity of NAs when using these approaches.

FID and MS detections are always associated to gas or high-performance liquid chromatography (GC or HPLC). A GC-FID method with a low-polarity capillary column was reported by Ré-Poppi et al. (2009) with lots of NAs being detected from Brazilian gasoline samples, yielding values of relative standard deviation lower than those of standard methods. FT-ICR-MS was used to analyze crude oil samples, providing some practical information on the size and composition of NAs, but with uncertainty about the presence of NAs with higher hydrogen deficiency. To avoid this drawback, other approaches like ToF-MS have been used (Barrow et al., 2003). A two-dimensional gas chromatography/ToF-MS (GC×GC/ToF-MS) technique was reported for the characterization of commercial mixtures and tailing extractions which provided detailed structural information on individual NAs (Hao et al., 2005). This approach has also been tested to effectively analyze diamondoid and aromatic NAs in OSPWs (Rowland et al., 2011a; Jones et al., 2012). Hindle et al. (2013) combined HPLC with ToF-MS for quantitative analysis of NAs from OSPW with particular sensitivity toward oxy-NAs. HPLC-LTQ-Orbitrap-MS was successfully used to detect about 3000 species in each OSPW sample including classical as well as S- and N-containing related compounds (Pereira et al., 2013a). Clemente and Fedorak (2005) and Brown and Ulrich (2015) summarized analytical methods for NAs determination. Table 1 collects the available identification approaches for non-conventional NAs including aromatic, oxy- and diamondoid ones from petroleum-sources worldwide.

TABLE 1 Identification approaches for non-conventional NAs

Categories of NAs	Source of NAs	Sample preparation	Identification Techniques	Reference
Saturated and aromatic	Distilled Brazilian petroleum supplied by PETROBRAS	Not mentioned	FTIR Spectrometer	Luna et al. (2008)
Aromatic	Syncrude Canada Ltd.'s West In-pit settling basin	Acidified by HCl and dissolved in NaOH	GC-MS; Synchronous fluorescence spectroscopy (SFS)	Kavanagh et al. (2009)
Aromatic	Individual butylphenylbutanoic acid (BPBA) isomers	Acidified by HCl; Use N,O-bis(trimethylsilyl)trifluoroacetamide to form trimethylsilyl derivatives; Extracted with ethyl acetate	GC-MS	Johnson et al. (2011)
Aromatic	OSPW	Demethylated by BF_3-MeOH; argentation solid phase extraction (SPE) by elution with hexane	Multidimensional comprehensive gas chromatography–mass spectrometry (GC × GC–MS)	Jones et al. (2012)
Aromatic	Hydrocarbon-contaminated sediments from Avonmouth, UK	Acidified by HCl; Use N,O-bis(trimethylsilyl)trifluoroacetamide to form trimethylsilyl derivatives; Extracted with ethyl acetate	GC-MS	Johnson et al. (2012)
Aromatic	Synthesized by n-BPBA and t- BPBA	Acidified by HCl; Use N,O-bis(trimethylsilyl)trifluoroacetamide to form trimethylsilyl derivatives; Extracted with ethyl acetate	GC-MS	Johnson et al. (2013)
Aromatic	Concentrated OSPW from Syncrude Canada Ltd. West In-pit settling basin in Fort McMurray, Alberta, Canada	Demethylated by BF_3-MeOH; acidified with HCl; extracted with ethyl acetate	GC × GC–MS	Reinardy et al. (2013); Rowland et al. (2011b); Scarlett et al. (2013)
Polycyclic aromatic hydrocarbons and NAs	Individual NAs; Tailings pond water in Alberta, Canada	Acidified by HCl; Use N,O-bis(trimethylsilyl)trifluoroacetamide to form trimethylsilyl derivatives; Extracted with ethyl acetate	GC–MS	Folwell et al. (2016)

Oxy-NAs	Individual oxy-NAs; Syncrude Canada Ltd. from the clarified zone of the West In-pit	Liquid-liquid extraction and solid-phase extraction (SPE); dissolved in ethyl acetate	HPLC/QTOF-MS	Bataineh et al. (2006)
Classic and Oxy-NAs	Individual NAs; Mildred Lake Settling Basin OSPWs, Canada	Liquid-liquid extraction and solid-phase extraction (SPE). dissolved in ethyl acetate	FTIR; HPLC/HRMS	Han et al. (2009)
Classic and Oxy-NAs	Individual 14 NAs and 3 oxy-NAs; oil production platform in Hebei; oil sands extraction plants in Xinjiang, China; OSPWs in North China	Derivatized with dansyl chloride; a solid-phase extraction (SPE) and resolved in acetonitrile	An ACQUITY UPLC system coupled to a Xevo QTOF-MS equipped with an electrospray ionization (ESI) source. (UPLC-ESI+-QTOF-MS)	Wang et al. (2013a) Wang et al. (2015a)
Classic and Oxy-NAs	35 model NAs and 4 oxy-NAS; Acros and Merichem mixed NAs	Dissolved in isopropyl alcohol (IPA)	HPLC high resolution accurate mass time-of-flight mass spectrometry (HPLC-HRQTOF-MS)	Hindle et al. (2013)
Diamondoids	Oils and petroleum products (including gasoline, kerosene, diesel fuels, residual, bunker B, and bunker C lubricating oils) from various oil companies worldwide	Eluted in order with n-hexane (12 mL) and followed by n-hexane DCM	GC-MS and GC-FID	Wang et al. (2006)
Diamondoids	Individual and Syncrude Canada Ltd. West Endpit settling basin in Fort McMurray, Alberta, Canada	Refluxing with BF_3-methanol	Two-dimensional comprehensive gas chromatography-timeof-flight-mass spectrometry (GCxGC-ToF-MS) analyses	Rowland et al. (2011a)
Isomeric diamondoid-structure like acids	A: a currently used tailings pond in Alberta, Canada; B: storage in-pit settling basin	Demethylated by BF_3-MeOH; extracted into hexane	GCxGC/ToF-MS	Rowland et al. (2012)

4. Treatment of NAs-containing wastewaters

Research on the abatement of NAs from aqueous effluents has been carried out in the past half century, including biological, physical and chemical techniques. The

substrates used in these studies mainly fall into three categories: the surrogate NAs, the commercial NAs and the NAs in real industrial wastewaters (Vaiopoulou et al., 2015; Klamerth et al., 2015; Xu et al., 2016). Generally, investigations performed using surrogate NAs are always focused on the representative aspects of the treatment approaches like the reaction pathways.

Scott et al. (2008a) claimed that biodegradation is the most cost-effective solution for mitigating the hazard of NAs-containing wastewaters. The study of Herman et al. (1994) concluded that NAs collected from OSPWs were more recalcitrant than the commercial ones. The study of Hwang et al. (2013) demonstrated the important role of aerobic bacteria in the degradation of NAs. Specific bacterial groups were found able to partially degrade those methyl-substituted NAs (Smith et al., 2008). In a more recent study, Mahdavi et al. (2015) reported an algae–bacteria consortium allowing NAs degradation with significant toxicity reduction.

The biodegradation of aliphatic or alicyclic acids may occur via β-oxidation (Biryukova et al., 2007), α- and β- co-oxidation (Rontani and Bonin, 1992) and aromatization (Han et al., 2008) depending on the structural characteristics. NAs with lower molecular weight and fewer rings are more susceptible to biodegradation (Clemente and Fedorak, 2005) whereas those with higher branching were found much more recalcitrant (Han et al., 2008). Besides, the number of carbon atoms also affects to the resistance of NAs to biodegradation. It has been reported that those with even numbers commonly give rise to cyclohexyl acetic acid formation, which possibly hinders the β- oxidation reactions in the biodegradation pathway (Kannel and Gan, 2012).

NAs from real OSPWs have been found in general more bio-recalcitrant due to higher molecular weight and cyclicity. Marsh (2006) reported that the indigenous microorganisms found in the OSPWs of the tailing ponds were not able to degrade a significant percentage of NAs even upon long time periods. Long-term evolution of OSPWs in the tailing ponds suggests that considerable amounts of NAs can remain for over 10 years (Kannel and Gan, 2012). Therefore, effective solutions are needed, based on chemical or physico-chemical approaches.

Adsorption has been reported for the removal of NAs. Several adsorbents, like organic-rich soil (Janfada et al., 2006), petroleum coke (El-Din et al., 2011) cyclodextrin-based polymers (Mohamed et al., 2011) and activated carbon (Iranmanesh et al., 2014) have been tested for that purpose. Mohamed et al. (2011) demonstrated that granular activated carbon yield better performance for NAs removal than organic polymeric adsorbents. Petroleum coke showed to efficiently remove NAs allowing significant detoxification (El-Din et al., 2011). However, health and operational maintenance concerns are associated to petroleum-coke, since vanadium and/or other heavy metals can be leached (Jia et al., 2002). Anyway, the main drawback of adsorption derives from its non-destructive character, which determines the need of further treatment and/or disposal of the exhausted adsorbent.

4.1 Application of AOPs for NAs abatement

Advanced oxidation processes (AOPs) have been widely studied in the literature for the removal of water pollutants mainly focused on recalcitrant harmful species. The traditional AOP concept refers to a series of techniques based on the oxidizing capacity of $HO^{\bullet}$ radicals under ambient-like conditions. However, this concept is currently accepted in a broader sense since it is well known the contribution of other radical species and temperature and pressure beyond the ambient have been used in many cases. There is a diversity of recognized AOPs, depending on the reagents or activation approaches used. Among the former, ozone, hydrogen peroxide and persulfate are the most common (Andreozzi et al., 1999; Yang et al., 2014).

The oxidation of NAs proceeds through a complex network of multiple series-parallel reactions involving radical species derived from the oxidizing reagents as well as from the organic substrate and the intermediates in the reaction pathway. Under appropriate operating conditions, the end products consist of CO_2 and H_2O (mineralization) but also low molecular-weight carboxylic acids can remain in different extent depending on the specific character and strength of the oxidation process. The kinetics of such complex systems has been commonly described by useful approaches like simple pseudo-first or second order models rather than rigorous ones involving the time-course of radical species whose validation is hindered by analytical limitations (Beltran, 2003).

Figure 3 depicts the time-course and the relative presence in the literature of different AOPs for NAs. In the following, those contributions are reviewed. Table 2 contains a list of the most recent works on AOPs application to NAs abatement.

4.1.1. Ozonation

Ozonation is a clean and efficient approach for the breakdown of organic pollutants with ozone playing the role of the oxidant and precursor of other oxidizing radicals.

Earlier work on NAs abatement by ozonation was conducted by Scott et al. (2008b). Ozonation of NAs-containing OSPW significantly improved the biodegradability, according to El-Din et al. (2011). Highly recalcitrant alkyl-branched NAs can be readily converted into more biodegradable species (Hwang et al., 2013). It was postulated that the reactive species from O_3, including $O_3^{\bullet-}$ and $HO^{\bullet}$ radicals, attack selectively the hydrogen atoms of the tertiary carbons which exist mainly in the more complex NAs, like alkyl-branched and ring-bearing structures. Scott et al. (2008b) found that the proportion of higher molecular weight NAs in the effluent from OSPW ozonation decreased by over 95 %. In the meantime, an increase of lower ones also occurred, which has been confirmed by Pérez-Estrada et al. (2011) and Wang et al. (2013b). A recent study reports the synergistic effect of ozone coupled with H_2O_2 allowing almost complete degradation of NAs from OSPW (Afzal et al., 2015).

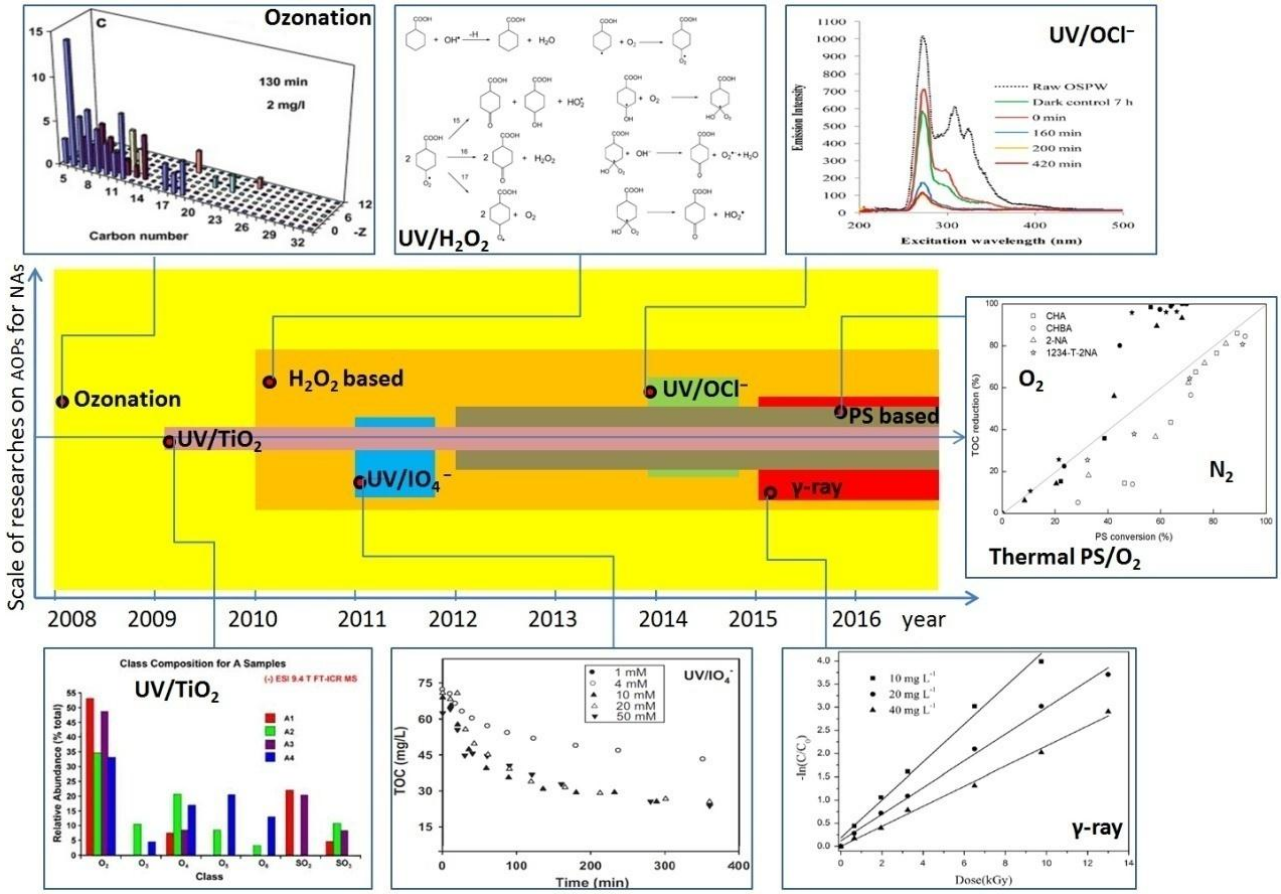

FIGURE 3 The brief time-course of the development of AOPs for NAs treatment categorized by oxidizing sources. The area of each block stands for the period and the relative number of publications ascribed to each AOP group with the figures of iconic works. (reprinted with permissions from Drzewicz et al. (2010), Headley et al. (2010), Jia et al. (2015), Liang et al. (2011), Scott et al. (2008b), Shu et al. (2014) and Xu et al. (2016), respectively. Copyright (2011 and 2014) American Chemical Society; (2010) John Wiley and Sons; (2008, 2011, 2015 and 2016) Elsevier)

Based on the improved biodegradability, biological treatment following previous ozonation has been studied for OSPW treatment with fairly good results (Martin et al., 2010; Wang and Kasperski, 2010). Ozonation hardly allows complete mineralization, especially for the lower molecular weight components, thus uncertainty about the remaining toxicity is a major issue and it is necessary to assess the health risk for practical application (Langlais et al., 1993; He et al., 2012).

Islam et al. (2014) fitted the time-course of surrogate NAs, including the acid-extractable fraction (AEF), COD, NAs, oxy-NAs, and (classical + oxy)-NAs upon ozone oxidation to a first-order kinetic model, which provided fairly good prediction. That simple approach was used by Al-jibouri et al. (2015) for the ozonation of model NAs at various temperatures. The values of the rate constants ranged within 0.67 and 8.85 M^{-1} s^{-1} and ≈ 89 kJ mol^{-1} was reported for the activation energy (Al-jibouri et al., 2015). Most recently, Wu and Upreti (2017) proposed models based on mass balance

to describe the evolution of commercial NAs, dissolved ozone and gaseous ozone during NAs ozonation. Although the developed models successfully predicted the concentrations of commercial NAs and gaseous ozone, the actual ozone consumption was higher than the predicted within the earlier process due to the inapplicability of the gas-liquid equilibrium condition in the initial high-rate stage of reaction.

The most recent works on NAs ozonation are included in Table 2. Those before 2015 can be seen in the review of Brown and Ulrich (2015).

TABLE 2 Summary of AOPs for NAs treatment

AOPs	NAs source	Reaction conditions	Main results	Other conclusions	references
Ozone-based AOPs (from 2015)					
Ozonation; O_3/H_2O_2	Cyclohexa-noic acid (CHA) and OSPW from Syncrude Canada Ltd.	pH = 9, in the presence and absence of scavengers	NA removal = 97.7% by O_3 and 99% by O_3/H_2O_2	$HO^{\bullet}$ radicals are responsible and direct ozonaton is quite significant	Afzal et al. (2015)
Ozonation; ozonation-biodegradation combination	Commercial mixture and individual NAs	[NA] = 25−35 mg L^{-1}; $[O_3]$ = 9.3 mg L^{-1}; T = 23 ^oC	NA removal = 89% by ozonation-biodegradation combined system	Ozone reacted preferentially with NAs of higher cyclicity and molecular weight, toxicity decreased by 6.7-fold	Vaiopoulou et al. (2015)
Ozonation	four fractions of OSPW	[NA] = 50 mg L^{-1}; $[O_3]$ = 37−41 mg L^{-1}; pH = 8	NA removal = 55% to 98% with different NA categories	Organic extracts at different pH differentiate NAs; Residual toxicity attributed to degradation products	Klamerth et al. (2015)
Ozonation	model NAs	T = 5, 15 and 25 ^oC	k = 0.67, 2.71 and 8.85 M^{-1} s^{-1} at 5, 15 and 25 ^oC, respectively	E_a = 88.85 kJ mol^{-1}	Al-jibouri et al. (2015)
Ozonation combined with integrated fixed-film activated sludge (IFAS)	OSPW	$[O_3]$ = 30mg L^{-1}; 11 months of retention time	Acid extractable fraction (AEF) removal = 42%	NA biodegradation decreased as the NA cyclization number increased	Huang (2016)
Ozonation	OSPW	$[O_3]$ = 2.0 mM	Complete removal	Efficient reduction of the acute toxicity towards *Vibrio fischeri* was observed by ozonation	Wang et al. (2016)
Ozonation followed by modified	OSPW	$[O_3]$ = 30 mg L^{-1}; Retention time = 426 days	Classical NAs removal = 70%	No severe membrane fouling was observed as the transmembrane pressure	Zhang et al. (2016d)

Luzack-Ettinger membrane bioreactor (MLE-MBR)				controlled below 12 kPa	
Ozone pretreated noxic-aerobic membrane bioreactor	OSPW	$[O_3]$ = 30mg L^{-1}; Retention time = 742 days	Ozonation pretreatment enhanced the OSPW NA degradation and the system's fouling control	Ozonation reshaped the microbial community structure of the MBR by changing relative abundances of the dominating species	Xue et al. (2016)
Fenton-based AOPs					
NTA-modified Fenton	CHA	[CHA] = 0.39 mM; $[H_2O_2]$ = 0.29−5.88 Mm; $[Fe^{III}NTA]$ = 0.27−0.89 mM; [NTA:Fe] = 1:1; pH = 8	CHA removal reached 90%	$HO^{\bullet}$ radicals played the main role with minor role of $O_2^{\bullet-}$ found for CHA degradation	Zhang et al. (2016b)
EDDS-modified Fenton	CHA	[CHA] = 0.39 mM; $[H_2O_2]$ = 0.74 mM; $[Fe^{II}]$ = 0.11 mM; [EDDS:Fe] = 2:1; pH=7−9	84% CHA removal	$E_{1/2}$ = 186 mV, −39 mV, and −89 mV at pH = 7, 8 and 9; The EDDS and $HO^{\bullet}$ reaction rate constant k = 2.48 ± 0.43 × 109 M^{-1} s^{-1} at pH 8	Zhang et al. (2016c)
Chelate-UV/Fenton	OSPW	UV lamp (200 nm to 530 nm); $[H_2O_2]$ = 5.88 Mm; [Fe] = 0.8 − 3 mg L^{-1}; [NTA] = [EDDS] = 0.72 mM	At optimal conditions: NA removal = 66.8% for UV-NTA-Fenton and 50.0% for UV-EDDS-Fenton)	No significant toxicity change of the NTA containing systems; EDDS increased the acute toxicity of the solution	Zhang et al. (2016a)
PS-based AOPs					
UV/PS	CHA	[CHA] = 100 mg L^{-1}; [PS] = 1−20 mM; pH=8−10	Half-life: 18.3 to over 360 min	Not mentioned	Liang et al. (2011)
Thermally-activated PS; ZVI/PS	CHA and OSPW	[CHA] = 50 mg L^{-1}; [NAs] = 30 mg L^{-1}; [PS] = 0−2000 mg L^{-1}; [ZVI] = 20g L^{-1}; T = 40, 60, 80 °C; pH = 9	100% CHA removal with 2000mg L^{-1} PS at 80 °C; over 90% OSPW NA removal with 100 mg L^{-1} PS and ZVI	Chloride show little effect on NA removal, but chloro-CHA was formed	Drzewicz et al. (2012)
Thermally-activated PS with O_2	Model NAs: CHA, Cyclohexa-nebutyric	[NAs] = 50 mg L^{-1}; [PS] = 10−100% stoichiometric; T = 40−97 °C, pH = 8	100% CHA removal achieved with 40% stoichiometric PS at 80 °C	Oxygen were demonstrated to take a role in NA mineralization	Xu et al. (2016)

	acid (CHBA), 1234-T-2NA, 2-NA				
Other AOPs					
Vacuum UV/H_2O_2; UV/H_2O_2	CHA	[CHA] = 20 mg L^{-1}; Vacuum UV lamp (172 nm); UV lamp (254 nm)	4-oxo-CHA, and hydroxy-CHA are the main intermediates; oxyl radical may be formed during the process	Scission of the cyclohexane ring was also observed from the acyclic byproducts including heptadioic acid and other short-chain carboxylic acids	Drzewicz et al. (2010)
UV/H_2O_2	CHA	[CHA] = 100 mg L^{-1}; [H_2O_2] = 1−50 mM pH = 8−12	Half-life: 17.2 to over 360 min; TOC drop from 64 to 3.4 mg L^{-1}	-	Liang et al. (2011)
UV/H_2O_2	CHA	[CHA] = 10−50 mg L^{-1} ; UV lamp (254 nm); irradiance = 0.11 mW cm^2	Highest reaction rate $k = 2.5 \times 10^{-2}$ min^{-1} at [H_2O_2] = 80 mg L^{-1}	pH had no significant effect on the CHA degradation; Chloride and carbonate ions decreased the treatment efficiency	Afzal et al. (2012a)
UV/H_2O_2	Model NAs and OSPW NAs	[NA] = 10−50 mg L^{-1}; UV lamp (254 nm); irradiance = 0.11 mW cm^2	Large, branched and cyclic NAs may be better oxidized in the UV/H_2O_2 process than small, linear and acyclic ones	No structure–reactivity was observed in the case of OSPW NAs	Afzal et al. (2012b)
UV/H_2O_2	OSPW	H_2O_2 = 2.0 mM; UV dose = 950 mJ cm^{-2} UV	Classical NAs removal = 42.4%	^{1}H NMR analyses confirmed the removal of aromatics NAs	Wang et al. (2016)
fluorescent and natural solar with TiO_2	oil sands NA mixtures; NAs mixture (FlukaNAs); model-NAs (4MACH)	[NA] = 40−100 mg L^{-1}; [TiO_2] = 0.3 g L^{-1}	75% removal of compounds in the oil sands NA mixture; 100% removal of 4MACH	The efficacy of the photo-catalysis was structure of NA related that ones with $-z < 6$ were more readily degraded	Headley et al. (2009)
UV/TiO_2; Microwave+UV /TiO_2	OSPW NA; Fluka NAs	[NA] = 40−100 mg L^{-1}; [TiO_2] = 0.3 g L^{-1}; UV lamp: 245nm; Microwave: 1200 W, 2.45 GHz	Samples treated with UV and microwave radiation have a lower relative abundance of other heteroatomic classes	Species containing SO_2 were found only in non-UV-treated samples which may serve as possible indicators of process-amended OSPW	Headley et al. (2010)

UV/TiO_2	OSPW NA; Fluka NAs	[NA] = 40−100 mg L^{-1}; [TiO_2] = 0.3 g L^{-1}; UV lamp: 245 nm	Commercial NAs and OSPW NA degraded rapidly, with half-life values ranging between 1.55 and 17.37 h	Complete toxicity of NAs as confirmed using Microtox tests	Sabyasachi et al. (2010)
Solar/TiO_2	OSPW NAs	[NA] = 54 mg L^{-1}; [TiO_2] = 0.5 g L^{-1}; Solar light: 25 MJ m^2 over 14 h daylight	Acid extractable organics (AEO): 39.8→0.6 mg L^{-1}; total organic carbon: (TOC): 45.1→3.5 mg L^{-1}; chemical oxygen demand (COD): 135→54 mg L^{-1}; biological oxygen demand (BOD): 0.2→4.4 mg L^{-1}; Microtox 15 min IC20 (% v/v): 77.2→>90	Complete mineralization was achieved within 7 days; A mechanism of superoxide bond cleavage was suggested	Leshuk et al. (2016)
Solar/film-fixed TiO_2	Fluka NAs	[NA] = 63 mg L^{-1}; Thickness of silicone film < 0.2 cm, 28 × 43 cm; solution deep < 1 cm	NA removal > 90%; removal rate: 15.5 mg L^{-1} h^{-1}; half-life: 2 h	Complete toxicity was achieved	McQueen et al. (2016)
UV alone, UV/TiO_2, UV/TiO_2-Graphene	Commercial NAs mixture	[NA] = 100 mg L^{-1}; GO:P25 = 0.5, 1, 5 and 10 wt%; [catalyst] = 100 mg L^{-1}; UV lamp: 254 nm	NA removal > 90% in UV/TiO_2-Graphene; 80% with UV/TiO_2	Lower pH is better for NA treatment; macromolecular NAs were easier to be degraded than the micromolecular ones	Liu et al. (2016b)
UV/chlorine	OSPW NAs and fluorophore organic compounds	[NA] = 21.6 mg L^{-1}; [OCl^-] = 200-300 mg L^{-1}; pH = 8−10; UV (303 nm) irradiance = 0.50 mW cm^{-2}	NA removal = 75 − 84%	Structure-dependent effect is observed that the NAs with higher molecular weight are easier to degrade	Shu et al. (2014)
Gamma radiation	CHBA	[CHBA] = 10−40 mg L^{-1}; absorbed doses: 0–13 kGy	CHBA removal = 99%; COD removal = 92%	The removal rate of CHBA increased with the absorbed dose and the decrease of its initial concentration	Jia et al. (2015)
Gamma	OSPW and	90% by volume was	NAs removal = 97%;	Acute toxicity to *Vibrio*	Boudens et

radiation	fluid fine tailings (FFT)	gamma irradiated mixed with 10% untreated inoculum from the pond source; Retention time: 2-52 weeks	FFT removal = 85%	*fischeri* was reduced by gamma radiation of OSPW	al. (2016)
UV/IO_4^-	CHA	[CHA] = 100 mg L^{-1}; $[IO_4^-]$ = 4−50 mg L^{-1}; pH = 8−12	Half-life = 100 → > 300min	Not mentioned	Liang et al. (2011)

4.1.2. Fenton-based technologies

The Fenton process is a well-known oxidation system using H_2O_2 as starting reagent and Fe^{2+} as catalyst, which promotes the generation of strongly oxidizing hydroxyl radicals through the main reaction:

$$H_2O_2 + Fe^{2+} + H^+ \rightarrow Fe^{3+} + HO^{\bullet} + H_2O \quad (1)$$

Regeneration of Fe^{2+} takes place, among other, by:

$$H_2O_2 + Fe^{3+} \rightarrow Fe^{2+} + HOO^{\bullet} + H^+ \quad (2)$$

which produces hydroperoxide radicals, also powerful oxidizing species. There are other numerous reactions participating in this complex chemical system which represents so far the most stablished advanced oxidation technology, together with ozonation.

Based on this concept, a number of related approaches have been developed, which can be considered as emerging technologies. The application (real or potential) of Fenton and Fenton-like oxidation to the abatement of recalcitrant water pollutants has been widely reported in the literature (Neyens and Baeyens, 2003; Bautista et al., 2008; Munoz et al., 2015; Pliego et al., 2015).

The pH of NAs-containing OSPWs (≈ 8) hinders the application of conventional Fenton oxidation to these effluents, since this process requires a pH around 3. To overcome this drawback, iron chelates have been used for the activation of H_2O_2 to prevent iron precipitation. Cyclohexanoic acid (CHA) has been effectively removed by Zhang et al. (2016a, b and c) using Fe-nitrilotriacetic acid (NTA) and Fe-Ethylenediamine-N, N'-disuccinic acid (EDDS) chelates. They also studied the reaction mechanism and kinetics. A competition-kinetic model was used with p-chlorobenzoic acid (pCBA) as reference compound to study the evolution of CHA by chelate-Fenton oxidation at pH = 8 under initial H_2O_2 concentration in excess respect to the chelates, CHA, and pCBA.

A further study thoroughly investigated the effects of EDDS and NTA as chelate agents in the treatment of OSPW by UV/Fenton. EDDS was found not only to reduce the reaction rate by scavenging the $HO^{\bullet}$ radicals but also showed worse toxicity effects (Zhang et al., 2016a). Therefore, the scavenging effect of chelating agents can reduce the efficiency of H_2O_2 consumption, which is a critical issue on the economy of Fenton-based technologies. Besides, the addition of chelate agents bring about the concern on

the effect on the toxicity of the resulting effluents.

Those studies followed the disappearance of the model NAs tested but results on mineralization, namely TOC reduction, were not provided. Further research on the oxidation intermediates and byproducts is still needed to gain insight into the potential application of Fenton-based treatments to the abatement of NAs.

4.1.3. Persulfate (PS)-based oxidation

The PS ion ($S_2O_8^{2-}$) is a well-known oxidant, whose action is based on the formation of highly oxidizing sulfate radicals ($SO_4^{\bullet-}$) ($E_0 = 2.5 - 3.1$) (Neta et al., 1988; Fang et al., 2012) upon energy- or metal-activated decomposition. The application of PS-based oxidation to the abatement of a diversity of priority and emerging pollutants is widely represented in the literatures, with a growing presence in the last fifteen years (Anipsitakis and Dionysiou, 2003 and 2004; Furman et al., 2010; Xu et al., 2012; Yang et al., 2014; Liu et al., 2016; Peng et al., 2017). Differing from Fenton-based processes, PS oxidation can efficiently work within a wide pH range from acidic to basic with the sulfate radicals as the dominant reactive species, but with other also participating. In fact, numerous studies provide evidences that PS can react with OH^- ions or even water to produce $HO^\bullet$ radicals:

$$SO_4^{\bullet-} + HO^- \rightarrow SO_4^{2-} + HO^\bullet \quad (3)$$

$$SO_4^{\bullet-} + H_2O \rightarrow SO_4^{2-} + HO^\bullet + H^+ \quad (4)$$

Moreover, dissolved oxygen has been demonstrated to increase the oxidizing efficiency of PS with the positive effect of $O_2^{\bullet-}$ radicals (Fang et al., 2013; Liu et al., 2016a; Xu et al., 2016).

Thermally-activated PS has been used for the abatement of model and OSPW NAs. Complete conversion of CHA was observed upon 2 h of reaction with 1.2 times the stoichiometric amount of persulfate (Drzewicz et al., 2012). Similarly, high efficiency was reported by Liang et al. (2011) with model NAs in a comparative study. Recently, Xu et al. (2016) reported the important role of dissolved oxygen in thermally-activated PS oxidation of model NAs at 80 ºC. Oxygen molecules were found not only to increase the reaction rate but also allow complete mineralization of NAs under PS doses well below the corresponding stoichiometric amount, due to the contribution of superoxide and hydroperoxide radicals resulting from:

$$SO_4^{\bullet-} + R{-}H \rightarrow HSO_4^- + {}^\bullet R \quad (5)$$

$${}^\bullet R + O_2 \rightarrow R^+ + O_2^{\bullet-} \quad (6)$$

$$O_2^{\bullet-} + H^+ \leftrightarrow HO_2^\bullet \quad (7)$$

Based on the experimental findings, the overall oxidation reactions for the model NAs tested in that work were reformulated to include the contribution of oxygen. The kinetics of mineralization was described by a pseudo-first-order rate equation and normalized values of the rate constants were provided (Figure 4).

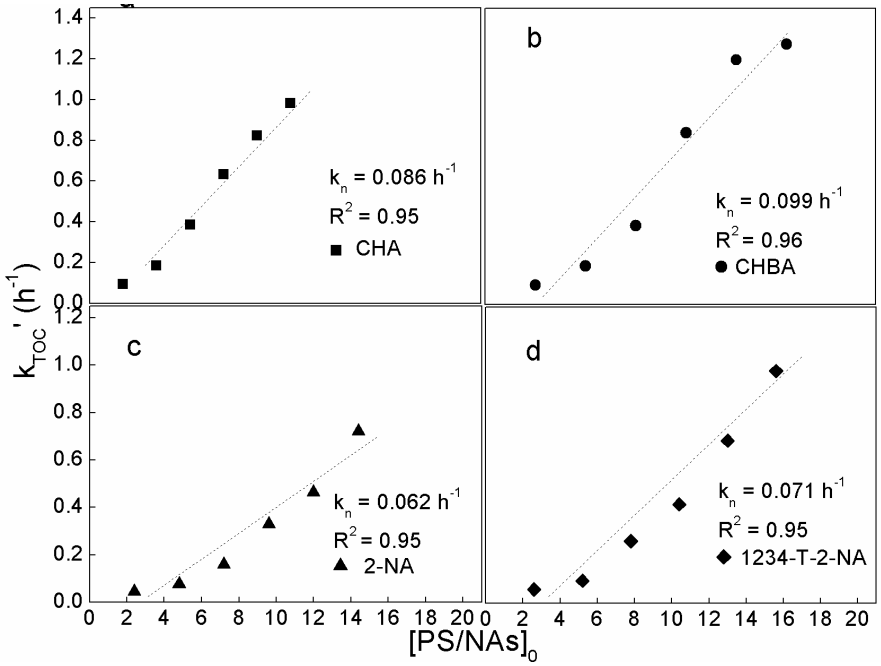

FIGURE 4. Values of the pseudo-first order rate constant of NAs mineralization at different initial PS/NAs molar ratios. (reprinted with permissions from Xu et al. (2016). Copyright (2016) Elsevier)

Compared to the HO• radical-driven processes, PS readily causes the decarboxylation of NAs giving rise to the corresponding aliphatic radicals which undergo further decomposition. Therefore, the sulfate radical becomes a more effective oxidant than HO• for aliphatic acids oxidation (Madhavan et al., 1978; Drzewicz et al., 2012). Nevertheless, the PS-based systems have some drawbacks, such as the high relative cost of the reagent and the increased conductivity of the resulting effluent due to sulfates.

4.1.4. NAs abatement by other AOPs

Degradation of model NAs with UV-activated H_2O_2 has been studied by Drzewicz et al. (2010) and Afzal et al. (2012 a and b). The former identified 4-oxo-CHA as the main intermediate, resulting from the attack of HO• to the para-position on the saturated ring. Ring-opening starts by β-scission of the cyclohexane ring according to the acyclic byproducts, which included heptadioic acid and various short-chain carboxylic acids. Liang et al. (2011) compared UV-activated H_2O_2, TiO_2, IO_4^-, and $S_2O_8^{2-}$ treatments applied to CHA. The efficiency of HO• for the breakdown of saturated hydrocarbon chains is lower than for unsaturated ones (Drzewicz et al., 2012). However, classical NAs do not contain olefin structures so that HO• radicals provoke mainly hydrogen abstraction. This reaction is less effective than the decarboxylation caused by sulfate radicals which can yield aliphatic radicals from saturated rings allowing more in-depth degradation (Madhavan et al., 1978; Drzewicz et al., 2012). Most recently, Wang et al. (2016) compared the efficiency of UV/H_2O_2, potassium ferrate(VI), and ozone in the oxidation of the organic fraction of OSPW. The important role of molecular ozone and

$HO^{\bullet}$ radicals was confirmed by scavenging tests and ^{1}H NMR analyses further suggested the removal of aromatic NAs. Those three oxidation systems reduced the acute toxicity towards *Vibrio fischeri* and goldfish primary kidney macrophages (PKMs), being ozonation the most efficient.

UV/TiO_2 and solar/TiO_2 treatments have been applied to degrade NAs (Headley et al., 2009; Leshuk et al., 2016). The light radiation can cause electron-hole pairs on TiO_2 which promote the formation of $O_2^{\bullet-}$ and $HO^{\bullet}$ radicals from water and dissolved oxygen. Headley et al. (2009) reported complete conversion of 4-methyl-cyclohexaneaceticic acid (4-MCHAA) with close to 75% TOC reduction upon 8 h under solar radiation over a TiO_2 suspension. In a further work, Sabyasachi et al. (2010) reported half-life values of OSPW NAs by UV/TiO_2 degradation ranging between 1.55 and 4.80 h. Significant toxicity reduction was achieved. Headley et al. (2010) used an UV/microwave system to activate TiO_2 for the abatement of OSPW NAs. More recently, Leshuk et al. (2016) reported on the effective solar-driven TiO_2 degradation of NAs in OSPW. Acid extractable organics in OSPW disappeared after one day of natural solar irradiation (25 MJ m^{-2} for 14 h daylight) in the presence of TiO_2. Complete mineralization was achieved within 7 days where toxicity reduction also occurred.

UV/chlorine oxidation has also been tested for the degradation of OSPW NAs (Shu et al., 2014). This process effectively removed NAs (75−84% conversion) from OSPW. Structure-dependent effects were also observed, being NAs with higher number of rings and carbon atoms more readily degradable. $HO^{\bullet}$, $O^{\bullet-}$ and $Cl^{\bullet}$ were claimed as the main oxidizing species from photo-excitation of water and chloride.

The breakdown of model NAs with gamma-ray irradiation was checked by Jia et al. (2015). Reactive species like $HO^{\bullet}$ radicals, hydrated electrons (e_{aq}^{-}) and atomic hydrogen can be formed by γ-excitation (Wang and Wang, 2007). Liang et al. (2011) attempted UV/IO_4^- oxidation of CHA. This system showed to be less efficient than H_2O_2- and PS-based approaches. The time course of NAs upon UV/TiO_2 (Leshuk et al., 2016) and gamma-ray (Jia et al., 2015) treatments was fitted to pseudo-first-order rate equation.

The scavenging effect of certain components of real NAs-containing wastewaters, like chloride and bicarbonate, must be considered and addressed. Adverse environmental effects can even result from the formation of related toxic species, like chlorate and organo-chlorinated byproducts. This aspect has been not considered so far in the literature on Fenton-based oxidation of NAs (Zhang et al., 2016c), while several interesting works have been conducted for PS-based oxidation of NAs. Drzewicz et al. (2012) investigated the role of chloride in CHA degradation by PS upon thermal and zero-valent iron activation. Although no significant hampering effect was observed in terms of CHA removal, they reported the formation of chloro-CHA during PS oxidation in the presence of chloride anions. Xu et al. (2016) studied the effect of chloride and bicarbonate on thermally-activated PS oxidation of model NAs. The former showed negative effect whereas it was negligible or even positive in the case of bicarbonate. Apart from those inorganic components, the scavenging potential of some organic species in the OSPW tailing ponds, such as unrecovered bitumen (oil and grease),

polyaromatic hydrocarbons (PAH), BTEX (benzene, toluene, ethyl benzene, and xylenes), as well as fulvic and humic acids, should also be addressed in the future regarding the application of AOP systems (Zhang et al., 2016c).

5. Conclusion and outlook

The exploitation of unconventional hydrocarbon sources causes serious environmental problems, derived from the generation of large volumes of wastewater containing a series of recalcitrant species (mainly NAs) of high toxicity. Different advanced oxidation treatments have been reported in the literature as promising solutions for the abatement of those pollutants. Among them, O_3-, H_2O_2- and PS-based techniques appear as the most likely for potential application in the next future. PS-based systems with thermal-activation have proved a high efficiency in terms of mineralization. The contribution of dissolved oxygen has shown to reduce the amount of reagent needed. Compared with O_3 and H_2O_2, however, PS introduces sulfur-containing ionic species into the final effluent. Future development of cost-effective solutions based on AOPs is a main challenge, given the growing environmental concern associated to OSPW and other related NAs-containing effluents. In that sense, advanced oxidation technologies can be used alone or combined. The tandem based on PS followed by further Fenton oxidation has proved to be highly efficient for NAs mineralization, reducing the cost derived from reagents consumption. Also, AOP-based treatments can be used as previous step addressed to improve the biodegradability, thus allowing an effective application of further biological treatment.

An important issue refers to the implementation of more sensitive analytical techniques for NAs and their related oxidation species. That would allow a more in-depth understanding of the reaction mechanisms involved, which is a crucial issue regarding the selection and design of potential solutions for the effective treatment of aqueous waste streams containing this kind of pollutants.

Acknowledgements

We are grateful to the Chinese Scholarship Council (CSC) for supporting the Ph.D. program of Xiyan Xu (CSC, File No. 201308410047). Spanish MINECO is also gratefully acknowledged for the financial support through the project CTQ2013-41963-R.

References

Afzal, A., Chelme-Ayala, P., Drzewicz, P., Martin, J.W. and Gamal El-Din, M. (2015) Effects of

ozone and ozone/hydrogen peroxide on the degradation of model and real oil-sands-process-affected-water naphthenic acids. Ozone: Science & Engineering 37(1), 45-54.

Afzal, A., Drzewicz, P., Martin, J.W. and Gamal El-Din, M. (2012a) Decomposition of cyclohexanoic acid by the UV/H_2O_2 process under various conditions. Sci. Total. Environ. 426, 387-392.

Afzal, A., Drzewicz, P., Pérez-Estrada, L.n.A., Chen, Y., Martin, J.W. and Gamal El-Din, M. (2012b) Effect of molecular structure on the relative reactivity of naphthenic acids in the UV/H_2O_2 advanced oxidation process. Environ. Sci. Technol. 46(19), 10727-10734.

Al-jibouri, A.K.H., Wu, J. and Upreti, S.R. (2015) Ozonation of Naphthenic Acids in Water: Kinetic Study. Water, Air, & Soil Pollution 226(10), 1-11.

Andreozzi, R., Caprio, V., Insola, A. and Marotta, R. (1999) Advanced oxidation processes (AOP) for water purification and recovery. Catal. Today 53(1), 51-59.

Anipsitakis, G.P. and Dionysiou, D.D. (2003) Degradation of organic contaminants in water with sulfate radicals generated by the conjunction of peroxymonosulfate with cobalt. Environ. Sci. Technol. 37(20), 4790-4797.

Anipsitakis, G.P. and Dionysiou, D.D. (2004) Radical generation by the interaction of transition metals with common oxidants. Environ. Sci. Technol. 38(13), 3705-3712.

Armstrong, S.A. (2008) Dissipation and phytotoxicity of oil sands naphthenic acids in wetland plants. (Doctoral dissertation)

Baffes, J., Kose, M.A., Ohnsorge, F. and Stocker, M. (2015) The great plunge in oil prices: Causes, consequences, and policy responses. Consequences, and Policy Responses (June 2015).

Barrow, M.P., McDonnell, L.A., Feng, X., Walker, J. and Derrick, P.J. (2003) Determination of the nature of naphthenic acids present in crude oils using nanospray Fourier transform ion cyclotron resonance mass spectrometry: The continued battle against corrosion. Anal. Chem. 75(4), 860-866.

Barrow, M.P., Peru, K.M., Fahlman, B., Hewitt, L.M., Frank, R.A. and Headley, J.V. (2015) Beyond naphthenic acids: Environmental screening of water from natural sources and the Athabasca oil sands industry using atmospheric pressure photoionization Fourier transform ion cyclotron resonance mass spectrometry. J. Am. Soc. Mass Spectr. 26(9), 1508-1521.

Barrow, M.P., Witt, M., Headley, J.V. and Peru, K.M. (2010) Athabasca oil sands process water: Characterization by atmospheric pressure photoionization and electrospray ionization Fourier transform ion cyclotron resonance mass spectrometry. Anal. Chem. 82(9), 3727-3735.

Bataineh, M., Scott, A., Fedorak, P. and Martin, J. (2006) Capillary HPLC/QTOF-MS for characterizing complex naphthenic acid mixtures and their microbial transformation. Anal. Chem. 78(24), 8354-8361.

Bauer, A.E., Frank, R.A., Headley, J.V., Peru, K.M., Hewitt, L.M. and Dixon, D.G. (2015) Enhanced characterization of oil sands acid□extractable organics fractions using electrospray ionization–high□resolution mass spectrometry and synchronous fluorescence spectroscopy. Environ. Toxicol. Chem. 34(5), 1001-1008.

Bautista, P., Mohedano, A., Casas, J., Zazo, J. and Rodriguez, J. (2008) An overview of the application of Fenton oxidation to industrial wastewaters treatment. J. Chem. Technol. Biot. 83(10), 1323-1338.

Beltran, F.J. (2003) Ozone reaction kinetics for water and wastewater systems, CRC Press.

Biryukova, O.V., Fedorak, P.M. and Quideau, S.A. (2007) Biodegradation of naphthenic acids by

rhizosphere microorganisms. Chemosphere 67(10), 2058-2064.

Boudens, R., Reid, T., VanMensel, D., MR, S.P., Ciborowski, J.J. and Weisener, C.G. (2016) Biophysicochemical effects of gamma irradiation treatment for naphthenic acids in oil sands fluid fine tailings. Sci. Total. Environ. 539, 114-124.

Brient, J.A., Wessner, P.J. and Doyle, M.N. (1995) Naphthenic acids. Kirk-Othmer encyclopedia of chemical technology.

Brown, L.D. and Ulrich, A.C. (2015) Oil sands naphthenic acids: A review of properties, measurement, and treatment. Chemosphere 127, 276-290.

Brunswick, P., Hewitt, L.M., Frank, R.A., van Aggelen, G., Kim, M. and Shang, D. (2016) Specificity of high resolution analysis of naphthenic acids in aqueous environmental matrices. Anal. Methods, 8(37), 6764-6773.

Clemente, J.S. and Fedorak, P.M. (2005) A review of the occurrence, analyses, toxicity, and biodegradation of naphthenic acids. Chemosphere 60(5), 585-600.

Da Campo, R., Barrow, M.P., Shepherd, A.G., Salisbury, M. and Derrick, P.J. (2009) Characterization of naphthenic acid singly charged noncovalent dimers and their dependence on the accumulation time within a hexapole in Fourier transform ion cyclotron resonance mass spectrometry. Energ. Fuel 23(11), 5544-5549.

Dias, H.P., Pereira, T.M., Vanini, G., Dixini, P.V., Celante, V.G., Castro, E.V., Vaz, B.G., Fleming, F.P., Gomes, A.O. and Aquije, G.M. (2014) Monitoring the degradation and the corrosion of naphthenic acids by electrospray ionization Fourier transform ion cyclotron resonance mass spectrometry and atomic force microscopy. Fuel 126, 85-95.

Dissanayake, A., Scarlett, A.G. and Jha, A.N. (2016) Diamondoid naphthenic acids cause in vivo genetic damage in gills and haemocytes of marine mussels. Environ. Sci. Pollut. R., 23(7), 7060-7066.

Dokholyan, B. and Magomedov, A. (1984) The effect of sodium naphthenate on the viability and physiological and biochemical indices of fish. Voprosy Ikhtiologii 23(6), 1013-1019.

Drzewicz, P., Afzal, A., El-Din, M.G. and Martin, J.W. (2010) Degradation of a model naphthenic acid, cyclohexanoic acid, by vacuum UV (172 nm) and UV (254 nm)/H_2O_2. J Phys Chem A 114(45), 12067-12074.

Drzewicz, P., Perez-Estrada, L., Alpatova, A., Martin, J.W. and Gamal El-Din, M. (2012) Impact of peroxydisulfate in the presence of zero valent iron on the oxidation of cyclohexanoic acid and naphthenic acids from oil sands process-affected water. Environ. Sci. Technol. 46(16), 8984-8991.

El-Din, M.G., Fu, H., Wang, N., Chelme-Ayala, P., Pérez-Estrada, L., Drzewicz, P., Martin, J.W., Zubot, W. and Smith, D.W. (2011) Naphthenic acids speciation and removal during petroleum-coke adsorption and ozonation of oil sands process-affected water. Sci. Total. Environ. 409(23), 5119-5125.

Fang, G.-D., Dionysiou, D.D., Al-Abed, S.R. and Zhou, D.-M. (2013) Superoxide radical driving the activation of persulfate by magnetite nanoparticles: Implications for the degradation of PCBs. Appl. Catal. B-Environ. 129, 325-332.

Fang, G.-D., Dionysiou, D.D., Wang, Y., Al-Abed, S.R. and Zhou, D.-M. (2012) Sulfate radical-based degradation of polychlorinated biphenyls: effects of chloride ion and reaction kinetics. J. Hazard. Mater. 227, 394-401.

Folwell, B.D., McGenity, T.J., Price, A., Johnson, R.J. and Whitby, C. (2016) Exploring the capacity

for anaerobic biodegradation of polycyclic aromatic hydrocarbons and naphthenic acids by microbes from oil-sands-process-affected waters. Int. Biodeter. Biodegr. 108, 214-221.

Frank, R.A., Fischer, K., Kavanagh, R., Burnison, B.K., Arsenault, G., Headley, J.V., Peru, K.M., Kraak, G.V.D. and Solomon, K.R. (2008) Effect of carboxylic acid content on the acute toxicity of oil sands naphthenic acids. Environ. Sci. Technol. 43(2), 266-271.

Furman, O.S., Teel, A.L. and Watts, R.J. (2010) Mechanism of base activation of persulfate. Environ. Sci. Technol. 44(16), 6423-6428.

Gautier, D.L., Bird, K.J., Charpentier, R.R., Grantz, A., Houseknecht, D.W., Klett, T.R., Moore, T.E., Pitman, J.K., Schenk, C.J. and Schuenemeyer, J.H. (2009) Assessment of undiscovered oil and gas in the Arctic. Science 324(5931), 1175-1179.

Grewer, D.M., Young, R.F., Whittal, R.M. and Fedorak, P.M. (2010a) Naphthenic acids and other acid-extractables in water samples from Alberta: what is being measured? Sci. Total. Environ. 408(23), 5997-6010.

Grewer, D.M., Young, R.F., Whittal, R.M. and Fedorak, P.M. (2010b) Naphthenic acids and other acid-extractables in water samples from Alberta: what is being measured? Sci. Total. Environ. 408(23), 5997-6010.

Han, X., MacKinnon, M.D. and Martin, J.W. (2009) Estimating the in situ biodegradation of naphthenic acids in oil sands process waters by HPLC/HRMS. Chemosphere 76(1), 63-70.

Han, X., Scott, A.C., Fedorak, P.M., Bataineh, M. and Martin, J.W. (2008) Influence of molecular structure on the biodegradability of naphthenic acids. Environ. Sci. Technol. 42(4), 1290-1295.

Hao, C., Headley, J.V., Peru, K.M., Frank, R., Yang, P. and Solomon, K.R. (2005) Characterization and pattern recognition of oil–sand naphthenic acids using comprehensive two-dimensional gas chromatography/time-of-flight mass spectrometry. J. Chromatogr. A 1067(1), 277-284.

Hayes, T.M.E. (2007) Examining the ecological effects of naphthenic acids and major ions on phytoplankton in the Athabasca oil sands region, Library and Archives Canada= Bibliothèque et Archives Canada.

He, Y., Patterson, S., Wang, N., Hecker, M., Martin, J.W., El-Din, M.G., Giesy, J.P. and Wiseman, S.B. (2012) Toxicity of untreated and ozone-treated oil sands process-affected water (OSPW) to early life stages of the fathead minnow (Pimephales promelas). Water Res. 46(19), 6359-6368.

Headley, J.V., Du, J.-L., Peru, K.M. and McMartin, D.W. (2009) Electrospray ionization mass spectrometry of the photodegradation of naphthenic acids mixtures irradiated with titanium dioxide. J. Environ. Sci. Heal. A 44(6), 591-597.

Headley, J.V. and McMartin, D.W. (2004) A Review of the Occurrence and Fate of Naphthenic Acids in Aquatic Environments. J. Environ. Sci. Heal. A 39(8), 1989-2010.

Headley, J.V., Peru, K.M. and Barrow, M.P. (2016) Advances in mass spectrometric characterization of naphthenic acids fraction compounds in oil sands environmental samples and crude oil—a review. Mass spectrometry reviews 35(2), 311-328.

Headley, J.V., Peru, K.M., Mishra, S., Meda, V., Dalai, A.K., McMartin, D.W., Mapolelo, M.M., Rodgers, R.P. and Marshall, A.G. (2010) Characterization of oil sands naphthenic acids treated with ultraviolet and microwave radiation by negative ion electrospray Fourier transform ion cyclotron resonance mass spectrometry. Rapid Commun. Mass S. 24(21), 3121-3126.

Headley, J.V., Peru, K.M., Mohamed, M.H., Wilson, L., McMartin, D.W., Mapolelo, M.M., Lobodin, V.V., Rodgers, R.P. and Marshall, A.G. (2013) Atmospheric pressure photoionization Fourier

transform ion cyclotron resonance mass spectrometry characterization of tunable carbohydrate-based materials for sorption of oil sands naphthenic acids. Energ. Fuel 28(3), 1611-1616.

Herman, D.C., Fedorak, P.M., MacKinnon, M.D. and Costerton, J. (1994) Biodegradation of naphthenic acids by microbial populations indigenous to oil sands tailings. Can. J. Microbiol. 40(6), 467-477.

Hindle, R., Noestheden, M., Peru, K. and Headley, J. (2013) Quantitative analysis of naphthenic acids in water by liquid chromatography-accurate mass time-of-flight mass spectrometry. J. Chromatogr. A 1286, 166-174.

Huang, C. (2016) Treatment of Oil Sands Process-affected Water (OSPW) Using Integrated Fixed-film Activated Sludge (IFAS) Reactors, University of Alberta.

Hughes, J.D. (2013) Energy: A reality check on the shale revolution. Nature 494(7437), 307-308.

Hwang, G., Dong, T., Islam, M.S., Sheng, Z., Pérez-Estrada, L.A., Liu, Y. and El-Din, M.G. (2013) The impacts of ozonation on oil sands process-affected water biodegradability and biofilm formation characteristics in bioreactors. Bioresource technology 130, 269-277.

Iranmanesh, S., Harding, T., Abedi, J., Seyedeyn-Azad, F. and Layzell, D.B. (2014) Adsorption of naphthenic acids on high surface area activated carbons. J. Environ. Sci. Heal. A 49(8), 913-922.

Islam, M.S., Moreira, J., Chelme-Ayala, P. and Gamal El-Din, M. (2014) Prediction of naphthenic acid species degradation by kinetic and surrogate models during the ozonation of oil sands process-affected water. Sci. Total. Environ. 493, 282-290.

Janfada, A., Headley, J.V., Peru, K.M. and Barbour, S. (2006) A laboratory evaluation of the sorption of oil sands naphthenic acids on organic rich soils. J. Environ. Sci. Heal. A 41(6), 985-997.

Jia, L., Anthony, E. and Charland, J. (2002) Investigation of vanadium compounds in ashes from a CFBC firing 100 petroleum coke. Energ. Fuel 16(2), 397-403.

Jia, W., He, Y., Ling, Y., Hei, D., Shan, Q., Zhang, Y. and Li, J. (2015) Radiation-induced degradation of cyclohexanebutyric acid in aqueous solutions by gamma ray irradiation. Radiat. Phys. Chem. 109, 17-22.

Johnson, R.J., Smith, B.E., Rowland, S.J. and Whitby, C. (2013) Biodegradation of alkyl branched aromatic alkanoic naphthenic acids by Pseudomonas putida KT2440. Int Biodeter Biodegr 81, 3-8.

Johnson, R.J., Smith, B.E., Sutton, P.A., McGenity, T.J., Rowland, S.J. and Whitby, C. (2011) Microbial biodegradation of aromatic alkanoic naphthenic acids is affected by the degree of alkyl side chain branching. ISME J 5(3), 486-496.

Johnson, R.J., West, C.E., Swaih, A.M., Folwell, B.D., Smith, B.E., Rowland, S.J. and Whitby, C. (2012) Aerobic biotransformation of alkyl branched aromatic alkanoic naphthenic acids via two different pathways by a new isolate of Mycobacterium. Environmental microbiology 14(4), 872-882.

Jones, D., Scarlett, A.G., West, C.E. and Rowland, S.J. (2011) Toxicity of individual naphthenic acids to Vibrio fischeri. Environ. Sci. Technol. 45(22), 9776-9782.

Jones, D., Watson, J., Meredith, W., Chen, M. and Bennett, B. (2001) Determination of naphthenic acids in crude oils using nonaqueous ion exchange solid-phase extraction. Anal. Chem. 73(3), 703-707.

Jones, D., West, C.E., Scarlett, A.G., Frank, R.A. and Rowland, S.J. (2012) Isolation and estimation

of the ‘aromatic’ naphthenic acid content of an oil sands process-affected water extract. J. Chromatogr. A 1247, 171-175.

Kamaluddin, M. and Zwiazek, J.J. (2002) Naphthenic acids inhibit root water transport, gas exchange and leaf growth in aspen (Populus tremuloides) seedlings. Tree physiology 22(17), 1265-1270.

Kannel, P.R. and Gan, T.Y. (2012) Naphthenic acids degradation and toxicity mitigation in tailings wastewater systems and aquatic environments: a review. J. Environ. Sci. Health. A 47(1), 1-21.

Kavanagh, R.J., Burnison, B.K., Frank, R.A., Solomon, K.R. and Van Der Kraak, G. (2009) Detecting oil sands process-affected waters in the Alberta oil sands region using synchronous fluorescence spectroscopy. Chemosphere 76(1), 120-126.

Kean, S. (2009) Eco-alchemy in Alberta. Science 326(5956), 1052-1055.

Kister, J., Pieri, N., Alvarez, R., Diez, M. and Pis, J. (1996) Effects of preheating and oxidation on two bituminous coals assessed by synchronous UV fluorescence and FTIR spectroscopy. Energ. Fuel 10(4), 948-957.

Klamerth, N., Moreira, J., Li, C., Singh, A., McPhedran, K.N., Chelme-Ayala, P., Belosevic, M. and El-Din, M.G. (2015) Effect of ozonation on the naphthenic acids' speciation and toxicity of pH-dependent organic extracts of oil sands process-affected water. Sci. Total. Environ. 506, 66-75.

Langlais, B., Legube, B., Beuffe, H. and Dore, M. (1993) Study of the nature of the by-products formed and the risks of toxicity when disinfecting a secondary effluent with ozone. Water. Sci. Technol. 27, 135-135.

Leshuk, T., Wong, T., Linley, S., Peru, K.M., Headley, J.V. and Gu, F. (2016) Solar photocatalytic degradation of naphthenic acids in oil sands process-affected water. Chemosphere 144, 1854-1861.

Leung, S.S., MacKinnon, M.D. and Smith, R.E. (2003) The ecological effects of naphthenic acids and salts on phytoplankton from the Athabasca oil sands region. Aquatic Toxicology 62(1), 11-26.

Leung, S.S.C., MacKinnon, M.D. and Smith, R.E. (2001) Aquatic reclamation in the Athabasca, Canada, oil sands: naphthenate and salt effects on phytoplankton communities. Environ. Toxicol. Chem. 20(7), 1532-1543.

Liang, X., Zhu, X. and Butler, E.C. (2011) Comparison of four advanced oxidation processes for the removal of naphthenic acids from model oil sands process water. J. Hazard. Mater. 190(1-3), 168-176.

Liu, H., Bruton, T.A., Li, W., Buren, J.V., Prasse, C., Doyle, F.M. and Sedlak, D.L. (2016a) Oxidation of benzene by persulfate in the presence of Fe (III)-and Mn (IV)-containing oxides: stoichiometric efficiency and transformation products. Environ. Sci. Technol. 50(2), 890-898.

Liu, J., Wang, L., Tang, J. and Ma, J. (2016b) Photocatalytic degradation of commercially sourced naphthenic acids by TiO_2-graphene composite nanomaterial. Chemosphere 149, 328-335.

Luna, F.M.T., Pontes-Filho, A.A., Trindade, E.D., Silva, I.J., Azevedo, D.C. and Cavalcante, C.L. (2008) Removal of aromatic compounds from mineral naphthenic oil by adsorption. J Ind Eng Chem 47(9), 3207-3212.

Madhavan, V., Levanon, H. and Neta, P. (1978) Decarboxylation by SO_4-radicals. Radiation Research 76(1), 15-22.

Madill, R.E., Orzechowski, M.T., Chen, G., Brownlee, B.G. and Bunce, N.J. (2001) Preliminary

risk assessment of the wet landscape option for reclamation of oil sands mine tailings: bioassays with mature fine tailings pore water. Environmental Toxicology 16(3), 197-208.

Mahdavi, H., Prasad, V., Liu, Y. and Ulrich, A.C. (2015) In situ biodegradation of naphthenic acids in oil sands tailings pond water using indigenous algae-bacteria consortium. Bioresour. Technol. 187, 97-105.

Marentette, J.R., Frank, R.A., Bartlett, A.J., Gillis, P.L., Hewitt, L.M., Peru, K.M., Headley, J.V., Brunswick, P., Shang, D. and Parrott, J.L. (2015) Toxicity of naphthenic acid fraction components extracted from fresh and aged oil sands process-affected waters, and commercial naphthenic acid mixtures, to fathead minnow (Pimephales promelas) embryos. Aquatic Toxicology 164, 108-117.

Marsh, W.P. (2006) Sorption of naphthenic acids to soil minerals, Library and Archives Canada= Bibliothèque et Archives Canada.

Martin, J.W., Barri, T., Han, X., Fedorak, P.M., El-Din, M.G., Perez, L., Scott, A.C. and Jiang, J.T. (2010) Ozonation of oil sands process-affected water accelerates microbial bioremediation. Environ. Sci. Technol. 44(21), 8350-8356.

Martin, N., Burkus, Z., McEachern, P. and Yu, T. (2014) Naphthenic acids quantification in organic solvents using fluorescence spectroscopy. J. Environ. Sci. Heal. A 49(3), 294-306.

McQueen, A.D., Kinley, C.M., Kiekhaefer, R.L., Calomeni, A.J., Rodgers Jr, J.H. and Castle, J.W. (2016) Photocatalysis of a Commercial Naphthenic Acid in Water Using Fixed-Film TiO_2. Water, Air, & Soil Pollution 227(5), 1-11.

Melvin, S.D. and Trudeau, V.L. (2012) Toxicity of naphthenic acids to wood frog tadpoles (Lithobates sylvaticus). J. Toxicol. Env. Heal. A 75(3), 170-173.

Mohamed, M.H., Wilson, L.D., Headley, J.V. and Peru, K.M. (2011) Sequestration of naphthenic acids from aqueous solution using β-cyclodextrin-based polyurethanes. Phys Chem Chem Phys 13(3), 1112-1122.

Munoz, M., de Pedro, Z.M., Casas, J.A. and Rodriguez, J.J. (2015) Preparation of magnetite-based catalysts and their application in heterogeneous Fenton oxidation–a review. Appl. Catal. B-Environ. 176, 249-265.

Myhre, O. and Fonnum, F. (2001) The effect of aliphatic, naphthenic, and aromatic hydrocarbons on production of reactive oxygen species and reactive nitrogen species in rat brain synaptosome fraction: the involvement of calcium, nitric oxide synthase, mitochondria, and phospholipase A. Biochem. pharmacol. 62(1), 119-128.

Neta, P., Huie, R.E. and Ross, A.B. (1988) Rate constants for reactions of inorganic radicals in aqueous solution. J. Phys. Chem. ref. Data 17(3), 1027-1284.

Neyens, E. and Baeyens, J. (2003) A review of classic Fenton's peroxidation as an advanced oxidation technique. J. Hazard. Mater. 98(1), 33-50.

Ortiz, X., Jobst, K.J., Reiner, E.J., Backus, S.M., Peru, K.M., McMartin, D.W., O'Sullivan, G., Taguchi, V.Y. and Headley, J.V. (2014) Characterization of naphthenic acids by gas chromatography-Fourier transform ion cyclotron resonance mass spectrometry. Anal. Chem. 86(15), 7666-7673.

Pérez-Estrada, L.A., Han, X., Drzewicz, P., Gamal El-Din, M., Fedorak, P.M. and Martin, J.W. (2011) Structure–reactivity of naphthenic acids in the ozonation process. Environ. Sci. Technol. 45(17), 7431-7437.

Pereira, A.S., Bhattacharjee, S. and Martin, J.W. (2013a) Characterization of oil sands process-

affected waters by liquid chromatography orbitrap mass spectrometry. Environ. Sci. Technol. 47(10), 5504-5513.

Pereira, A.S., Islam, M., Gamal El-Din, M. and Martin, J.W. (2013b) Ozonation degrades all detectable organic compound classes in oil sands process□affected water; an application of high□performance liquid chromatography/obitrap mass spectrometry. Rapid Commun. Mass S. 27(21), 2317-2326.

Pliego, G., Zazo, J.A., Garcia-Muñoz, P., Munoz, M., Casas, J.A. and Rodriguez, J.J. (2015) Trends in the intensification of the Fenton process for wastewater treatment: an overview. Crit. Rev. Env. Sci. Tec. 45(24), 2611-2692.

Pollard, S.J., Hrudey, S.E., Fuhr, B.J., Alex, R.F., Holloway, L.R. and Tosto, F. (1992) Hydrocarbon wastes at petroleum-and creosote-contaminated sites: rapid characterization of component classes by thin-layer chromatography with flame ionization detection. Environ. Sci. Technol. 26(12), 2528-2534.

Purcell, J.M., Hendrickson, C.L., Rodgers, R.P. and Marshall, A.G. (2006) Atmospheric pressure photoionization Fourier transform ion cyclotron resonance mass spectrometry for complex mixture analysis. Anal. Chem. 78(16), 5906-5912.

Quinlan, P.J. and Tam, K.C. (2015) Water treatment technologies for the remediation of naphthenic acids in oil sands process-affected water. Chem. Eng. J. 279, 696-714.

Ré-Poppi, N., Almeida, F., Cardoso, C., Raposo, J., Viana, L., Silva, T., Souza, J. and Ferreira, V. (2009) Screening analysis of type C Brazilian gasoline by gas chromatography–Flame ionization detector. Fuel 88(3), 418-423.

Reinardy, H.C., Scarlett, A.G., Henry, T.B., West, C.E., Hewitt, L.M., Frank, R.A. and Rowland, S.J. (2013) Aromatic naphthenic acids in oil sands process-affected water, resolved by GCxGC-MS, only weakly induce the gene for vitellogenin production in zebrafish (Danio rerio) larvae. Environ. Sci. Technol. 47(12), 6614-6620.

Rontani, J. and Bonin, P. (1992) Utilization of n-alkyl-substituted cyclohexanes by a marine Alcaligenes. Chemosphere 24(10), 1441-1446.

Rowland, S.J., Scarlett, A.G., Jones, D., West, C.E. and Frank, R.A. (2011a) Diamonds in the rough: identification of individual naphthenic acids in oil sands process water. Environ. Sci. Technol. 45(7), 3154-3159.

Rowland, S.J., West, C.E., Jones, D., Scarlett, A.G., Frank, R.A. and Hewitt, L.M. (2011b) Steroidal aromatic 'naphthenic acids' in oil sands process-affected water: structural comparisons with environmental estrogens. Environ. Sci. Technol. 45(22), 9806-9815.

Rowland, S.J., West, C.E., Scarlett, A.G., Ho, C. and Jones, D. (2012) Differentiation of two industrial oil sands process□affected waters by two□dimensional gas chromatography/mass spectrometry of diamondoid acid profiles. Rapid Commun. Mass S. 26(5), 572-576.

Rowland, S.M., Robbins, W.K., Corilo, Y.E., Marshall, A.G. and Rodgers, R.P. (2014) Solid-phase extraction fractionation to extend the characterization of naphthenic acids in crude oil by electrospray ionization Fourier transform ion cyclotron resonance mass spectrometry. Energ. Fuel 28(8), 5043-5048.

Sabyasachi, M., Venkatesh, M., Ajay K, D., Dena W, M., John V, H. and Kerry M, P. (2010) Photocatalysis of naphthenic acids in water. Journal of Water Res.ource and Protection 2010.

Scarlett, A., Reinardy, H., Henry, T., West, C., Frank, R., Hewitt, L. and Rowland, S. (2013) Acute toxicity of aromatic and non-aromatic fractions of naphthenic acids extracted from oil sands

process-affected water to larval zebrafish. Chemosphere 93(2), 415-420.

Schindler, D. (2010) Tar sands need solid science. Nature 468(7323), 499-501.

Schramm, L.L., Stasiuk, E.N. and MacKinnon, M. (2000) Surfactants in Athabasca oil sands slurry conditioning, flotation recovery, and tailings processes, Cambridge University Press: Cambridge.

Scott, A.C., Young, R.F. and Fedorak, P.M. (2008a) Comparison of GC-MS and FTIR methods for quantifying naphthenic acids in water samples. Chemosphere 73(8), 1258-1264.

Scott, A.C., Zubot, W., MacKinnon, M.D., Smith, D.W. and Fedorak, P.M. (2008b) Ozonation of oil sands process water removes naphthenic acids and toxicity. Chemosphere 71(1), 156-160.

Shu, Z., Li, C., Belosevic, M., Bolton, J.R. and El-Din, M.G. (2014) Application of a solar UV/chlorine advanced oxidation process to oil sands process-affected water remediation. Environ. Sci. Technol. 48(16), 9692-9701.

Smith, B.E., Lewis, C.A., Belt, S.T., Whitby, C. and Rowland, S.J. (2008) Effects of alkyl chain branching on the biotransformation of naphthenic acids. Environ. Sci. Technol. 42(24), 9323-9328.

Tokic, D. (2015) The 2014 oil bust: Causes and consequences. Energy Policy 85, 162-169.

Tollefsen, K.E., Petersen, K. and Rowland, S.J. (2012) Toxicity of synthetic naphthenic acids and mixtures of these to fish liver cells. Environ. Sci. Technol. 46(9), 5143-5150.

Toor, N.S., Han, X., Franz, E., MacKinnon, M.D., Martin, J.W. and Liber, K. (2013) Selective biodegradation of naphthenic acids and a probable link between mixture profiles and aquatic toxicity. Environ. Toxicol. Chem. 32(10), 2207-2216.

Vaiopoulou, E., Misiti, T.M. and Pavlostathis, S.G. (2015) Removal and toxicity reduction of naphthenic acids by ozonation and combined ozonation-aerobic biodegradation. Bioresour. Technol. 179, 339-347.

Wang, B., Wan, Y., Gao, Y., Yang, M. and Hu, J. (2013a) Determination and characterization of oxy-naphthenic acids in oilfield wastewater. Environ. Sci. Technol. 47(16), 9545-9554.

Wang, B., Wan, Y., Gao, Y., Zheng, G., Yang, M., Wu, S. and Hu, J. (2015a) Occurrences and behaviors of naphthenic acids in a petroleum refinery wastewater treatment plant. Environ. Sci. Technol. 49(9), 5796-5804.

Wang, C., Klamerth, N., Messele, S.A., Singh, A., Belosevic, M. and El-Din, M.G. (2016) Comparison of UV/hydrogen peroxide, potassium ferrate (VI), and ozone in oxidizing the organic fraction of oil sands process-affected water (OSPW). Water Res. 100, 476-485.

Wang, J., Feng, L., Steve, M., Tang, X., Gail, T.E. and Mikael, H. (2015b) China's unconventional oil: A review of its resources and outlook for long-term production. Energy 82, 31-42.

Wang, J. and Wang, J. (2007) Application of radiation technology to sewage sludge processing: a review. J. Hazard. Mater. 143(1), 2-7.

Wang, N., Chelme-Ayala, P., Perez-Estrada, L., Garcia-Garcia, E., Pun, J., Martin, J.W., Belosevic, M. and Gamal El-Din, M. (2013b) Impact of ozonation on naphthenic acids speciation and toxicity of oil sands process-affected water to Vibrio fischeri and mammalian immune system. Environ. Sci. Technol. 47(12), 6518-6526.

Wang, X. and Kasperski, K.L. (2010) Analysis of naphthenic acids in aqueous solution using HPLC-MS/MS. Anal. Methods 2(11), 1715.

Wang, Z., Yang, C., Hollebone, B. and Fingas, M. (2006) Forensic fingerprinting of diamondoids for correlation and differentiation of spilled oil and petroleum products. Environ. Sci. Technol.

40(18), 5636-5646.

West, C.E., Jones, D., Scarlett, A.G. and Rowland, S.J. (2011) Compositional heterogeneity may limit the usefulness of some commercial naphthenic acids for toxicity assays. Sci. Total. Environ. 409(19), 4125-4131.

Wort, D. and Patel, K. (1970) Response of plants to naphthenic and cycloalkanecarboxylic acids. Agronomy Journal 62(5), 644-646.

Wu, J. and Upreti, S.R. (2017) Application of mass balance models in the process of ozone removal of naphthenic acids from water. Can. J. Chem. Eng. 95(1), 39-45.

Xu, X.-Y., Zeng, G.-M., Peng, Y.-R. and Zeng, Z. (2012) Potassium persulfate promoted catalytic wet oxidation of fulvic acid as a model organic compound in landfill leachate with activated carbon. Chem. Eng. J. 200, 25-31.

Xu, X., Pliego, G., Zazo, J.A., Casas, J.A. and Rodriguez, J.J. (2016) Mineralization of naphtenic acids with thermally-activated persulfate: The important role of oxygen. J. Hazard. Mater. 318, 355-362.

Xue, J., Zhang, Y., Liu, Y. and El-Din, M.G. (2016) Effects of ozone pretreatment and operating conditions on membrane fouling behaviors of an anoxic-aerobic membrane bioreactor for oil sands process-affected water (OSPW) treatment. Water Res. 105, 444-455.

Yang, Y., Pignatello, J.J., Ma, J. and Mitch, W.A. (2014) Comparison of halide impacts on the efficiency of contaminant degradation by sulfate and hydroxyl radical-based advanced oxidation processes (AOPs). Environ. Sci. Technol. 48(4), 2344-2351.

Zhang, Y., Klamerth, N., Chelme-Ayala, P. and Gamal El-Din, M. (2016a) Comparison of nitrilotriacetic acid and [S, S]-ethylenediamine-N, N'-disuccinic acid in UV-Fenton for the treatment of oil sands process-affected water at natural pH. Environ. Sci. Technol., 50(19), 10535-10544.

Zhang, Y., Klamerth, N. and El-Din, M.G. (2016b) Degradation of a model naphthenic acid by nitrilotriacetic acid–modified Fenton process. Chem. Eng. J. 292, 340-347.

Zhang, Y., Klamerth, N., Messele, S.A., Chelme-Ayala, P. and El-Din, M.G. (2016c) Kinetics study on the degradation of a model naphthenic acid by ethylenediamine-N, N'-disuccinic acid-modified Fenton process. J. Hazard. Mater. 318, 371-378.

Zhang, Y., Xue, J., Liu, Y. and El-Din, M.G. (2016d) Treatment of oil sands process-affected water using membrane bioreactor coupled with ozonation: A comparative study. Chem. Eng. J. 302, 485-497.

Two-step persulfate and Fenton oxidation of naphthenic acids in water

Xiyan Xu; Gema Pliego; Juan A. Zazo; Jose A. Casas; Juan J. Rodriguez

Graphical abstract

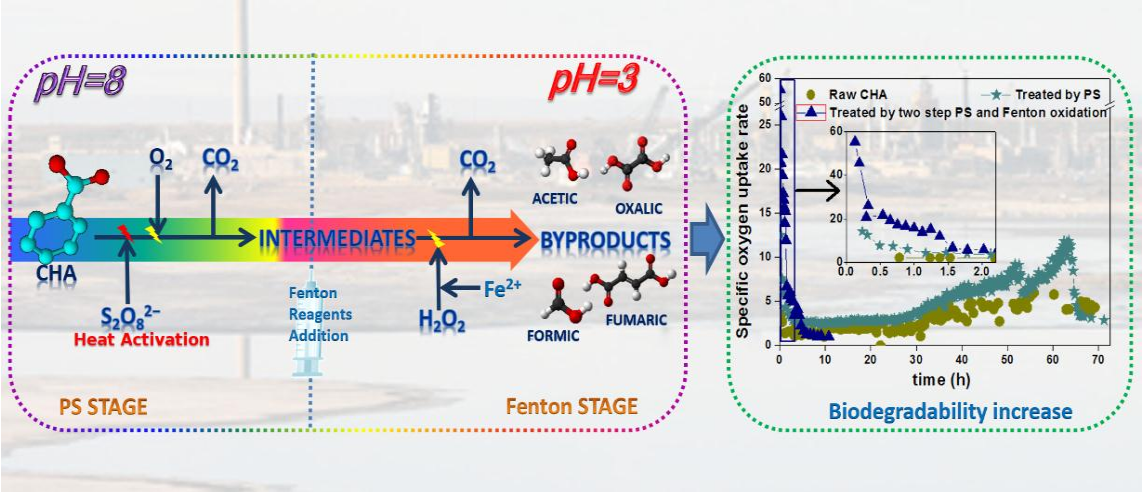

Abstract

Two-step persulfate (PS) and Fenton oxidation has been investigated for the mineralization of naphthenic acids (NAs) at 80 ºC and initial pH = 8. The effects of PS and H_2O_2 doses, iron concentration, duration of the PS oxidation step and operating temperature have been assessed using cyclohexanoic acid (CHA, 50 mg L^{-1}) as the model compound. The combined treatment allowed up to ≈ 80% mineralization of CHA with using fairly low relative amounts of reagents (20 and 30% of the stoichiometric for PS and H_2O_2, respectively). A kinetic model combining both the PS and Fenton oxidation stages is proposed to describe the rate of TOC removal, where the values of rate constants and apparent activation energy are provided. The system was also successfully tested with other NAs including saturated ring as well as aromatic structures, namely cyclohexanebutyric acid (CHBA), 2-naphthoic acid (2-NA) and 1,2,3,4-tetrahydro-2-naphthoic acid (1234-T-2-NA). Treatment of the NAs tested by this system gave rise to easily biodegradable effluents which included mainly short-chain organic acids, as confirmed by ionic chromatography (IC), BOD_5/COD ratio and respirometric tests. The results show the potential application of this approach as a promising cost-effective solution for the treatment of NAs-bearing aqueous wastes.

Key words: Naphthenic acids; Persulfate; Fenton; Oxidation; Mineralization; Kinetics.

1. Introduction

The negative environmental impacts of naphthenic acids (NAs) raise increasing attention(Kannel and Gan 2012, Niasar et al. 2016, Shah et al. 2016, Sun et al. 2014). NAs have been reported as persistent pollutants present in marine oil spills(Wan et al. 2014) and oil sands processes-affected wastewaters (OSPWs) with high toxicity toward a wide variety of organisms, including microorganisms, plants and animals(Clemente and Fedorak 2005, Tollefsen et al. 2012, Zhang et al. 2011). NAs are carboxylic acids including in their structure aromatic and naphthenic rings together with aliphatic chains in lower proportion. They can be represented by a common chemical formula of $C_nH_{2n+Z}O_2$(Drzewicz et al. 2012), but also include some diacids, keto- and heteroatomic groups(Purcell et al. 2007). In addition, positional and stereo isomerism of alicyclic NAs result in numerous cis-/trans isomers, and the branching of acyclic NAs can even further increase their complexity(Quinlan and Tam 2015). Surrogate model NAs, such as cyclohexanoic acid (CHA), are used to investigate their environmental related features(Xu et al. 2016, Zhang et al. 2016a).

Different techniques addressed to the removal of NAs from aqueous wastes have been investigated. Those include adsorption(Iranmanesh et al. 2014), biodegradation(Gunawan et al. 2014) and advanced oxidation processes (AOPs)(Drzewicz et al. 2010, Drzewicz et al. 2012, Liang et al. 2011). Adsorption, being a non-destructive operation, give rise to secondary wastes while conventional biological treatments are limited by the toxicity and recalcitrant character of NAs(Kannel and Gan 2012). AOPs have proved their ability for the mineralization of a wide diversity of target organics. H_2O_2 and persulfate (PS) are known precursors of hydroxyl ($HO^{\bullet}$) and sulfate ($SO_4^{\bullet-}$) radicals, under the action of different catalytic agents, like activated carbon(Xu et al. 2012), metals(Rodriguez et al. 2014, Zazo et al. 2006) and their oxides(Do et al. 2013), or by some energy source, including thermal(Ji et al. 2016), light (UV(Khan et al. 2014, Umar et al. 2014)/solar(Pliego et al. 2014a)/LED(Umar et al. 2015)) and electricity(Yuan et al. 2014). NAs have been degraded by ozonation(Garcia-Garcia et al. 2011), thermally-activated PS(Xu et al. 2016), zero valent iron (ZVI)-activated PS(Drzewicz et al. 2012), UV/PS, UV/H_2O_2, chelate-Fenton(Zhang et al. 2016b), UV(solar)/TiO_2(Leshuk et al. 2015, Liang et al. 2011) and UV/Chlorine(Shu et al. 2014). $HO^{\bullet}$ radicals preferentially attack the α position of the aliphatic chains and the para-position of the naphthenic ring of CHA(Drzewicz et al. 2010), while $SO_4^{\bullet-}$ radicals are believed to firstly cause the decarboxylation of CHA(Drzewicz et al. 2012, Madhavan et al. 1978).

Our previous work demonstrated that thermally-activated PS oxidation can efficiently cause the mineralization of NAs with dissolved oxygen participating as oxidizing speciess(Xu et al. 2016). The reaction between NAs and sulfate radicals generated from thermal activation of PS give rise to the corresponding organic radicals which can react with oxygen yielding reactive $O_2^{\bullet-}$/$HO_2^{\bullet}$(Fang et al. 2013, Liu et al. 2016, Xu et al. 2016). However, the draw backs of PS-based approach impede its potential application, including the introduction of copious sulfur element and, particularly, the high reagent cost.

Fenton oxidation is one of the main AOP systems and has been recognized as a cost-effective solution for a number of industrial wastewaters compared to the PS-based ones(Bautista et al. 2008, Pignatello et al. 2006). It uses H_2O_2 as starting reagent and Fe^{2+} as catalyst, which promotes the generation of strongly oxidizing hydroxyl radicals. Fenton process can also be intensified by increasing the temperature (i.e. high temperature Fenton, HTF)(Pliego et al. 2014b, Zazo et al. 2010). However, this approach has been rarely attempted for NAs breakdown, due partially to the basic pH of the OSPWs containing NAs(Drzewicz et al. 2012, Liang et al. 2011) and also to the complexation of Fe by NAs which hinders the activity of Fe ion in the solution(Laredo et al. 2004). In fact, several efforts have been made to adapt the Fenton-based technology to a wider range of pH(Barona et al. 2015). Recently, Zhang et al.(Zhang et al. 2016a, Zhang et al. 2016b, Zhang et al. 2016c) used chelate-Fenton systems to treat CHA at basic condition. However, the scavenging effect of the chelate agents toward $HO^{\bullet}$ radicals represents a main drawback regarding H_2O_2 consumption and on the other hand it has to be considered the possible increase of toxicity derived from them and/or their degradation byproducts.

The reactions involved in PS oxidation yield important amounts of protons(Drzewicz et al. 2012, Xu et al. 2012), thus giving rise to strong decrease of pH. The as-generated OSPWs are commonly characterized by a moderately basic pH (≈ 8) and a temperature well above the ambient (≈ 80 ^{o}C) used in the oil sand extraction process(Hong et al. 2013, Kannel and Gan 2012). Therefore, a treatment based on thermally-activated PS oxidation followed Fenton to deal with NAs from OSPWs could achieve several objectives. The first step allows a significant mineralization of NAs(Xu et al. 2016) while reducing the pH to the optimum range for the Fenton process. The effluent from this step would also reduce the Fe-NA complexation, improving the following Fenton oxidation step. A convenient combination of those two AOPs could provide a high mineralization of NAs giving rise to a final effluent of lower toxicity and easily biodegradable at much lower expense by replacing PS with more cost-effective Fenton reagents without the need of acidifying agents.

The aim of this study is to assess the efficiency of this approach for the abatement of model NAs, namely cyclohexanoic acid (CHA), cyclohexanebutyric acid (CHBA), 2-naphthoic acid (2-NA) and 1,2,3,4-tetrahydro-2-naphthoic acid (1234-T-2-NA), which include naphthenic ring and aromatic structures(Xu et al. 2016). To that end, CHA was used as model compound to analyze the effect of the operating variables as well as the kinetics of TOC removal. Then, the effluents from the oxidation of all the four NAs tested were studied to address the improvement of biodegradability by the current approach.

2. Materials and methods

2.1 Experimental procedure

The two-step PS and Fenton oxidation experiments were carried out in batch, in

100 mL stoppered glass flasks placed in a constant-temperature water bath with a shacking frequency equivalent to 200 rpm. In each run, 50 mL of NAs (CHA, CHBA, 2-NA and 1234-T-2-NA, purity over 98%, purchased from Sigma-Aldrich) were preheated for over 15 min at different temperatures (60−97 ºC ± 1) after adjusting the pH to 8. Then, sodium persulfate (1−20% of the stoichiometric amount) was added to start the PS oxidation stage. After certain reaction time (0.5−2 h), H_2O_2 (10−80% of the stoichiometric) and Fe^{2+} (0.5−20 mg L^{-1}, using $FeSO_4•7H_2O$) were added simultaneously for reaction of another 4 h. The effluents were collected and analyzed immediately. The results shown are the average of duplicates with the corresponding error bars presented. The degradation of the starting NAs during the preheating stage was checked and was always negligible. The stoichiometric doses mentioned in the current work always refer to the original NAs and are calculated according to previous work(Xu et al. 2016). In the case of CHA at 50 mg L^{-1}, the stoichiometric amounts are 1673.4 and 239 mg L^{-1} for sodium persulfate and hydrogen peroxide, respectively. The experiments were carried out without aeration since the amount of oxygen in the upper part of the reactor (where air is enclosed) is in excess respect to the needed according to the reactions for PS-oxidation in pressure of O_2 (see supporting information).

Chemical oxygen demand (COD) was determined by oxidation with potassium dichromate following the Standard Method (ISO 6060) using UV-vis spectrometer (Shimadzu, mod. UV-1603). BOD_5 tests were conducted in a Velps Scientifica apparatus using the standard procedure available from previous work(Sanchis et al. 2013). 400 mL samples of the initial or treated NAs were mixed with activated sludge at 75 mg VSS L^{-1} and pH = 7.2 in the presence of phosphate buffer. $CaCl_2$, KCl and $MgSO_4$ were added as micronutrients and 1.25 mg L^{-1} N-allylthiourea was used as nitrification inhibitor. The biodegradability index was calculated as the BOD_5/COD ratio(Xu et al. 2012). The data of BOD_5 and COD were averages of triplicates with error bars.

A well-developed respirometric test was carried out for the assessment of the biodegradability before and after AOP reactions. A LSS respirometer was used with intermittent aeration during 72 h using(Polo et al. 2011, Sanchis et al. 2014). Two limited values of oxygen concentration were set lower than water-solubility at the given conditions. Each specific oxygen uptake rate (SOUR) data was recorded once the amount of dissolved oxygen dropped to the bottom limit due to the microbial respiration. The aeration started at the mean time, and then stopped until the oxygen concentration reached the upper limit. A biomass concentration of 350 mg VSS L^{-1} was used according to the preliminary tests. The reactors were placed in a thermostatic water bath at 25 ºC with magnetic stirring at 500 rpm.

2.2 Analytical methods

The concentrations of CHA and CHBA were measured by Gas Chromatography with Flame Ionization Detector (GC-FID) in a GC 3900 Varian provided with a 30 m length × 0.25 mm i.d. capillary column (CP-Wax 52 CB, Varian) using nitrogen as carrier gas. For CHA, the initial oven temperature was set at 70 ºC and then increased up to 240 ºC at a rate of 30 ºC min^{-1}. For CHBA, the only difference was lowering the

heating rate to 20 ºC min^{-1}. The concentration of the cyclohexanone as an intermediate of PS oxidation of CHA was also determined by GC-FID according the method for CHA analysis. 2-NA and 1234-T-2-NA were determined by high-performance liquid chromatography (HPLC; Varian Pro-Start 240) with a UV detector and Microsorb C18 5 μm column (250 × 4.6 mm) as stationary phase. Acetonitrile and 4 mM H_2SO_4 (1/1) were used as mobile phase at an injection rate of 1 mL min^{-1} with the oven temperature set at 60 ºC.

Total organic carbon (TOC) was measured by a TOC analyzer (Shimadzu, mod. TOC VSCH) and PS concentration by a spectrophotometric determination method based on modification of the iodometric titration analysis(Liang et al. 2008). The concentration of hydrogen peroxide was analyzed by colorimetric titration using the $TiOSO_4$ method(Eisenberg 1943). Iron ions were determined by the o-phenantroline method(Sandell 1959).

Short-chain carboxyl acids by ionic chromatography with chemical suppression (Metrohm 790 IC) using a conductivity detector. A Metrosep A supp 5−250 column (25 cm length, 4 mm i.d.) was used as stationary phase and an aqueous solution of 3.2 mM Na_2CO_3 and 1 mM of $NaHCO_3$ at pumping rate of 0.7 mL min^{-1} as mobile phase.

3. Results and discussion

CHA mineralization by conventional Fenton oxidation was firstly checked at initial pH = 3 and 80 ºC with 40 and 100% of the stoichiometric amount of H_2O_2 and 5 mg L^{-1} Fe^{2+}. The results are shown in Fig. 1 together with those obtained upon PS only and PS/H_2O_2 simultaneous oxidation at the same temperature and initial pH = 8, using 20 % of the stoichiometric amount.

Fairly poor mineralization (≈ 18%) was achieved by only Fenton oxidation even using H_2O_2 at 239 mg L^{-1} (i.e. 100% of the stoichiometric). Slow decomposition of H_2O_2 was observed (≈ 25%, after 6 h of reaction) associated to a continuous reduction of the measured Fe concentration down to less than 1 mg L^{-1} whereas the pH was still at the optimum value for the Fenton process (≈ 3). That might be due to the complexation of Fe by CHA(Laredo et al. 2004). On the other hand, PS oxidation yielded 40% mineralization at 20% of the stoichiometric amount. Simultaneous PS/Fenton oxidation with PS and H_2O_2 at 20 and 40% of the stoichiometric, respectively, led to only slightly higher mineralization than the sole PS at the same dose (20%), in spite that certain synergetic effect has been reported by other authors in PS/H_2O_2 oxidation(Hilles et al. 2016, Liang et al. 2014).

3.1 Two-step PS and Fenton oxidation

Based on the important pH reduction caused by PS oxidation, a combination of PS and subsequent Fenton oxidation was investigated. The amount of PS as well as the reaction time in the PS oxidation step will affect to the pH and composition of the resulting effluent which enters the following Fenton oxidation step. Different experiments were performed using 1, 5, 10 and 20% of the stoichiometric PS with CHA at 50 mg L^{-1} and 2 h reaction time, followed by Fenton oxidation with 95.6 mg L^{-1} of

H_2O_2 (40% of the stoichiometric) and 5 mg L^{-1} Fe^{2+}.

The results are shown in Fig. 2, where it can be seen the important effect of increasing the PS dose within the range tested. Below 10% of the stoichiometric, the subsequent Fenton step has no significant effect. Beyond that PS dose, further Fenton oxidation becomes increasingly efficient while effective H_2O_2 decomposition was observed and the measured Fe concentration remained stable in the vicinity of 5 mg L^{-1}. This can be explained by the pre-degradation extent of CHA so that iron naphthenates are not formed, but also by the fact that the pH of the effluent from the PS step approaches to the optimum for Fenton oxidation (≈ 3) as the PS dose is increased. In fact, PS oxidation alone at higher dose of around 35% of the stoichiometric allows achieving 80% mineralization of CHA(Xu et al. 2016). Now, the combination with a subsequent Fenton treatment provides a way of reducing the PS needs by 43% using much cheaper Fenton reagents while still maintaining close to that mineralization extent. The remaining TOC in the current system corresponds to short-chain organic acids of very low significance in terms of toxicity. It is true that the reduction of the PS amount is accompanied by a complementary addition of H_2O_2 to accomplish further Fenton oxidation, so the amount of H_2O_2 must be conveniently adjusted to minimize total reagent consumption.

Fig. 3 shows the results obtained with different H_2O_2 doses expressed as percent of the theoretical stoichiometric amount relative to initial CHA. The PS amount in the previous step was always 20% of the stoichiometric. As can be seen, the extent of mineralization in the Fenton step increased significantly with the H_2O_2 dose up to around 30% of the stoichiometric and then the remaining TOC (corresponding mostly to short-chain organic acids) seems refractory to Fenton oxidation. Increasing the Fe^{2+} dose above 5 mg L^{-1} neither showed any significant effect on the Fenton step.

The duration of the PS step was also varied since it can affect the extent of CHA breakdown in that stage and consequently to the evolution of TOC upon further Fenton oxidation. Fig. 4 shows the results obtained upon different time durations for the PS reaction. As can be seen, the overall TOC removal of the combined system decreased significantly when the PS oxidation step lasted less than 1.5-2 h.

Finally, the effect of initial pH was studied within the range of 3 to 12, using 20% of the stoichiometric amount of PS in the first step, and 40% of the stoichiometric H_2O_2 with 5 mg L^{-1} Fe^{2+} in the sequent Fenton. As can be observed in Fig. 5, the initial pH had no significant effect on CHA mineralization, given the fact that the pH evolved always to around 3 in the PS oxidation step. Therefore, this two-step PS and Fenton system does not need any artificial correction of the initial pH of the wastewater to be treated.

Summarizing, the combined PS and Fenton system shows significant advantage compared to the only thermally-activated PS and to Fenton oxidation. It mineralizes close to 80% of CHA (50 mg L^{-1}) working at 80 ºC (thermally-activated PS) with PS and H_2O_2 at 20 and 30% of the stoichiometric amount, respectively. That represents ≈ 335 mg L^{-1} of sodium PS and 75 mg L^{-1} of H_2O_2 (plus 5 mg L^{-1} Fe^{2+}) in terms of reagents consumption. Fenton alone is far from achieving that objective even at high H_2O_2 doses

(100% of the stoichiometric) whereas PS oxidation by itself would require around 35% of the stoichiometric amount, i.e. ≈ 586 mg L^{-1} of sodium PS. Therefore, about 251 mg L^{-1} sodium PS are substituted by ≈ 75 mg L^{-1} of H_2O_2 in the combined treatment. At average industrial prices of around 1100 \$ t^{-1} for the former, and 250 \$ t^{-1} for H_2O_2 (35% solution) and 46 \$ t^{-1} for $FeSO_4 \cdot 7H_2O$, the combined treatment system means a much lower cost in terms of reagent consumption (reduced by ≈ 80% for the Fenton oxidation step and 35% for the overall cost) and also has the additional advantage of significantly lower sulfate and sodium concentration in the final effluent. In addition, the required thermal energy for PS activation can be conveniently achieved by making use of the elevated processing temperature of OSPWs (≈ 80 ºC)(Hong et al. 2013), which further emphasizes the potential application of this combined system.

3.2 Kinetic analysis

The rates of PS and H_2O_2 decomposition in the two steps, respectively, can be expressed by first-order kinetics:

$$-\frac{dC_{PS}}{dt} = k_{PS}C_{PS} \quad (E1)$$

$$-\frac{dC_{H_2O_2}}{dt} = k_{H_2O_2}C_{H_2O_2} \quad (E2)$$

where C_{PS} and $C_{H_2O_2}$ represent the concentrations of PS and H_2O_2, respectively and k_{PS} and $k_{H_2O_2}$ the corresponding rate constants.

Oxygen can be considered in excess with respect to the reactants at the working conditions, so that its effect can be seen as invariable during the PS stage. For TOC removal, the following equation is proposed:

$$-\frac{dC_{TOC}}{dt} = k_1 C_{TOC} C_{PS} + k_2 C_{TOC}^2 C_{H_2O_2} \quad (E3)$$

where C_{TOC} is the concentrations of TOC, and k_1 and k_2 are the apparent rate constants of mineralization of the species tested in the PS and Fenton oxidation steps, respectively. Mineralization of NAs with PS has been well described by a first-order rate equation respect to TOC in a previous work(Xu et al. 2016) whereas second-order dependence has been used in the literature for phenol mineralization upon Fenton oxidation(Bautista et al. 2008). Scientist 3.0 software was used to fit the experimental data to equation (E3).

The results are shown in Fig. 6, where fairly good fitting can be observed. The values of the corresponding apparent rate constants are listed in Table 1 together with the correlation coefficients. A difference of two orders of magnitude among the rate constants at 60 and 97 ºC can be observed, suggesting that the system is quite temperature-dependent. The Arrhenius plots are depicted in Fig. 7. A value of 115 kJ mol^{-1} (r^2 = 0.998) was obtained for the apparent activation energy of the PS oxidation step and 87 kJ mol^{-1} for the Fenton one (in this case, the value of the rate constant at 60 ºC was not considered since desirable pH for Fenton was not achieved working at that temperature).

3.3 Degradation of other NAs

Other individual NAs, namely CHBA, 2-NA and 1234-T-2-NA, as well as a mixture of them (including CHA), were tested. These NAs include saturated-ring as well as aromatic structures. The amounts of PS and H_2O_2 used for the treatment of the NAs mixture were calculated according to the proportionof each NA (equally in volumn). As can be seen from Fig. 8, the mineralization efficiency was significantly improved after the addition of Fenton reagent in all cases. The corresponding rate constants are collected in Table 2. Regarding the NAs mixture, it is remarkable that the extent of mineralization was close to the observed for the most reactive ones, suggesting some kind of synergistic effect which requires further research given its importance to cope with the complexity of real OSPWs.

3.4 Evolution of the NAs and oxidation byproducts upon two-step PS and Fenton oxidation

Fig. 9 provides the time-course of NAs upon oxidation by thermally-activated PS with 20% of the stoichiometric amount. As can be observed, that PS dose was enough to achieve complete conversion of the four model NAs tested. Moreover, the results show that the aromatic ring-bearing NAs, namely 2-NA and 1234-T-2-NA, are more resistant to oxidation than the saturated ring-bearing ones (CHA and CHBA). Several oxidation by-products were detected, mainly short-chain organic acids from the ring-opening. In all cases, fumaric acid appears as the primary product from the ring-opening and evolves to formic, acetic and oxalic acid, the two latest being refractory to Fenton oxidation under the operating conditions of the experiments.

Fig. 10 shows the carbon balance throughout the two-step treatment. As can be observed, a large proportion of unidentified organic matter (measured as TOC) was found in the earlier oxidation stages (PS step) in all cases, decreasing gradually as oxidation proceeds upon the Fenton step. Apparently, the nature of those species is related to the starting NA, which also affects to the final breakdown. In the case of the two saturated ring-bearing NAs tested, those compounds appear quite easily oxidized by Fenton, achieving final mineralization percentages up to 80 and 91% for CHA and CHBA after the 6 h of the experiments, where the final identified carbon mass was 85 and 97%, respectively. On the opposite, in the case of the aromatic ring-bearing NAs, the oligomeric byproducts are more refractory, giving rise to significantly lower mineralization (48 and 51% for 2-NA and 1234-T-2-NA, respectively). Thus, only 51 and 63% of carbon could be identified after oxidation. Therefore, it is important to assess the biodegradability of the remaining matter in order to learn on its potential behavior in a further biological treatment.

3.5 Biodegradability

Fig. 11 shows the evolution of the BOD_5 and COD values as well as the BOD_5/COD ratio upon the oxidative treatments of the NAs. The amount of PS used was 20% of the stoichiometric and the reaction conditions in the two-step PS/Fenton oxidation were similar to those of the experiments of Fig. 10. It can be seen that COD values decreased upon the treatment due to oxidation. Looking at the BOD_5/COD ratio, the starting NAs tested yield quite different values, being particularly low in the case

of the aromatic ring-bearing ones (2-NA and 1234-T-2-NA). PS oxidation at 20% of the stoichiometric amount led to a significantly better biodegradability, which was then improved upon the application of the further Fenton treatment.

The respirometric profiles serve to learn on the behavior of the oxidation effluents upon further biological treatment(Polo et al. 2011, Sanchis et al. 2014). Since fairly low TOC remains after the two-step oxidation approach using the aforementioned doses of reactants (PS at 20% of the stoichiometric amount, H_2O_2 at 40 % of the stoichiometric and Fe^{2+} at 5.0 mg L^{-1}), now only 20% of the stoichiometric amount of H_2O_2 was used in the Fenton stage. The results of the respirometric tests with the starting NAs (100 mg L^{-1}) and the effluents from PS oxidation alone and PS+Fenton are depicted in Fig. 12 (for the saturated-ring bearing ones) and Fig. 13 (for the aromatic ones).

Relatively slow sludge respiration of the raw CHA was observed throughout the respirometric test especially within the starting stages (inserted graph in Fig. 12) with less than 15% of TOC consumed at the end of 72 h, confirming its bio-recalcitrant character, in agreement with the literature(Kannel and Gan 2012) and consistently with the previous value of the BOD_5/COD ratio. Regarding the effluent from thermally-activated PS oxidation of CHA, the respirometric test showed obvious activity at the beginning with a sharp decline of SOUR within the first 2 hours (corresponding insert graph in Fig. 12), indicating a fast consumption of some readily biodegradable intermediates. The microbial activity was then maintained at slow SOUR and after around 25 h an increased microbial activity was observed, which dramatically decreased at ≈ 65 h, suggesting the recalcitrant character of the degradation byproducts at that point of the respirometric test. With the effluents from the oxidative treatments much higher microbial activity can be seen within the initial period of the respirometric tests, but then fairly low values of SOUR were measured given the strong reduction of TOC.

With regard to CHBA, some higher respirometric intensity was registered within the starting period with the effluents from both the thermally-activated PS and the two-step PS and Fenton treatments. However, with the former, no more data could be recorded after a sharp increase of SOUR at around 10 h, suggesting some toxic incidence on the microorganisms since about 60% of the initial TOC was still remaining so that a lack of available carbon source cannot be postulated.

In the case of the aromatic-ring-bearing NAs (2-NA and 1234-T-2-NA), the effluents from the two-step oxidation always showed the best biodegradability within the starting hours, compared with the thermally-activated PS-treated and the original NAs (Fig. 13). The two-step oxidation effluents from those species show almost complete decline, most probably due to the almost complete degradation of the TOC remaining after the oxidative treatment. This is consistent with the high value of the BOD_5/COD ratio (≈ 1) of that effluent.

4 Conclusions

Two-step PS and Fenton oxidation provides a promising cost-effective approach

for the degradation of NAs. About 80% TOC reduction was achieved from CHA (50 mg L^{-1}) with 20 and 30% of the stoichiometric amount of PS and H_2O_2, respectively. This system is much more effective than Fenton oxidation alone and allows reducing the reagent cost with respect to single PS-oxidation while introducing less sulfate in the final effluent. Other individual NAs and their mixture were also tested and high mineralization efficiencies were achieved as well. A simple and practical kinetic model has been proposed, which describes fairly well the time-course of TOC. Values of the rate constants are provided. For CHA mineralization, 115 and 87 kJ mol^{-1} were obtained as representative values of the apparent activation energy for the PS and Fenton oxidation steps, respectively. The remaining TOC corresponded mainly to short-chain organic acids easily biodegradable as demonstrated by IC, BOD_5/COD ratio and respirometric tests.

Acknowledgement

Spanish MINECO is gratefully acknowledged for the financial support through the project CTQ2013-41963-R. We are also grateful to the Chinese Scholarship Council (CSC) for supporting the Ph.D. program of Xiyan Xu (CSC, File No. 201308410047).

References

Barona, J.F., Morales, D.F., González-Bahamón, L.F., Pulgarín, C. and Benítez, L.N. (2015) Shift from heterogeneous to homogeneous catalysis during resorcinol degradation using the solar photo-Fenton process initiated at circumneutral pH. Applied Catalysis B: Environmental 165, 620-627.

Bautista, P., Mohedano, A., Casas, J., Zazo, J. and Rodriguez, J. (2008) An overview of the application of Fenton oxidation to industrial wastewaters treatment. Journal of Chemical Technology and Biotechnology 83(10), 1323-1338.

Clemente, J.S. and Fedorak, P.M. (2005) A review of the occurrence, analyses, toxicity, and biodegradation of naphthenic acids. Chemosphere 60(5), 585-600.

Do, S.-H., Kwon, Y.-J., Bang, S.-J. and Kong, S.-H. (2013) Persulfate reactivity enhanced by Fe 2 O 3–MnO and CaO–Fe 2 O 3–MnO composite: Identification of composite and degradation of CCl 4 at various levels of pH. Chemical Engineering Journal 221, 72-80.

Drzewicz, P., Afzal, A., El-Din, M.G. and Martin, J.W. (2010) Degradation of a model naphthenic acid, cyclohexanoic acid, by vacuum UV (172 nm) and UV (254 nm)/H2O2. The Journal of Physical Chemistry A 114(45), 12067-12074.

Drzewicz, P., Perez-Estrada, L., Alpatova, A., Martin, J.W. and El-Din, M.G. (2012) Impact of Peroxydisulfate in the Presence of Zero Valent Iron on the Oxidation of Cyclohexanoic Acid and Naphthenic Acids from Oil Sands Process-Affected Water. Environ Sci Technol 46(16), 8984-8991.

Eisenberg, G. (1943) Colorimetric determination of hydrogen peroxide. Industrial & Engineering Chemistry Analytical Edition 15(5), 327-328.

Fang, G., Gao, J., Dionysiou, D.D., Liu, C. and Zhou, D. (2013) Activation of persulfate by quinones: Free radical reactions and implication for the degradation of PCBs. Environ Sci Technol 47(9), 4605-4611.

Garcia-Garcia, E., Ge, J.Q., Oladiran, A., Montgomery, B., El-Din, M.G., Perez-Estrada, L.C., Stafford,

J.L., Martin, J.W. and Belosevic, M. (2011) Ozone treatment ameliorates oil sands process water toxicity to the mammalian immune system. Water Res 45(18), 5849-5857.

Gunawan, Y., Nemati, M. and Dalai, A. (2014) Biodegradation of a surrogate naphthenic acid under denitrifying conditions. Water Res 51, 11-24.

Hilles, A.H., Amr, S.S.A., Hussein, R.A., El-Sebaie, O.D. and Arafa, A.I. (2016) Performance of combined sodium persulfate/H 2 O 2 based advanced oxidation process in stabilized landfill leachate treatment. Journal of Environmental Management 166, 493-498.

Hong, P.A., Cha, Z., Zhao, X., Cheng, C.-J. and Duyvesteyn, W. (2013) Extraction of bitumen from oil sands with hot water and pressure cycles. Fuel Processing Technology 106, 460-467.

Iranmanesh, S., Harding, T., Abedi, J., Seyedeyn-Azad, F. and Layzell, D.B. (2014) Adsorption of naphthenic acids on high surface area activated carbons. Journal of Environmental Science and Health, Part A 49(8), 913-922.

Ji, Y., Shi, Y., Dong, W., Wen, X., Jiang, M. and Lu, J. (2016) Thermo-activated persulfate oxidation system for tetracycline antibiotics degradation in aqueous solution. Chemical Engineering Journal 298, 225-233.

Kannel, P.R. and Gan, T.Y. (2012) Naphthenic acids degradation and toxicity mitigation in tailings wastewater systems and aquatic environments: a review. J Environ Sci Health A Tox Hazard Subst Environ Eng 47(1), 1-21.

Khan, J.A., He, X., Shah, N.S., Khan, H.M., Hapeshi, E., Fatta-Kassinos, D. and Dionysiou, D.D. (2014) Kinetic and mechanism investigation on the photochemical degradation of atrazine with activated H 2 O 2, S 2 O 8 2− and HSO 5−. Chemical Engineering Journal 252, 393-403.

Laredo, G.C., López, C.R., Alvarez, R.E. and Cano, J.L. (2004) Naphthenic acids, total acid number and sulfur content profile characterization in Isthmus and Maya crude oils. Fuel 83(11), 1689-1695.

Leshuk, T., Wong, T., Linley, S., Peru, K., Headley, J. and Gu, F. (2015) Solar photocatalytic degradation of naphthenic acids in oil sands process-affected water. Chemosphere 144, 1854-1861.

Liang, C., Guo, Y.-Y. and Pan, Y.-R. (2014) A study of the applicability of various activated persulfate processes for the treatment of 2, 4-dichlorophenoxyacetic acid. International Journal of Environmental Science and Technology 11(2), 483-492.

Liang, C., Huang, C.-F., Mohanty, N. and Kurakalva, R.M. (2008) A rapid spectrophotometric determination of persulfate anion in ISCO. Chemosphere 73(9), 1540-1543.

Liang, X., Zhu, X. and Butler, E.C. (2011) Comparison of four advanced oxidation processes for the removal of naphthenic acids from model oil sands process water. J Hazard Mater 190(1-3), 168-176.

Liu, H., Bruton, T.A., Li, W., Buren, J.V., Prasse, C., Doyle, F.M. and Sedlak, D.L. (2016) Oxidation of benzene by persulfate in the presence of Fe (III)-and Mn (IV)-containing oxides: stoichiometric efficiency and transformation products. Environ Sci Technol 50(2), 890-898.

Madhavan, V., Levanon, H. and Neta, P. (1978) Decarboxylation by SO4-radicals. Radiation Research 76(1), 15-22.

Niasar, H.S., Li, H., Kasanneni, T.V.R., Ray, M.B. and Xu, C.C. (2016) Surface amination of activated carbon and petroleum coke for the removal of naphthenic acids and treatment of oil sands process-affected water (OSPW). Chemical Engineering Journal 293, 189-199.

Pignatello, J.J., Oliveros, E. and MacKay, A. (2006) Advanced oxidation processes for organic contaminant destruction based on the Fenton reaction and related chemistry. Critical reviews in environmental science and technology 36(1), 1-84.

Pliego, G., Xekoukoulotakis, N., Venieri, D., Zazo, J.A., Casas, J.A., Rodriguez, J.J. and Mantzavinos,

D. (2014a) Complete degradation of the persistent anti‐depressant sertraline in aqueous solution by solar photo‐Fenton oxidation. Journal of Chemical Technology and Biotechnology 89(6), 814-818.

Pliego, G., Zazo, J.A., Casas, J.A. and Rodriguez, J.J. (2014b) Fate of iron oxalates in aqueous solution: The role of temperature, iron species and dissolved oxygen. Journal of Environmental Chemical Engineering 2(4), 2236-2241.

Polo, A., Tobajas, M., Sanchis, S., Mohedano, A. and Rodriguez, J. (2011) Comparison of experimental methods for determination of toxicity and biodegradability of xenobiotic compounds. Biodegradation 22(4), 751-761.

Purcell, J.M., Juyal, P., Kim, D.-G., Rodgers, R.P., Hendrickson, C.L. and Marshall, A.G. (2007) Sulfur speciation in petroleum: Atmospheric pressure photoionization or chemical derivatization and electrospray ionization Fourier transform ion cyclotron resonance mass spectrometry. Energy & Fuels 21(5), 2869-2874.

Quinlan, P.J. and Tam, K.C. (2015) Water treatment technologies for the remediation of naphthenic acids in oil sands process-affected water. Chemical Engineering Journal 279, 696-714.

Rodriguez, S., Vasquez, L., Costa, D., Romero, A. and Santos, A. (2014) Oxidation of Orange G by persulfate activated by Fe(II), Fe(III) and zero valent iron (ZVI). Chemosphere 101, 86-92.

Sanchis, S., Polo, A., Tobajas, M., Rodriguez, J. and Mohedano, A. (2014) Coupling Fenton and biological oxidation for the removal of nitrochlorinated herbicides from water. Water Res 49, 197-206.

Sanchis, S., Polo, A.M., Tobajas, M., Rodriguez, J.J. and Mohedano, A.F. (2013) Degradation of chlorophenoxy herbicides by coupled Fenton and biological oxidation. Chemosphere 93(1), 115-122.

Sandell, E.B. (1959) Colorimetric determination of traces of metals. Interscience Pubs. New York.

Shah, S.N., Chellappan, L.K., Gonfa, G., Mutalib, M.I.A., Pilus, R.B.M. and Bustam, M.A. (2016) Extraction of naphthenic acid from highly acidic oil using phenolate based ionic liquids. Chemical Engineering Journal 284, 487-493.

Shu, Z., Li, C., Belosevic, M., Bolton, J.R. and El-Din, M.G. (2014) Application of a Solar UV/Chlorine Advanced Oxidation Process to Oil Sands Process-Affected Water Remediation. Environ Sci Technol 48(16), 9692-9701.

Sun, N., Chelme-Ayala, P., Klamerth, N., McPhedran, K.N., Islam, M.S., Perez-Estrada, L., Drzewicz, P., Blunt, B.J., Reichert, M. and Hagen, M. (2014) Advanced Analytical Mass Spectrometric Techniques and Bioassays to Characterize Untreated and Ozonated Oil Sands Process-Affected Water. Environ Sci Technol 48(19), 11090-11099.

Tollefsen, K.E., Petersen, K. and Rowland, S.J. (2012) Toxicity of synthetic naphthenic acids and mixtures of these to fish liver cells. Environ Sci Technol 46(9), 5143-5150.

Umar, M., Roddick, F. and Fan, L. (2014) Effect of coagulation on treatment of municipal wastewater reverse osmosis concentrate by UVC/H< sub> 2</sub> O< sub> 2</sub>. J Hazard Mater 266, 10-18.

Umar, M., Roddick, F., Fan, L., Autin, O. and Jefferson, B. (2015) Treatment of municipal wastewater reverse osmosis concentrate using UVC-LED/H< sub> 2</sub> O< sub> 2</sub> with and without coagulation pre-treatment. Chemical Engineering Journal 260, 649-656.

Wan, Y., Wang, B., Khim, J.S., Hong, S., Shim, W.J. and Hu, J. (2014) Naphthenic acids in coastal sediments after the Hebei Spirit oil spill: a potential indicator for oil contamination. Environ Sci

Technol 48(7), 4153-4162.

Xu, X.-Y., Zeng, G.-M., Peng, Y.-R. and Zeng, Z. (2012) Potassium persulfate promoted catalytic wet oxidation of fulvic acid as a model organic compound in landfill leachate with activated carbon. Chemical Engineering Journal 200, 25-31.

Xu, X., Pliego, G., Zazo, J.A., Casas, J.A. and Rodriguez, J.J. (2016) Mineralization of naphtenic acids with thermally-activated persulfate: The important role of oxygen. J Hazard Mater 318, 355-362.

Yuan, S., Liao, P. and Alshawabkeh, A.N. (2014) Electrolytic manipulation of persulfate reactivity by iron electrodes for trichloroethylene degradation in groundwater. Environ Sci Technol 48(1), 656-663.

Zazo, J.A., Casas, J.A., Mohedano, A.F. and Rodríguez, J.J. (2006) Catalytic wet peroxide oxidation of phenol with a Fe/active carbon catalyst. Applied Catalysis B: Environmental 65(3-4), 261-268.

Zazo, J.A., Pliego, G., Blasco, S., Casas, J.A. and Rodriguez, J.J. (2010) Intensification of the Fenton process by increasing the temperature. Industrial & engineering chemistry research 50(2), 866-870.

Zhang, X., Wiseman, S., Yu, H., Liu, H., Giesy, J.P. and Hecker, M. (2011) Assessing the toxicity of naphthenic acids using a microbial genome wide live cell reporter array system. Environ Sci Technol 45(5), 1984-1991.

Zhang, Y., Klamerth, N., Chelme-Ayala, P. and Gamal El-Din, M. (2016a) Comparison of nitrilotriacetic acid and [S, S]-ethylenediamine-N, N'-disuccinic acid in UV-Fenton for the treatment of oil sands process-affected water at natural pH. Environ Sci Technol.

Zhang, Y., Klamerth, N. and El-Din, M.G. (2016b) Degradation of a model naphthenic acid by nitrilotriacetic acid–modified Fenton process. Chemical Engineering Journal 292, 340-347.

Zhang, Y., Klamerth, N., Messele, S.A., Chelme-Ayala, P. and El-Din, M.G. (2016c) Kinetics study on the degradation of a model naphthenic acid by ethylenediamine-N, N'-disuccinic acid-modified Fenton process. J Hazard Mater 318, 371-378.

Figures

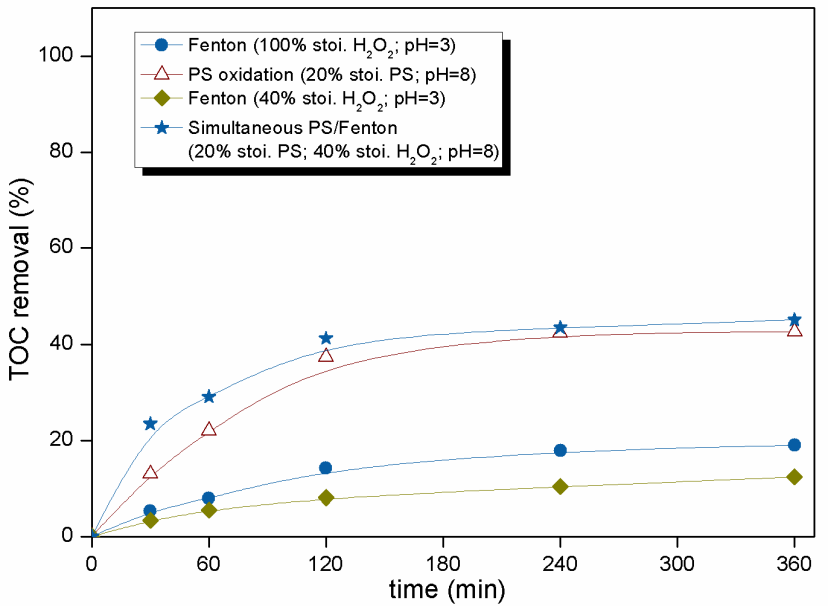

Fig. 1 CHA mineralization by various oxidation approaches (Fe^{2+} at 5 mg L^{-1} in Fenton; T = 80 ºC).

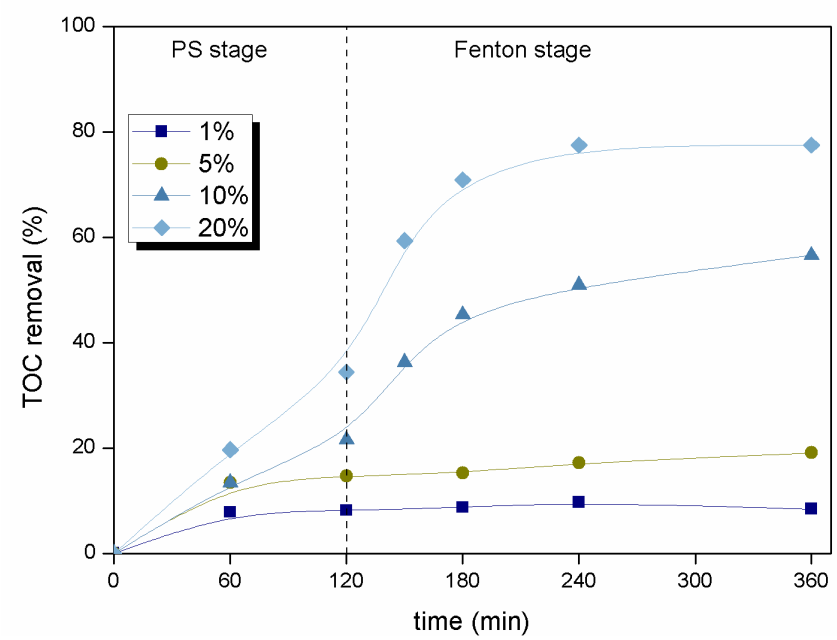

Fig. 2 Two-step PS (120 min) and Fenton oxidation of CHA (50 mg L^{-1}) at 80 ºC with different PS amounts (% of the stoichiometric). Fenton step with H_2O_2 at 40% of the stoichiometric and Fe^{2+} at 5 mg L^{-1}.

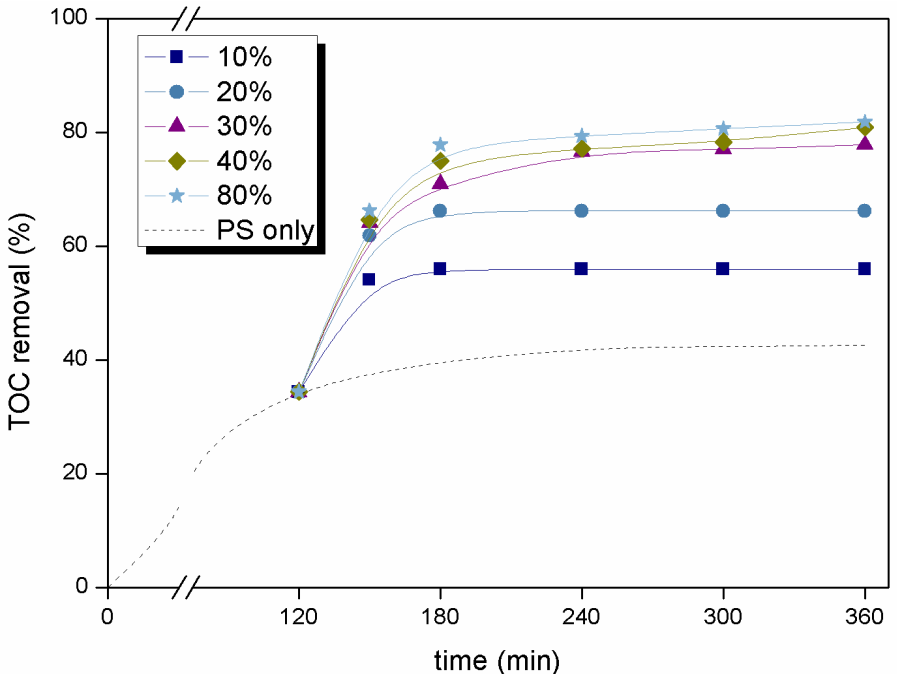

Fig. 3 Two-step PS (120 min) and Fenton oxidation of CHA (50 mg L^{-1}) at 80 ºC with different H_2O_2 amounts (% of the stoichiometric) in the Fenton step. PS at 20% of the stoichiometric and Fe^{2+} at 5 mg L^{-1}.

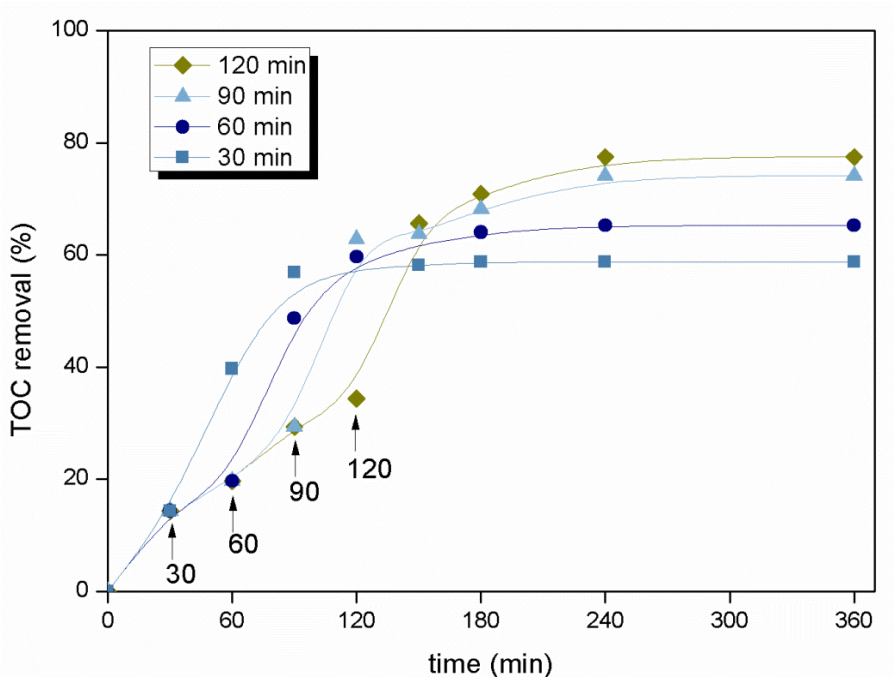

Fig. 4 Two-step PS and Fenton oxidation of CHA (50 mg L^{-1}) at 80 ºC with different times for the PS step durations. PS and H_2O_2 at 20 and 40% of the stoichiometric, respectively.

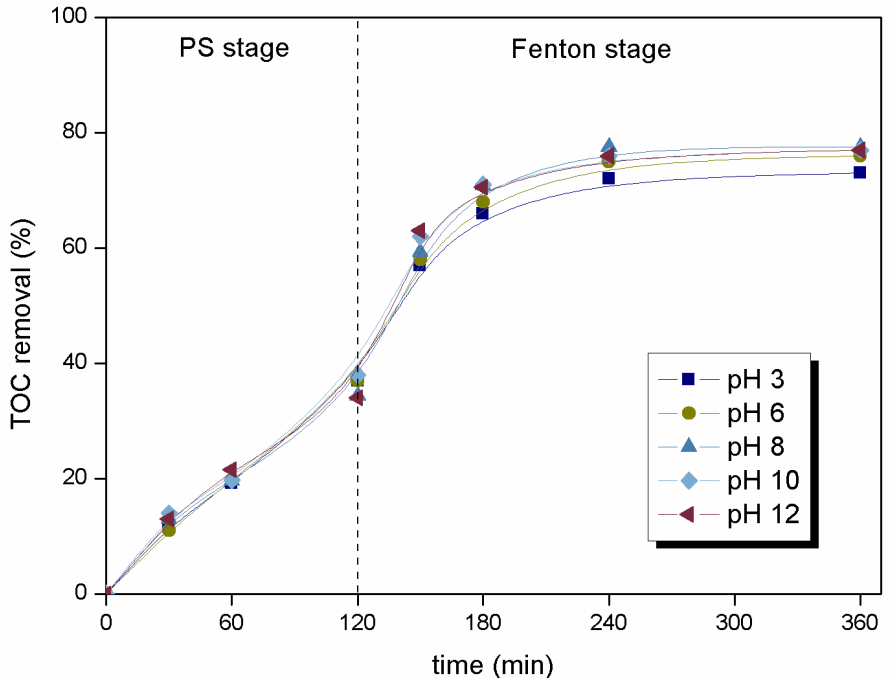

Fig. 5 The effect of initial pH.

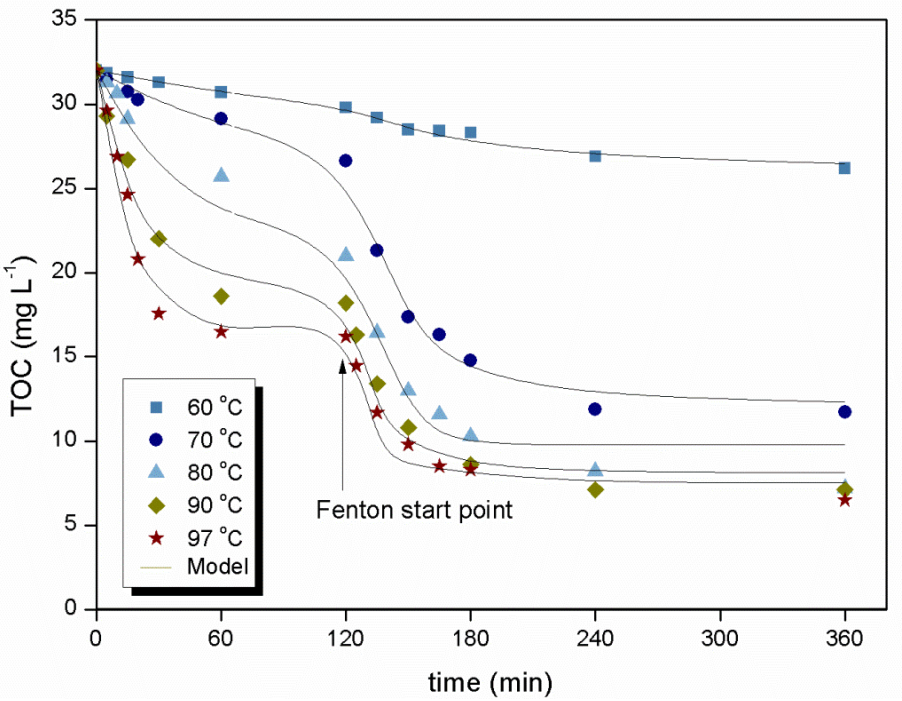

Fig. 6 Experimental (points) and predicted (lines) TOC values vs reaction time at different temperatures.

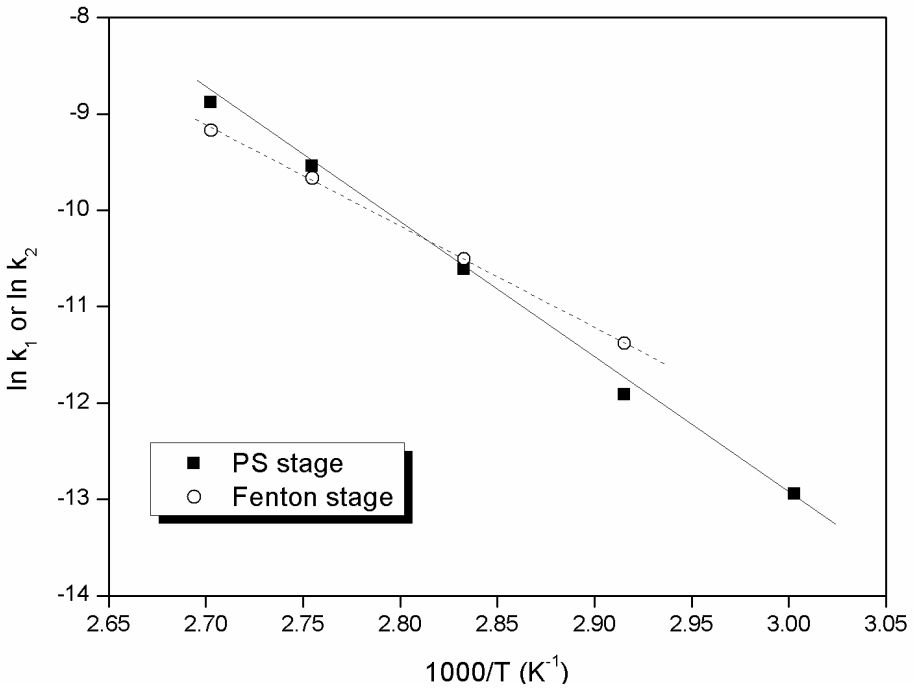

Fig. 7 Arrhenius plots for the PS and Fenton mineralization of CHA.

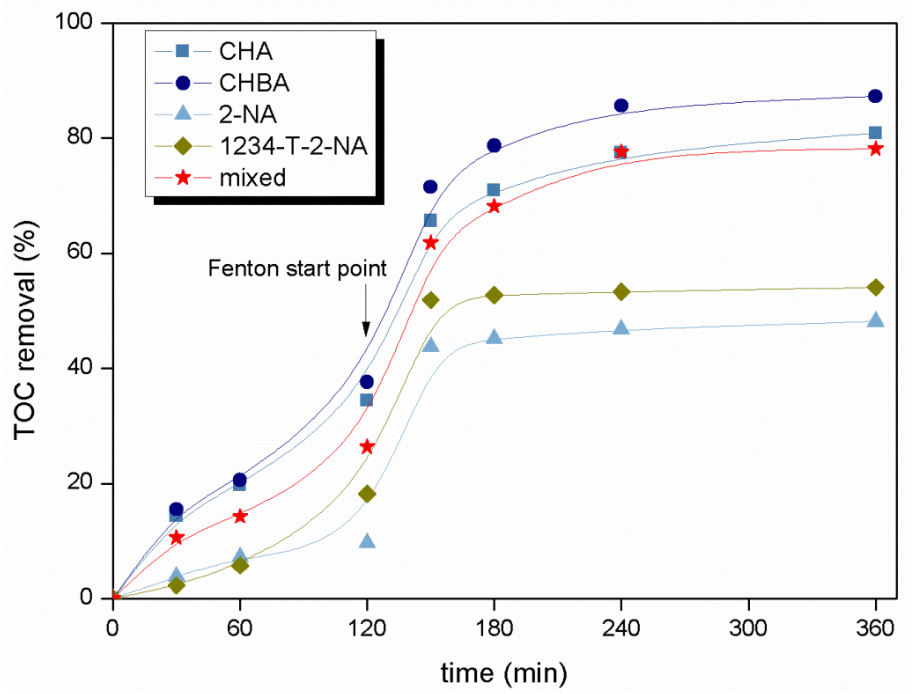

Fig. 8 Mineralization of different NAs and their mixture.

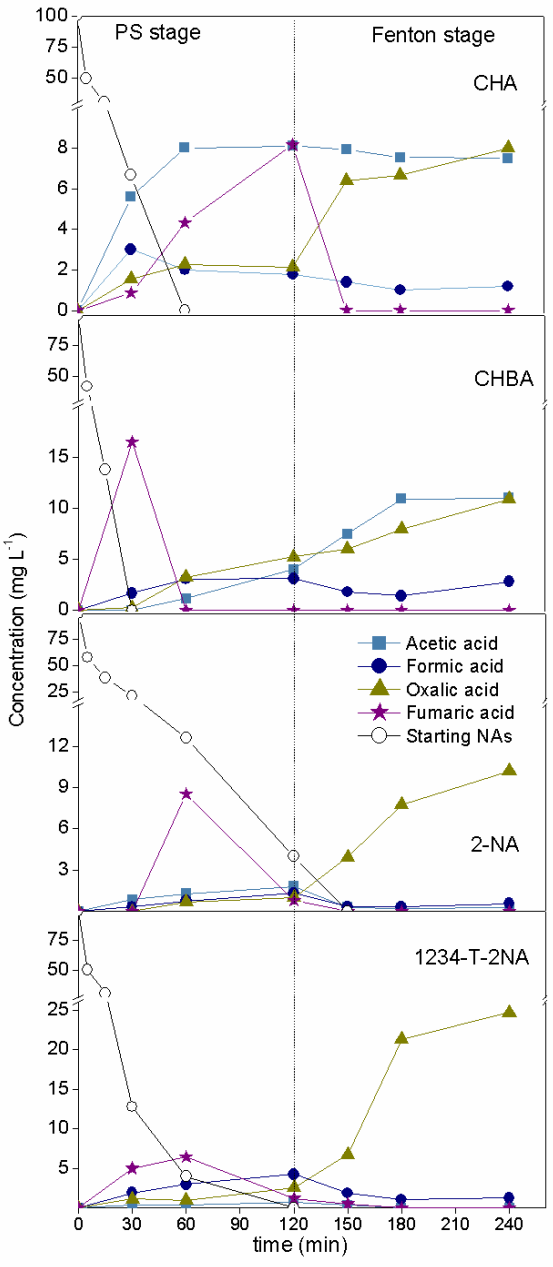

Fig. 3.9 Time-course of the starting NAs and short-chain acids upon the two-step PS(2 h) and Fenton oxidation of NAs. $[NAs]_0$ = 100 mg L^{-1}; [PS] = 20% of the stoichiometric; $[H_2O_2]$ = 40 % of the stoichiometric; $[Fe^{2+}]$ = 5.0 mg L^{-1}; pH_0 = 8; T = 80 °C.

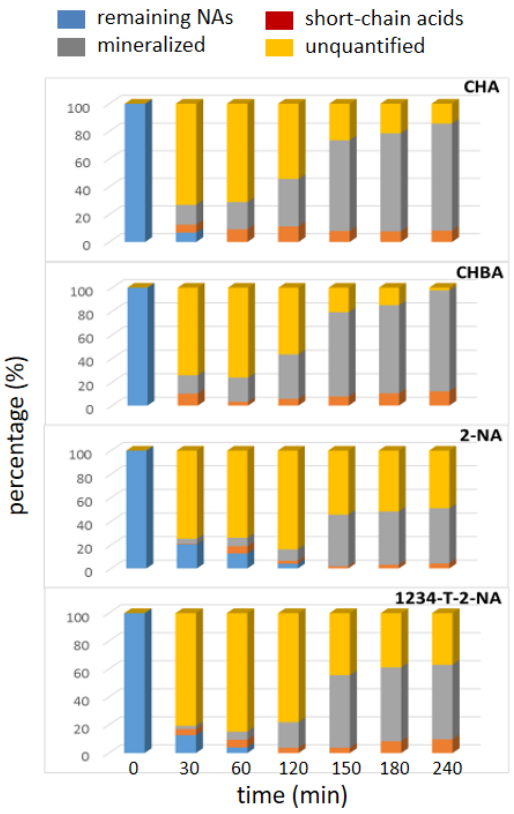

Fig. 10 Carbon balance upon the two-step PS(2 h) and Fenton oxidation. [PS] = 20% of the stoichiometric; [H_2O_2] = 40 % of the stoichiometric; [Fe^{2+}] = 5.0 mg L^{-1}; pH_0 = 8; T = 80 °C.

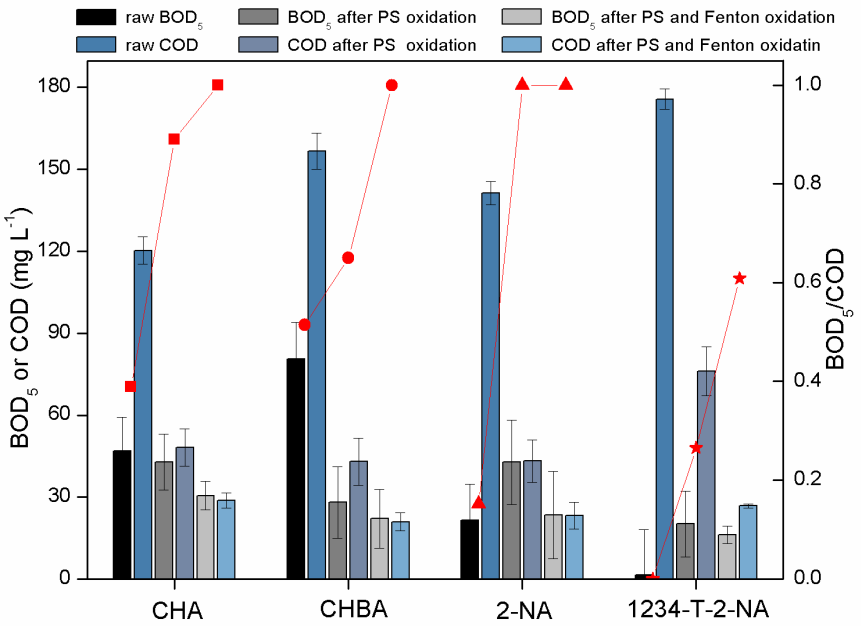

Fig. 11 BOD_5 and COD values of NAs after reactions at different conditions (bars) and the corresponding BOD_5/COD values (line+symbols).

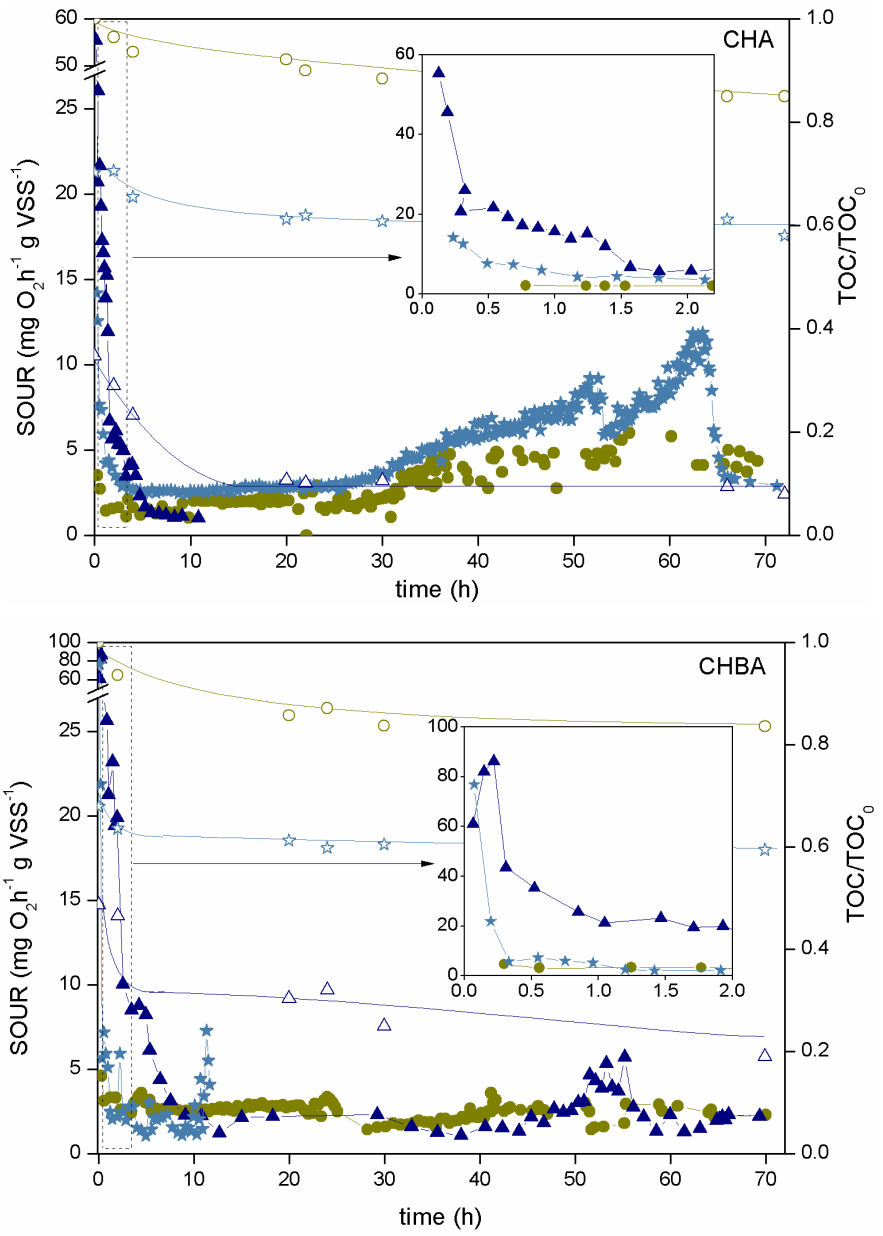

Fig. 12 Time-course of SOUR (solid symbols) and TOC (opened symbols) upon respirometric tests with the starting CHA and CHBA and the effluents from the oxidation treatments. Initial NAs (circle), NAs after thermally-activated PS oxidation (star) and two-step PS(2 h) and Fenton(2 h) oxidation (triangle). The inset figures show the profiles within the earlier stages.

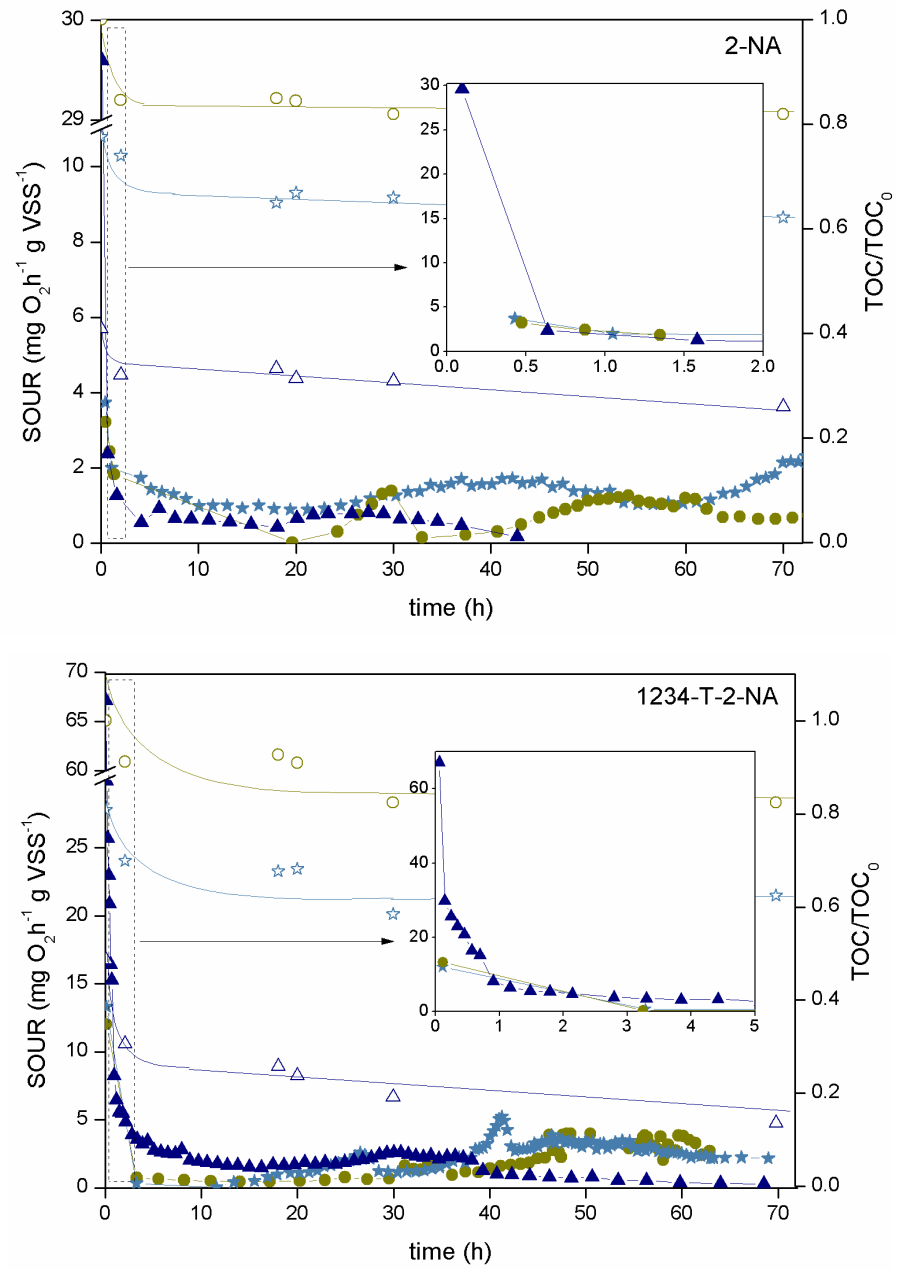

Fig. 13 Time course of SOUR (solid symbols) and TOC (opened symbols) upon respirometric tests with the starting 2-NA and 1234-T-2-NA and the effluents from the oxidation treatments. Symbols as in Fig. 12.

Tables

Table 1 Values of the apparent rate constants of CHA mineralization upon PS and Fenton oxidation under different working temperatures. PS and H_2O_2 at 20 and 40% of the stoichiometric, respectively; Fe^{2+} at 5 mg L^{-1}.

T	PS stage				Fenton stage			
(°C)	$k_1 \times 10^5$	r^2	$k_{PS} \times 10^2$	r^2	$k_2 \times 10^5$	r^2	$k_{H_2O_2} \times 10^2$	r^2
	L mg^{-1} min^{-1}		min^{-1}		L^2 mg^{-2} min^{-1}		min^{-1}	
97	13.9±3.22	0.992	7.98±0.43	0.995	10.4±2.47	0.978	20.4±2.46	0.999
90	7.19±1.57	0.998	4.56±0.10	0.999	6.33±2.54	0.972	12.6±2.91	0.999
80	2.46±1.25	0.998	1.56±0.12	0.993	2.74±0.54	0.988	4.18±0.61	0.975
70	0.669±0.32	1.000	0.798±0.04	0.998	1.14±0.61	0.998	2.46±0.35	0.967
60	0.239±0.15	1.000	0.521±0.02	0.999	0.065±0.04	1.000	1.41±0.22	0.965

Table 2 Values of the apparent rate constants for the PS and Fenton oxidation of individual NAs and mixture of them. PS and H_2O_2 at 20 and 40% of the stoichiometric, respectively. Fe^{2+} = 5 mg L^{-1}; T = 80 °C.

	PS stage				Fenton stage			
NAs	$k_1 \times 10^5$	r^2	$k_{PS} \times 10^2$	r^2	$k_2 \times 10^5$	r^2	$k_{H_2O_2} \times 10^2$	r^2
	L mg^{-1} min^{-1}		min^{-1}		L^2 mg^{-2} min^{-1}		min^{-1}	
CHBA	2.91±0.23	0.998	1.84±0.16	0.991	5.51±1.54	0.976	4.22±0.58	0.992
2-NA	0.482±0.12	1.000	1.13±0.14	0.986	7.79±0.38	1.000	5.29±0.64	0.986
1234-T-2-NA	0.699±0.25	1.000	1.02±0.17	0.987	6.31±0.32	0.999	5.12±0.59	0.987
Mixed	1.50±0.22	0.999	1.58±0.19	0.985	5.95±1.58	0.987	4.98±0.71	0.980